# 18th AIVC Conference
# Ventilation and Cooling

held at Astir Palace, Vouliagmeni Complex, Athens, Greece
23rd-26th September 1997

Proceedings
Volume 2

# PREFACE

## International Energy Agency

The International Energy Agency (IEA) was established in 1974 within the framework of the Organisation for Economic Co-operation and Development (OECD) to implement an International Energy Programme. A basic aim of the IEA is to foster co-operation among the twenty one IEA Participating Countries to increase energy security through energy conservation, development of alternative energy sources and energy research development and demonstration (RD&D). This is achieved in part through a Programme of collaborative RD&D consisting of forty-two Implementing Agreements, containing a total of over eighty separate energy RD&D projects. This publication forms one element of this Programme.

## Energy Conservation in Buildings and Community Systems

The IEA sponsors research and development in a number of areas related to energy. In one of these areas, energy conservation in buildings, the IEA is sponsoring various exercises to predict more accurately the energy use of buildings, including comparison of existing computer programs, building monitoring, comparison of calculation methods, as well as air quality and studies of occupancy.

## The Executive Committee

Overall control of the Programme is maintained by an Executive Committee, which not only monitors existing projects but identifies new areas where collaborative effort may be beneficial.

To date the following have been initiated by the Executive Committee (completed projects are identified by *):

| | |
|---|---|
| Annex 1 | Load Energy Determination of Buildings* |
| Annex 2 | Ekistics and Advanced Community Energy Systems* |
| Annex 3 | Energy Conservation in Residential Buildings* |
| Annex 4 | Glasgow Commercial Building Monitoring* |
| Annex 5 | Air Infiltration and Ventilation Centre |
| Annex 6 | Energy Systems and Design of Communities* |
| Annex 7 | Local Government Energy Planning* |
| Annex 8 | Inhabitant Behaviour with Regard to Ventilation* |
| Annex 9 | Minimum Ventilation Rates* |
| Annex 10 | Building HVAC Systems Simulation* |
| Annex 11 | Energy Auditing* |
| Annex 12 | Windows and Fenestration* |
| Annex 13 | Energy Management in Hospitals* |
| Annex 14 | Condensation* |
| Annex 15 | Energy Efficiency in Schools* |
| Annex 16 | BEMS - 1: Energy Management Procedures* |
| Annex 17 | BEMS - 2: Evaluation and Emulation Techniques |
| Annex 18 | Demand Controlled Ventilating Systems* |
| Annex 19 | Low Slope Roof Systems |
| Annex 20 | Air Flow Patterns within Buildings* |
| Annex 21 | Thermal Modelling* |
| Annex 22 | Energy Efficient Communities* |
| Annex 23 | Multizone Air Flow Modelling (COMIS)* |
| Annex 24 | Heat Air and Moisture Transfer in Envelopes* |
| Annex 25 | Real Time HEVAC Simulation* |
| Annex 26 | Energy Efficient Ventilation of Large Enclosures* |

| | |
|---|---|
| Annex 27 | Evaluation and Demonstration of Domestic Ventilation Systems* |
| Annex 28 | Low Energy Cooling Systems |
| Annex 29 | Energy Efficiency in Educational Buildings |
| Annex 30 | Bringing Simulation to Application |
| Annex 31 | Energy Related Environmental Impacts of Buildings |
| Annex 32 | Integral Building Envelope Performance Assessment. |
| Annex 33 | Advanced Local Energy Planning |
| Annex 34 | Computer-aided Evaluation of HVAC System Performance |

# Annex V Air Infiltration and Ventilation Centre

The Air Infiltration and Ventilation Centre was established by the Executive Committee following unanimous agreement that more needed to be understood about the impact of air change on energy use and indoor air quality. The aim of the Centre is to promote an understanding of the complex behaviour of air flow in buildings and to advance the effective application of associated energy saving measures in both the design of new buildings and the improvement of the existing building stock.

*The Participants in this task are Belgium, Canada, Denmark, Germany, Finland, France, Netherlands, New Zealand, Norway, Sweden, United Kingdom and the United States of America.*

# 18TH AIVC CONFERENCE PROGRAMME
# "Ventilation and Cooling"

**CONTENTS** **Page**

## Volume 1

**SESSION 1: VENTILATION AND INDOOR AIR QUALITY**



**SESSION 2: INNOVATIVE COOLING**

# VENTILATION AND COOLING

**18TH ANNUAL AIVC CONFERENCE**
**ATHENS, GREECE, 23-26 SEPTEMBER, 1997**

## A METHOD FOR THE ECONOMICAL OPTIMIZATION OF DESIGN TEMPERATURES AND THE CONNECTING FLOWS OF A COOLING SYSTEM


Author: Sarkomaa, Pertti

Department of Energy Technology, Lappeenranta University of Technology,
Skinnarilankatu 34, 53850 Lappeenranta, Finland,
tel +358-5-6212700, fax. +358-5-6212799, e-mail pertti.sarkomaa@lut.fi


Optimalisation of a simple cooling system

interessant voor formules, etc..

Vraag Stewie: (Wat bedoel je met effectivness)

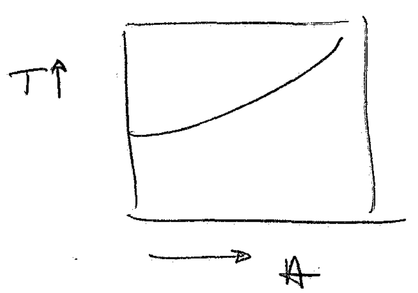


vereen-voudiging

## SYNOPSIS

The planning parameters of a cooling system for ventilation, for example the vaporization and condensing temperatures, heat capacity flow rates, design temperatures and design temperature differences have a strong influence on the investment and operating costs.

The target of this research is to find economically optimized design parameters by minimizing the present value of investment and the operating costs of the cooling system. The cooling system may have several series-connected heat exchangers on the vaporization and condensing sides of the cooling machine.

When the optimization is carried out, such factors as the price of electricity, maintenance costs, operating time, interest rate, annual running time, the coefficient of performance, marginal costs of heat transfer surface areas and the overall heat transfer coefficients of the vaporizer, the condenser and the other heat exchangers which are connected to the same system, are taken into account.

This new method is useful for the economical optimization of the design parameters of ventilation and other cooling systems.

## SYMBOLS

| | |
|---|---|
| $A$ | heat transfer surface area, m$^2$ |
| $\dot{C}$ | heat capacity flow rate, W/K |
| COP | coefficient of performance |
| $J$ | economical efficiency of a heat exchanger, W/US$ K |
| $K$ | present value of costs, US$ |
| $K_0$ | constant part of the investment costs, US$ |
| $P$ | electric power of compressor motor, W |
| $S$ | economic number, K |
| $T$ | temperature, K |
| $a$ | factor of present value of periodic payment during the operating time |
| $c_p$ | specific heat , J/kgK |
| $e$ | unit price of electricity, US$/kWh |
| $q_m$ | mass flow rate, kg/s |
| $h$ | marginal cost of a heat transfer surface area, US$/m$^2$ |
| $k$ | overall heat transfer coefficient, W/m$^2$K |
| $r$ | ratio of annual maintenance cost and investment cost |
| $s^*$ | dimensionless optimization parameter |
| $t$ | annual peak-load power time, h |

Greek letters

| | |
|---|---|
| $\varepsilon$ | effectiveness of a heat exchanger |
| $\Phi$ | design cooling power, W |
| $\eta$ | efficiency of a total process |
| $\eta_{cd}$ | ratio of process efficiencies of real ideal process and Carnot process |
| $\eta_i$ | indicated efficiency which takes into account differences between the real indicated process and the real ideal process |
| $\eta_m$ | efficiency of driving motor and gear |
| $\eta_{mk}$ | mechanical efficiency of compressor |
| $\theta$ | temperature difference, K |
| $\sigma$ | dimensionless economy number |

Subscripts

| | |
|---|---|
| R | reduced |
| a | ambient |
| c | condenser |
| ln | logarithmic |
| v | vaporizer |
| r | room |

## 1. INTRODUCTION

Cooling systems have usually been optimized by using thermodynamic or economical methods. There are examples of the recent research in references /1/, /2/ and /3/.

In this research a new technical and economical method to optimize a cooling system is presented. The cooling system may have several series-connected heat exchangers on the vaporization and condensing sides of the cooling machine (fig. 1). Planning parameters like vaporizing temperature $T_v$, condensing temperature $T_c$ (fig. 2) as well as heat capacity flows between heat exchangers and their design temperatures have big influence on the economy of the cooling system.

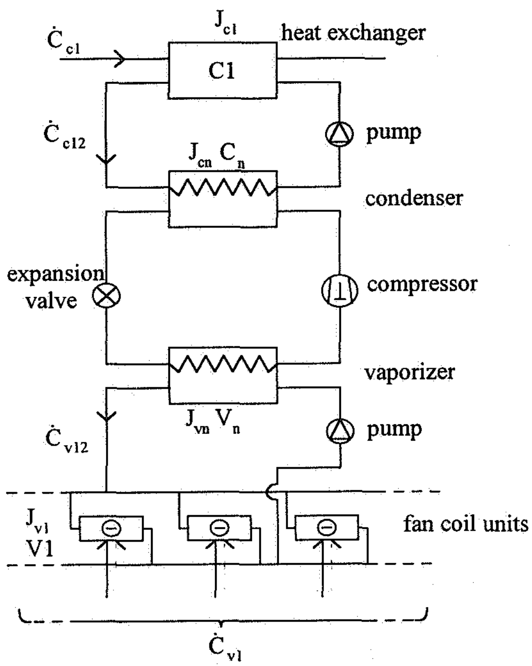


Figure 1. Optimized cooling system.

The target of the research is to determine economically optimal dimensioning parameters for the cooling system presented in fig. 1, where the vaporizer and the condenser are thought to be counterflow heat exchangers in which the other side temperatures are approximately constant and the values of effectivenesses are $\varepsilon_v$ and $\varepsilon_c$, fig. 2. The following factors are taken into account in the optimization: overall heat transfer coefficient, $k$; marginal costs of heat transfer surface area, $h$; maintenance costs, which are estimated by the ratio of annual maintenance costs and investment costs, $r$; the factor of present value of periodic payment during the operating time, $a$; annual peak-load power time, $t$; efficiency of the process, $\eta$; and unit price of electricity, e.

Remarks

As a result, when the system is optimized by the new method, economically optimal values of effectivenesses and surface areas of the condenser and the vaporizer are obtained. If the cooling system has several series-connected heat exchangers on the vaporization and condensing sides of the cooling machine (fig. 1) also economically optimal surface areas and connecting heat capacity flows of heat exchangers and temperatures in corresponding conditions are obtained as a result.

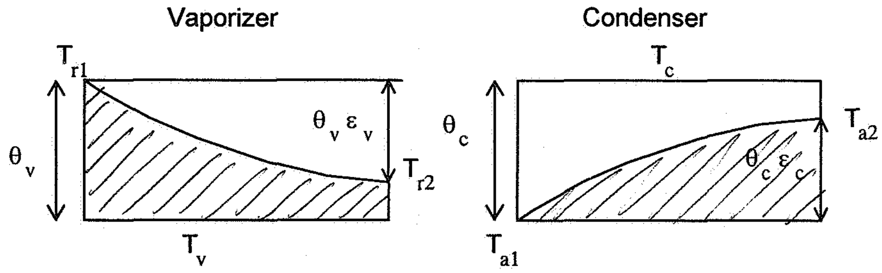


Figure 2. Temperatures of the vaporizer and the condenser.

figuur 2

## 2. DEFINITIONS AND FUNDAMENTAL EQUATIONS

The heat transfer surface areas of a vaporizer and a condenser are /4/

$$A_v = \frac{\dot{C}_v}{k_v} ln\left(\frac{1}{1-\varepsilon_v}\right), \quad (1) \qquad A_c = \frac{\dot{C}_c}{k_c} ln\left(\frac{1}{1-\varepsilon_c}\right), \quad (2)$$

where $\dot{C}_v$ is the cooled heat capacity flow and $\dot{C}_c$ is the heat capacity flow which cools the condenser. $k_v$ and $k_c$ are the overall heat transfer coefficients of the vaporizer and the condenser. $\varepsilon_v$ and $\varepsilon_c$ are the effectivenesses of a vaporizer and a condenser.

In optimization the design cooling power $\Phi_v$ is constant ( je hebt een zekere $\phi_v$ nodig)

$$\phi_v = q_{mv} c_{pv} \left(T_{r1} - T_{r2}\right) = \dot{C}_v \varepsilon_v \theta_v = constant. \quad (3)$$

The cooling power of the condenser is

$$\phi_c = \dot{C}_c \varepsilon_c \theta_c = \phi_v + P = \phi_v \left(1 + \frac{1}{COP}\right) = \phi_v \left(1 + \frac{1}{\eta} \frac{T_{a1} - T_{r1} + \theta_c + \theta_v}{T_{r1} - \theta_v}\right), \quad (4)$$

where $P$ is the electrical power of compressor, COP is the coefficient of performance.

The COP of the refrigerator is

$$COP = \frac{\Phi_v}{P} = \eta \frac{T_v}{T_c - T_v} = \eta \frac{T_{r1} - \theta_v}{T_{a1} - T_{r1} + \theta_c + \theta_v}, \quad (5)$$

where $\eta = \eta_m \eta_{mk} \eta_{cd} \eta_i$, (6) $\quad \theta_v = T_{r1} - T_v$, (7) $\quad \theta_c = T_c - T_{a1}$. (8)

Efficiencies are: $\eta_m$ efficiency of the driving motor and the gear, $\eta_{mk}$ mechanical efficiency of the compressor and $\eta_{cd}$ ratio of process efficiencies of the real ideal process and the Carnot process and $\eta_i$ indicated efficiency.

The economical efficiency of the heat exchanger is determined by equation

$$J = \frac{k}{h(1 + ra)}, \quad (9)$$

where $h$ is the marginal costs of the heat transfer surface area and $r$ is the ratio of annual maintenance costs and investment costs and $a$ is the factor of present value of periodic payment

## 3. OPTIMAL SOLUTION FOR THE PRESENT VALUE OF INVESTMENT COSTS AND OPERATING COSTS OF THE COOLING SYSTEM

The present value of investment costs and operating costs are determined by discounting all costs to the present time. The cost function is

$$K = K_0(1+r_0a)+A_ch_c(1+r_ca)+A_vh_v(1+r_va)+Ptea$$
$$= K_0(1+r_0a)+\frac{\dot{C}_ch_c}{k_c}(1+r_ca)ln\left(\frac{1}{1-\varepsilon_c}\right)+\frac{\dot{C}_vh_v}{k_v}(1+r_va)ln\left(\frac{1}{1-\varepsilon_v}\right)+\left[\frac{\phi_v tea}{\eta}\frac{T_{a1}-T_{r1}+\theta_c+\theta_v}{T_{r1}-\theta_v}\right], \quad (10)$$

where $K_0$ is the piecewise continuous constant part of the investment costs of the cooling system and $e$ is the unit price of electricity. The cost function is piecewise continuous, but between discrete points it is the function of two independent variables, the effectivenesses of the vaporizer and the condenser, $\varepsilon_v$ and $\varepsilon_c$.

The conditions of the optimization are

$$\frac{\delta K}{\delta \varepsilon_c}=\frac{\dot{C}_c}{J_c}\frac{1}{(1-\varepsilon_c)}-\frac{\dot{C}_c tea((\eta-1)T_v+T_{a1})}{\left(\eta T_v\frac{\dot{C}_c\varepsilon_c}{\phi_v}-1\right)^2}=0, \quad (11)$$

$$\frac{\delta K}{\delta \varepsilon_v}=\frac{\dot{C}_v}{J_v}\frac{1}{(1-\varepsilon_v)}-\frac{tea}{\eta T_v}\frac{\phi_v^{\ 2}}{\dot{C}_v\varepsilon_v^2}\left(\frac{\eta\left(\frac{\dot{C}_c\varepsilon_c}{\phi_v}T_{a1}+1\right)-1}{\left(\eta T_v\frac{\dot{C}_c\varepsilon_c}{\phi_v}-1\right)^2}+\frac{T_c}{T_v}\right)=0. \quad (12)$$

The optimization parameters $s_v^*$ and $s_c^*$ are determined by equations (13) and (14)

$$s_v^* = 0{,}5(T_{r1}-T_{r2})^2\frac{teaJ_v}{\eta T_v}\left(\frac{\eta\left(\frac{\dot{C}_c\varepsilon_c}{\phi_v}T_{a1}+1\right)-1}{\left(\eta\frac{\dot{C}_c\varepsilon_c}{\phi_v}T_v-1\right)^2}+\frac{T_c}{T_v}\right), \quad (13)$$

$$s_c^* = 0{,}5(T_{a2}-T_{a1})^2\frac{teaJ_c}{(\eta-1)T_v+T_{a1}}. \quad (14)$$

The economically optimal effectivenesses of the vaporizer and the condenser are

$$\varepsilon=\sqrt{s^{*2}+2s^*}-s^*. \quad (15)$$

## 4. OPTIMAL SOLUTION OF SERIES-CONNECTED HEAT EXCHANGERS ON THE VAPORIZATION AND CONDENSING SIDES

If series-connected heat exchangers are of the counterflow type they can be reduced to one counterflow heat exchanger /5/, which is furthermore optimized by the method presented in chapter 3, where $J_v$ and $J_c$ in equations (13) and (14) are substituted for their reduced values in equations (16) and (17).

$$J_{vR} = \frac{J_{v1}}{1+\sigma_v}, \qquad (16) \qquad J_{cR} = \frac{J_{c1}}{1+\sigma_c}. \qquad (17)$$

Generally $$\sigma = \sum_{i=2}^{n} \sqrt{\frac{J_1}{J_i}} \qquad (18)$$

and for the system in fig. 1 $$\sigma_c = \sqrt{\frac{J_{c1}}{J_{cn}}}, \qquad (19) \qquad \sigma_v = \sqrt{\frac{J_{v1}}{J_{vn}}}. \qquad (20)$$

Furthermore for the system in fig. 1, the optimal heat capacity flows between heat exchangers are

$$\dot{C}_{c12} = \dot{C}_{c1}\left(1+\frac{1}{\sigma_c}\right), \qquad (21) \qquad \dot{C}_{v12} = \dot{C}_{v1}\left(1+\frac{1}{\sigma_v}\right). \qquad (22)$$

The heat transfer surface areas $A_{c1}$ and $A_{v1}$ in fig. 1 are obtained from equations

$$A_{c1} = \frac{\dot{C}_{c1}}{k_{c1}}(1+\sigma_c)\, ln\left(\frac{1}{1-\varepsilon_{cR}}\right), \qquad (23) \qquad A_{v1} = \frac{\dot{C}_{v1}}{k_{v1}}(1+\sigma_v)\, ln\left(\frac{1}{1-\varepsilon_{vR}}\right). \qquad (24)$$

And, finally, economically optimal heat transfer surface areas of the vaporizer and the condenser are

$$A_{cn} = \frac{k_{c1}}{k_{cn}}\sqrt{\frac{J_{c1}}{J_{cn}}}A_{c1}, \qquad (25) \qquad A_{vn} = \frac{k_{v1}}{k_{vn}}\sqrt{\frac{J_{v1}}{J_{vn}}}A_{v1}. \qquad (26)$$

Usually different kinds of parallel fan units with different k and h values are installed to cooled rooms. They have to be reduced to one counterflow heat exchanger for the optimization. The reduced heat exchanger has the same cooling power, same heat capacity flow and same differential of price of the heat transfer surface area as the original fan units. If the fan units are designed so that the ratios between heat capacity flows in each unit are equal and optimal the optimization parameters for one reduced heat exchanger are

$$\dot{C}_{v1} = \sum_{i=1}^{n} \dot{C}_{v1i}, \qquad (27) \qquad \varepsilon_{v1} = \sum_{i=1}^{n} \frac{\dot{C}_{v1i}}{\dot{C}_{v1}}\varepsilon_{v1i}, \qquad (28)$$

$$J_{v1} = \left(\sum \frac{\dot{C}_{v1i}}{\dot{C}_{v1}} \frac{1-\varepsilon_{v1}}{1-\varepsilon_{v1i}} \frac{1-R_{v1}\varepsilon_{v1}}{1-R_{v1}\varepsilon_{v1i}} \frac{1}{J_{v1i}}\right)^{-1}, \qquad (29) \qquad \phi_{v1} = \sum_{i=1}^{n} \phi_{v1i}. \qquad (30)$$

## 5.1 EXAMPLE

The cooling demand for an office building is 400 kW. The rooms are cooled by fan coil units. The number of fan coil units, cooling power, heat capacity flow of air and the ratio of overall heat transfer coefficient and marginal costs with installation costs for each unit are: 47 pc., $\phi_{v1}$=1 kW, $\dot{C}_{v1}$=85 W/K, $k_{v1}/h_{v1}$=0,45 W/(K US$); 100 pc., 2,33 kW, 195 W/K, 0,685 W/(K US$); 20 pc., 4 kW, 335 W/K, 0,905 W/(K US$); 4 pc., 10 kW, 835 W/K, 1,09 W/(K US$). Air is cooled in the fan coil unit from the temperature of +27 °C to + 15 °C. The effectivenesses of the fan coil units are equal. The ratio of overall heat transfer coefficient and marginal costs with installation costs of the water cooler and the air condenser are 0,95 W/(K US$) and 1,8 W/(K US$). Air temperature difference in the condenser is 8 K and the inlet temperature of cooling air is 32 °C. The ratio of annual maintenance costs and investment costs in the fan coil units is $r_{v1}$=0,03, in the water cooler (vaporizer) $r_{vn}$=0,04 and in the air condenser $r_c$= 0,02. The interest rate is 10 % and operating time of the investment 15 years and thus the factor of present value of periodic payment a=12,39. $\eta$=0,55. Annual peak-load power time of the compressor is 2500 h. The unit price of electricity is 0,06 US$/kWh.

## 5.2 SOLUTION

Economical efficiency of the air condenser, eq. (9) $J_{cn}$= 1,44 W/US$K. Vaporizing temperature $T_v = T_{r1} - (T_{r1} - T_{r2}) / \varepsilon_v = 276$ K. Dimensionless optimization parameter of the condenser, eq. (14) $s_c^*$=0,429. Optimal effectiveness of the condenser, eq. (15) $\varepsilon_c$=0,592. Heat capacity flow of the fan coil units, eq. (27) $C_{v1}$=33,5 kW/K. Condensing temperature $T_c = T_{a1} + (T_{a2} - T_{a1}) / \varepsilon_c = 318$ K. Economical efficiency of the fan coil units, eq. (9) and eq. (29) $J_{v1}$=0,51 W/US$ K. Economical efficiency of the water cooler, eq. (9) and eq. (29) $J_{vn}$=0,64 W/US$ K. Dimensionless economy number of the vaporizer, eq. (20) $\sigma_v$=0,90. Reduced economical efficiency of the vaporizer, eq. (16) $J_{vr}$=0,27 W/US$ K. COP, eq. (5) COP=3,57. $\phi_v / \dot{C}_c = (\phi_c / \dot{C}_c)(COP/(1+COP))$=6,25 K. Dimensionless optimization parameter of the vaporizer, eq. (13) $s_v^* = 1{,}17$. Reduced effectiveness of the vaporizer eq.(15) $\varepsilon_{vr}$=0,76. The second iteration round: $T_v$=284 K; $\varepsilon_c$=0,59; $T_c$=318 K; $\varepsilon_v$=0,52. The third iteration round. $T_v$=277 K; $\varepsilon_c$=0,59; $T_c$=319 K; $\varepsilon_v$=0,53. The fourth iteration round: $T_v$=277 K; $\varepsilon_c$=0,59; $T_c$=319 K; $\varepsilon_v$=0,53. The heat capacity flow between the water cooler and fan coil units, eq. (22) $\dot{C}_{v12}$=70,9 kW/K Mass flow of water $q_m = \dot{C}_{v12}/c_{pv}$=16,9 kg/s. The sum of the fan coil unit conductances, eq. (24) $G_{v1}=k_{v1}A_{v1}$=47,5 kW/K, which consists of 47 pc. 0,119 kW/K, 100 pc. 0,276 kW/K, 20 pc. 0,475 kW/K and 4 pc. 1,19 kW/K. The conductance of the vaporizer of the water cooler, eq. (26) $G_{vn}$=42,6 kW/K. The conductance of condenser, eq. (2) $G_c=k_cA_c$=188 kW/K.

The sensitivities of effectivenesses $\varepsilon_v$ and $\varepsilon_c$ and logarithmic mean temperature differences $\theta_{lnv}$, eq. (33) and $\theta_{lnc}$, eq. (34) are presented in fig. 3 and fig. 4 as a function of the ratio of economic numbers $S_v/S_{v0}$, eq. (31) and $S_c/S_{c0}$, eq. (32) and efficiency $\eta$.

$$S_v = 0{,}5(T_{r1} - T_{r2})^2 teaJ_{vR}, \quad (31) \qquad S_c = 0{,}5(T_{a2} - T_{a1})^2 teaJ_c, \quad (32)$$

$$\theta_{ln\,v} = \frac{T_{r1} - T_{r2}}{ln\left(\dfrac{T_{r1} - T_v}{T_{r2} - T_v}\right)}, \qquad (33) \qquad \theta_{ln\,c} = \frac{T_{a2} - T_{a1}}{ln\left(\dfrac{T_c - T_{a1}}{T_c - T_{a2}}\right)}. \qquad (34)$$

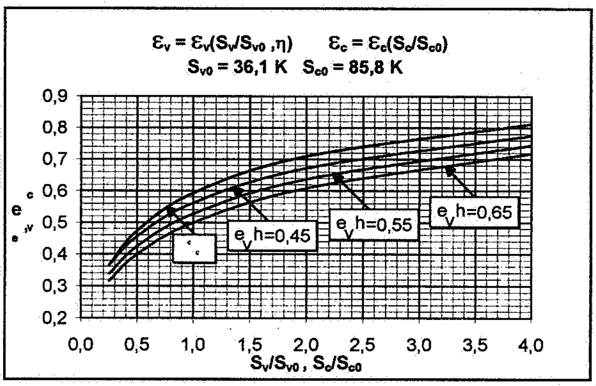


Figure 3. Sensitivity of effectivenesses

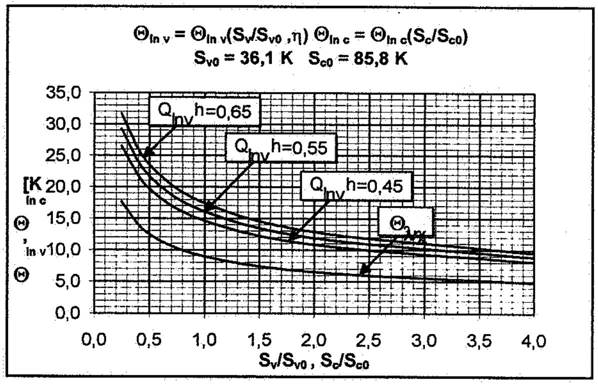


Figure 4. Sensitivity of log mean temperature difference

## 6. DISCUSSION

Ratio between the lifetime electricity costs and the marginal costs of the heat transfer areas are described by the optimization parameters $s_v^*$ and $s_c^*$. The bigger the optimization parameters $s^*$, the bigger the economically optimal effectiveness of the heat exchanger. Annual operating time, price of electricity, interest rate of investment and operating life of the cooling system vary considerably in practice. Therefore economic design parameters should be chosen optimically especially for big cooling systems.

The optimization equations are solved by iteration. Iteration converges rapidly, and usually only four calculation rounds are needed, if $\varepsilon_v = \varepsilon_c = 0{,}6$ is the first approximation in the beginning.

## REFERENCES

1. *GOKTUN, S.*
   *"Optimal Performance of an Irreversible Refrigerator with Three Heat Sources"*
   *Energy (Oxford), v 22, n 1, Jan 1997, p 27-31.*
2. *YAN, Z. and CHEN L.*
   *"Optimization of the Rate of Energy Output for an Endoreversible Carnot Refrigerator"*
   *Journal of Physics D: Applied Physics, v 29, n 12, Dec 14 1996, p 3017-3021.*
3. *Wu, C. and Chen, L. and Sun, F.*
   *"Optimization of Steady Flow Refrigeration Cycles"*
   *International Journal of Ambient Energy, v 17, n 4, Oct 1996, p 199-206.*
4. *INCROPERA, F.P. and DEWITT, D.P.*
   *"Introduction to Heat Transfer"*
   *John Wiley & Sons, New York, 1996.*
5. *SARKOMAA, P.*
   *"Economic Optimization of industrial heat exchangers (in Finnish)"*
   *Energiansäästö kiinteistöissä ja teollisuudessa, Helsinki University of Technology, Espoo, 1994, p 267-276.*

# VENTILATION AND COOLING
# 18TH ANNUAL AIVC CONFERENCE
# ATHENS, GREECE, 23-26 SEPTEMBER, 1997

## Guidance and tools for night and evaporative cooling in office buildings

1 zone model →
x controle op ≠ cooling install..
x veel resultaten
→ o a ook verbruik water.


Jean-Robert MILLET

Centre Scientifique et Technique du Bâtiment, Marne la Vallée, France

## 1. INTRODUCTION

In France, mechanical cooling is increasingly used in office buildings. This situation is related to a demand for a better comfort, the increase of the thermal insulation and internal gains, and the changes in the building design.

Nevertheless, in many cases, it is possible to achieve a thermally comfortable environment by passive means - as thermal inertia, and solar protection of the external envelope - and use of low energy techniques as night or evaporative cooling. When mechanical cooling is yet required, the same approach can be used to reduce the peak demand and the energy needs.

These parameters have to be taken into account at the early stages of building design. Therefore, there is a need for simple tools enabling to give first guidance to the designer. On another hand, these tools must be produced by a more precise one in order to improve the design in further stages, or to take into account specific situations.

In addition, the development of efficient strategies in this field requires to take into account the fact that the maximum cooling power is generally available at night, and the cooling peak demand occurs in the middle of the day. This leads to two consequences :

1. The tools must take into account in a quite accurate way the non steady state thermal behaviour of the rooms,
2. The control strategies must compensate the lack of maximum cooling power by precooling the building at night, while keeping the indoor climate comfortable during occupancy.

The works conducted at CSTB aims to fulfil the above requirements. Developed within the framework of IEA annex 28 "low energy cooling", they are based on two kinds of tools : detailed tools, and guidance ones.

## 2. DETAILED DESIGN TOOLS :

The air handling plant shown in fig 1 has the following components :

- a rotating exchanger,
- a humidifier for the return air,
- a heating coil,
- a humidifier for the supply air,
- a cooling coil,
- two fans providing different airflow rates (equal for both fans).

The system control is based on a set of set point temperatures related to the running possibilities of the different components of the system. The running of one component is modified within a temperature band where the control is assumed to be linear or equivalent to it for the timestep.

Additional control can be taken into account in order to avoid misfunctionings. The system heating or cooling power is then related only to the indoor air temperature Ti by Fsyst (Ti). On another hand, the room behaviour for a given timestep can be described as Froom (Ti) function, which describes the indoor temperature resulting from a given heating (or cooling) power. It is here considered that this relationship is linear.

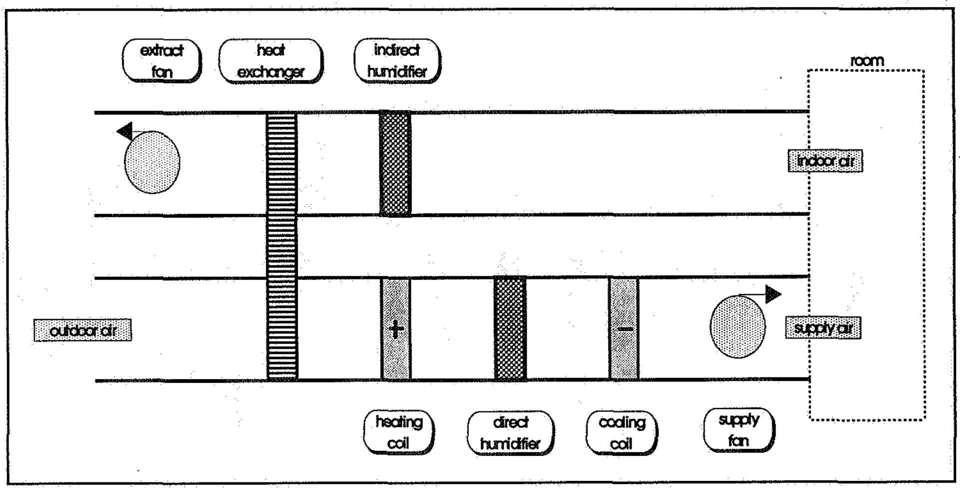


**figure1 air handling plant components**

The calculation model for the room behaviour COMET developed at CSTB is based on the simplification of the heat transfers between the internal and external environment reported in figure 2.

RC model
voor 1 zone

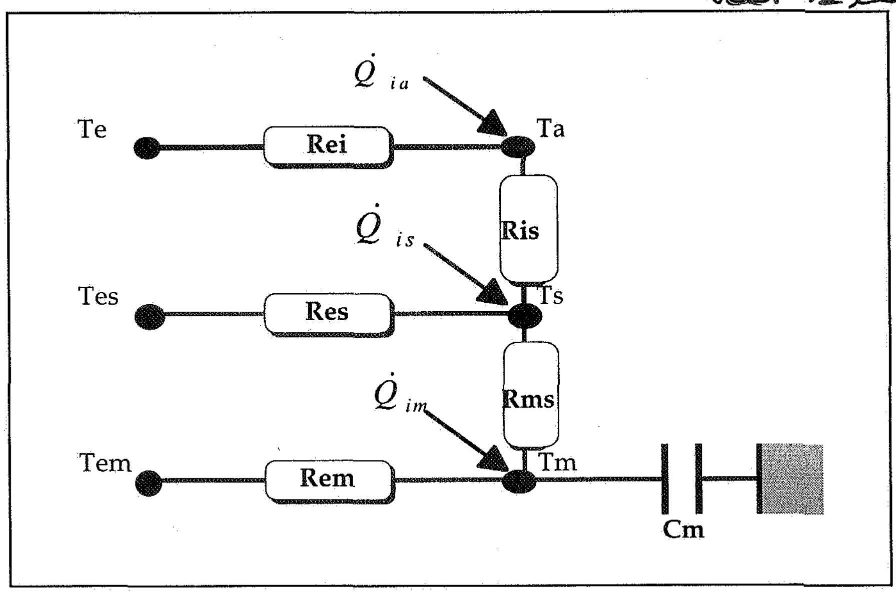


Figure 2 - Equivalent electric representation of the building model

Compared to other programs, this calculation model requires less detailed input datas as more detailed codes (as TRNSYS for example) : for example, external components are only described by their U value, solar factor and depth.

On the other hand, it enables to distinguish between the indoor operative and air temperature, which can be up to 2 or 3 K for air conditioned buildings when most of the simplified method only uses one value for both.
It has been validated using TRNSYS as a reference. (figure 3) . Starting of a base room, main parameters (orientation, window solar factor,inertia, internal gains, ventilation, system control) where modified and yearly heating and cooling needs calculated.

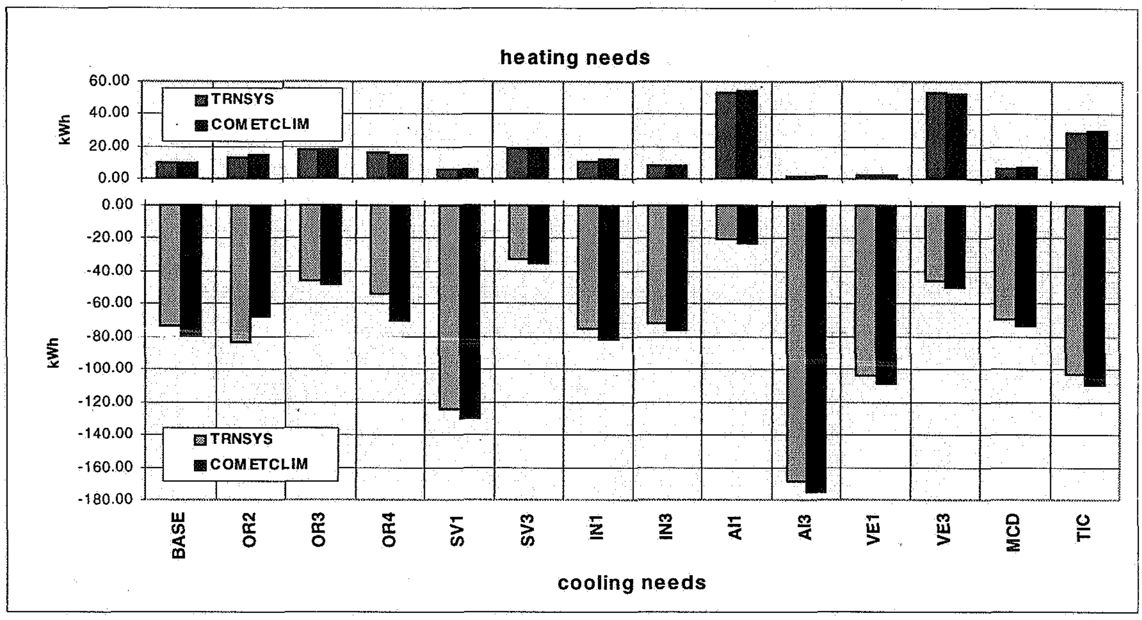


**figure 3 - Comparison between TRNSYS and COMET**

The functioning set point is obtained by solving the two equations at each timestep. A simple algorithm is then used to calculate the actual indoor temperature as shown in the figure 4.

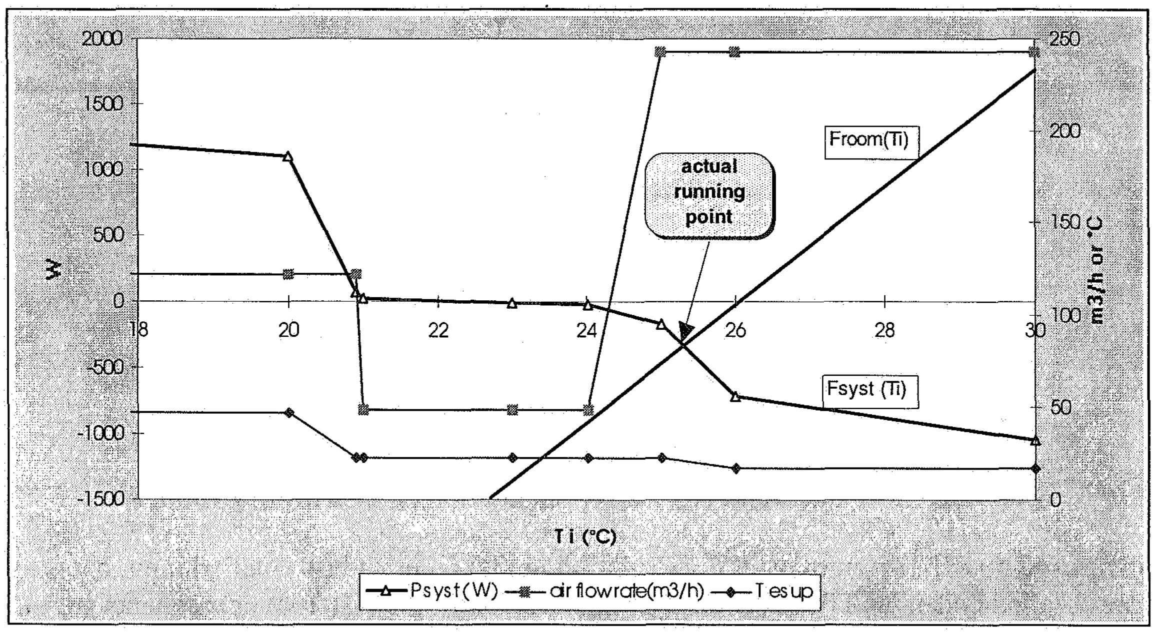


**figure 4 - example of running point calculation**

## 2.1 SYSTEM CONTROL

Each component is controlled by an on-off or by fixing values through a temperature band. It is important to notice that the control description must be based on its equivalent behaviour for the calculation timestep. As a general rule, it is considered here that the behaviour is linear within the band control.

For example, if the heating band control is 20 °C - 21 °C, it is assumed that the heating power will be at its maximum value for Ti < 20°C, equal to 0 for Ti > 21 °C and vary linearly between 20 °C and 21 °C. This does not mean that the control system must be a proportional one : a simple on-off control can lead to the same equivalent behaviour. A second rule here applied is that a control band must corresponds to a linear variation of supply air temperature and air flow. The set point temperatures can be constant or vary with time (the set point for heating can for example be reduced at night in winter).

### *2.1.1 control matrixes*

For each system, we have defined control matrixes for summer and for winter conditions, during occupancy and inoccupancy (24 control matrixes). Examples of such matrixes are shown in fig 5.

### *2.1.2 transition*

When we do a calculation for a complete typical year, we have to define transitions between winter control matrix and summer control matrix. When calculation is done with winter control matrix, we check the indoor air temperature between 7h and 8h. If this temperature becomes higher than 23°C, the transition with summer control matrix is done. When calculation is done with summer control matrix, we check the indoor air temperature between 8h and 9h. If this temperature becomes lower than 19°C, the transition with winter control matrix is done.

### *2.1.3 additional controls*

- indirect humidification is used if permitted by the set point control and if the humidified air Thum as a temperature lower than the outdoor air Te . The control is as follows :

Te > Thum + dThic $\Rightarrow$ control by set point

Te $\leq$ Thum + dThic $\Rightarrow$ no humidification

The dThic value is used to avoid humidification if it is of low efficiency regarding outdoor temperature. It can be for example fixed to 2 K.

- heat exchange

When the room requires cooling, the heat exchanger is stopped if outdoor air has a temperature lower than extract air before heat exchanger. In any case, the heat exchanger is controlled in order to avoid temperature lower than a limit value Teexlim (16°C during occupancy and 11°C during non occupancy). If this limitation occurs, direct humidification can't be used.

- direct humidification. The direct humidification is controlled in order to avoid air absolute humidity higher than a limit value wehumlim.

| ti-occ | -20 | 20 | 21 | 22 | 23 | 24 | 25 | 26 | 70 |
|---|---|---|---|---|---|---|---|---|---|
| air flow rate ratio (% vol/h) | 0.17 | 0.17 | 0.17 | 0.17 | 0.17 | **1.0** | 1.0 | 1.0 | 1.0 |
| use of | 0 | 0 | 0 | 0 | 0 | 1 | 1 | 1 | 1 |
| add ind.humid | 0 | 0 | 0 | 0 | 0 | 1 | 1 | 1 | 1 |
| use of | 1 | 1 | 1 | 1 | 1 | 1 | 1 | 1 | 1 |
| add heat exch. | 1 | 1 | 1 | 1 | 1 | 1 | 1 | 1 | 1 |
| use of heating | 0 | 0 | 0 | 0 | 0 | 0 | 0 | 0 | 0 |
| use of direct | 0 | 0 | 0 | 0 | 0 | 0 | 1 | 1 | 1 |
| use of cooling | 0 | 0 | 0 | 0 | 0 | 0 | 0 | 0 | 0 |

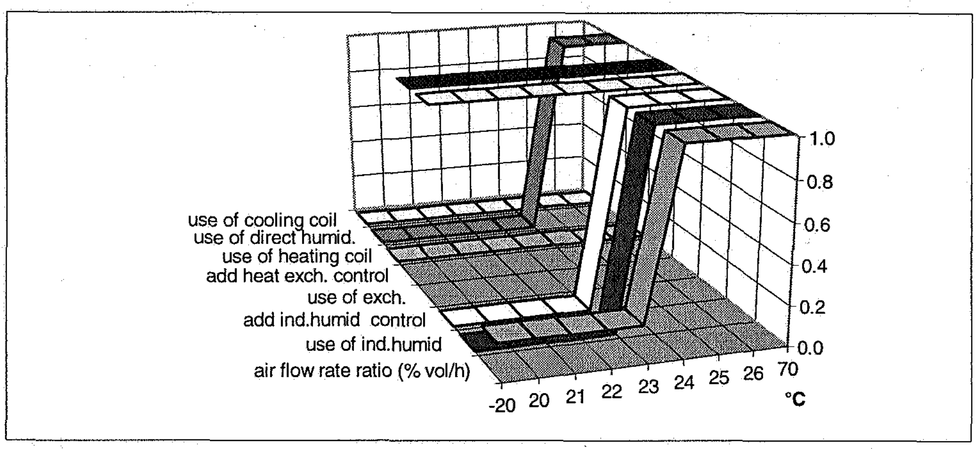


during occupancy time

| ti-inoc | -20 | 15 | 16 | 19 | 20 | 21 | 22 | 26 | 70 |
|---|---|---|---|---|---|---|---|---|---|
| air flow rate ratio (% vol/h) | 0.01 | 0.01 | 0.01 | 0.01 | 0.17 | **1.0** | 1.0 | 1.0 | 1.0 |
| use of | 0 | 0 | 0 | 0 | 1 | 1 | 1 | 1 | 1 |
| add ind.humid | 0 | 0 | 0 | 0 | 1 | 1 | 1 | 1 | 1 |
| use of | 1 | 1 | 1 | 1 | 1 | 1 | 1 | 1 | 1 |
| add heat exch. | 1 | 1 | 1 | 1 | 1 | 1 | 1 | 1 | 1 |
| use of heating | 0 | 0 | 0 | 0 | 0 | 0 | 0 | 0 | 0 |
| use of direct | 0 | 0 | 0 | 0 | 0 | 1 | 1 | 1 | 1 |
| use of cooling | 0 | 0 | 0 | 0 | 0 | 0 | 0 | 0 | 0 |

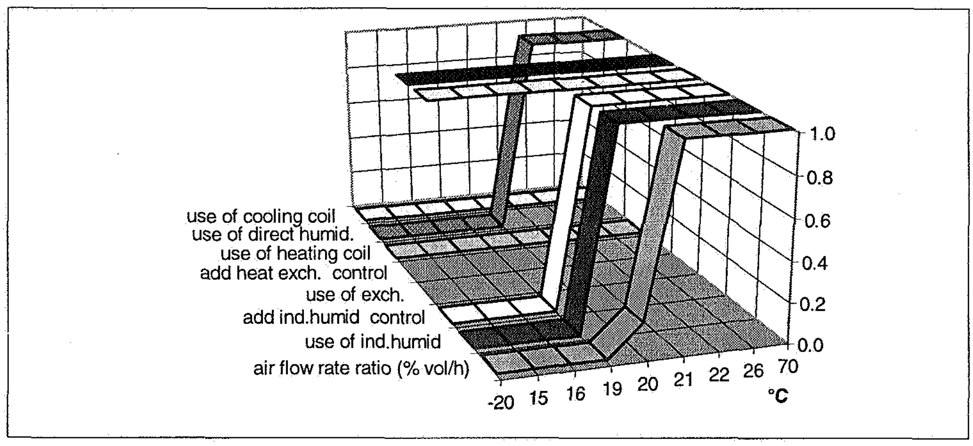


during non occupancy time

**fig 5 - example of control scheme for an evaporative indirect/direct system in summer**

We give hereafter detailed results for a typical warm day in summer (system dimensioning) at Trappes (Paris area). The system is a direct + indirect evaporative one. The building is of high inertia and East oriented.

| Dept : | Trappes | Simulation of Air Handling Plant (dimensioning) | 31-jan-97 |
|---|---|---|---|
| Cooling plant : | None | Evaporative system : direct+indirect | Air flow (m3/h) : 243 · N° simul: 177 |
| Int . Gains (W/m2) : | 10 | Inertia : high · Orientation : East | Fs : 0.25 |

| Climatic data | | | | Internal gains | | | Pconv: | (Wh) | (gr/h) | Ventilation | | | | (vol/h) | |
|---|---|---|---|---|---|---|---|---|---|---|---|---|---|---|---|
| Dept | idmer (km) | alt (m) | Lat | | from (h) | to (h) | 0.5 | sens. | lat | | from (h) | to (h) | | Air flow | |
| 78 | 400 | 0 | 48.8 | occ : | 8 | 18 | vacc | 0 | 0 | occ : | 8 | 18 | vacc | 0 | Teexlim |
| | | | | Stop days /week : | | 2 | occ | 150 | 110 | Stop days /week : | | 2 | occ | 0 | occ |
| System | Effnhi | Rexch | EffnhD | Pch | Rch | Tadp | Bp | Effri | Fanrefaf | Fanpratio | Fanrefeff | Dtihc | Wehumlim | | 16 |
| | 0.8 | 0.7 | 0.8 | 2000 | 1 | 12 | 1 | 2 | 243 | 0.8 | 0.4 | 2 | 15 | | vacc |
| Running summer | from | 7 | to (h) | 18 | stop | 2 | Running winter | from | 5 | to (h) | 18 | stop | 2 | | 10 |

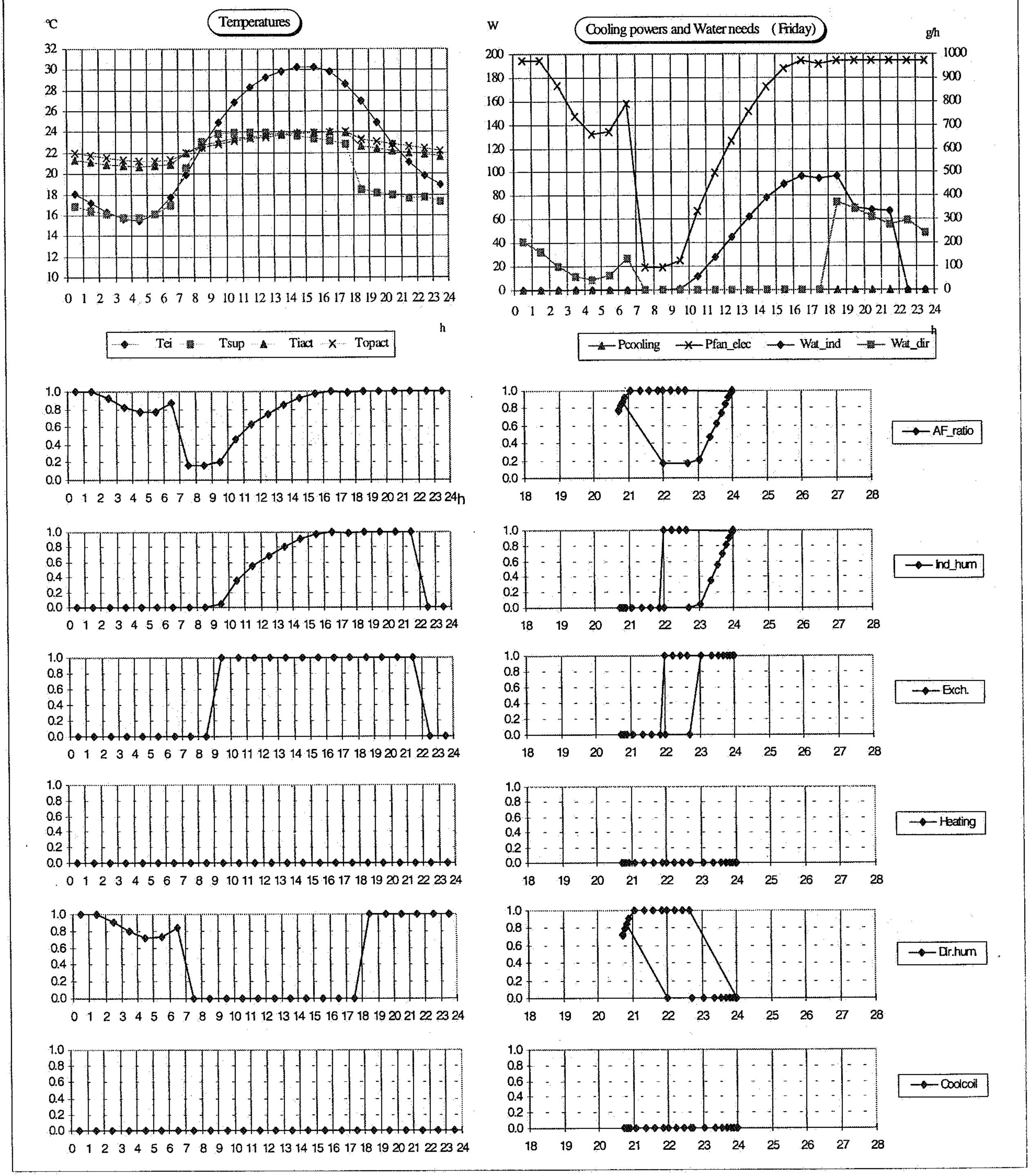


**figure 6 example of result for a reference warm day**

## 3. SIMPLIFIED DESIGN TOOLS

We choose to present basic results directly as indoor temperatures ,required coil cooling power and yearly energy and water needs for typical cases. The "worst" cases here taken into account are the worst possibles ones, considering that the use of evaporative and night cooling requires a minimum attention on the building design.

### *3.1.1 climatic area*

3 climatic areas : center of France (Trappes) ; south interland (Carpentras) and south near the Mediterranean coast (Nice).

### *3.1.2 building characteristics*

- **internal gains :** Occupants , equipment and lighting : 10 and 30 W/m² .

- **solar gains :** we define the ratio S Ab /Al with two reference values :0.05 ; 0.15 with S : window solar factor; Ab : window area, Al : room area

- **inertia :** low and high . Low means one ceiling or floor of high inertia; high means both ceiling and floor and side walls of high inertia.

- **orientation :** East and West.

### *3.1.3 system characteristics*

- **air flow :** We choose 4 air flows corresponding to 2, 4, 6, 8 a.c./h.and 6 systems :

| without cooling plant : | with cooling plant : |
|---|---|
| - no evaporative system ("night cooling" only),<br>- direct evaporative system,<br>- indirect evaporative system,<br>- direct + indirect evaporative system. | - without "night cooling" + cooling coil,<br>- indirect evaporative + cooling coil. |

For all systems, "night cooling" is used if of interest.

For each system, we have defined control matrixes for summer and for winter conditions, during occupancy and inoccupancy (24 control matrixes).

### *3.1.4 simplified tool*

Two sets of simulations were made for the three different sites (Trappes, Carpentras, Nice), using the equivalent RC dynamic model Comet developed at CSTB . The first set is related to sizing and dimensioning and is based on a reference warm day (figure 7). In this case we focus on indoor temperature and required cooling power if a cooling coil is used. The second set of runs were done for a complete typical year. Then, we focus on heating, cooling, fan electrical energy and water needs. About 2500 runs were performed , either on the typical day or on a complete reference year.

| | |
|---|---|
| (white) | Correspond to maximum operative temperature in occupancy during the reference warm day <=26°C |
| (light shading) | Correspond to maximum operative temperature in occupancy during the reference warm day >26°C and <30°C |
| (dark shading) | Correspond to maximum operative temperature in occupancy during the reference warm day >=30°C and < 33°C |
| (black) | Correspond to maximum operative temperature in occupancy during the reference warm day >=33°C |

## Trappes (Dept : 78)

Reference warm day

### Maximum operative temperature in occupancy

| Solar gains S*Aglaz/Aroom | | 0.05 | | | | | | | | 0.15 | | | | | | | | | | |
|---|---|---|---|---|---|---|---|---|---|---|---|---|---|---|---|---|---|---|---|---|
| Int. gain w/m² (8h to 18h) | | 10 | | | | 30 | | | | 10 | | | | 30 | | | | | | |
| Inertia | | High | | Low | | High | | Low | | High | | Low | | High | | Low | | | | |
| Orientation | | E | W | E | W | E | W | E | W | E | W | E | W | E | W | E | W | | | |
| Air flow | Evap.system | Without cooling plant | | | | | | | | | | | | | | | | min | Ave | max |
| 2 vol/h | none | 30 | 30 | 32 | | | | | | | | | | | | | | 30 | | |
| | direct | 26 | 26 | 28 | 29 | 30 | 30 | | | | | | | | | | | 26 | | |
| | indirect | 28 | 28 | 30 | 30 | 32 | 32 | | | | | | | | | | | 28 | | |
| | direct+indirect | 25 | 26 | 27 | 28 | 29 | 29 | 32 | | 32 | | | | | | | | 25 | 32 | |
| 4 vol/h | none | 28 | 28 | 31 | 31 | 31 | 31 | | | 32 | | | | | | | | 28 | | |
| | direct | 24 | 24 | 25 | 26 | 26 | 26 | 29 | 30 | 28 | 28 | 30 | | 30 | 31 | | | 24 | 29 | |
| | indirect | 25 | 26 | 27 | 28 | 28 | 28 | 31 | 32 | 30 | 31 | | | | | | | 25 | 31 | |
| | direct+indirect | 24 | 25 | 25 | 26 | 26 | 26 | 28 | 29 | 27 | 28 | 29 | 32 | 29 | 30 | 32 | | 24 | 28 | |
| 6 vol/h | none | 27 | 28 | 30 | 31 | 30 | 30 | | | 31 | 32 | | | | | | | 27 | 32 | |
| | direct | 23 | 24 | 24 | 25 | 25 | 25 | 27 | 28 | 26 | 26 | 28 | 30 | 28 | 28 | 31 | | 23 | 27 | |
| | indirect | 24 | 25 | 26 | 27 | 26 | 27 | 29 | 30 | 28 | 28 | 30 | | 30 | 31 | | | 24 | 29 | |
| | direct+indirect | 24 | 24 | 25 | 25 | 25 | 25 | 26 | 27 | 25 | 26 | 27 | 30 | 27 | 28 | 29 | 32 | 24 | 27 | 32 |
| 8 vol/h | none | 27 | 27 | 30 | 30 | 29 | 30 | 32 | | 30 | 31 | | | 32 | 32 | | | 27 | 32 | |
| | direct | 23 | 23 | 24 | 25 | 24 | 24 | 26 | 27 | 25 | 26 | 27 | 29 | 26 | 27 | 29 | 31 | 23 | 26 | 31 |
| | indirect | 24 | 24 | 26 | 27 | 26 | 26 | 28 | 29 | 27 | 27 | 29 | 31 | 28 | 29 | 31 | | 24 | 28 | |
| | direct+indirect | 24 | 24 | 25 | 25 | 25 | 25 | 25 | 26 | 25 | 26 | 26 | 28 | 26 | 27 | 28 | 30 | 24 | 26 | 30 |
| | min | 23 | 23 | 24 | 25 | 24 | 24 | 25 | 26 | 25 | 26 | 26 | 28 | 26 | 27 | 28 | 30 | 23 | | |
| | Ave | 26 | 26 | 27 | 28 | 28 | 28 | 30 | 31 | 29 | 30 | 32 | | 32 | 32 | | | | 30 | |
| | max | 30 | 30 | 32 | | | | | | | | | | | | | | | | |
| Air flow | Evap.system | With cooling plant | | | | | | | | | | | | | | | | min | Ave | max |
| 2 vol/h | ind.+Cool. plant | 24 | 25 | 25 | 27 | 27 | 27 | 30 | 31 | 30 | 30 | 32 | | | | | | 24 | 30 | |
| | cool.plant only | 25 | 25 | 26 | 27 | 27 | 28 | 31 | 32 | 30 | 31 | | | | | | | 25 | 31 | |
| 4 vol/h | ind.+Cool. plant | 24 | 24 | 24 | 25 | 24 | 25 | 26 | 27 | 25 | 26 | 27 | 30 | 27 | 28 | 30 | | 24 | 27 | |
| | cool.plant only | 24 | 24 | 24 | 25 | 25 | 25 | 27 | 28 | 26 | 27 | 29 | 31 | 28 | 28 | 31 | | 24 | 27 | |
| 6 vol/h | ind.+Cool. plant | 24 | 24 | 24 | 25 | 24 | 24 | 25 | 25 | 25 | 25 | 26 | 28 | 25 | 26 | 27 | 30 | 24 | 25 | 30 |
| | cool.plant only | 24 | 24 | 24 | 25 | 24 | 25 | 25 | 26 | 25 | 26 | 27 | 29 | 26 | 27 | 29 | 31 | 24 | 26 | 31 |
| 8 vol/h | ind.+Cool. plant | 24 | 24 | 24 | 24 | 24 | 24 | 24 | 25 | 24 | 25 | 25 | 27 | 25 | 25 | 26 | 28 | 24 | 25 | 28 |
| | cool.plant only | 24 | 24 | 24 | 25 | 24 | 25 | 25 | 25 | 25 | 25 | 26 | 27 | 25 | 26 | 27 | 29 | 24 | 25 | 29 |
| | min | 24 | 24 | 24 | 24 | 24 | 24 | 24 | 25 | 24 | 25 | 25 | 27 | 25 | 25 | 26 | 28 | 24 | | |
| | Ave | 24 | 24 | 25 | 25 | 25 | 25 | 26 | 27 | 26 | 27 | 28 | 30 | 28 | 29 | 31 | | | 27 | |
| | max | 25 | 25 | 26 | 27 | 27 | 28 | 31 | 32 | 30 | 31 | | | | | | | | | |

### Maximum cooling power (W/m2)

| Solar gains S*Aglaz/Aroom | | 0.05 | | | | | | | | 0.15 | | | | | | | | | | |
|---|---|---|---|---|---|---|---|---|---|---|---|---|---|---|---|---|---|---|---|---|
| Int. gain w/m² (8h to 18h) | | 10 | | | | 30 | | | | 10 | | | | 30 | | | | | | |
| Inertia | | High | | Low | | High | | Low | | High | | Low | | High | | Low | | | | |
| Orientation | | E | W | E | W | E | W | E | W | E | W | E | W | E | W | E | W | | | |
| Air flow | Evap.system | | | | | | | | | | | | | | | | | min | Ave | max |
| 2 vol/h | ind.+Cool. plant | 13 | 13 | 14 | 14 | 14 | 14 | 15 | 15 | 15 | 15 | 16 | | | | | | 13 | 16 | |
| | cool.plant only | 18 | 18 | 19 | 21 | 21 | 21 | 23 | 23 | 23 | 23 | | | | | | | 18 | 22 | |
| 4 vol/h | ind.+Cool. plant | 12 | 15 | 18 | 26 | 26 | 26 | 27 | 27 | 26 | 26 | 28 | 29 | 28 | 28 | 30 | | 12 | 25 | |
| | cool.plant only | 27 | 31 | 33 | 36 | 37 | 39 | 40 | 43 | 39 | 39 | 44 | 46 | 43 | 43 | 47 | | 27 | 39 | |
| 6 vol/h | ind.+Cool. plant | 10 | 12 | 17 | 27 | 24 | 28 | 34 | 39 | 29 | 38 | 39 | 40 | 39 | 39 | 41 | 43 | 10 | 31 | 43 |
| | cool.plant only | 30 | 35 | 36 | 48 | 49 | 53 | 54 | 56 | 54 | 54 | 58 | 64 | 58 | 58 | 67 | 69 | 30 | 53 | 69 |
| 8 vol/h | ind.+Cool. plant | 9 | 11 | 17 | 26 | 23 | 27 | 33 | 44 | 28 | 37 | 41 | 52 | 42 | 50 | 52 | 54 | 9 | 34 | 54 |
| | cool.plant only | 34 | 38 | 39 | 52 | 53 | 57 | 61 | 71 | 59 | 70 | 71 | 77 | 72 | 73 | 78 | 86 | 34 | 62 | 86 |
| | min | 9 | 11 | 14 | 14 | 14 | 14 | 15 | 15 | 15 | 15 | 16 | 17 | 17 | 17 | 18 | 19 | 9 | | |
| | Ave | 19 | 22 | 24 | 31 | 31 | 33 | 36 | 40 | 34 | 38 | 40 | 43 | 40 | 41 | 44 | | | 35 | |
| | max | 34 | 38 | 39 | 52 | 53 | 57 | 61 | 71 | 59 | 70 | | | | | | | | | |

**figure 7 - example of simplified tool sheet for evaporative cooling system :**
The maximum operative temperature, and the required cooling power (if use of a cooling coal) can be checked according to the building and system characteristics

## 4. CONCLUSION

The results of the works are as follows :

1. a simplified reference calculation method enabling to calculate the indoor temperature profile for a reference warm day according to a zoning of metropolitan French territory. Apart from the buildings characteristics, a focusing point is the description and the control of the air handling plant. This tool is based on an equivalent RC model and gives also the energy and water needs for a reference warm day and all over the year. A particular point of interest is the electrical needs for fans, as they can compensate in some case the reduction of energy required for cooling.

2. a predesign guidance document, which makes it possible for the most common cases to define the required buildings and air unit characteristics to achieve a given level of comfort by use of charts and tables and to evaluate the additional required cooling power if needed as well as the yearly water and energy needs.

Used primarily for new buildings, these tools will be also a help for retrofitting .

## 5. REFERENCES


Review of low energy cooling technologies IEA Annex 28 - substask 1 report - Natural Resources Canada / CANMET

Dominique Marchio, Jean-Robert Millet, Olivier Morisot, "simple modelling for energy consumption estimation in air conditioned buildings" CLIMA 2000 BRUSSELS 1997

Jean-Robert Millet "COMETRES : a predesign tool for the improvement of summer comfort" First international conference "Building and the environment" Garston, U.K. 16-20 May 1994


## 6. ACKNOWLEDGEMENTS


The study was sponsored by Gaz de France and Ademe (Agence de l'Environnement et de la Maîtrise de l'Energie).

# VENTILATION AND COOLING
# 18TH AIVC CONFERENCE, ATHENS, GREECE
# 23-26 SEPTEMBER, 1997

**Title:** **Increased Ventilation Airflow Rate: Night and Day Cooling of an Office Building**


**Author(s):** **Christophe Martin**

Metingen van nachtkoeling.
op een gebouw

**Affiliation:** **CETIAT, 27-29 Bd.du 11 Novembre 1918, BP 2042, 69603 Villeurbanne Cedex, France**

**INCREASED VENTILATION AIRFLOW RATE :
NIGHT AND DAY COOLING OF AN OFFICE BUILDING**

*by Christophe MARTIN - CETIAT*


## Abstract

This study aims at evaluating the energetical benefits of increased ventilation airflow rate to cool buildings. Different operating modes have been tested :
- increased ventilation airflow rate during the night to take advantage of the building thermal capacity to cool it,
- increased ventilation airflow rate during night and day when the outside air temperature is lower than the inside air temperature.

This three-year study (from 1994 to 1996) has been carried out in 4 steps :
1) bibliographic study to learn results of studies already led in this field;
2) experimental phase on a real building in La Rochelle (France);
3) experimental phase on a real building in Chambery (France);
4) parametric study by numerical simulation.

This paper concerns only the 3rd step of the global study : the experimental phase in Chambery. This experimental study consisted in implementing different working scenarios of increased ventilation airflow rate (up to 10 vol/h) during night and day on a office building. The experiments were carried out during summers 1995 and 1996 and gave us useful information to optimize increased ventilation airflow rate working scenarios, such as :
- solar impact on efficiency,
- working periods in night and day,
- control based on difference between outside air temperature and inside air temperature,
- potential energy savings with regard to energy consumption of the fans.

## 1 - Experiments

The experiments took place on an office building in Chambery which is located in the south-east part of France, close to the Alps and submitted to a continental outdoor climate. Preliminary experiments were carried out during summer 1995 to assess the performance and to adjust the operating parameters of the system. Based on these results, final experiments were carried out during summer 1996.

floor
ceiling ?
internal walls

### 1.1 - The building

The building, built in 1992, seems to have a low thermal inertia. The walls are made of metallic beams and siding with fiberglass thermal insulation. The experimental part consisted of the western part of the first floor, constituted of 7 offices : 3 facing north and 4 facing south, as shown in figure 1.

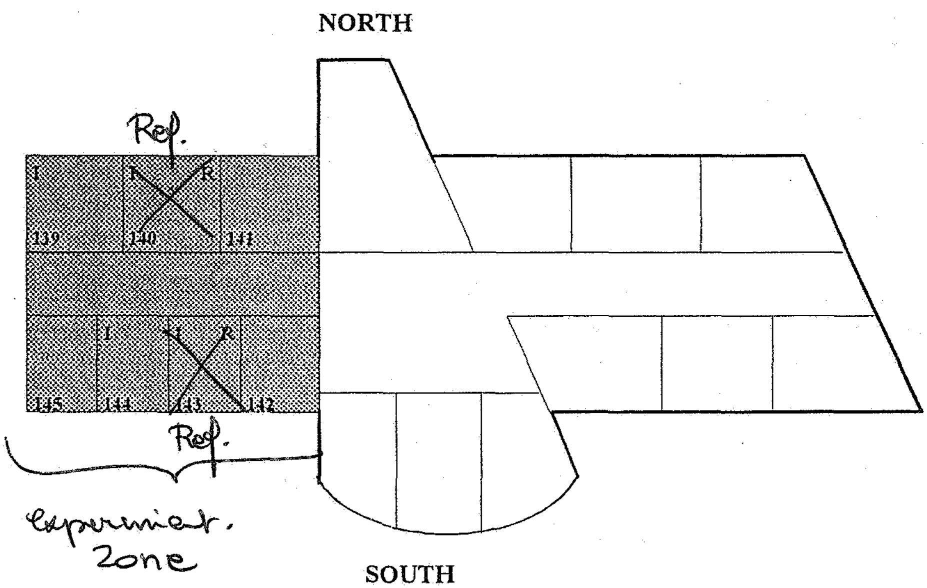


*Figure 1 : Experimental building*

### 1.2 - The ventilation systems

The experimental building is equipped with two different ventilation systems : one exhaust ventilation system for sanitary fresh air (0,5 vol/h) and ~~one exhaust~~ and supply ventilation system which was modified to reach airflow rates of about 6 to 10 vol/h. The detailed airflow rates reached in each office are presented in table 1.

*Table 1 : Airflow rates in the offices*

| N° office | Floor area [m²] | Room volume [m³] | Sanitary exhaust ventilation system [m³/h] | Increased supply airflow rate [m³/h] | Increased exhaust airflow rate [m³/h] | Total exhaust airflow rate [m³/h] | [vol/h] |
|---|---|---|---|---|---|---|---|
| 139 | 23,35 | 65,38 | 33 | 280 | 360 | 393 | 6,0 |
| 140 | 23,65 | 66,22 | 33 | 0 | 0 | 33 | 0,5 |
| 141 | 22,80 | 63,84 | 32 | 355 | 390 | 422 | 6,6 |
| 142 | 16,80 | 47,04 | 24 | 450 | 480 | 504 | 10,7 |
| 143 | 17,65 | 49,42 | 25 | 0 | 0 | 25 | 0,5 |
| 144 | 17,65 | 49,42 | 25 | 415 | 440 | 465 | 9,4 |
| 145 | 17,35 | 48,58 | 24 | 425 | 310 | 334 | 6,9 |

The offices n° 140 (north) and 143 (south) are not connected to the increased ventilation airflow rate system and were considered as reference to assess the effects of increased ventilation airflow rate.

The sanitary exhaust ventilation system works permanently when the increased ventilation airflow rate system is controlled by a BMS (Building Management System).

## 1.3 - The instrumentation

Four offices were instrumented : the two reference offices (140 and 143) and two offices (139 north and 144 south) with increased ventilation airflow rate. Three temperature probes were installed in the middle of each office at 1.00, 1.50 and 2.00 m from the floor.

One air temperature probe was installed in the inlet duct of the air handling unit (used to generate the increased exhaust and supply airflow rate) and one in the outlet duct.

A measurement station was already available on the roof of the building, for recording the outdoor conditions (air temperature and solar intensity).

The BMS was equipped with probes and recorded the outdoor air temperature (with a probe on the north side of the building), the minimum inside air temperature (with one air temperature probe in each office), the supply air temperature and the operating status of the increased ventilation airflow rate system.

## 1.4 - The scenarios

Different scenarios were carried out to assess the potential energy savings of such a system. ~~Working limits~~ were selected to manage the increased airflow rate ventilation system. It could only work when the difference between the minimum inside air temperature and the outdoor air temperature was greater than 2 °C.

The three different experiments carried out during summer 1996 are described in table 2.

*Table 2 : Experimental periods carried out during summer 1996*

| Period | Scenario |
|---|---|
| August 14 to 18 | No increased ventilation airflow rate : reference period |
| August 19 to 26 | Increased ventilation airflow rate when it is allowed without time ~~limit~~ restriction $\Delta(T_i - T_e) > 2°C$ |
| September 1 to 9 | Increased ventilation airflow rate when it is allowed only during the night from 8 pm to 8 am |

During all these different periods, the sanitary exhaust ventilation system was working permanently.

**2 - The results**

The records showed that there were no significant differences between the three air temperature probes of an office or between the different outdoor air temperature probes.

2.1 - Period without increased ventilation airflow rate

During this period, it seemed obvious that the different offices had a different behaviour : the air temperatures in the offices facing north were lower than those facing south. Even on the same side, offices 143 and 144 showed differences because of different exposure to sun : office 143 could benefit from the shadow of the projecting middle part of the building. Nevertheless, the evolution of these differences seemed to be similar from one day to the other and it was decided to define an average evolution on 24 hours as shown in figure 2. It was necessary to take into account these differences to understand correctly the effects of increased ventilation airflow rate during the other periods.

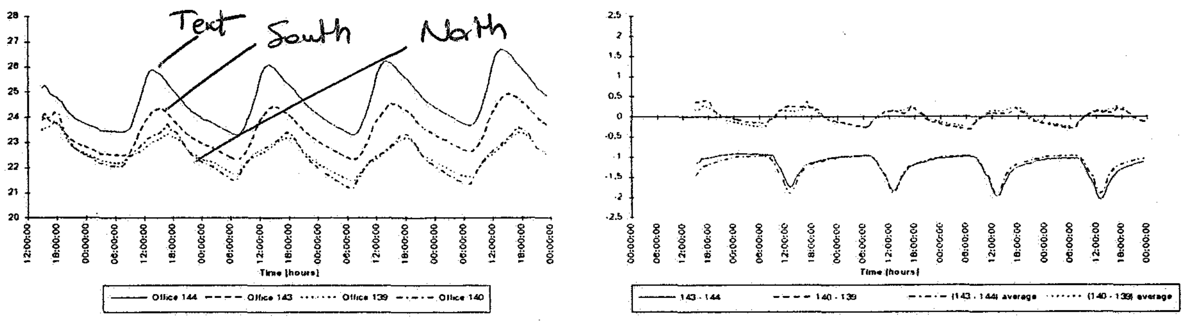


*Figure 2 : Inside air temperature evolution during the period without increased ventilation airflow rate*

2.2 - Period with increased ventilation airflow rate during the night

During this period, increased ventilation airflow rate system worked only during the night from 8 pm to 8 am when the difference between the outdoor air temperature and the minimum inside air temperature was greater than 2 °C.

To analyse the results of the experiments, the difference in inside air temperatures between the ventilated offices with high airflow rates (139 and 144) and the reference offices (140 and

143) had to be taken into account. The normal air temperature difference between the ventilated offices and the reference offices noticed during the period without increased ventilation airflow rate had to be substracted. Finally, an average evolution on 24 hours was necessary to reach a conclusion on general tendancis. Figures 3 and 4 show the different steps of this procedure.

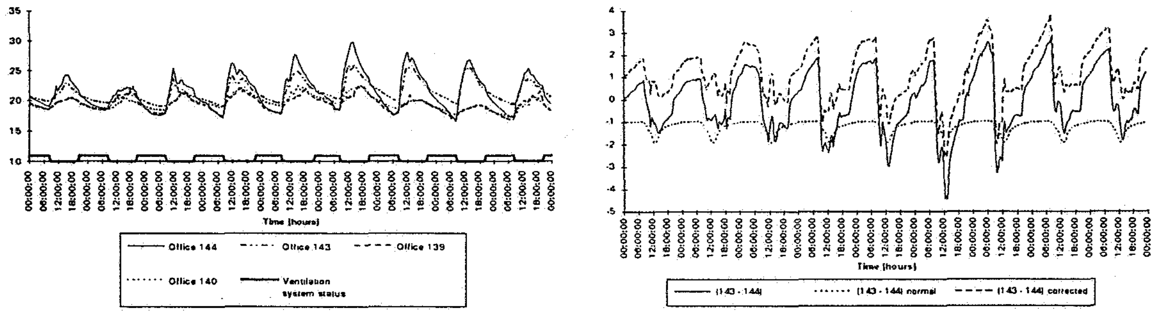


***Figure 3 : Inside air temperature evolution during the period with increased ventilation air flow rate during the night***

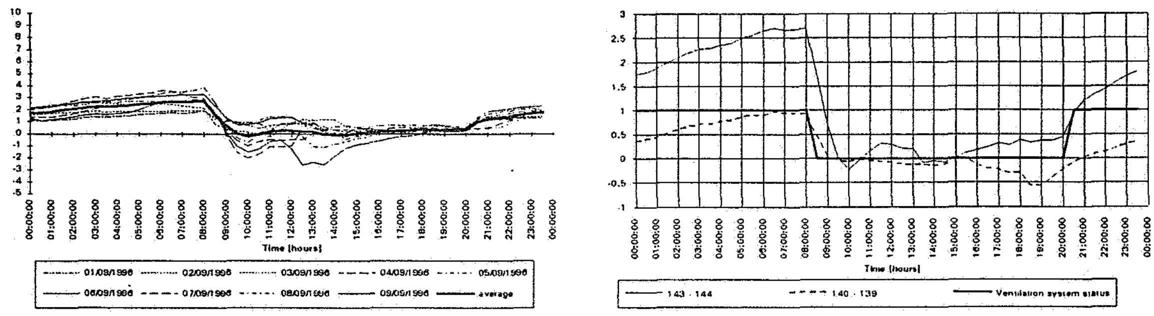


***Figure 4 : Average inside air temperature evolution during the period with increased ventilation air flow rate during the night***

Figure 4 shows that the inside air temperature difference between the ventilated offices and the reference offices increases when the increased ventilation airflow rate system is working, but as soon as it stops, the inside air temperature difference between the offices decreases very quickly and reaches zero in less than one hour. This can be explained by the very low thermal inertia of the building.

For this case, it appears that increased ventilation airflow rate during the night is not profitable.

2.3 - Period with increased ventilation airflow rate without time limit

During this period, the increased ventilation airflow rate system worked without any time restriction when the difference between the outdoor air temperature and the minimum inside air temperature was greater than 2 °C.

In order to analyse the results, a calculation procedure similar to that used in section 2.2 was adopted. Figure 5 shows directly the average inside temperature difference between the ventilated offices and the reference offices on a 24-hour period.

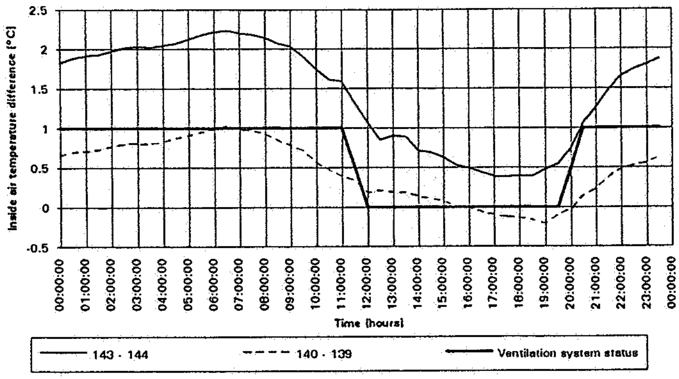


*Figure 5 : Average inside air temperature evolution during the period with increased ventilation air flow rate without time restriction*

With this scenario, the increased ventilation airflow rate system worked until 12.00 and the inside air temperature could be lowered by 2 °C in the southern offices and by 1 °C in the northern offices. Moreover, previous results showed that it was not necessary to ventilate the building all night and it could be possible to optimize the working scheme to start the ventilation system only 4 hours before the occupied period.

To evaluate the energy savings potentiality, an index was defined as follows :

$$I_{ji} = \int_{8h00}^{20h00} (T_{ref} - T_i)dt$$

Iji : temperature gain index for office n° i
Ti : inside air temperature of the office n° i
Tref : inside air temperature of the reference office associated to the office n° i

Figure 6 shows the evolution of Iji with the solar intensity and the outdoor air temperature.

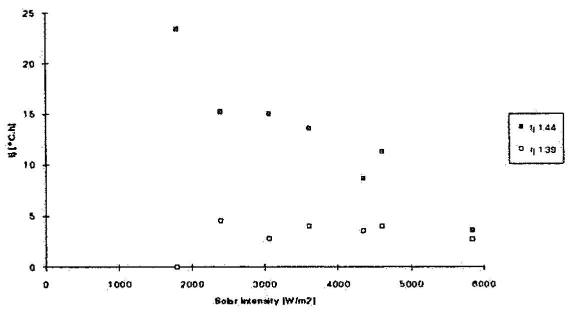

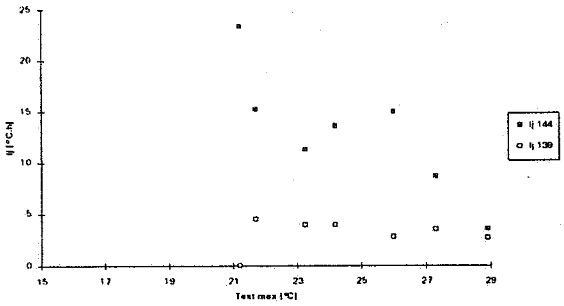

*Figure 6 : Evolution of Ij with solar intensity and maximum outdoor air temperature*

It appears that the nothern offices are less sensitive to the outdoor climate conditions. For the southern offices, the lower the outdoor air temperature and the solar intensity are, the higher the temperature gain index is.

## 2.4 - Influence of outdoor temperature

To optimize the working scenario of such a system, it was necessary to take into account the evolution of the inside air temperature of both the ventilated offices and the reference offices against outdoor air temperature.

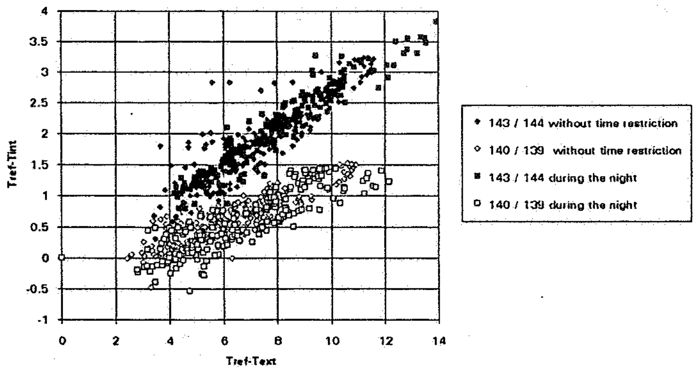


***Figure 7 : Inside air temperature difference between reference offices and ventilated offices against air temperature difference between inside air temperature of reference offices and outdoor air temperature***

Figure 7 shows that the tendance is the same for the northern offices and for the southern offices but the effect is much more important for the southern offices. For both cases, it appears not profitable to start the high ventilation airflow rate system for an air temperature difference between inside air temperature and outdoor air temperature lower than 4°C.

A theoretical coefficient of performance (COP) was defined as :

$$COP = \frac{\int \dot{M} C_p (T_r - T_s) dt}{2 \times P_{abs}} \quad \text{with } P_{abs} = \frac{Q_v . \Delta P}{\eta}$$

$\dot{M}$ : mass airflow rate,
$C_p$ : specific heat capacity of air,
$T_r$ : exhaust air temperature,
$T_s$ : supply air temperature,
$P_{abs}$ : electrical power of the fans (hypothesis exhaust = supply),
$Q_v$ : volume airflow rate ($\dot{M} = Q_v . \rho$ , with $\rho$ : specific mass of air),
$\Delta P$ : pressure losses,
$\eta$ : efficiency of the fan.

Figure 8 shows the evolution of the COP with realistic values for the parameters : $Q_v$=1980 $m^3/h$, $\Delta P$=300 Pa and $\eta$=30 %.

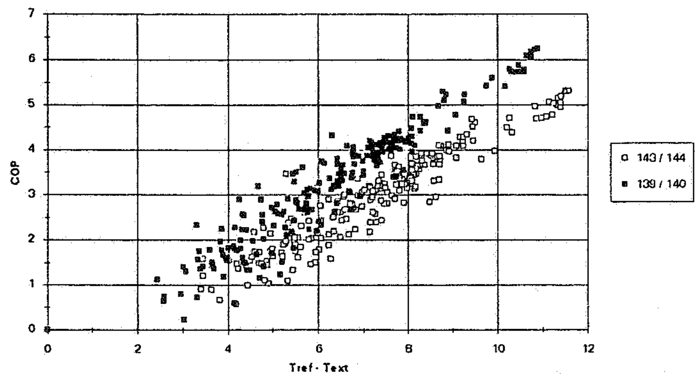


***Figure 8 : COP evolution with air temperature difference between inside air temperature of the reference offices and outdoor air temperature***

A profitable system should have a COP greater than 1. Figure 8 shows that the difference between the inside air temperature of the reference offices and the outdoor air temperature must be greater than 4 °C, which is in accordance with the previous conclusion. Obviously, with a simple exhaust system, the COP of the system would be multiplied by two (only one fan electrical consumption).

### 3 - Conclusion

This following conclusions can be drawn from the experiments :
- the northern and southern offices present the same tendancis but the southern offices seem to be more sensitive to the outdoor conditions;
- since the thermal inertia of the experimental building is low, it is not useful to let the system work all night, but just a few hours before the occupied period;
- the efficiency of this system decreases when the solar intensity and the outdoor temperature increase. It is then important to take care of sun protection on the southern wall of the building;
- to be profitable, the system has to work only when the air temperature difference between the indoor and outdoor is of 4 °C at least;
- to be profitable, the increased ventilation airflow rate system has to work without time restriction during day-time. Such an operative scheme allows it to work until 11.00 am and to reduce the inside air temperature by 2 °C in the southern offices and by 1 °C in the northern offices;

As a conclusion, in this case, this increased ventilation airflow rate system seems to be interesting in term of energy savings in mid-season (spring and autumn), when the solar intensity is not to high and when the outdoor air temperature is reasonably low.

### Acknowledgements

This study was coordinated by the French Technical Centre of Heating and Air Handling Industries (CETIAT) and led in collaboration with the University of La Rochelle (LEPTAB) and the University of Savoie (LGCH), with the participation of the french manufacturers ABB VIM and CIAT. It was partially financed by the Agence de l'Environnement et de la Maîtrise de l'Energie (ADEME), Région Rhône-Alpes and Gaz de France (GDF).

**VENTILATION AND COOLING**
**18TH AIVC CONFERENCE, ATHENS, GREECE**
**23-26 SEPTEMBER, 1997**

**Title:** **Dehumidification by Alternative Cooling Systems**

**Author(s):** **Prof.Dr.Ing.Fritz Steimle, Dipl.Ing. Jurgen Roeben**

**Affiliation:** **Institute of Applied Thermodynamics and Air Conditioning,**
**University of Essen, Universitatsstrasse 15, 45141 Essen, Germany**

# 18th AIVC Conference

# VENTILATION AND COOLING

# Call for Papers

**Venue: Greece,**

**Tuesday 23rd to Friday 26th September 1997**

**Proposed Paper for submission by February17th, 1997**

Title ~~Dehumidification by alternative cooling systems~~


Author ~~Prof. Dr.-Ing. Fritz Steimle, Dipl.-Ing. Jürgen Röben~~

Address (including country) ~~Institute of Applied Thermodynamics and Air Conditioning~~

~~University of Essen~~

~~Universitätsstraße 15, 45141 Essen, Germany~~

Tel: 0201-183-2600 Fax: 0201-183-2584


**Abstract**

(Please type in space below and mail to AIVC or fax: +44 (0)1203 416306)

**Dehumidification by alternative cooling systems**


The traditional way to dehumidify the outdoor air in a heating, ventilating and air conditioning (HVAC) system is by cooling down the air temperature below the dew point. For this process a refrigeration system is necessary to realise these low temperatures. Nowadays everybody knows the disadvantages by using refrigeration systems. An alternative method to dehumidify the air is by separating the process of dehumidification and cooling. There are different ways to get low supply air temperatures for cooling the indoor spaces. It is possible for example to use well water, an evaporative cooling system or of course a refrigeration system with relatively high evaporation temperature. This cooling components are well known and already in practice so that the main interest of this paper is the dehumidification process.

The paper will give a general view of the adsorptive and absorptive dehumidification components. Then a new dehumidifier which use a liquid dessicant will be described. A small prototype has been tested in an experimental plant in the laboratory of the Institute of Applied Thermodynamics and Air Conditioning in Essen. The design of the dehumidifier and the first results of the measurements will be presented.


[ ] Please check box if poster presentation preferred

# VENTILATION AND COOLING
## 18TH ANNUAL AIVC CONFERENCE
## ATHENS, GREECE, 23-26 SEPTEMBER 1997


**Title**: Applying Night Ventilation Techniques in Office Buildings


**Authors**: V. Geros[1,2], M. Santamouris[1] and G. Guarraccino[2]

**Affiliation**:
1. Group Building Environmental Studies, Department of Applied Physics, University of Athens, Building PHYS-V, Athens 15784, Greece.
2. LASH-ENTPE, Rue Maurice Audin 69120, Vaulx en Velin, France.

## Applying Night Ventilation Techniques in Office Buildings

V. Geros[1,2], M. Santamouris[1] and G. Guarraccino[2]

1. Group Building Environmental Studies, Department of Applied Physics, University of Athens, Building PHYS-V, Athens 15784, Greece.
2. LASH-ENTPE, Rue Maurice Audin 69120, Vaulx en Velin, France.

### 1. Synopsis

In this paper the potential of night ventilation techniques is investigated. Extended real scale measurements have been performed, in three buildings, under free floating and air conditioned operation. Two of the buildings have been studied by using a theoretical model developed in TRNSYS[1] software. Simulation results have been validated by using the measured data. Specific studies concerning the indoor air temperature and the cooling load of the buildings have been carried out in order to identify the influence of night ventilation techniques on the buildings thermal performance. A sensitivity analysis, for various air flow rates during night ventilation, have been performed for one of the studied buildings. The impact of night ventilation on the cooling load (for A/C operation) and indoor temperature (for free floating operation) is studied as well. A significant impact of night ventilation in buildings of high thermal mass is found.

### 2. Introduction.

Night ventilation is one of the most efficient passive cooling techniques. During summer, night ventilation provides cooling by using the outdoor air to carry away the heat from the building. The efficiency of night ventilation is strongly related with two parameters. The relative difference between the indoor and outdoor temperature, and the rate supply of the fresh air. The lower the outdoor temperature and the higher the fresh air supply, the higher is the effectiveness. Thermal mass of the building as well as the building's interior planning determine the usefulness of night ventilation.

To investigate the cooling potential of night ventilation techniques, extended measurements have been performed in three office buildings, during the summer of 1995 and 1996. In particular, the following three buildings, presenting different characteristics, were studied :

- Office building "Meletitiki Ltd. A.N. Tombazis and Associates" (summer of 1995 and 1996).
- Office located in "University of Athens, Department of Applied Physiscs" (summer of 1996).
- Office located in "National Observatory of Athens" (summer of 1996).

Continuous measurements of the indoor temperature as well as of the air flow rates during the application of night ventilation have been carried out. In the last two buildings the indoor air temperature of the adjusted spaces was also measured.

### 3. Description of the Studied Buildings and Measurement System.

4 "Meletitiki Ltd" is mainly composed by seven zones as shown in Figure 1, without internal partitions as the building is a unique volume construction. It has a heavy structure and it is ventilated during the night by mechanical and natural means. It is also thermostatically

controlled and cooled by air to air heat pumps. The design air flow rate during night is close to 26 air changes per hour.
Various operational schedules, have been studied both experimentally and theoretically :

- Free floating conditions during day and night without applying night ventilation techniques.
- Thermostatically controlled conditions during the day period (operation of the air conditioning system), without any use of night ventilation.
- Night ventilation followed by a free floating operation during the day period.
- Night ventilation followed by thermostatically controlled operation (operation of the air conditioning system), during the day period.

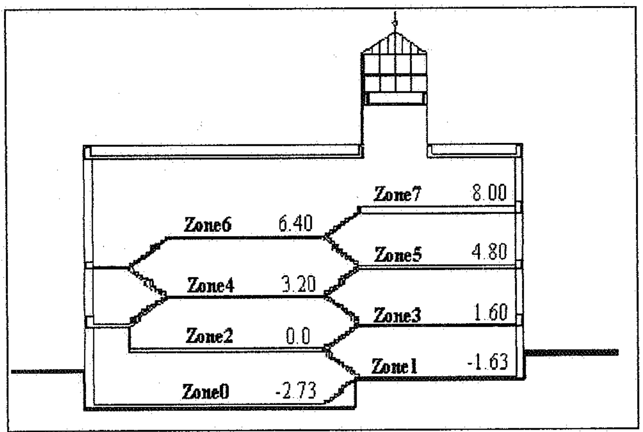

**Figure 1. Section of the "Meletitiki Ltd." building showing the different zones and levels.**

Night ventilation is achieved mainly through two exhaust fans located on the roof of Zones 6 and 7 over the two staircases. During the night period windows of zones 2, 3, 5 and 7 remain open. The capacity of each fan is close to 25000 $m^3$/hour. The estimated air flow when night ventilation applied was close to 25 air changes per hour. The mean air flow when fans where off and the windows open varied between 1 to 3 air changes per hour. In the summer of 1995 measurements have been carried out during the summer holidays (July 26th to August 11th). The indoor air temperature was measured in the main zones of the building (zones 2, 4, 6 and 7). In total, indoor temperature was measured at eight different points of the building. Night ventilation has been used for hours between 10pm to 6am. Figure 2 gives the ambient and the average indoor temperature during the experimental period.

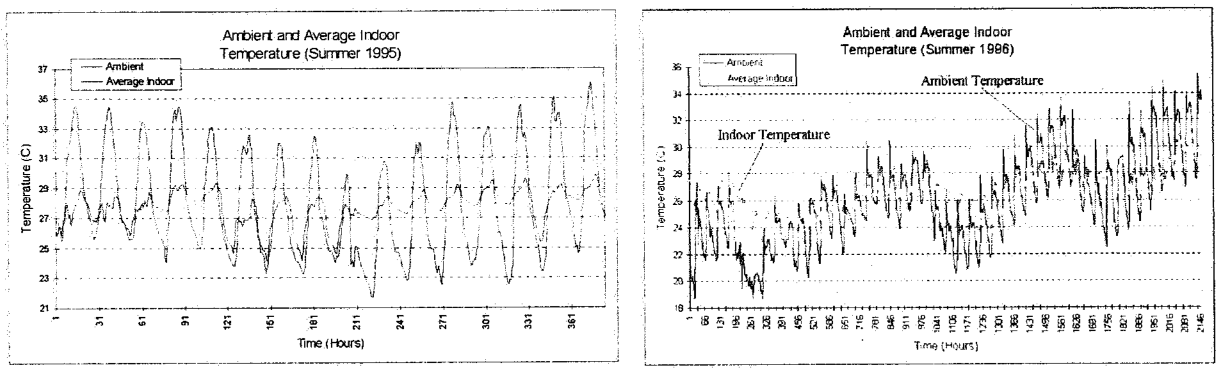

**Figure 2. Ambient and average indoor temperature in "Meletitiki Ltd." (Summer 1995 and 1996).**

During the summer of 1996 the indoor and ambient temperatures were measured from May 24th to July 8th. Indoor air temperature was measured in zones 2, 4, 6 and 7 of the building. Night ventilation has been applied between 10pm to 6am. Figure 2 gives the ambient and the average indoor temperature during the experimental period.

single side

B The office of the "University of Athens", is a room located on the third floor of a six storey building. The building has a light structure and the studied room is cooled by an air to air heat pump. In order to apply night ventilation techniques the two windows of the room were open during the night period. Both windows are located at the same side of the room and therefore the building is single side ventilated. Continuous tracer gas measurements, (constant injection), have been carried out so as to measure the air flow rate. The operational schedules followed for the "Meletitiki Ltd" building, have been also studied, in this building.

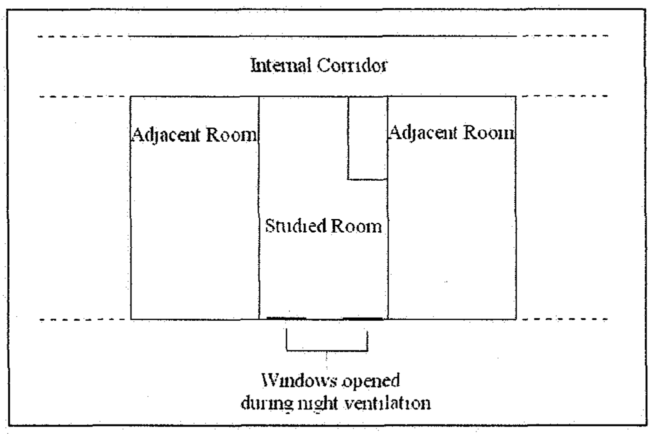


**Figure 3. Plan of the office located in "University of Athens" building, showing the location of the studied room.**

During summer of 1996 the indoor and ambient temperatures were measured from July 9th to July 23rd. Figure 4 gives the ambient and the indoor temperature during the experimental period of 1996 as well as the corresponding air changes per hour. Night ventilation techniques were applied during twelve nights of the above period.

light structure
single sided
↳ 6 to 12 ACH/h

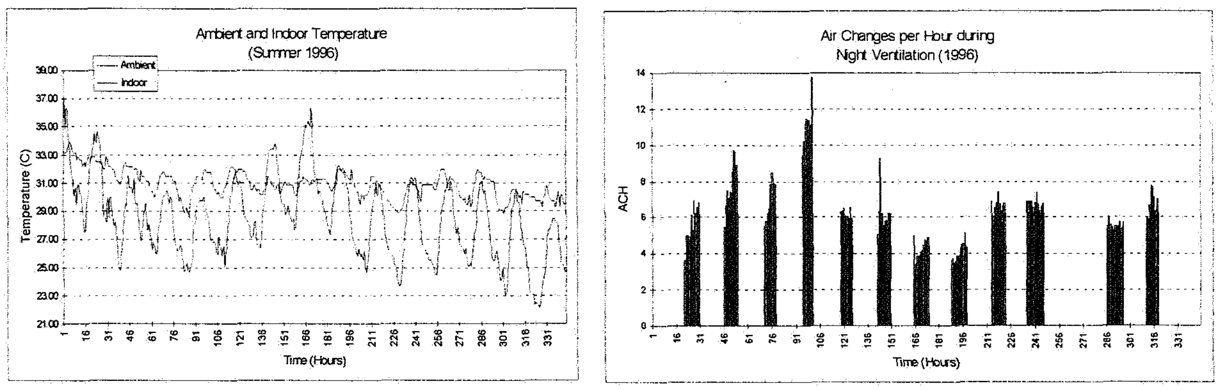


**Figure 4. Ambient temperature, indoor temperature and the corresponding air changes per hour during night ventilation in "University of Athens" (Summer 1996).**

C The office located in "National Observatory of Athens", is a room located on a one storey building. It is composed by one zone (Figure 5). It is a non air conditioned building having a very heavy structure. Night ventilation is applied and measured the same way as in the previous building.

werkt ok ; vermoeden dat by hoge airflows → geen contact tussen massa & lucht !!

ventilation effectiveness

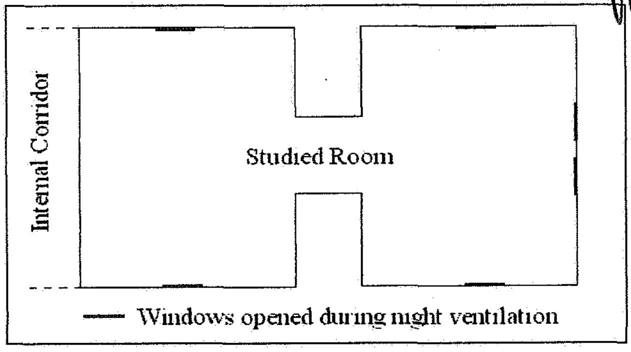


**Figure 5. Plan of the office located in "National Observatory of Athens" building, showing the location of the studied room.**

During the summer of 1996 the indoor and ambient temperatures (three temperature sensors) were measured from September 7th to September 18th. Figure 6 gives the ambient and the average indoor temperatures during the experimental period of 1996 as well as the corresponding air changes per hour achieved during the night. Night ventilation techniques were applied during twelve nights of the above period.

10 – 17 ACH/hr !

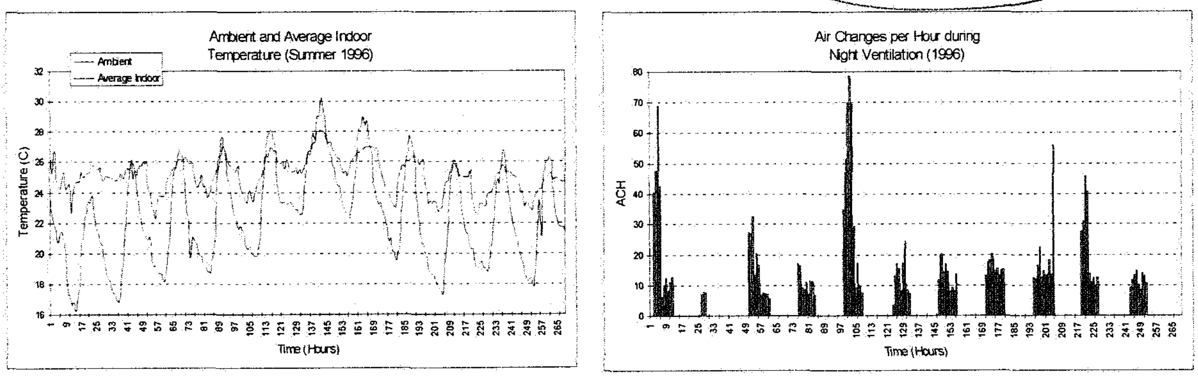


**Figure 6. Ambient temperature, indoor temperature and the corresponding air changes per hour during night ventilation in "National Observatory of Athens" (Summer 1996).**

## 4. Simulations and Theoretical Studies for the "Meletitiki Ltd" building (Summer 1995).

In order to evaluate the performance of night ventilation techniques and to analyze the experimental data, simulations of the thermal performance of the building have been performed using the TRNSYS software, during the measurement period of the summer of 1995. An additional air flow model based on the network approach has been coupled to TRNSYS to simulate air flow through internal and external openings under natural and forced air flow. The basics of the model as well as the validation procedure and results are described in (2). It should be noticed that during the above measurement period the building was under free floating conditions and without internal gains.

The simulated as well as the measured temperatures for zones 2, 4, 6 and 7 and for the whole measurement period, are given in Figures 7 and 8, respectively. As shown, the agreement between all simulated and measured values is satisfactory for all the possible operational conditions. The average difference between measured and simulated temperatures is close to 0.4 C. Thus it was assured that the developed theoretical model of the building represents accurately the thermal behavior of the building under all the studied conditions.

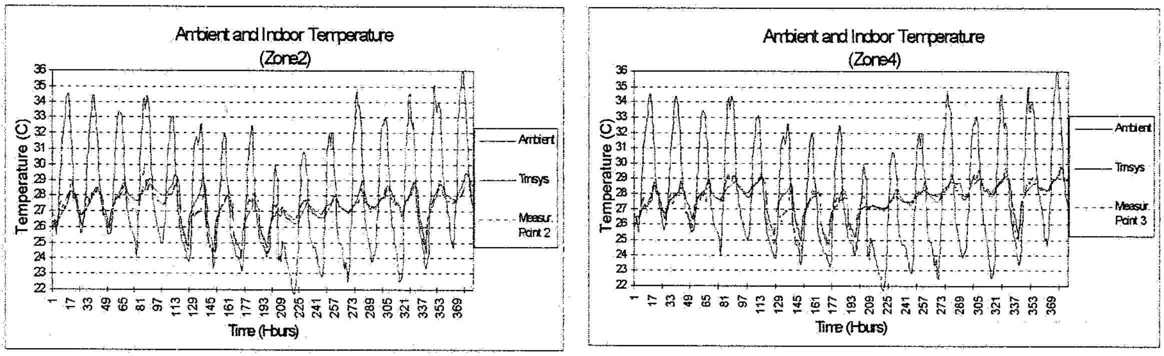


**Figure 7. Measured, simulated and ambient values of the air temperature, for Zones 2 and 4.**

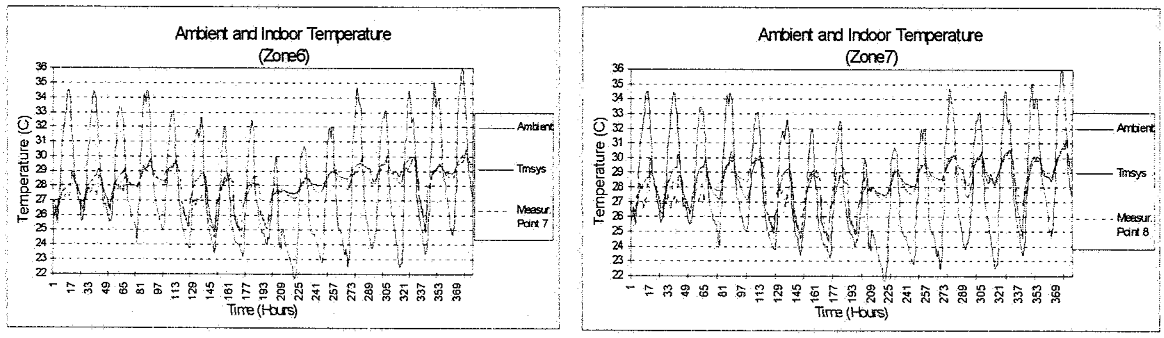


**Figure 8. Measured, simulated and ambient values of the air temperature, for Zone 6 and 7.**

In order to investigate the influence of night ventilation to indoor temperature, the building was simulated under the above conditions but without night ventilation. Figures 9 and 10 give the indoor air temperature with and without night ventilation for free floating operations. This comparative approach has clearly shown that under free floating conditions, application of night ventilation techniques contributes to decrease the next day peak indoor temperature of the building, up to 2.5 °C. It should be noticed that under air conditioning conditions the corresponding temperature decrease was close to 1 °C.

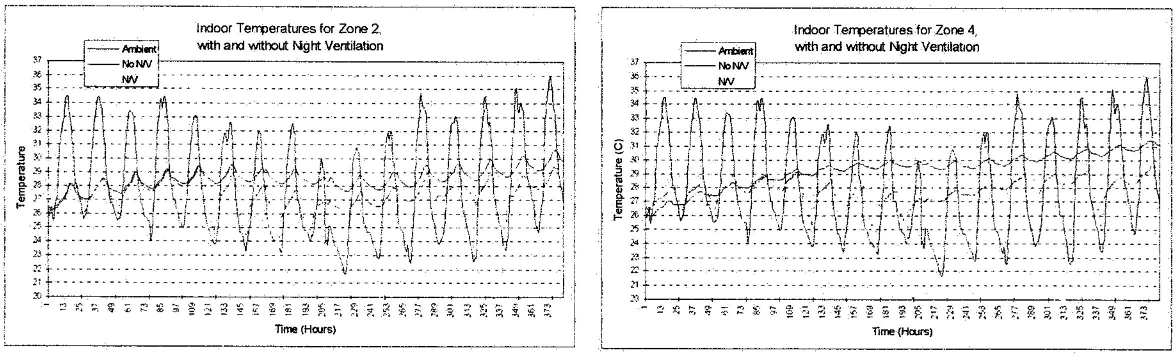


**Figure 9. Indoor temperature with and without night ventilation, for Zone 2 and 4.**

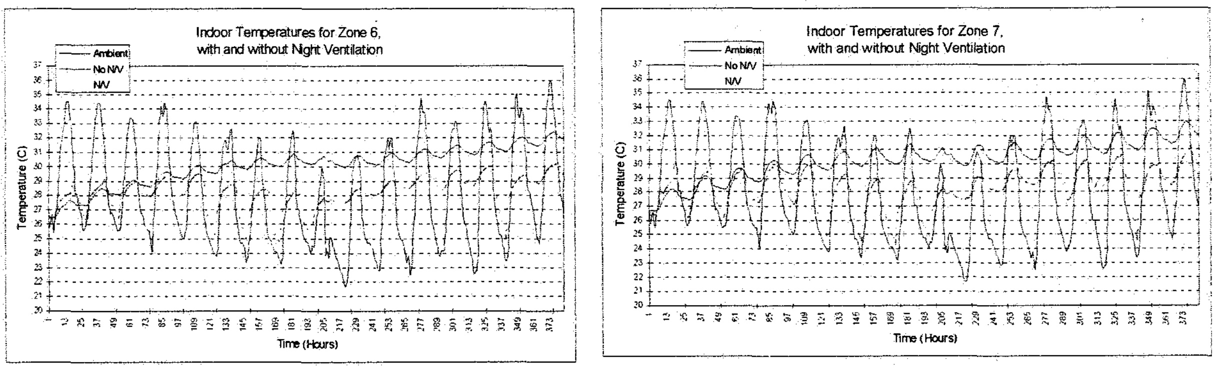


**Figure 10. Indoor temperature with and without night ventilation, for Zone 6 and 7.**

In order to investigate the cooling potential of night ventilation techniques and to examine the impact of the various possible air flow levels, simulations have been performed under air conditioning conditions with and without night ventilation. The previously mentioned validated TRNSYS model, is used. Simulations were carried out for a complete summer period, (May to September), and for 5, 10, 20 and 30 air changes per hour. The building was considered to be under thermostatic control between 9 a.m. to 7 p.m., while night ventilation is applied between 10 p.m. to 6 a.m. Simulations have been performed for an indoor set point temperatures of 27 C.

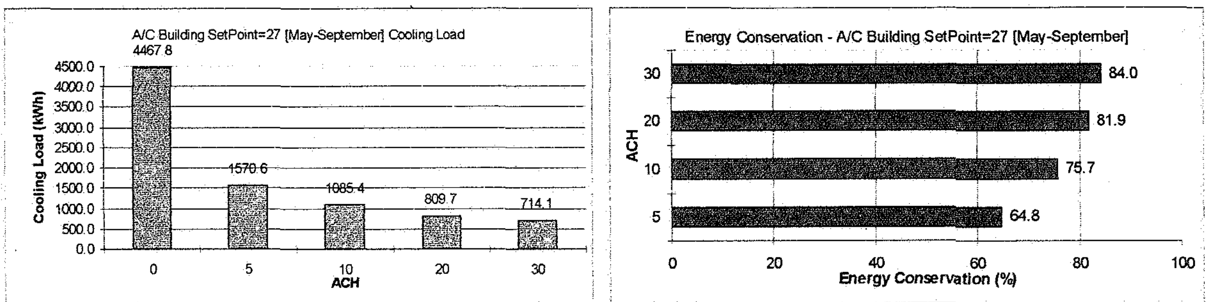


**Figure 11. Cooling energy and energy conservation due to night ventilation (set point 27C).**

Figure 11 gives the obtained results for the studied scenarios. The absolute value of the cooling load as well as the corresponding energy savings for cooling are given. It is found that the expected energy conservation, for this specific building, varies between 65 to 84 percent when air flow rate varies between 5 to 30 ACH. As clearly shown, the higher the air flow rate, the higher the calculated energy conservation due to night ventilation.

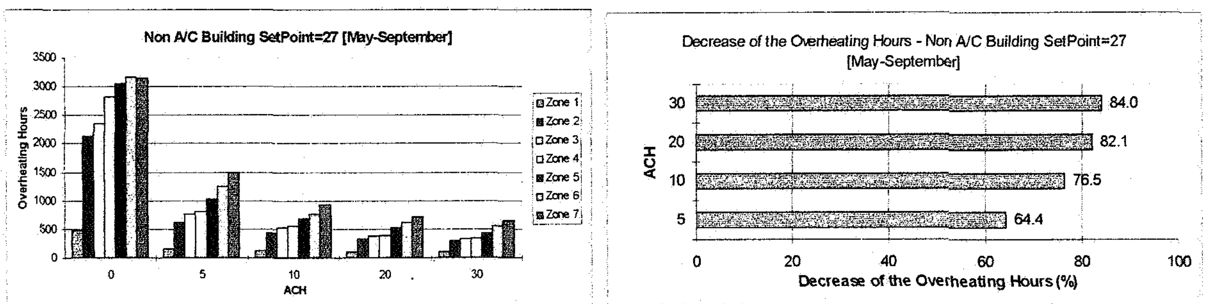


**Figure 12. Number and decrease of the overheating hours (set point 27 °C)**

To investigate the potential of night ventilation techniques, to improve indoor comfort conditions when A/C systems are not in use, the building was simulated under free floating conditions. In this case the number of hours for which indoor temperature exceeds 27 C were calculated (Figure 12).

## 5. Simulations and Theoretical Studies for the "University of Athens" building (Summer 1996).

Simulations of the thermal performance of the building, during the measurement period of the summer of 1996, have been performed using the TRNSYS software. The measured air flow rates during night ventilation (Figure 4) have been used in all thermal model. In contrast with the previous building, the present was occupied during the experimental period. The simulated as well as the measured indoor temperatures are given in Figure 13. As shown, the simulated and measured temperatures are almost identical. The average difference between measured and simulated temperatures is close to 0.3 C.

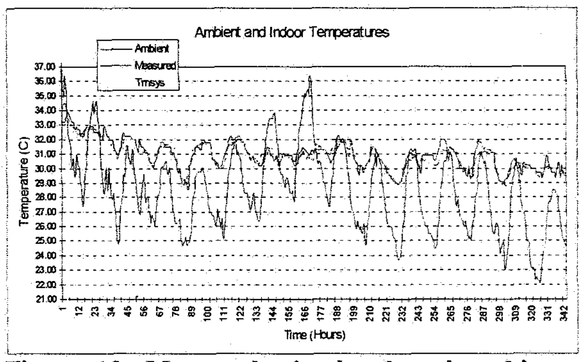


**Figure 13. Measured, simulated and ambient values of the air temperature.**

In order to investigate the impact of night ventilation on the indoor air temperature, comparisons with simulation results of non night ventilated configuration have been performed. In both cases the building was considered as thermostatically controlled. Application of night ventilation techniques was found to decrease the next day peak indoor temperature of this building by 0.1 up to 0.2 °C (Figure 14).

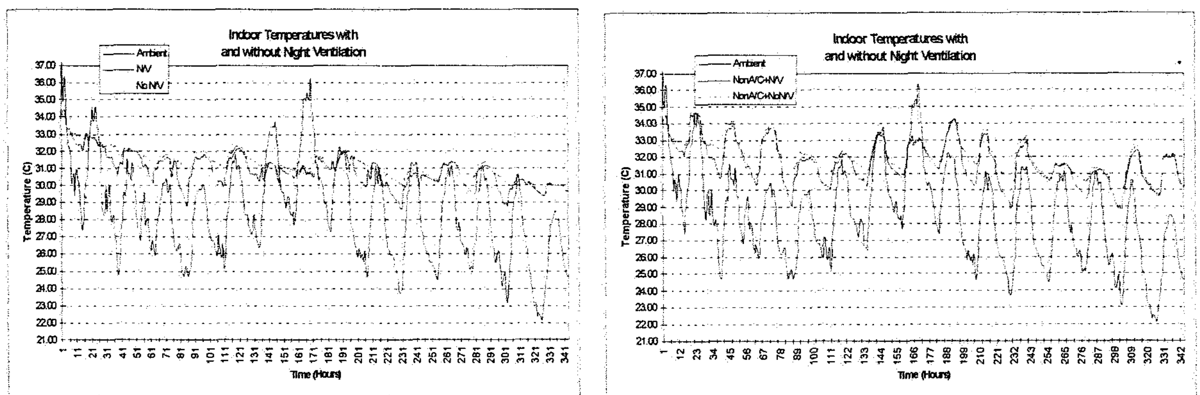


**Figure 14. Indoor temperature with and without night ventilation (A/C and non A/C operation)**

It is concluded that the use of the air conditioning system, the high internal gains and the low thermal mass of the building decrease the efficiency of night ventilation techniques. In a second attempt, the building was simulated under free floating conditions. Figure 14 gives the indoor air temperatures with and without night ventilation, when the A/C system is not in use. As shown the influence of night ventilation on the thermal performance of the building is not important. The application of night ventilation decreases the next day peak indoor temperature of the building by 0.1 to 0.3 C.

## 6. Conclusions

Night ventilation techniques have been applied in three real scale office buildings, of different mass, ventilation and layout characteristics (in Athens, Greece). The "Meletitiki Ltd" building has important thermal mass and it was studied during a period of very low internal gains, and non operation of the air conditioning system. On the contrary, the "University of Athens" building has a light structure and it was studied when internal gains were important and the air conditioning system was in use. The two cases are extreme conditions and in a way they indicate the limits of the potential of night ventilation techniques.

It was found that in the "Meletitiki Ltd", application of night ventilation techniques decrease the next day peak indoor temperature of the building, during free floating conditions, up to 2.5C, while under A/C conditions the corresponding temperature decrease was close to 1 C. Sensitivity analysis has shown that under A/C conditions, the expected energy conservation, for this specific building, varies between 65% to 84% when the air flow rate varies between 5 to 30 ACH respectively. It is shown that the higher the air flow rate, the higher the calculated energy conservation due to night ventilation. Under free floating conditions, the expected decrease of overheating hours varies between 64% to 84% when the air flow rate varies between 5 to 30 ACH respectively.

In the building of the University of Athens, night ventilation decreases the next day's peak indoor temperature of the building during A/C conditions by 0.1 to 0.2 C, while under free floating conditions the temperature decrease is 0.1 to 0.3 C.

In conclusion, night ventilation techniques when applied, may contribute to decrease considerably or not the cooling load of A/C and improve or not the comfort levels of free floating buildings. The exact contribution of night ventilation for a specific building has to be calculated as a function of the building characteristics, the climatic conditions, the applied air flow rate and the assumed operational conditions.

## 7. References

1. Solar Energy Laboratory, University of Wisconsin - Transsolar Stuttgart.
Trnsys version 14 - A Transient System Simulation Program.
2. M. Bruant, A.I. Dounis, G. Guarracino, P. Michel and M. Santamouris
"Indoor air Quality Control by a fuzzy reasoning machine in naturally ventilated buildings" Journal of Applied Energy, In Press, 1996.

VENTILATION AND COOLING
18TH AIVC CONFERENCE, ATHENS, GREECE
23-26 SEPTEMBER, 1997

**Title:** Reducing Cooling Loads With Under Roof Air Cavities


**Author(s):** Prof. G V Fracastoro, Ing.L.Giai, Ing.M. Perino

**Affiliation:** Department of Energetics, Politecnico di Torino, Italy


idee : in zomer dakstructuur ventileren →
minder zonnewinste

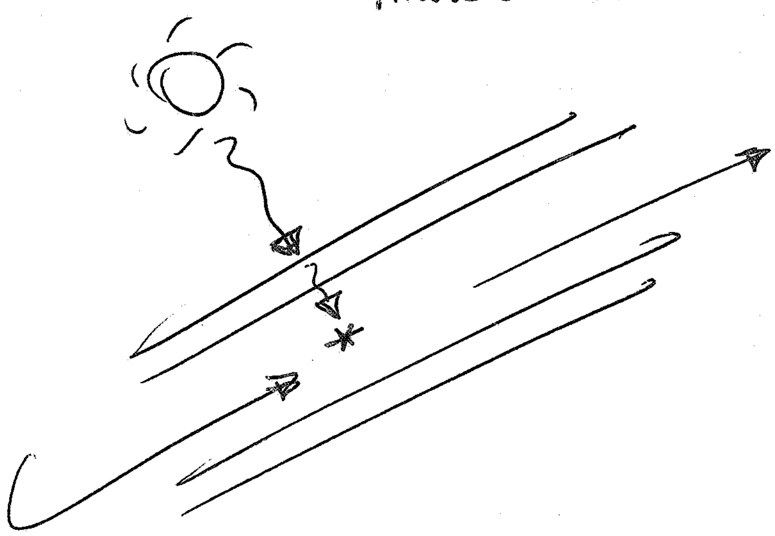

(interessant
pak vglen)

## Synopsis

In the present paper a model for steady-state thermal analysis of ventilated and unventilated light roofs is proposed. The aim of the work is to study the influence of thermo-physical and geometric parameters of the roof and boundary conditions (solar radiation) on the entering heat flow and the temperature distribution within the roof structure. Knowledge of this relationship, in fact, is important to optimise the roof "thermal" design in order to reach acceptable indoor conditions with low energy costs.
In the first part of the paper a calculation procedure for the forecast of internal temperatures and induced air flow rates is presented. The model can be used to analyse both closed and ventilated air cavities for different boundary conditions. From the mathematical point of view it is composed by a system of non-linear equation solved numerically.
The model output are: air temperature distributions, surface temperatures, heat fluxes and air flow rates (in the case of ventilated cavities).
The second part of the paper deals with the development of two simplified models, directly providing the entering heat flows. A non-dimensional analysis based on the Π-theorem provided the structure of the monomial expression, and the free parameters were determined through a parametric analysis performed by the complete model described in the first part.
The resulting model predicts the performance of light roofs with good accuracy.

## Introduction

The under roof cavities represent a system characterised by the presence of two solid layers with an air space in between. These kinds of envelopes are specially used in the case of light roofs and allow an effective increase of the thermal insulation of the building, without a great increase of the structure weight. For these reasons these types of surfaces are widely employed in the roofing of large spaces such as atria, sporting halls and auditoria.
The correct design of these roofs requires a suitable calculation procedure producing information about the thermal fluxes going into the space, needed for thermal load calculation and HVAC plant design, and the temperature field inside the layers, which may give relevant information about the thermal stresses induced in the structure. Moreover, the availability of an automatic procedure, able to predict the behaviour of the system with little computational resources, allows the design optimisation of the roof thermal structure, aiming at achieving acceptable indoor conditions at lower energy costs.
As the aim is to provide an easy to use and time saving tool, the calculation procedure described in this paper has been implemented into a well known spreadsheet (Excel®), widely used and available to a great number of designers. More detailed and sophisticated calculation procedure are available, like CFD codes. However, these computer programs, that supply three-dimensional flow and thermal fields of the system, require a large amount of computational time and resources, and may not be used in practice to develop sensitivity analyses or design optimisation.
The calculation procedure takes into account two different kinds of roof cavities:
*Closed air cavities*: in which the air space is confined inside a closed volume by non-permeable surfaces.
*Ventilated air cavities*: in which the lower and upper part of the air cavity are open and the air is free to flow by means of natural or forced draught through the air space. Forced ventilation cavities are usually less employed and, besides, easier to analyse, because the air flow is imposed, while the air flow in natural ventilated cavities is an output itself. For these reasons in the following paragraphs attention will be devoted only to the last type of cavity roofs.
Since these two kinds of roof air cavities have different physical behaviour, two distinct predictive models are required.

## Calculation models

### *Basic hypotheses common to closed and ventilated cavity roofs*

The simplifying hypotheses, common for open and closed cavities, are:

- steady-state thermal and flow fields,
- solar radiance and optical properties of surfaces uniform along the roof surface and along the direction perpendicular to the air flow pattern,
- thermal gradients negligible along the cross direction of the roof.

For what concerns convective heat transfer the larger between the two following correlations has been adopted:

for natural convection (ASHRAE, 1977) $$h_c = 1.52 \cdot |\Delta T|^{\frac{1}{3}} \qquad (1)$$

for mixed convection (ASHRAE, 1977) $$h_c = 5.62 + 3.9 \cdot v \qquad (2)$$

where $\Delta T$ is the temperature difference between air and surface and v is the air velocity.
The steady-state behaviour assumption is justified by two factors: the first is that these types of roofs are usually made with light structures, with quite low thermal inertia, and hence the time constant of the system is low and heat flows almost instantaneously. The second is that the computer code is intended for design purpose, where the steady-state assumption is usually made.
For the calculation of atmospheric radiation the Cole's relation has been adopted (Fracastoro, 1985):

$$G_a = 222 + 4.94 \cdot T_e + 65 \cdot cc + 1.39 \cdot cc \cdot T_e \qquad (3)$$

where $T_e$ is the outdoor air temperature, measured in °C and cc, is the cloud cover factor, expressed as a fraction of unity.

### *Closed cavities*

A roof with a closed air cavity is usually configured as:

- an upper layer made of a thin metal plate, often coupled with a thermal insulating panel,
- an air cavity, of quite low thickness (compared with the longitudinal roof length)
- a lower layer made of one or more panel with suitable thermo-acoustic properties.

Neglecting the thermal resistance of the metal plate, the calculation model for the closed cavities may be reduced to the scheme of figure 1.
For the inside surfaces of the air cavity the convective heat transfer coefficient has been calculated by means of the Raithby-Hollands (1985) correlation for closed, tilted cavities.
The total solar radiation I and infrared atmospheric radiation $G_a$ impinging on the outdoor surface of the roof, inclined of an angle $\theta$ with respect to the horizontal plane, are absorbed with two different absorption coefficients, $\alpha_s$ and $\alpha_l$, whose values depend on the optical properties of the outside roof surface. As a consequence, the equilibrium temperature of the upper layer is determined by the incident solar radiation, the re-radiation of the hot surface and the convective heat flow. Neglecting the longitudinal thermal gradients, the model will become one-dimensional, and the specific thermal flow rate,

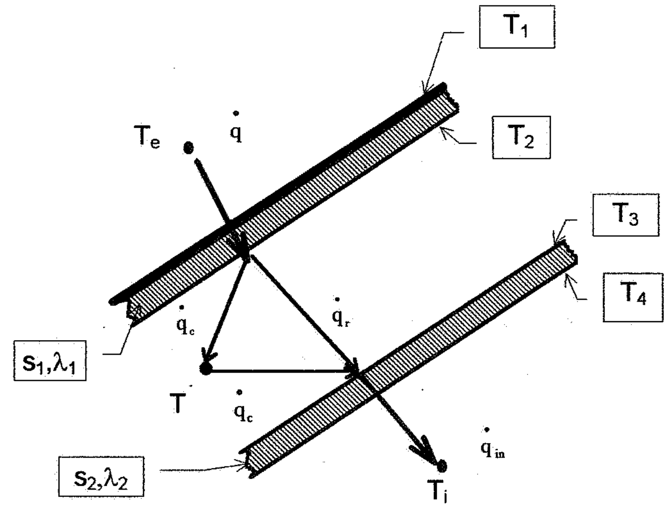


$$\dot{q} = \alpha_s \cdot I + \alpha_1 \cdot G_a - \varepsilon_1 \cdot \sigma \cdot T_1^4 - h_{ce} \cdot (T_1 - T_e)$$

$$\dot{q}_r = F_\varepsilon \cdot \sigma \cdot (T_2^4 - T_3^4)$$

$$\dot{q}_c = h_c \cdot (T_2 - T_3)$$

$$\dot{q}_{in} = \left(\frac{s}{\lambda}\right)^{-1} \cdot (T_3 - T_4)$$

$$\dot{q}_{in} = h_i \cdot (T_4 - T_i) + F_\varepsilon \cdot \sigma \cdot (T_4^4 - T_i^4)$$

**Figure 1** - Calculation model for closed air cavity.

$q = \dot{Q}/S$, will be uniform over the whole roof surface. Furthermore, the energy balance of the roof yields:

$$\begin{cases} \dot{q} = \dot{q}_c + \dot{q}_r \\ \dot{q}_c + \dot{q}_r = \dot{q}_{in} \end{cases} \qquad (4)$$

More details on the mathematical models of the closed cavity may be found in (Fracastoro et al., 1997).

### *Ventilated cavities*

When the air cavities are tilted respect to the horizontal the air flows upwards due to natural draught ("chimney effect") and exchanges heat with the adjacent surfaces, progressively increasing its enthalpy and temperature. Therefore, there will be thermal gradients along the air flow direction and the heat flows crossing the roof will increase in the air flow direction. The system is now strongly two-dimensional, and the mathematical model that describes the thermal and fluodynamic behaviour of the roof will be made of a set of non-linear differential equations. This system has been solved numerically, discretizing the real system in a number of elements adopting an up-wind scheme. The resulting algebraic system is described in figure 2 for the generic jth-element.

- $S_j$ is the area of the j-th element, with $S = \sum_j S_j$,
- $s_1$ ed $s_2$ are the thickness of the two (upper and lower) insulating panels.

The energy balance of the roof yields:

$$\begin{cases} \dot{Q}_1 = \dot{Q}_r + \dot{Q}_2 \\ \dot{Q}_4 = \dot{Q}_r + \dot{Q}_3 \end{cases} \qquad (5)$$

In order to complete the mathematical model the enthalpy balance has to be written for the air flow inside the cavity:

$$\dot{Q}_{aria,j} = \dot{m} \cdot c_p \cdot (T_{j+1} - T_j) = \dot{Q}_{3,j} + \dot{Q}_{4,j} \qquad (6)$$

insolation

surface

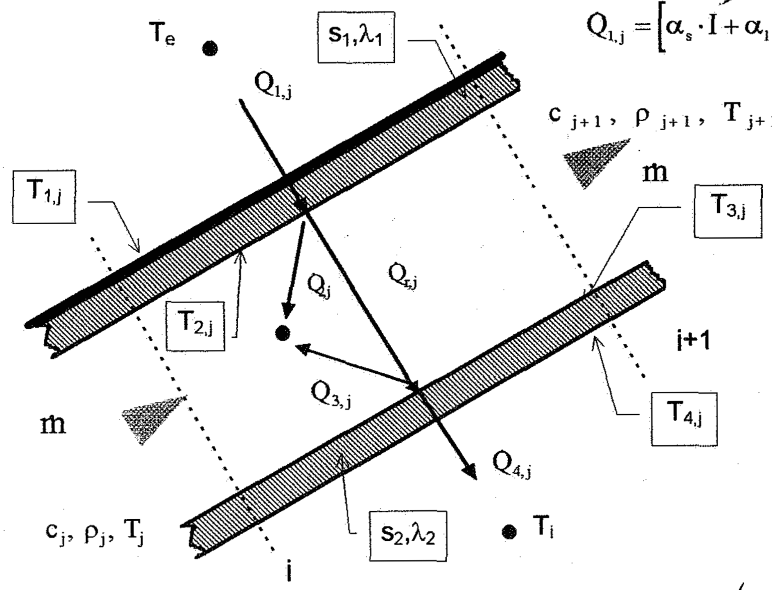


$$Q_{1,j}=\left[\alpha_s\cdot I+\alpha_l\cdot G_a-\sigma\cdot\varepsilon_l\cdot T_{1,j}^4-h_{ce,j}\cdot\left(T_{1,j}-T_e\right)\right]\cdot S_j$$

$$Q_{1,j}=\frac{\lambda_1}{s_1}\cdot\left(T_{1,j}-T_{2,j}\right)\cdot S_j$$

$$Q_{2,j}=h_{c2,j}\cdot\left(T_{2,j}-T_j\right)\cdot S_j$$

$$Q_{3,j}=h_{c3,j}\cdot\left(T_{3,j}-T_j\right)\cdot S_j$$

$$Q_{4,j}=\frac{\lambda_2}{s_2}\cdot\left(T_{3,j}-T_{4,j}\right)\cdot S_j$$

$$Q_r=\sigma\cdot F_\varepsilon\cdot\left(T_{2,j}^4-T_{3,j}^4\right)\cdot S_j$$

$$Q_{4,j}=h_i\cdot\left(T_{4,j}-T_i\right)\cdot S_j+F_\varepsilon\cdot\sigma\cdot(T_{4,j}^4-T_i^4)\cdot S_j$$

**Figure 2** - Calculation model for open air cavity.

The air mass flow rate is also a function of the fluodynamic properties of the flow channel. In fact, the sum of all the pressure drops, due to distributed and concentrated losses in the various elements along the roof shall equal the total static pressure difference existing in the outdoor air between the entrance and the exit of the air cavity:

$$\sum_j \Delta p_j=\sum_j -\rho_j\cdot\left(\frac{c_{j+1}^2-c_j^2}{2}+g\cdot\Delta z_j+l_{w,j}\right)=-\rho_{aria,est}\cdot g\cdot\Delta z_{tot} \qquad (7)$$

## Numerical solution

In order to solve the non-linear system of algebraic equations obtained from the mathematical model of air cavities discussed in the previous paragraph, a numerical iterative procedure has been used. The two models have been implemented into an Excel® spreadsheet that, following the two schematic flow-charts shown in figure 3, allows a quick solution of the problem.

The computational time needed for the closed cavity analysis is negligible, and no problems of convergence have been experienced.

For what concerns the open cavities, the calculation procedure may require some minutes of CPU time (employing a PC Pentium pro 200 MHz with 32 Mb of system memory). Critical boundary conditions for convergence are: low solar radiation, high degree of thermal insulation and low tilt angle roof. A suitable guess of the outside surface temperature field and of the air mass flow rate is also needed for the first step calculation. A recommendable procedure is to use the results of the closed cavity as a first guess for the open case simulation.

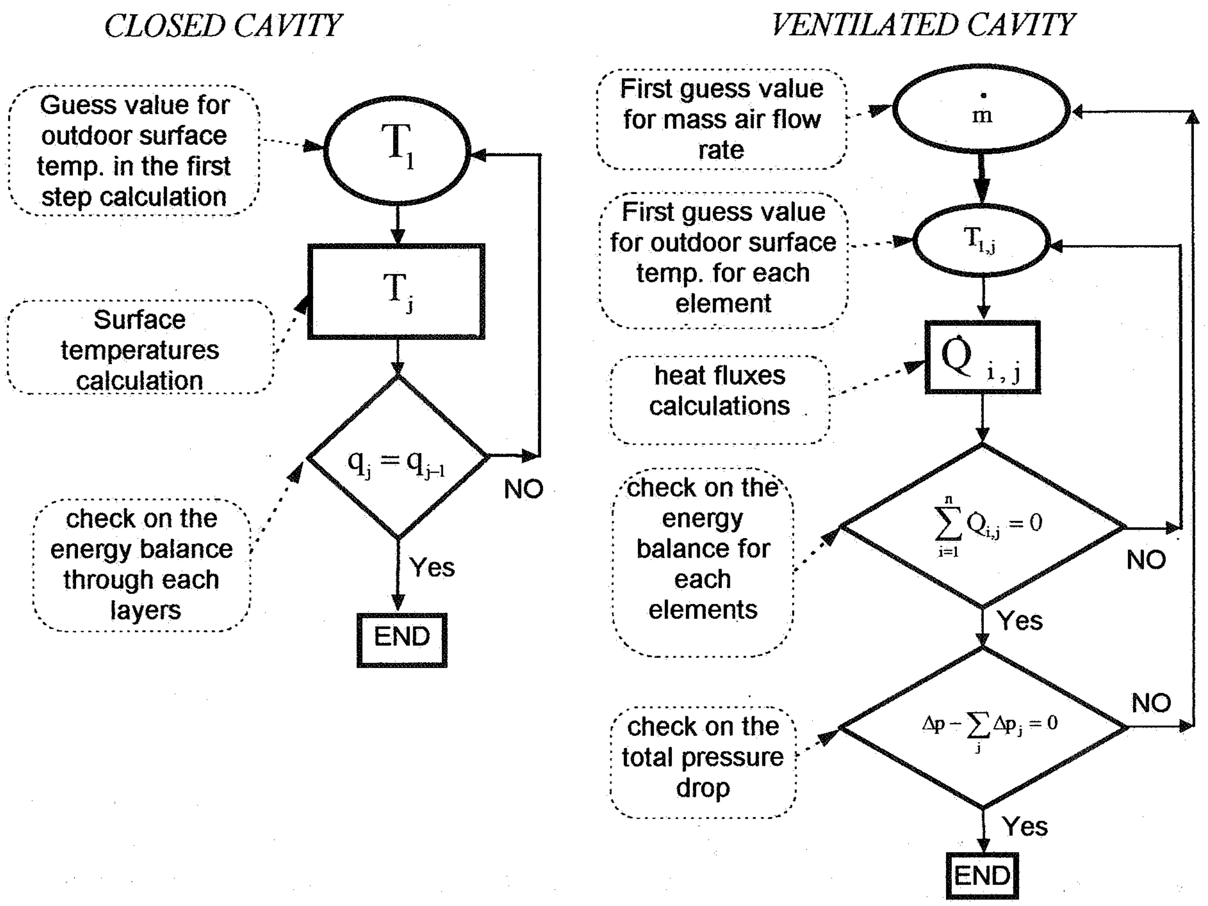


**Figure 3** - Flow chart of the solution procedure for the close and open air cavity model.

## Models application

### *Closed air cavity*

Once the entering heat flow is normalized respect to the absorbed solar radiation, it turns out to be dependent only on the ratio of the outside film resistance to the total roof resistance, according to the classical expression:

$$\frac{Q}{\alpha \cdot I \cdot S} = \frac{R_{out}}{R_{tot}} \tag{8}$$

where

$R_{out}$ is the value of the outside surface coefficient,

$R_{tot}$ is the total thermal resistance of the roof, which may be calculated adding to the conductive thermal resistance of the insulation layers the outside and inside surface resistances and the thermal resistance of the air cavity.

The air cavity thermal resistance is, in practice, inversely proprtional to the gray surfaces view factor, $F_\varepsilon$, according to the expression:

$$R_{int} = \frac{0.12}{F_\varepsilon}.$$

Figure 4 compares the performance of ventilated and closed air cavities in reducing the solar heat load. This chart plots the non-dimensional parameters:

$$\xi = \frac{Q_{in,vent.}}{Q_{in,closed}} \quad \text{and} \quad \eta = \frac{Q_{in}}{I \cdot S},$$

versus the total conductive thermal resistance. The presence of the closed air cavity, even with very low total conductive resistance, allows to reduce the solar heat load to 15% of the solar radiance. This fraction may be further reduced to a value of 5%, when the total thermal resistance is higher than 1 $m^2K/W$.

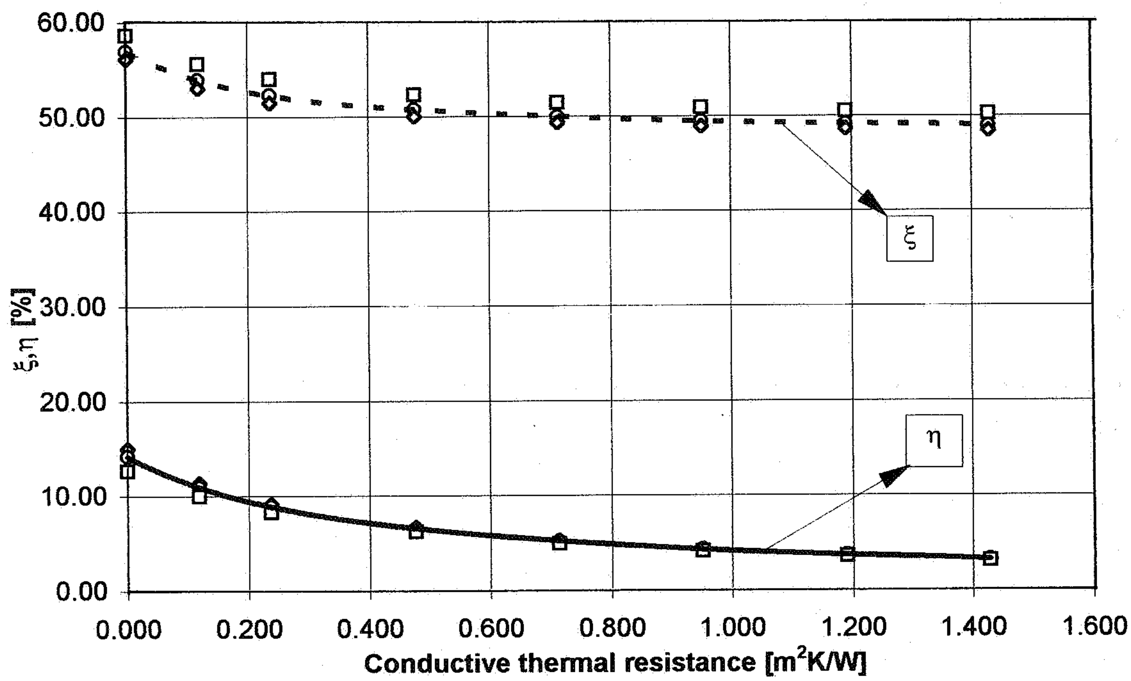


**Figure 4** - Ventilated and closed air cavity performances.

These positive effects are amplified if the air cavity is ventilated, with entering heat fluxes lower than 60 % of the closed case, down to less than 50 % when $R_{tot}$ becomes higher than 1 $m^2K/W$ (fig. 4 has been plotted supposing the insulation concentrated in the lower panel).

**Simplified model for ventilated air cavity**

The numerical procedure obtained for the naturally ventilated configurations is a flexible calculation tool, that however requires a certain amount of computational resources and time. In order to provide a procedure for first attempt calculations, a simplified method, based on dimensionless analysis, has been developed.

The study has been split into two different parts:

1) investigate the behaviour of a non-insulated ("bare") ventilated roof considering only the effects of the boundary conditions (solar radiation, I) and geometrical parameters (roof length, L, duct roughness, e, and hydraulic diameter, D, roof angle referred to horizontal plane, $\theta$) (i.e. the roof is made of an upper and lower thin metal slab having a negligible conductive resistance, and only a radiation shield function).
2) analyse the influence of:

- total conductive thermal resistance of the insulating panels,
- distribution of the thermal resistance between upper and lower slab.

***Bare roof***

For what concerns the "bare" roof, applying the Π-theorem to the ventilated air cavity model, it is possible to reduce the relations between the main physical influencing variables into a monomial formula containing five dimensionless groups:

$$\Pi_1 = A \cdot \Pi_2^m \cdot \Pi_3^n \cdot \Pi_4^o \cdot \Pi_5^p$$

where:

$$\Pi_1 = \frac{\frac{Q_{in}}{a}}{I \cdot L} \qquad (9)$$

$$\Pi_2 = \frac{L \cdot \sin\theta}{D} \qquad \Pi_3 = \frac{R^* \cdot T_e}{g \cdot L \cdot \sin\theta} \qquad \Pi_4 = \frac{e}{L} \qquad \Pi_5 = \frac{\alpha \cdot I}{h_e \cdot T_e} = \frac{T_{s,a} - T_e}{T_e} \qquad (9')$$

being:

$Q/a$ the total net heat flux entering the enclosure per unit of roof width, $T_e$ air outdoor temperature, $T_{s,a}$ sol-air temperature, $h_e$ surface heat transfer coefficient, $\alpha$ external roof surface absorption coefficient, $R^*$ air elasticity constant, g gravity acceleration.
Applying the computer code described in the previous section to a set of more than 100 data[1], including different boundary conditions and air cavity configurations, it is then possible to derive a number of "working points" for the ventilated cavities, by means of which the unknown coefficients may be determined.
The best-fit of the calculated values has lead to the following formula:

$$\Pi_1 = 0.0033 \cdot \Pi_2^{0.2967} \cdot \Pi_3^{0.4245} \cdot \Pi_4^{0.0365} \cdot \Pi_5^{0.1545} \qquad (10)$$

The reliability of this formula is acceptable, as it is shown in figure 5 where the exact dimensionless parameter $\Pi_1$ is plotted versus the value "predicted" by means of eqn. 10. For all the considered configurations the prediction error lies inside a range from -10 % to +7 %.

***Effect of insulation***

The effect of the total conductive resistance and of the distribution of this resistance between the upper and lower slabs may be taken into account introducing a suitable dimensionless parameters ~~defined as~~:

$$\varphi = \frac{Q_{in,insulation}}{Q_{in,R=0}} \qquad (11)$$

[1] these calculations have been performed assuming: equal inside and outside air temperature (in order to take into account only the solar radiation shield effect), constant atmosphere radiation $G \approx 355\ W/m^2$, equal long and shorrt-wave absorption coefficients.

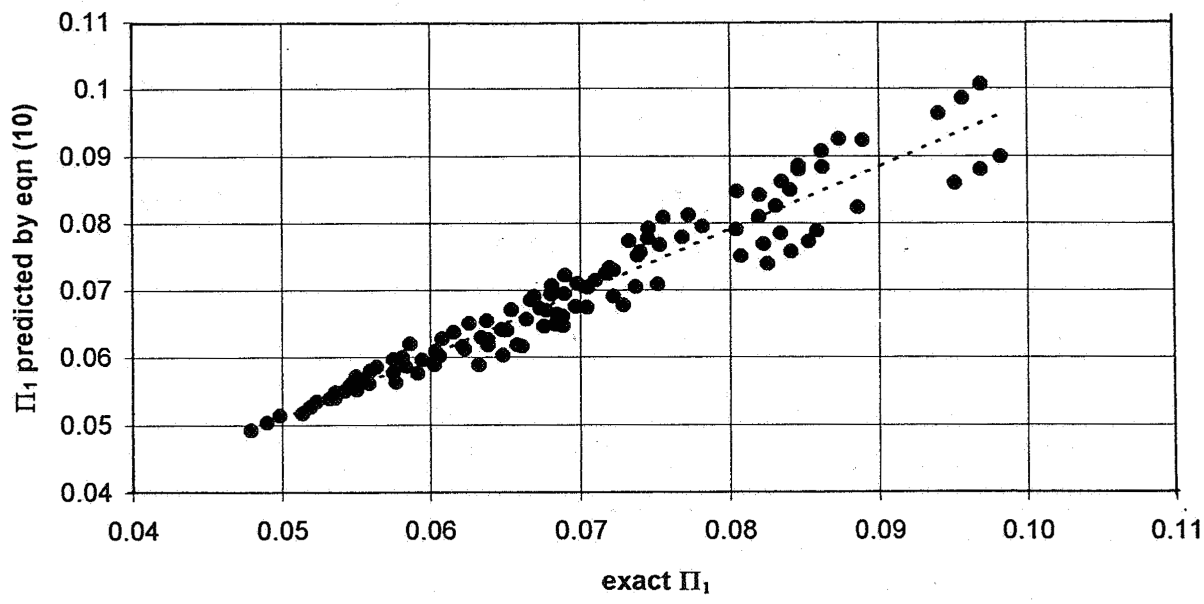


**Figure 5** - Comparison between predicted and calculated $\Pi_1$ value.

It is possible to express $\varphi$ only as a function of the total (upper plus lower slab) conductive thermal resistance and of the distribution of such resistance between the two slabs, having the other parameters, such as I, $\vartheta$, L, D, e, practically no influence.
This is clearly shown in figure 6 where $\varphi$ is plotted versus the fraction of thermal conductive resistance placed in the upper slab respect to the total.

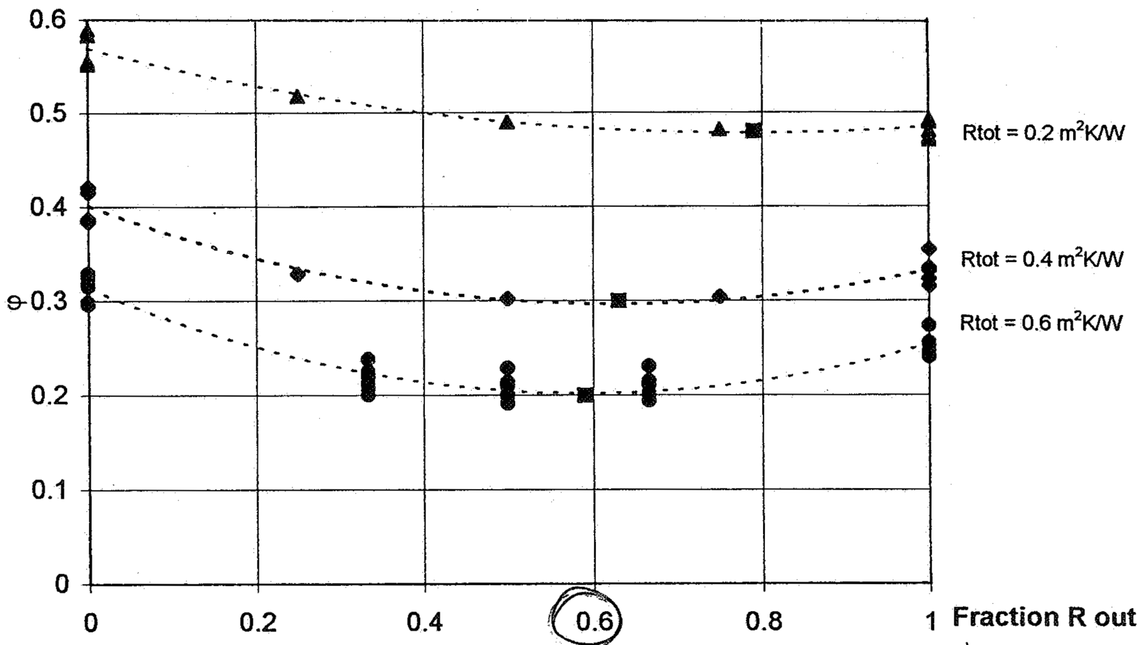


**Figure 6** - Influence of thermal insulation.

optimale positie
± 60 % van isolatie
in buitenste slab,
40% in binnenste

The points gather around a parabolic trend with quite low dispersion. The non-dimensional heat flux, $\varphi$, shows a minimum when the 60%-80% of the conductive thermal resistance is located in the upper panel. For these configurations the total heat flux entering the enclosure through the roof, is only 75 % of the heat flux that would be transmitted if all the insulation were located in the lower panel.

Finally, once the parameter $\Pi_1$ has been calculated by means of eqn. (10) and $\varphi$ has been read by means of figure 6, $Q_{in}$ may be determined as:

$$Q_{in} = \varphi \cdot \Pi_1 \cdot I \cdot L \cdot a \tag{12}$$

The assumptions under which the simplified model has been developed are given in Table 2.

**Table 2 - Ventilated cavity. Constant values adopted.**

| Parameter | Symbol | Value | Units |
|---|---|---|---|
| "long-wave" absorption coefficient | $\alpha_l$ | 0.85 | - |
| Cloud cover factor | cc | 0.10 | - |
| Outdoor air temperature | $T_e$ | 25 | °C |
| Indoor air temperature | $T_i$ | 25 | °C |

## Conclusions

The paper describes the models developed by the authors to simulate the thermal behaviour of roofs with closed and/or ventilated air cavities. The models have been implemented on a commercial spreadsheet and allow a quick and easy calculation of the relevant outputs, such as air flow rates, temperature distribution, and entering heat fluxes. Some examples are reported which provide some insight on the performance of these structures, and show the reduction of solar heat gains achievable both with closed and ventilated air cavities. In particular, ventilated roofs may lead to a reduction of 50 % and more respect to closed air cavity roofs. Furthermore, the model shows that there is an optimal positioning of insulation slabs in the case of ventilated air spaces, while positioning is unrelevant for closed ones.
A further step has led to the development of a procedure for "hand calculation" of the heat gain through a ventilated roof. This procedure yields results correct within ± 10 % respect to the computer model.
Future developments will include the experimental validation of the codes.

## References


ASHRAE, *Handbook of Fundamentals*, ASHRAE, New York 1977, cap. 2 "Heat transfer".

Fracastoro G.V. *Elementi di climatologia edilizia,* CELID, Torino 1985.

Fracastoro, G.V., Giai, L., Perino, M., *Analisi del comportamento termico di coperture di edifici con intercapedine d'aria,* Proc. 15th UIT National Heat Transfer Conf., Torino, 19-20 June 1997.

Raithby G.D., K.G.T. Hollands, *Handbook of heat transfer fundamentals*, McGraw Hill Book G., New York, 1985, chapter on "Natural convection".

**VENTILATION AND COOLING**

**18TH ANNUAL AIVC CONFERENCE**
**ATHENS, GREECE, 23-26 SEPTEMBER, 1997**

# Possibilities and limitations for evaporative and desiccant cooling technologies

samen → !

**Torbjörn Lindholm**

interessante tekst
↓
goede uitleg
over ≠ systemen

**Chalmers University of Technology**
**Department of Building Services Engineering**
**412 96 Gothenburg, Sweden**

interess - opm. - van spreker;
Als je demands vastzet
bvb.: nt > 25°C → zware installatie
beter: ( 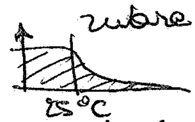
25°C


## Synopsis

Evaporative cooling is an interesting alternative to conventional compressor refrigeration systems for air-conditioning. However, the use of evaporative cooling presupposes all-air systems and is, to a large extent, limited by ambient conditions as well as the settled demands on the indoor climate. High outdoor humidity levels have a great influence on the supply-air temperature achievable, i.e. cooling loads possible to meet. One way to reduce the influence of these limitations is to use desiccant cooling, i.e. to dehumidify the ambient air before the evaporative stages. Here, a general methodology to describe possibilities and limitations for evaporative and desiccant cooling, is presented. The major advantage of using this methodology is that this may give rise to an increased understanding of these processes. This methodology can also be used for a rough estimation of the energy consumption for air-conditioning using evaporative or desiccant cooling. As an example, this methodology is applied on cooling loads of a base-case office building situated in Stockholm, Sweden.


## 1. Introduction

One of the primary demands for a good indoor climate in a building is that temperature and humidity are maintained at comfortable levels, regardless of the prevailing outdoor climate. Heating and cooling loads for the building can be calculated when specified requirements are stipulated with regard to room temperature and humidity. The heating and cooling loads are then mainly affected by the combination of building design, activities in the building and the outdoor climate. Commercial and office buildings often have a heat surplus a great part of the year due to internal activities, even in climates with moderate ambient temperatures. This heat surplus has to be compensated for in order to fulfil the specified requirements on the indoor climate. Thus, the specified requirements on the indoor climate and the prevailing outdoor climate have a great influence on the loads for the air-conditioning system. The energy consumption then depends on the choice of technical solution. The focus in this paper is on possibilities and limitations using evaporative and desiccant cooling to satisfy the cooling demands in buildings. A methodology used to give a rough estimation of the energy consumption for air-conditioning using evaporative or desiccant cooling is also described.

## 2. Indoor climate

Many studies have been carried out with the aim of determining how human beings are affected by different combinations of temperature and humidity. Most studies indicate that an indoor temperature around 24 °C and 30-70 % relative humidity are acceptable [1]. In this context, it is important to analyse the consequences of too strict demands on thermal comfort, as they can result in considerably increased investment and running costs. Thus, demands on thermal comfort, should be defined by an acceptable interval or by the number of hours, for example, when the indoor temperature may exceed or be below the desired level. The methodology presented in this paper, is based on the number of hours when a certain supply-air temperature can be obtained using different evaporative cooling technologies with common boundary conditions.

## 3. All-air, air-conditioning systems

A building's sensible cooling demand can be met by using an appropriate combination of supply-air temperature and air-volume flow. If the activities in the building generate moisture, and there is a specified upper humidity limit, then the absolute humidity content of the supply-air must be low enough. This internal moisture gain gives rise to the building's latent cooling demand.

The building's total cooling demand would then be the sum of the sensible and latent cooling demands. If a low supply-air temperature is provided for a given sensible cooling demand then a lower airflow can be used. This lower airflow means that the investment cost as well as fan electricity consumption can be reduced. However, too low supply-air temperatures would cause draught problems; therefore there is a lower temperature limit regarding practicable supply-air temperatures.

Generally, a compressor refrigeration system is used to obtain the necessary supply-air temperature in all-air systems. As a result of the greenhouse effect and the ozone depletion debate, the prerequisites for compressor refrigeration systems have been changed. Therefore, other methods of air-conditioning are considered. When the ambient climate conditions are opportune, a suitable alternative may be evaporative or desiccant cooling.

## 4. Evaporative and desiccant cooling

In arid climates the necessary supply-air temperature can be obtained by humidifying the air-stream in one or more stages (figure 1). In this context this method of air-conditioning is called evaporative cooling. When the humidity in the air-stream is increasing, in this humidifying process, the dry-bulb temperature is decreasing. The reason for this is that the heat necessary to evaporate the supplied water into vapour is essentially taken from the air-stream. There are different types of humidifying equipment available for this purpose.

The humidifying process is essentially an adiabatic process and therefore the wet-bulb temperature remains constant. The performance of a humidifier, or in this context an evaporative cooler, is specified by the so called saturation effectiveness. The saturation effectiveness specifies the extent to which the leaving dry-bulb temperature from an evaporative cooler approaches the thermodynamic wet-bulb temperature of the entering air. This dry-bulb temperature decrease can be used as direct evaporative cooling (figure 1a) by humidifying the outdoor-air stream. The evaporative cooler can also be located in the exhaust-air stream as so-called indirect evaporative cooling (figure 1b). The outdoor air-stream temperature is then decreased by using a sensible heat recovery device, i.e. a heat exchanger that does not transfer moisture. These two types of evaporative cooling configurations can be combined into indirect + direct evaporative cooling (figure 1c).

High outdoor humidity levels as well as the demands on the indoor climate have a great influence on the supply-air temperature possible to reach when using evaporative cooling. There are, thus, physical limitations with regard to the supply-air temperatures possible to achieve.

→ no moisture in input stream

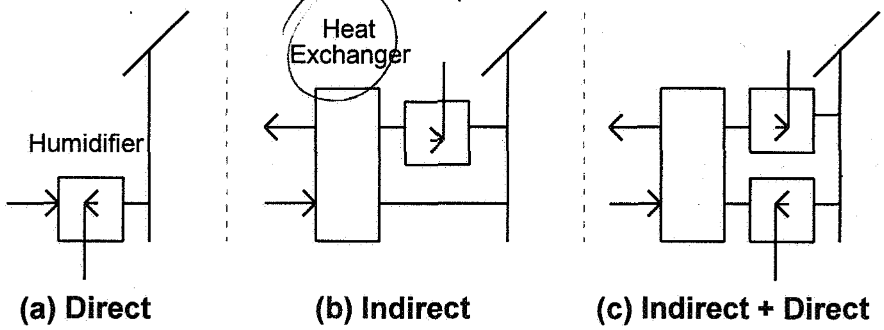


**Figure 1.** Evaporative cooling configurations.

One way to reduce the influence of these physical limitations is to use desiccant cooling, i.e. to dehumidify the ambient air before the evaporative stages with a desiccant dehumidifier. This dehumidification paves the way for the subsequent evaporative cooling system. The physical limitation regarding ambient conditions is, therefore, reduced.

RV↑

daarom vooraf drogen

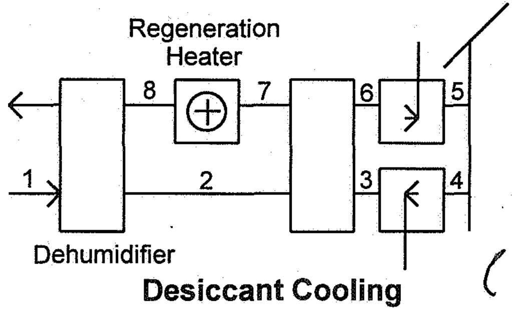


(pennington cycle)

**Figure 2.** Desiccant cooling, a combination of indirect + direct evaporative cooling and a desiccant dehumidification (in this case a desiccant wheel).

↳ or liquid system → zie Essen

There are mainly two different types of desiccant dehumidifiers, either based on solid desiccant materials or desiccants in liquid form. In both cases thermal energy is used to achieve the desired dehumidification. From here on in the report, the term dehumidifier will primarily be used to refer to a dehumidifier based on solid material, a so-called desiccant wheel. An ideal dehumidification process, in this case, is assumed to be a constant enthalpy process. In the real dehumidification process, the enthalpy would increase due to the so-called heat of adsorption as well as ordinary heat transfer.

In order to achieve the necessary dehumidification, the desiccant material has to be regenerated, i.e. the adsorbed moisture has to be removed. For this purpose thermal energy must be supplied to the regeneration heater (figure 2) to raise the temperature $t_8$. The amount of thermal energy necessary, is determined by how much moisture has to be removed as well as component performance. Different sources of energy can be considered for this regeneration. If a combustion process is used then it is possible to achieve just about any temperature $t_8$. Another source would be district heating, but in this case an upper temperature limit of approximately $t_8$ = 60 °C occurs.

Sweden !

Even a desiccant cooling system has physical limitations with regard to the supply-air temperatures possible to achieve. If the proposed thermal source causes limitations to possible regeneration temperature, then additional limitations will be experienced for the desiccant plant.

## 5. Building's cooling load

The building's total cooling load, i.e. the necessary heat extraction rate $\dot{Q}$, can be expressed:

$$\dot{Q} = \dot{M} \cdot (h_5 - h_4) \qquad (1)$$

Where $\dot{M}$ is supply-air mass flow and $h$ is specific enthalpy, with indices, 4 refers to the supply-air stream and 5 refers to the exhaust-air stream.

A useful expression for handling the relationship between sensible and latent cooling load is the sensible heat ratio *SHR*. *SHR* is defined as the ratio of sensible heat to the total value of heat. In equation 2 the expression for *SHR* for the building cooling load is given.

$$SHR = \frac{\dot{Q}_{sensible}}{\dot{Q}_{total}} = \frac{c_p \cdot (t_5 - t_4)}{(h_5 - h_4)} \qquad (2)$$

Where $t$ is dry-bulb temperature and $c_p$ is specific heat.

*SHR* = 1 means that no moisture is generated from the activities in the building. Office buildings are an example of buildings with small internal moisture gains. The origin of the heat surplus in office buildings is mainly from human beings, equipment, appliances, electric light and solar gains. Of these internal heat gains, only human beings normally contribute to an internal moisture gain. If human beings carrying out moderately active office work at normal room temperature were the only contributor to the internal gains, then the *SHR* would be approximately 0.55 [1]. If no more than 40 % of the internal heat gains were assumed to originate from human beings then the *SHR* would be greater than 0.8 in an office building.

## 6. Limitations for evaporative and desiccant cooling

The limitations caused by the ambient climate have been studied with regard to the supply-air temperatures possible to achieve. In some of these systems, the prevailing exhaust-air condition also affects the reachable supply-air temperatures and this fact must be taken into consideration. Certain combinations of ambient temperature and humidity mean that it is possible to reach a certain supply-air temperature. These ambient-air states can be identified if the room temperature, *SHR* and the effectiveness of the components are specified. These valid combinations of ambient temperature and humidity can then be combined in the psychometric chart as a limit-line.

sensible heat ratio : int. moisture gains (låge! värde)

In this case a room temperature of 24 °C and a *SHR* of 0.8 have been presumed. For the evaporative as well as the desiccant system, the heat exchanger sensible effectiveness is 0.8, and the humidifier's saturation effectiveness is 0.8. In this paper the performance of a commercial available desiccant wheel has been applied. With regard to the regeneration temperature, a maximum temperature limit has been assumed to exist.

In figure 3, limit-lines are shown on the psychometric chart describing the outdoor conditions when it is possible to reach a supply-air temperature of 17 °C. If the ambient climate is in the area in between this limit-line and the desired temperature level, in this case 17 °C, then it is possible to reach a supply-air temperature of 17 °C or lower . From here on, such an area is referred to as the psychometric area for each system or subsystem.

In figure 3, the boundary conditions of the Stockholm climate have been visualised, as well. The Stockholm climate is based on hourly measured values from 1983 to 1992.

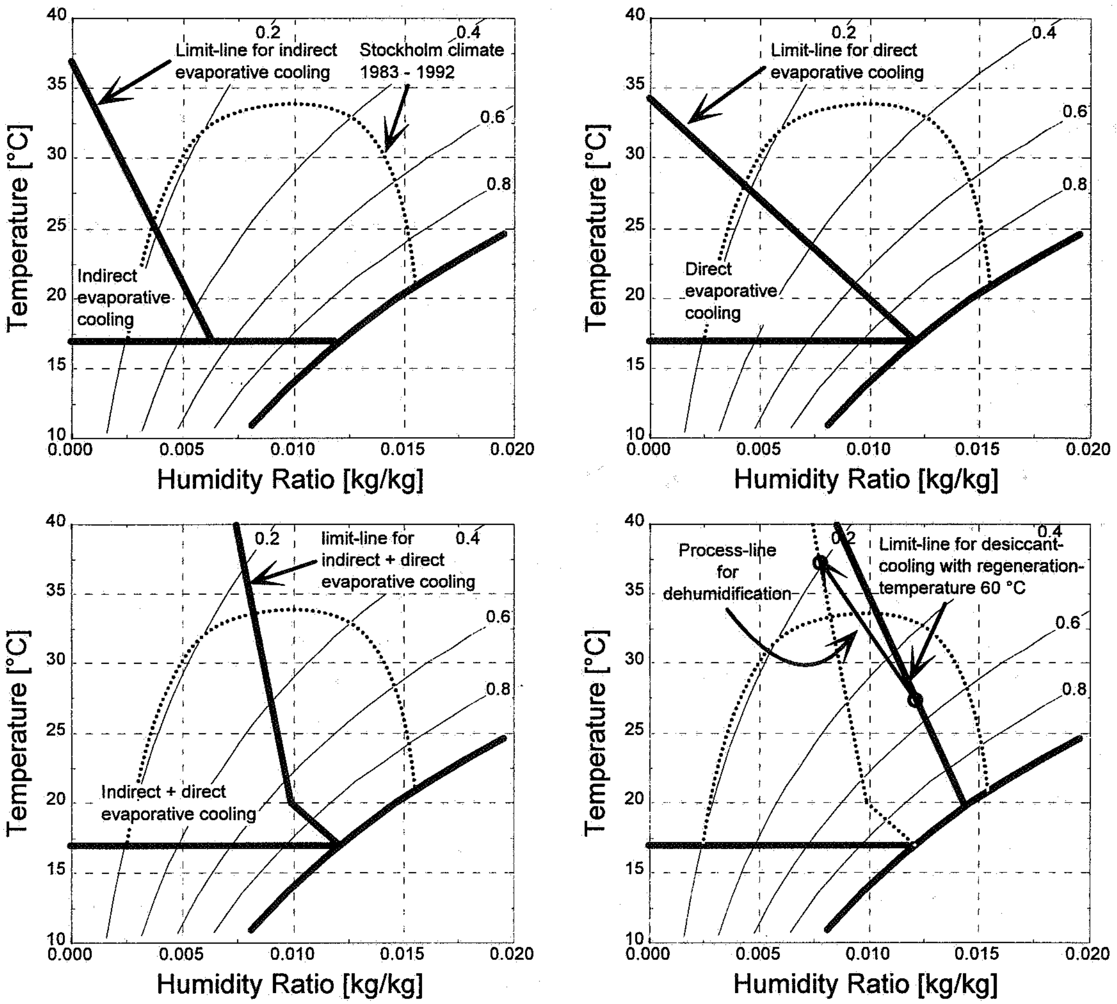


**Figure 3.** Limit-lines and psychometric areas.

The psychometric area of indirect evaporative cooling covers just a small part of the total area which describes the Stockholm climate in the psychometric chart. The corresponding psychometric area for direct as well as indirect + direct evaporative cooling covers a substantially greater part. The major part of the Stockholm climate area is covered by desiccant cooling, despite the regeneration temperature limit. There are, thus, limitations for all systems related to the ambient climate condition.

If climate data is available, for any location, it is possible to calculate the number of hours when the combination of ambient temperature and humidity is in each psychometric area. As an example, the Stockholm climate data is used. In this case the influence of different desired supply-air temperatures in between 14 and 18 °C has been studied. The number of hours when it is possible to reach a specific supply-air temperature, is shown in figure 4, i.e. the number of hours in each psychometric area. In this figure it is also possible to read the total number of hours, for an average year, when the ambient temperature is above the desired temperature.

In figure 4 it is shown that the ambient climate restricts the use of low supply-air temperatures when dimensioning an evaporative system in particular. By dehumidifying the ambient air this climatic restriction can be reduced.

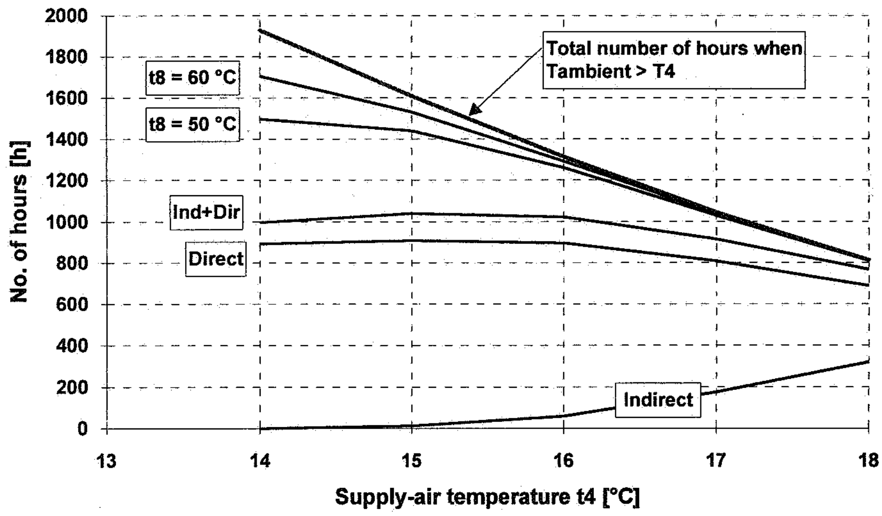


**Figure 4.** Number of hours when different evaporative and desiccant stages can be used to reach a specific supply-air temperature.

In this case it should be observed that the temperature referred to as supply-air temperature is the temperature of the air entering the supply-air fan. The magnitude of the temperature increase, when the air-stream passes the supply-air fan, is dependent on the dimensioning of the whole air-conditioning system, i.e. plant, selection of fan, duct-system, etc. This temperature increase is, in general, about 1 °C.

## 7. Ambient conditions and building's cooling load

The previously described psychometric areas can also be used for a rough estimation of the energy consumption for air-conditioning, using evaporative or desiccant cooling. If hourly values of the building's cooling load as well as ambient conditions are available, then the total energy demand can be calculated for each psychometric area. This information can then be used to estimate the energy consumption for air-conditioning, using evaporative or desiccant cooling.

As an example of this, a calculation of a building's hourly cooling load has been carried out. In this case the building model (Type56) in the simulation software TRNSYS has been used to calculate the hourly cooling demand for a base-case office building situated in Stockholm. A detailed description of this office building can be found in reference [2]. The internal sensible heat gain was defined as 12 W/m$^2$ during office hours (08 - 18), and 2 W/m$^2$ during night hours (18 - 08). The model was used to calculate the necessary sensible heat extraction rate to keep the room temperature below 24 °C day and night. Calculations were carried out with the same weather data as mentioned earlier, Stockholm 1983 - 1992. The maximum cooling load was calculated to be 22 W/m$^2$ during this 10 year period and the building's annual cooling demand was 24.6 kWh/m$^2$.

The cooling load was then calculated for each psychometric area. In figure 5, average values for the 10 year period are shown.

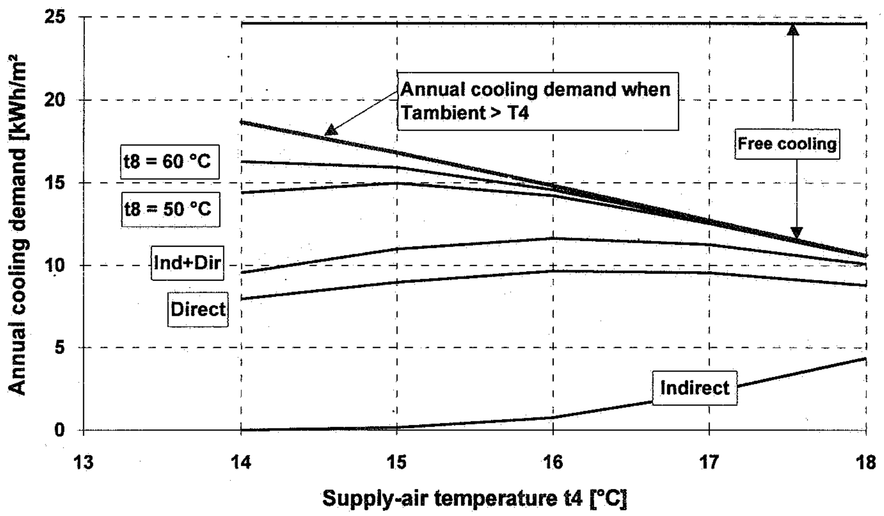


**Figure 5.** Annual cooling demand for a typical office building and the fraction possible to meet by evaporative or desiccant cooling.

The curves that describe the fraction of the building's total cooling demand possible to meet by evaporative or desiccant cooling, are shown in figure 5, and look similar to figure 4. The frequency of different ambient climate conditions, thus, has a great influence on this fraction.

## 8. Humidifying the supply-air stream

A commonly raised objection against using the direct humidifying stage, in an evaporative or desiccant plant, is that moisture would be added to the supply-air stream. This is expected to cause a worse indoor thermal climate. However, the maximum content of humidity in the supply-air, though, is restricted to saturated state at the prevailing temperature. In figure 6 is shown the maximum relative humidity that could occur in the room at different supply-air temperatures. This figure is valid for a room temperature of 24 °C and the internal moisture gain is specified by the *SHR*.

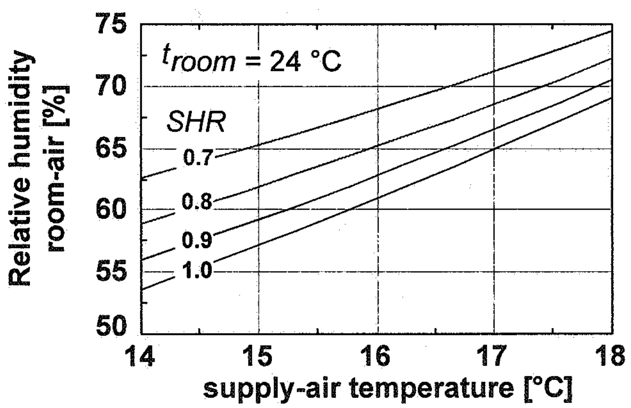


**Figure 6.** Relative humidity in the room-air when using a direct humidifying stage.

For a supply-air temperature of 15 °C, the maximum humidity content is 10.7 g/kg (100 % RH). If $SHR = 1$, the same absolute humidity would arise in the room-air, and for a room temperature of 24 °C the relative humidity would be 57 % RH. For $SHR = 0.8$, a supply-air temperature of 17.5 °C would give rise to a relative humidity of 70 % RH.

In this case, no consideration is taken to the temperature increase over the supply-air fan. This temperature rise would not influence the principal discussion regarding humidity in the room, though it would affect the sensible cooling load for the air-conditioning system.

## 9. Energy consumption

Use of the methodology described in this paper to discuss possibilities as well as limitations of evaporative and desiccant cooling technologies may increase the understanding of these processes. The methodology can also be used for a rough estimation of the energy consumption expected for air-conditioning when using evaporative or desiccant cooling. The expected number of hours in each psychometric area can be used to estimate the total energy consumption. The water consumption would be constant for each evaporative stage and the electricity consumption for the fans could be estimated with a value of specific fan power, *SFP*. The *SFP*-value, though, is dependent on the dimensioning of the whole air-conditioning system. It would also be possible to estimate the regeneration heat load by using limit-lines for different thermal coefficients of performance, $COP_{th}$. The $COP_{th}$ is in this case defined as the total heat extraction rate from the building divided by the necessary regeneration heat rate. These limit-lines would resemble the limit-lines for the regeneration temperature shown in figure 3. However, the total regeneration heat demand is still dependent on the number of hours when desiccant dehumidifying is necessary. In arid climates the cost for the regeneration may be of minor importance in some cases.

A common way of calculating the energy consumption for air-conditioning is to simulate the combined effects of building design, activities in the building and the outdoor climate. This seems to be the best way but the accuracy is always dependent on the used simulation models as well as inputs to the model and the control strategies, in particular. The calculated result would, to a great extend, be dependent on the used control strategy if settled without taking the physical limitations into consideration.

It is also important to take the physical limitations into consideration when comparing evaporative or desiccant cooling to, for example, a conventional compressor refrigeration system. In the conventional system there is usually no limitation regarding supply-air temperatures possible to reach. Different control strategies may be necessary in order to carry out an objective comparison of total energy consumption. Preference of the system chosen is, in the end dependent on the local prices of water, electricity and heat.

## References


[1] ASHRAE Handbook, 1993 Fundamentals , Chapter 8 and 26,
American Society of Heating, Refrigeration and Air-conditioning Engineers, Atlanta

[2] Nilsson Per-Erik "Heating and cooling requirements in commercial buildings"
Document D27:1994, Department of Building Services Engineering
Chalmers University of Technology, Sweden

eenvoudige paper
met ontwerpregels voor
architecten !!

van buiten te
kennen !

# VENTILATION AND COOLING

18TH ANNUAL AIVC CONFERENCE
ATHENS, GREECE, 23-26 SEPTEMBER, 1997

## Macroscopic Formulation and Solution of Ventilation Design Problems

no CFD,
but modes

STATIC → no heat capacity !

James W. Axley

Alles bekeken vanuit de
vraag: "Wat is de oppvl.
van de ramen"?

School of Architecture
Yale University
New Haven, Connecticut, USA
james.axley@yale.edu

## Synopsis

This paper will present a general approach that may be used to solve natural ventilation design problems typically addressed at the preliminary design stage – How wide should windows be opened in a given building for wind-driven cross ventilation on a moderate summer day? How should a ventilating monitor be configured to mitigate internal and solar gains on the same summer day? Established macroscopic equations governing airflow and heat transfer in multizone building systems will be reformulated to place airflow component characteristics – e.g., size of window opening, speed of a ventilating fan, or height of a monitor window – as key design parameters to be adjusted, selected, or in the special case of optimization, to be optimized. The resulting equations will establish constraints that must be placed on these design variables to guarantee the satisfaction of mass, momentum, and energy conservation. To these constraints, constraints relating to thermal comfort will be formulated in terms of the design parameters. It will be shown that together the conservation and comfort constraints serve to unambiguously define combinations of design parameters that are technically feasible – from these an optimal combination may be sought. The general approach will be applied to simple cases of cross ventilation and stack ventilation to demonstrate the utility of the approach.

## List of Symbols

Variables

- $A$ area of window opening ($m^2$)
- $[A]$ airflow coefficient matrix
- $\{B\}$ vector of buoyancy effects
- $c_p$ heat capacity of air, constant pressure ($J \cdot kg^{-1} \cdot {}^\circ K^{-1}$)
- $C_i$ concentration of species "$i$"
- $C_d$ orifice opening discharge coefficient; typically $\approx 0.60$
- $C_p$ wind pressure coefficient
- $[C]$ thermal capacitance matrix
- $\{E\}$ thermal excitation vector
- $f(u,v\ldots)$ function of $u,v,\ldots$)
- $g$ the acceleration of gravity ($m \cdot s^{-2}$)
- $[K]$ thermal conductance matrix
- $\dot{m}$ air mass flow rate ($kg \cdot s^{-1}$)
- $M$ (effective) molecular weight of dry air $\approx 28.97\ g \cdot mol^{-1}$
- $p$ pressure (Pa)
- $q_{gain}$ total cooling load (W)
- $R$ universal gas constant ($J \cdot {}^\circ K^{-1} \cdot mol^{-1}$)
- $RH$ relative humidity
- $t$ time (s)
- $T$ temperature (°C)
- $v$ air velocity vector ($m \cdot s^{-1}$)
- $x, y, z$ spatial coordinates (m)
- $\Delta z$ stack height (m)
- $\phi$ design parameter
- $\rho$ air density ($kg \cdot m^{-3}$)
- $\hat{\rho}$ spatial average air density (1.2 $kg \cdot m^{-3}$ is sufficiently accurate here)
- $\Sigma UA$ the sum of building conductances ($m^2 \cdot {}^\circ K \cdot W^{-1}$)

Subscripts & Marks

- $i$ associated with zone "$i$"; indoor zone
- $j$ associated with a specific point
- $k$ associated with a region
- $l$ associated with an airflow path
- $n$ associated with a surface
- $o$ associated with outdoor conditions
- $db$ dry bulb temperature
- $mrt$ mean radiant temperature
- $eff$ effective
- $res$ CIBSE dry resultant temperature
- $\hat{u}$ spatial average of $u$

## 1. Introduction

Advances made in methods to predict and measure building airflows have truly revolutionized the fields of building ventilation and air quality research and practice in the past two decades. Tracer gas techniques have been extended and refined to allow more accurate, better characterized, and more complete multizone measurements of airflows within buildings. A variety of rigorously defined ventilation effectiveness metrics have grown out of these advances and have placed ventilation system evaluation on a solid objective basis. Building pressurization techniques have been improved and extended to allow field measurement of building envelope, zone and component leakage air flow characteristics providing a more complete understanding of infiltration airflow paths in buildings and mathematical models to simulate them. Macroscopic methods of airflow analysis have been generalized to allow integrated modeling of wind-driven, buoyancy-driven, and mechanically-forced airflow in multizone building systems of arbitrary complexity. The global predictive capability of macroscopic simulation methods have been complimented by a constellation of microscopic methods of analysis, together placed under the more familiar rubric of Computational Fluid Dynamics, that allow investigation of the details of airflow around buildings and within single and, at this point, simply and well-connected collections of two or three rooms.

Consequently, we presently find ourselves armed with a veritable arsenal of tools to evaluate the thermal comfort, air quality and energy conservation efficacy of existing and proposed building ventilation systems that should, we hope, lead to improvements in building design, renovation, and operation. Yet, ironically, we have yet to develop tools to directly answer simple design questions relating to building ventilation: How wide should windows be opened in a given building for wind-driven cross ventilation on a moderate summer day? How should a ventilating monitor and building windows be configured to mitigate internal and solar gains on the same summer day? What size fan is needed to assist stack-driven air flow through the monitor on a more extreme summer day?

This paper seeks to address this problem.

## 2. Approach

A building system may be considered to be a three-dimensional continuum within which the *state variables* of temperature $T$, pressure $p$, air velocity $v$, and concentration $C_i$ vary in space, x, y, z, and in time, $t$.

*State Variables* $\quad T(x,y,z,t),\ p(x,y,z,t),\ v(x,y,z,t),\ C_i(x,y,z,t)$

The variation of these state variables is governed, fortunately, by fundamental mass, momentum, and energy conservation principles – bound by environmental and thermal/mechanical/chemical boundary conditions – that allow prediction of the spatial and temporal variation of these state variables. Broadly speaking, two numerical approaches are commonly used for this prediction:

- *Microscopic analysis*, based typically on finite difference or finite element techniques, approximates the continuously defined state variables by a finite set of spatially discrete but temporally continuous state variables defined at or associated with discrete (mesh) points "$j$" within the continuum:

  *Microscopic Discretization* $\quad T(x_j,y_j,z_j,t),\ p(x_j,y_j,z_j,t),\ v(x_j,y_j,z_j,t),\ C_i(x_j,y_j,z_j,t)$

  Room airflow analysis using computational fluid dynamics techniques and conduction heat transfer and moisture transfer analysis using finite element or finite difference methods are the most familiar examples of microscopic analysis used today for building performance evaluation.
- *Macroscopic analysis,* based on idealizing the building system as a collection of one or more control volumes linked by discrete heat or mass transport paths, also approximates the continuously defined state variables by a finite set of spatially discrete but temporally continuous state variables but now the discrete state variables are associated with either the

control volumes or discrete transport paths – i.e., discrete regions rather than geometric points within the continuum:

*Macroscopic Discretization* $T_k(t),\ p_k(t),\ \dot{m}_k(t),\ C_{i,k}(t)$

Here the subscript $k$ is used to identify the discrete region – the control volume or discrete transport path – as, for example, well-mixed zones, 1D heat transfer paths through walls, windows, and floors, and airflow through doors, windows, cracks, etc. Macroscopic analysis applies the conservation principles to the discrete regions idealized as control volumes within the building system and thereby forfeits the ability to predict the spatial detail within these control volumes. Importantly, air velocity is simply replaced by predictions of total air mass flow rate through discrete air flow paths – air velocity is not directly predicted.

Multizone building energy simulation, multizone indoor air quality analysis, and component-based approaches to HVAC system simulation are the familiar examples of macroscopic analysis used today for building performance evaluation.

In principle, these same state variables also determine the "state" of thermal comfort and air quality within the habitable portions of the building system – i.e., given the metabolic activity, clothing level, chemical sensitivity, etc. of occupants – however, the exact relation between these state variables and the state of thermal comfort and air quality is not presently understood with theoretical certainty. Nevertheless, a variety of semi-empirical thermal comfort indices have been developed over the years (see [1] for an overview) that relate thermal comfort to the primary comfort variables of dry bulb air temperature $T_{db}$, mean radiant temperature $T_{mrt}$, air velocity $v$, and relative humidity $RH$ within rooms:

*Primary Comfort Variables* $T_{db}(x,y,z,t),\ T_{mrt}(x,y,z,t),\ v(x,y,z,t),\ RH(x,y,z,t)$

Microscopic methods of analysis provide the means to predict these comfort variables and, importantly, their spatial variation within rooms – air dry bulb temperature and velocity are directly predicted while mean radiant temperature and RH distributions may be easily computed at each of the room air mesh points from computed surface temperatures and vapor-phase water concentrations respectively. As a result, microscopic analytical evaluation of comfort in rooms has become one of the primary applications of computational fluid dynamics (see, for example, [2, 3]). In spite of the direct utility of the microscopic approach to thermal comfort prediction, several limitations must be noted:

- microscopic analysis is presently limited to single or simply connected multiple rooms of relatively simple geometry; whole building system analysis is beyond the current capability of microscopic analysis,
- microscopic analysis is expensive due to the special expertise needed to implement it, the time necessary to formulate, solve, and evaluate the results from microscopic analysis, and the fact that it is computationally demanding; for this reason it remains a research tool in North America and is very seldom applied in practice, and
- microscopic analysis presently supports only a trial and error approach to building design.

How about macroscopic analysis? Macroscopic methods can provide an economic and accessible means to predict simple measures of thermal comfort within rooms (e.g., spatially averaged room air dry bulb temperature, mean radiant temperature, air velocity, and relative humidity) although, in North America, these methods are most commonly used to predict annual and peak energy demands of heating and cooling systems in buildings instead. While they can not provide the spatial detail offered by microscopic analysis, macroscopic methods can be readily applied to whole building systems and configured to allow an integrated consideration of interacting building systems – e.g. heat transfer in the building fabric and envelope, HVAC systems, lighting systems, and natural ventilation systems. As in the microscopic case, however, these methods have been formulated to support only a trial and error approach to building design, although in the most current examples this design approach has been expedited via automated comparative analysis and augmented with design rules of thumb [4].

Here we will take a more direct approach to design. Macroscopic conservation equations governing airflow and heat transfer in multizone building systems will be used to establish the relation between system response and key design parameters associated with discrete airflow paths – e.g., size of window opening, speed of a ventilating fan, or height of a monitor window. Using one of a number of comfort metrics, a second relation will be generated to establish the link between the comfort index and the design parameters. Finally, a comfort criteria will be applied to identify combinations the design parameters that are feasible from a comfort point of view. In some instances it may also prove useful to add an *objective function* to narrow the selection of feasible design parameters to an "optimal" choice.

### *1.1. Mass & Energy Conservation*

To begin, consider a building system idealized as a collection of well-mixed zones – not a necessary limitation of the approach, simply a convenience here – linked by discrete air flow paths and conductive heat transfer paths:

General case

difficult

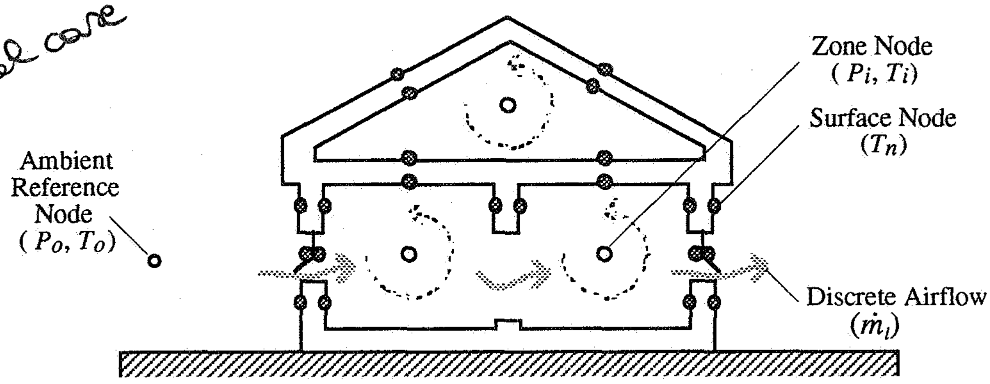


Fig. 1 Simplified representation of a multizone building idealization.

Macroscopic discrete state variables of pressure and temperature, $p_i$ and $T_i$, will be associated with each of the zones – i.e., the pressure associated with a specific elevation within the zone identified above by "zone nodes" and the temperature associated with the spatial mean air temperature within the zone. Similarly, an outdoor ambient reference node will be associated with ambient pressure and temperature, $p_o$ and $T_o$. Surface temperature variables, $T_n$, will be associated with the surfaces of each of the several conductive heat transfer paths within the building system and, finally, the mass flow rate of air, $\dot{m}_l$, through each of the several discrete airflow paths will be identified.

With these variables defined, one may apply mass and energy conservation principles to form systems of equations governing heat transfer and airflow in the building system (refer to [5-7] for details):

*Heat Transfer:* $$[K]\{T\} + [C]\frac{d\{T\}}{dt} = \{E\} \quad (1)$$

*Airflow:* $$[A]\{p\} = \{B\} \quad (2)$$

where:

- $\{T\}$ is a vector of zone and surface temperatures
- $\{E\}$ is the system "excitation vector" that accounts for thermal energy gains at each of the system nodes,
- $[K]$ is the system "conductance matrix" that is assembled from component or element conductances (i.e., $UA$ terms for conductive transfer paths) and from airflow

contributions (i.e., the product of the air mass flow rate and heat capacity, $\dot{m}\hat{c}_p$, for discrete airflow paths),

$[C]$ is the system "capacitance matrix" that is assembled from component or element contributions to the thermal capacity associated with each temperature node,

$\{p\}$ is a vector of zone pressures,

$[A]$ is the system airflow coefficient matrix assembled from the pressure-flow characteristics of the discrete airflow paths, and

$\{B\}$ is a vector associated with buoyancy effects.

Solution of Equation 1 directly yields predictions of system temperatures $\{T\}$. The determination of air mass flow rates is less direct – one first solves Equation 2 for the zonal pressures $\{p\}$ then uses these solutions along with the individual discrete airflow path pressure flow relations to determine specific air mass flow rates, $\dot{m}_l$.

As written, these equations appear to be two systems of uncoupled linear equations but, in the usual case, they are in fact rather complex coupled systems of nonlinear equations. Specifically, the system airflow coefficient matrix is most often nonlinearly dependent on the state of pressures in the system, $[A] = [A(\{p\}]$; the buoyancy effects vector is dependent on zone temperatures, $\{B\} = \{B(\{T\})$; and the system conductance matrix and excitation vector are both dependent on the air mass flow rates $\dot{m}_l$ which, in turn, are dependent on both the system temperature and pressure vectors via the dependencies just noted for $[A]$ and $\{B\}$.

The individual pressure-flow relations for the discrete flow paths are generally nonlinear but, nevertheless, depend on key design parameters, $\phi_l$, of the flow path (e.g., size of window opening, speed of a ventilating fan, or height of a monitor window). That is to say, the mass flow rate of air through a given "$l$" discrete flow path is related to the zonal pressures the path links, say $p_i$, $p_j$ and the design parameters:

$$\dot{m}_l = f(p_i, p_j, \phi_l) \tag{3}$$

Combining Equations 1, 2 and 3, one may, in principle, establish a relation between the system response (i.e., system temperatures and airflow rates) and the design parameters. In most practical situations, however, it will not be possible to establish this relationship formally as the combined system of equations will be hopelessly complex. Consequently, it will be necessary to establish the relation numerically by systematically varying key design parameters over a range of reasonable values and solving for the system response – i.e., for a given building and ambient and operating conditions. Whether formally or numerically derived, one may establish the relation between system response and the key design parameters for a given design problem:

$$\{T\} = \{f_T(\phi_l)\} \tag{4}$$

$$\{\dot{m}\} = \{f_{\dot{m}}(\phi_l)\} \tag{5}$$

### *1.2 Comfort Metrics and Criteria*

A number of comfort indices could be considered. Here we'll limit consideration to two – room dry bulb temperature $T_{db}$ and the CIBSE dry resultant temperature $T_{res}$ – see [1] for a complete discussion of these and other comfort indices.

As noted above, macroscopic analysis forfeits spatial detail for numerical economy so we'll accept predictions of zone air temperature as a spatial average estimate of room dry bulb temperature for a given zone "$i$":

*Metric 1:*
$$\hat{T}_{db} \approx T_i \tag{6}$$

The CIBSE dry resultant temperature is defined in terms of the room dry bulb temperature, mean radiant temperature $T_{mrt}$, and air velocity $v$. Again we'll accept spatial average approximations. An area weighted average of computed surface temperatures will be taken as the spatial average of the mean radiant temperature in a given zone:

$$\hat{T}_{mrt} \approx \frac{\sum_{\text{zone i}} A_n T_n}{\sum_{\text{zone i}} A_n} \tag{7}$$

For room air velocity, we may estimate the spatial average velocity $\hat{v}_l$ at a discrete flow path "$l$" as:

$$\hat{v}_l \approx \frac{\dot{m}_l}{\hat{\rho} A_l} \tag{8}$$

where:

$\hat{\rho}$ is, technically, the spatial average of the air density along the flow path but accuracy here is not important,

$A_l$ is the cross sectional area of the flow path

Here, we must be careful in the application of this approximation. At or in the "throw" of a ventilation opening, Equation 8 should provide a reasonable approximation of air velocities; away from the opening ventilation-driven velocities may diminish rapidly.

With these approximation in hand, the CIBSE dry resultant temperature may be defined as follows:

*Metric 2:*

$$\hat{T}_{res} \approx \begin{cases} 0.5\left(\hat{T}_{mrt} + \hat{T}_{db}\right) & ; \ \hat{v} \le 0.1 \ m/s \quad \textit{"still air"} \\ \left(\hat{T}_{mrt} + \hat{T}_{db}\sqrt{10\hat{v}}\right) \Big/ 1 + \sqrt{10\hat{v}} & ; \ \hat{v} > 0.1 \ m/s \end{cases} \tag{9}$$

We'll place simple limits on the first measure of comfort to establish a comfort criteria:

*Criteria 1:*

$$20\,°C \le \hat{T}_{db} \le 26°C \tag{10}$$

For the dry resultant temperature metric, CIBSE recommends $T_{res}$ = 20 °C for "still air" conditions in offices and provides a corrective increase in temperatures for air speeds greater than 0.1 m/s that may be approximated by $2.74\sqrt{\hat{v} - 0.1}$ °C. Thus the CIBSE comfort criteria for offices may be represented as:

*Criteria 2a:*

$$20\,°C \le \hat{T}_{res} \le 20\,°C + 2.74\sqrt{\hat{v} - 0.1} \tag{11}$$

In addition CIBSE recommends limiting air velocities to 0.3 m/s except in summers. Based on recent work of Arens and his colleagues [8] we'll add to the CIBSE criteria, Equation 11, an upper (summer) limit on air velocity of 1.5 m/s:

*Criteria 2b:*

$$\hat{v} \le 1.5 \ m/s \tag{12}$$

Note, we have not included RH humidity in our considerations. The CIBSE comfort criteria apply for relative humidities between 40 and 70%, consequently the applications to follow should be practically useful within this range. By adding system equations that allow a prediction of room RH to the above heat transfer and airflow equations – Equations 1 and 2 – and including additional comfort criteria for RH, however, the basic approach taken may be easily extended to include this important aspect of comfort.

### *1.3 Feasible & Optimal Design Configurations*

By combing the system response results developed in terms of the key design parameters, indicated functionally by Equations 4 and 5, with one of the comfort metrics, Equation 6 or 9, we may establish the relation between the comfort index and the design parameters. It is useful to think of this relation geometrically as a comfort index surface defined relative to the key design parameters – the "design space". The comfort criteria presented above also define surfaces in the "design space." The intersection of the comfort index surface and comfort criteria surface defines, rather unambiguously, combinations of the key design parameters that are technically feasible. If then we can define some objective function in terms of the key design parameters, we can search through the feasible combinations of design parameters to find an optimal configuration. The examples presented below should made this distinction between feasible and optimal clear and reveal the procedures used to evaluate them.

Optimization is a tempting objective yet the definition of a reasonable objective function may not be obvious nor have the technical rigor associated with the approach presented above to determine feasible solutions. Knowledge of a range of feasible configurations is likely to be of the greatest value to the building designer anyway, as the designer is invariably searching for design configurations in a far more complex "design space" that given by the ventilation problem – e.g., for windows, in addition to thermal comfort, the designer must consider an array of functional considerations such as daylighting and view potential, economic and constructional constraints, as well as more "formal" issues relating to planning strategies, spatial character and composition and detail of the building's facade.

## 3. Applications

In this section we'll apply the approach presented above to two relatively simple cases – wind-driven cross-ventilation and stack-ventilation of a simple single-zone building under steady-state conditions of heat transfer.

### *3.1 Wind-Driven Cross Ventilation of a Single Zone Building*

Consider a simple single-zone model of a building ventilated by wind-driven cross-ventilation:

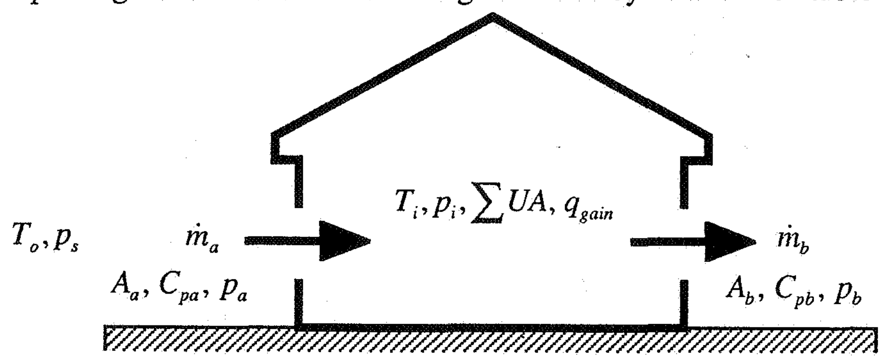


Fig. 2 Single-zone cross-ventilated building idealization and variables.

A steady wind, characterized by a stagnation pressure $p_s$, approaches the building from the left as air passes through a window "$a$" of cross sectional area $A_a$ and out through window "$b$" of cross sectional area $A_b$. $A_a$ and $A_b$ will be taken as the key design parameters that will be adjusted to achieve thermal comfort. Wind pressure coefficients at the windows $C_{pa}$ and $C_{pb}$; building conductances $\sum UA$; internal gains $q_{gain}$; and outdoor air temperature $T_o$ are assumed known a priori. Two unknown state variables are associated with this simple idealization – the zone air temperature $T_i$ and the zone pressure $p_i$ defined relative to a specific elevation which, here, will be taken along the horizontal centerline through the two windows.

With the problem thus defined, we can form the heat transfer system equations by demanding conservation of thermal energy (as experienced analyst we recognize kinetic energy and pressure work terms associated with the flow will be negligible in comparison to the uncertainty in the thermal energy terms):

$$\textit{Heat Transfer:} \qquad \sum UA\left(T_i - T_o\right) + \left(\hat{c}_p\dot{m}_bT_i - \hat{c}_p\dot{m}_aT_o\right) = q_{gain} \tag{13a}$$

or in the form of Equation 1 above:

1 kW
+ solar gains
+ ...

$$KT_i = E \quad with \quad K = \left(\sum UA + \hat{c}_p \dot{m}_b\right) \quad and \quad E = q_{gain} + \left(\sum UA + \hat{c}_p \dot{m}_a\right) T_o \tag{13b}$$

We'll model the airflow through the windows using the familiar orifice equation as it has proven (and continues to be proven [9]) to be a reliable model:

$$m_a = C_d A_a \sqrt{2\rho(p_a - p_i)} \quad and \quad m_b = C_d A_b \sqrt{2\rho(p_i - p_b)} \tag{14}$$

and estimate the wind pressures acting at each of the windows using the approach wind stagnation pressures and appropriate wind pressure coefficients, $C_{pa}$ and $C_{pb}$, although here more research is needed to provide proper estimates of these pressure coefficients as the size of the window openings increase the porosity of the building [10]:

$$p_a = C_{pa} p_s \quad and \quad p_b = C_{pb} p_s \tag{15}$$

With these relations in hand we may demand the conservation of air mass flow and form the system airflow equations for the problem:

*Airflow:*

$$\dot{m}_a - \dot{m}_b = 0 \tag{16a}$$

$$C_d A_a \sqrt{2\rho(C_{pa} p_s - p_i)} - C_d A_b \sqrt{2\rho(p_i - C_{pb} p_s)} = 0 \tag{16b}$$

In this case, the airflow equations are uncoupled from the heat transfer equations and thus we may directly solve for the airflow rates:

$$\dot{m}_a = \dot{m}_b = C_d \sqrt{\frac{A_a^2 A_b^2}{A_a^2 + A_b^2}} \sqrt{2\rho p_s (C_{pa} - C_{pb})} \tag{17}$$

Substituting this solution into the system heat transfer equation, Equation 13, we may solve for the zone air temperature in terms of the design parameters $A_a$ and $A_b$:

$$T_i = \frac{q_{gain}}{\hat{c}_p C_d \sqrt{\frac{A_a^2 A_b^2}{A_a^2 + A_b^2}} \sqrt{2\hat{\rho} p_s (C_{pa} - C_{pb})} + \sum UA} + T_o \tag{18}$$

Note the first square root term in the denominator defines, an equivalent single orifice opening $A_{eff}$ that plays a key role in these equations. For a series of openings in cross-ventilation flow, we may generalize the result ~~defined by Equation 18~~ by replacing this term with this effective orifice opening defined as ~~(after Flourentzou, 1996 #1314)~~:

$$\left(\frac{1}{A_{eff}}\right)^2 = \sum \left(\frac{1}{A_i}\right)^2 \tag{19}$$

Zeer bel. vgl!

Given the form of this expression, it becomes clear that the smallest opening in the series will tend to control the airflow.

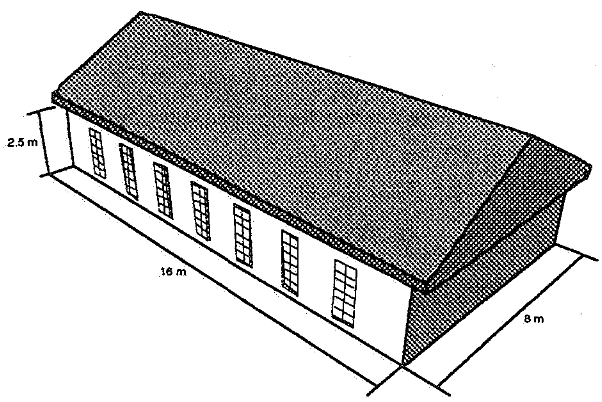


Fig. 3 Representative building for application of approach.

To better understand the character and use of Equation 18, consider the representative single story building illustrated above. With R20 (3.5 $m^2 {}^\circ K/W$) wall insulation, R30 (5.3 $m^2 {}^\circ K/W$) roof insulation, and R4 (0.7 $m^2 {}^\circ K/W$) windows the total building conductance of the envelope is $\Sigma UA = 71.1$ W/°K. For combined solar and occupant generated internal gains of 4 W/$ft^2$ (43 W/$m^2$) the total internal gain is $q_{gain} = 5{,}504$ W. Finally, an approach wind stagnation pressure of $p_s = 15$ Pa (corresponding to an approach wind velocity of 5 m/s or 11 mph), an outdoor air temperature of $T_o = 20$ °C, and wind pressure coefficients of $C_{pa} = 0.8$ and $C_{pb} = -0.7$ will be assumed and reasonable values will be assigned to the discharge coefficient ($C_d = 0.6$) and the average air density and heat capacity ($\hat{\rho} = 1.2$ kg/$m^3$ and $\hat{c}_p = 1{,}004$ J/kg-°K).

Substituting these values in Equation 18, the response becomes specific and may be plotted as shown below:

$$T_i = \frac{5{,}504\ W}{4{,}409\sqrt{\frac{A_a^2 A_b^2}{A_a^2 + A_b^2}}\ W/{}^\circ K + 71.1\ W/{}^\circ K} + 20\ {}^\circ C \tag{20}$$

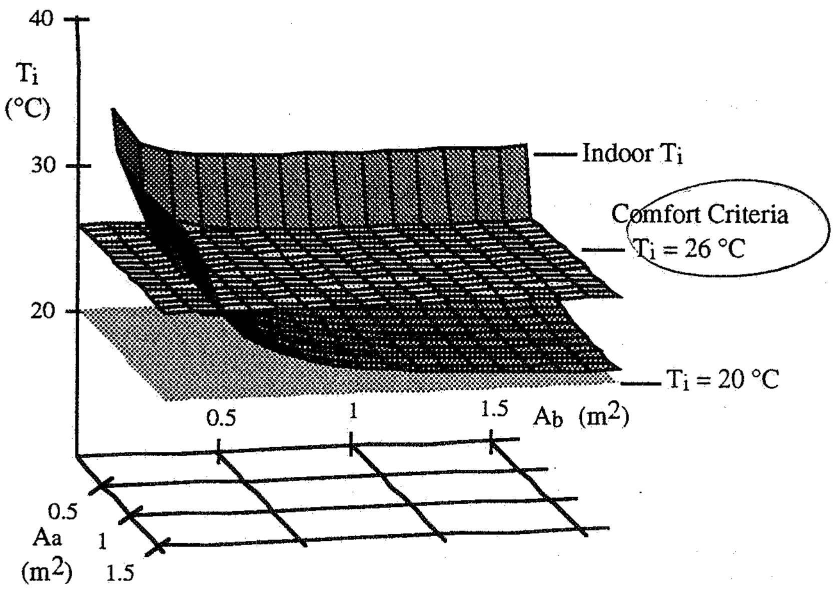


Fig. 4 Indoor air temperature response and comfort criteria for the representative building using cross ventilation with an approach wind velocity of 5 m/s.

As expected, the indoor air temperature response asymptotically approaches the outdoor air temperature for large window openings.

*Comfort Metric and Criteria 1*

The simple room air temperature comfort criteria defined by Equation 10 is also plotted on Figure 4 – simple horizontal planes corresponding to the upper and lower bounds of the comfort criteria, 26 °C and 20 °C. The intersection of the upper bound comfort criteria surface and the indoor temperature response - here, taken as the comfort index – then, establishes the minimum feasible combinations of window openings needed to achieve thermal comfort. This intersecting curve - the feasible solution curve for $T_i = 26$ °C - is plotted below as a solid line along with a more moderate feasible solution curve for $T_i = 23$ °C plotted as a dotted line:

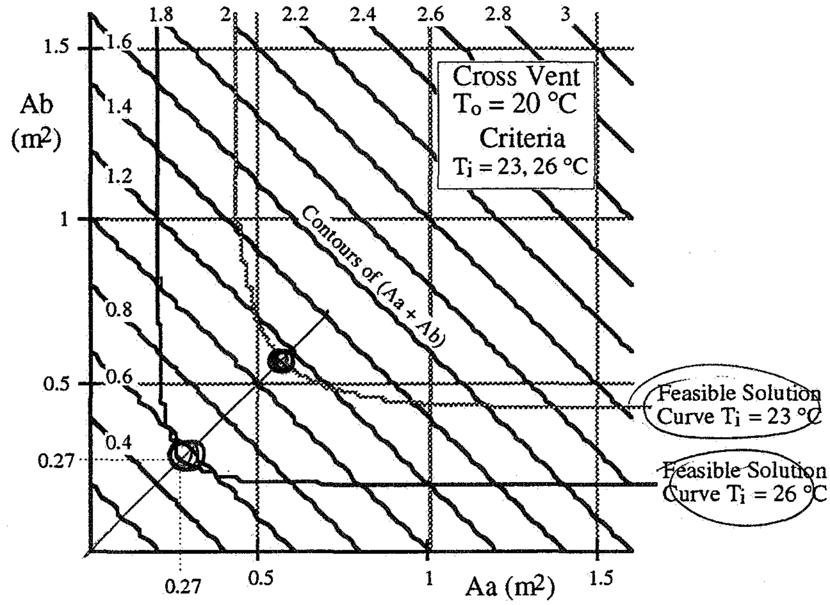


Fig. 5 The curve of feasible combinations of window openings for the cross-ventilation design problem for the simple air temperature comfort metric.

Using these curves, the building designer could select any number of window opening combinations to achieve a thermal comfort objective. For example, a combination of a 1 m$^2$ windward window opening, $A_a$, and a 0.20 m$^2$ leeward window opening, $A_b$, would achieve the 26 °C comfort objective while to achieve the 23 °C comfort objective with the same windward window opening, the leeward opening would have to approximately doubled to $A_b \approx 0.40$ m$^2$. Guided by a feasible solution curve, a building designer could attempt to meet other design objectives while maintaining a given thermal comfort objective without being constrained to a specific "optimal" solution.

Nevertheless, in some instances it may also be possible to establish an minimization objective that would allow the designer to narrow the search to a specific "solution." As a demonstration of this, consider the objective to minimize the sum of the window openings, $(A_a + A_b)$, possibly in an effort to minimize cost. Contours of equal values for this *objective function* are also plotted on Figure 5. Given the simplicity of this objective function and the fact that feasible solution curve, Equation 18, is symmetric about the line $A_a = A_b$, the minimum (or optimal) solution is obtained when $A_a = A_b$ which for the specific case at hand is $A_a = A_b = 0.27$ m$^2$. In the complex and rich world of architectural design, this particular objective function may or may not have much merit.

*Comfort Metric and Criteria 2* nieuwe comfort T°

With the general approach established by ~~this first example~~, we may move on to the far more complex case of utilizing the CIBSE dry resultant temperature comfort index, Equation 9, and the associated comfort criteria, Equation ~~11. We'll limit~~ consideration to conditions just inside the windward window where mean air velocities may be estimated, by Equation 8, as:

$$\hat{v} = \frac{m_a}{\hat{\rho} A_a} = C_d \sqrt{\frac{2\, p_s}{\rho} \frac{A_b^2 (C_{pa} - C_{pb})}{(A_a^2 + A_b^2)}} = 3.67 \sqrt{\frac{A_b^2}{(A_a^2 + A_b^2)}} \ \ m/s \qquad (21)$$

Using this result, the specific solution Equation 20, and the strategy outlined above to estimate the spatial average mean radiant temperature we may establish the relation between the dry resultant temperature and the design parameters – the window openings $A_a$ and $A_b$. For even this simple case, however, the algebra becomes formidable. Using a computational symbolic math processor the result below was obtained:

$$
\hat{T}_{res} = \begin{cases} 0.98\left[\dfrac{5500}{4409\,A_{eff} + 71.1} + 20\right] + 0.27 \;\; ; \;\; 3.67\dfrac{A_{eff}}{A_a} - 0.1 < 0 \\[2ex] \dfrac{0.96\left[\dfrac{5500}{4409\,A_{eff} + 71.1} + 20\right] + \left[\dfrac{5500}{4409\,A_{eff} + 71.1} + 20\right]\sqrt{36.7\dfrac{A_{eff}}{A_a}} + 0.53}{\sqrt{36.7\dfrac{A_{eff}}{A_a}} + 1} \;\; ; \;\; 3.67\dfrac{A_{eff}}{A_a} - 0.1 \geq 0 \end{cases}
$$

Plotting this result along with the CIBSE comfort criteria presented above we again obtain two intersecting surfaces that define the technically feasible design combinations that will achieve the thermal comfort objective. Two cases are plotted below – the first places no limit on indoor air velocity and the second places an upper limit of 1.5 m/s (i.e., as discussed above).

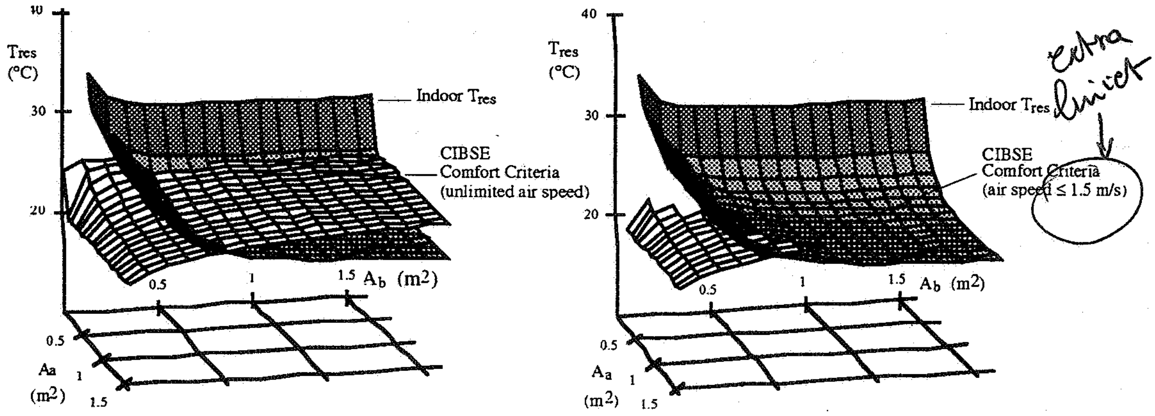


Figure 6. CIBSE dry resultant temperature response and comfort criteria for the representative building for cross ventilation with an approach wind velocity of 5 m/s.

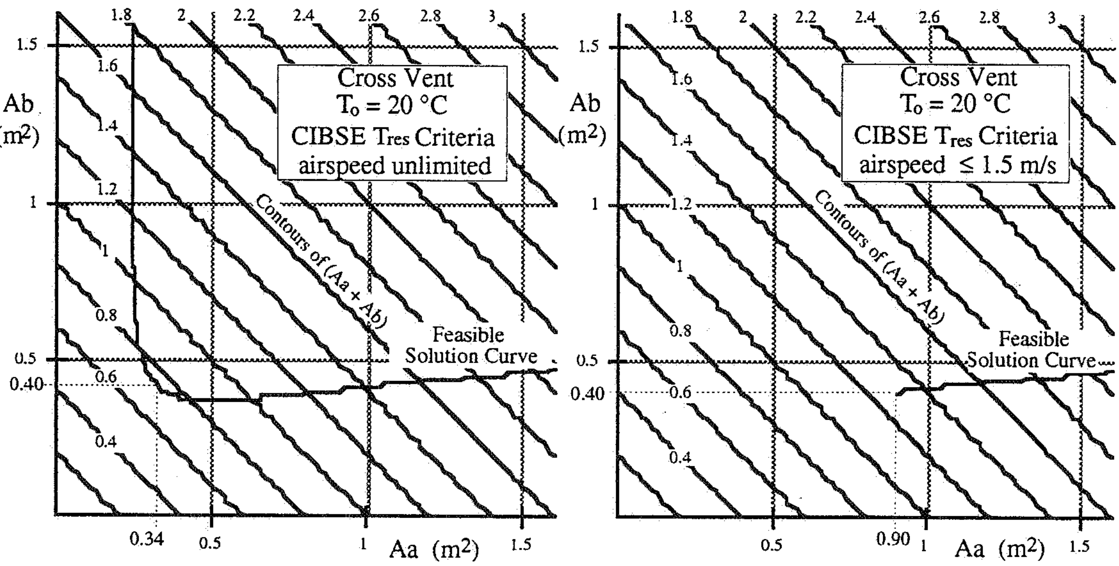


Fig. 7 Curves of feasible combinations of window openings for the cross-ventilation design problem for the CIBSE dry resultant temperature comfort metric.

With this more complete comfort metric the response and comfort criteria surfaces are geometrically more complex, but have the same general features found using the simpler comfort metric. The intersection of the response and comfort surfaces are, however, significantly different – the limit on indoor air speed quite literally limits the intersection of these curves. These intersections, again define the technically feasible combinations of window openings that may be used to achieve the comfort objective. They are plotted in Figure 7 for the two limits placed on indoor air speed.

In the unlimited indoor air velocity case, the feasible solution curve is seen to be similar to that obtained for the simpler comfort metric – falling, interestingly, between the feasible solution curves for $T_i = 23$ and 26 °C – but now it is no longer symmetric about the $A_a = A_b$ line. Consequently, if we apply the same objective function to minimize total window opening area (note the contours on these plots again) we'll obtain an "optimal" solution of $A_a = 0.34$ m$^2$ and $A_b = 0.40$ m$^2$ – a slight bias toward a larger leeward window opening, a position that has been presented as a cross ventilation design guideline [11]. On the other hand, if indoor air velocities are limited, all feasible solutions and the "optimal" least area solution ($A_a = 0.90$ and $A_b = 0.40$, as shown above) involve configurations where the windward opening is significantly greater than the leeward. That is to say, for this particular building case, inlet air velocities must be limited by increasing the resistance to flow at the leeward window(s) to satisfy the 1.5 m/s limit place on indoor air velocities.

### *3.2 Stack Ventilation of a Single Zone Building*

Consider, now, a similar simple single-zone model utilizing a stack ventilation strategy:

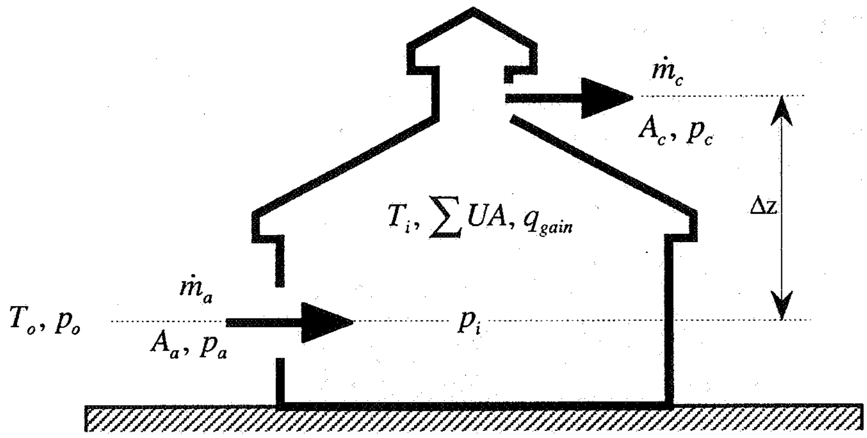


Fig. 8 Single-zone stack-ventilated building idealization and variables.

Again, air enters a window opening $A_a$, but now exits at a higher opening $A_c$ located a distance $\Delta z$ above the lower opening. These three variables – $A_a$ , $A_c$ , and $\Delta z$ – will be taken as the key design parameters that will be adjusted to achieve thermal comfort in this case. All other variables will be defined as before. The ambient pressure $p_o$ and the indoor pressure $p_i$ are defined here relative to the same elevation.

Again, heat transfer system equations may be formed by demanding the conservation of thermal energy:

$$\textit{Heat Transfer:} \qquad \sum UA\left(T_i - T_o\right) + \left(\hat{c}_p \dot{m}_c T_i - \hat{c}_p \dot{m}_a T_o\right) = q_{gain} \tag{22}$$

Again, airflow through the windows will be modeled using the orifice equation. In the absence of wind-driven pressures, both indoor and outdoor air pressures will be assumed to vary hydrostatically in proportion to the indoor and outdoor air densities, $\rho_i$ and $\rho_o$ respectively – the, now, conventional assumption of macroscopic airflow analysis [5-7]:

$$m_a = C_d A_a \sqrt{2\bar{\rho}(p_o - p_i)} \; and \; m_b = C_d A_b \sqrt{2\bar{\rho}\left((p_i - \rho_i g\Delta z) - (p_o - \rho_o g\Delta z)\right)} \quad (23)$$

The airflow system equations may be formed by demanding conservation of airflow:

*Airflow:* $$m_a + m_b = 0 \quad (24a)$$

$$C_d A_a \sqrt{2\bar{\rho}(p_o - p_i)} + C_d A_b \sqrt{2\bar{\rho}\left((p_i - \rho_i g\Delta z) - (p_o - \rho_o g\Delta z)\right)} = 0 \quad (24b)$$

Finally, we'll use the ideal gas law to estimate air densities indoor and out:

$$\rho = \frac{p\,M_{air}}{RT_{°K}} \; where \; \frac{p\,M_{air}}{R} \approx 352.6\,{}^{kg-°K}/_{m^3} \; and \; T_{°K} = T + 273.15 \quad (25)$$

In this case, the heat transfer and airflow equations are coupled through both the airflow rate and buoyancy terms and the resulting nonlinearity is pathological. Consequently, it was not possible to <u>explicitly</u> solve the resulting equations for the indoor air temperature $T_i$ in terms of the design variables, $A_a$ and $A_c$. Nevertheless, these equations may be combined to form an equation that <u>implicitly</u> defines such a relation:

$$\frac{q_{gain}^2}{\Delta T^2} - 2\frac{\Sigma UAq_{gain}}{\Delta T} + \Sigma UA^2 = \frac{\left(2\frac{\Sigma UA\,q}{\Delta T} - \Sigma UA^2 - \frac{q_{gain}^2}{\Delta T^2}\right)A_b^2}{A_a^2} + 2\frac{\bar{\rho}\Delta z C_d^2 \bar{c}_p^2\, 352.6\, g\Delta T A_b^2}{(Ti + 273.15)(To + 273.15)} \; ; \; \Delta T = T_i - T_o \quad (26)$$

This implicit solution may then be plotted using numerical root-finding methods available in popular math processing programs.

We'll apply this result to the representative building presented above – a reasonably conventional single story building with total cooling load $q_{gain}$ = 43 W/m$^2$ (4 W/ft$^2$). The indoor air temperature response is plotted below, for this stack-ventilated case, along with the indoor air temperature comfort criteria of $T_i$ = 26 °C:

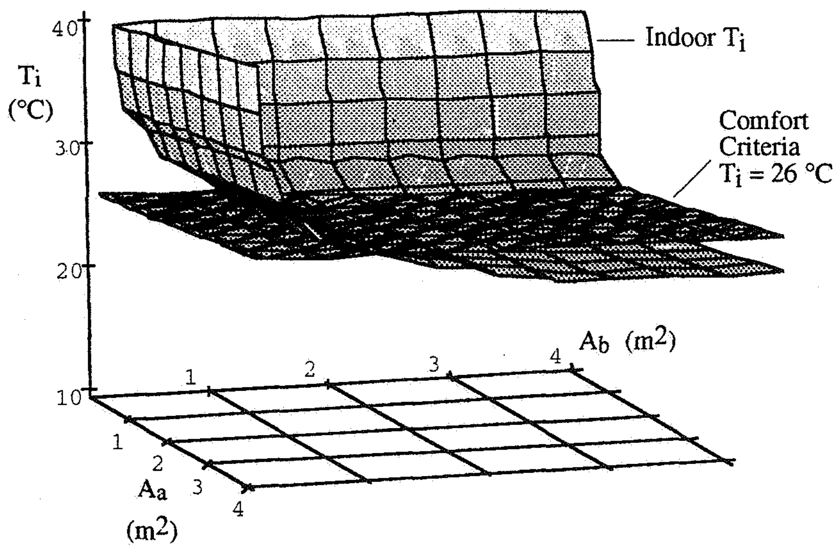


Fig. 9 Indoor air temperature and comfort criteria for the representative building using stack-ventilation with an outdoor air temperature of $T_o$ = 20 °C.

As expected, the indoor air temperature approaches the outdoor air temperature for large window openings. The intersection of the comfort criteria surface and the indoor air temperature response surface establishes combinations of window openings that will achieve the 26 °C comfort objective – the feasible solution curve. Feasible solution curves were generated for a range of stack heights, the third design parameter, and are plotted below. In addition, the inlet air velocity is also plotted as it varies with inlet window opening, $A_a$.

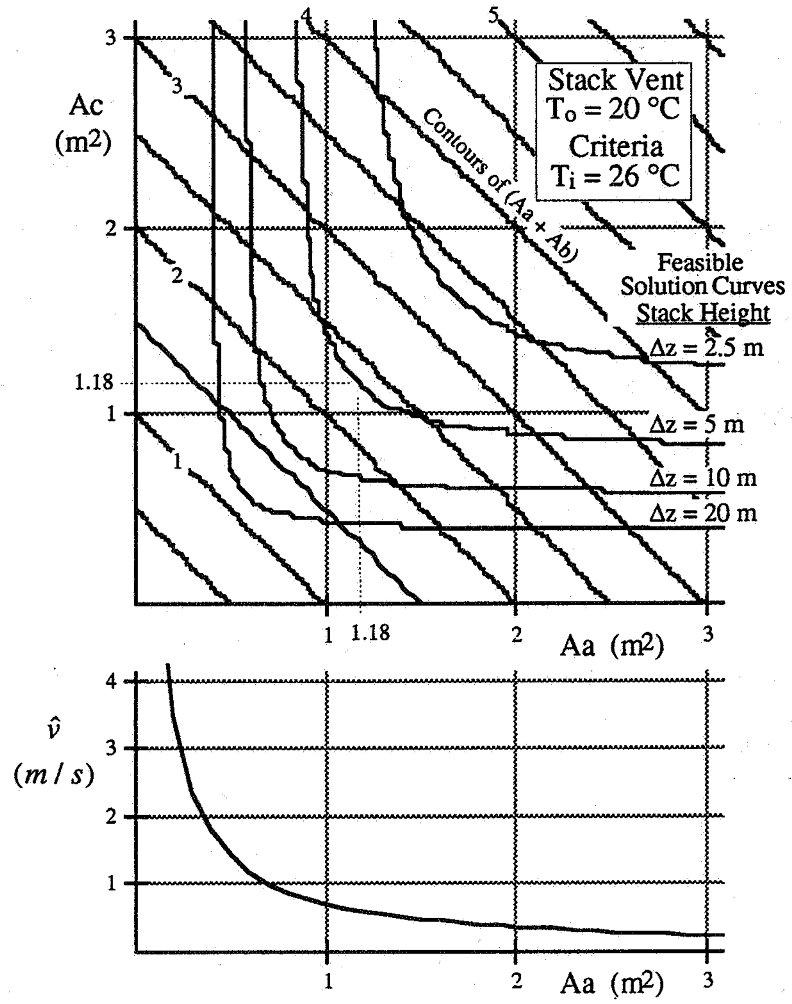


Fig. 10 Feasible solution curves for a range of stack heights, $\Delta z$, and inlet air velocity for the representative building using stack-ventilation with an outdoor air temperature of $T_o = 20$ °C.

A building designer could use these feasible solution curves in much the same way as before to guide design decisions while maintaining the comfort object (i.e., here $T_i = 26$ °C). For example, with a reasonable stack height of 5 m the designer could achieve the 26 °C comfort objective with $(A_a, A_c) \approx (3.0\ m^2, 0.8\ m^2)$, $(A_a, A_c) \approx (2.0\ m^2, 0.9\ m^2)$, $(A_a, A_c) \approx (1.0\ m^2, 1.4\ m^2)$, or choose the combination that minimizes the total window opening of $(A_a, A_c) \approx (1.18\ m^2, 1.18\ m^2)$. If the designer felt it was important to limit inlet air velocities to, say, 0.5 m/s then inlet window openings would have to greater than, approximately, 1.5 $m^2$ regardless of stack height (i.e., to simultaneously achieve the 26°C objective).

## 4. Conclusion

A general approach to solve ventilation design problems typically addressed at the preliminary design stage has been presented that is based on well-established macroscopic analysis theory. Equations, based on conservation of mass, momentum, and energy are formulated that relate room response to the key ventilation design parameters. These conservation equations may then be combined with comfort criteria also formulated in terms of these key design parameters to identify, unambiguously, feasible combinations of the design parameters that will achieve the thermal comfort objective. While it is argued that the description (i.e., curve, surface, or hypersurface) of these feasible combinations are likely to be of greatest use to the building designer, one may, in addition, add an objective function to allow the search for an "optimal" combination. It is likely, however, that the "optimal" solution will be sub-optimal from the point of view of a skilled designer in as much as such a designer will, in effect, be searching in a design space of far greater complexity than that defining the ventilation problem.

The application of the general approach to a simple single-zone building was demonstrated. Both wind-driven cross-ventilation and buoyancy-driven stack-ventilation schemes were considered along with thermal comfort assessed in terms of a) the indoor air temperature and b) the CIBSE dry resultant temperature with air velocity correction. Although simple, these cases are likely to be practically useful to designers of residential and small commercial and office buildings. From a general perspective, these simple cases demonstrate that the equations that result from the approach may be expected to be pathologically nonlinear and symbolically insoluble, thus, in general, numerical methods will have to be applied to evaluate both the relation between the chosen comfort index and the design parameters and the feasible combinations of these design parameters that will achieve the comfort objective. For simple problems this may readily be achieved with available math processing programs; for more complex cases it will be more reasonable to extend the capabilities of existing building energy simulation, airflow, and indoor air quality programs.

**References**


1. Awbi, H.B., *Ventilation of Buildings*. 1991, London: E & FN Spon. 313 pages.
2. Gan, G., *Effect of Combined Heat and Moisture Transfer on the Predicted Thermal Environment.* Indoor + Built Environment, 1996. **Vol 5**(No. 3): p. pp.170-180.
3. Awbi, H. and G. Gan, *Predicting Air Flow and Thermal Comfort in Offices.* ASHRAE Journal, 1994. **February**: p. pp. 17-21.
4. Prowler, D., *et al.*, *Designing Low-Energy Buildings: Passive Solar Strategies & Energy-10 Software 1.0*, . 1996, Passive Solar Industries Council: Washington, DC.
5. Walton, G. *Airflow Network Models for Element-Based Building Airflow Modeling.* in *ASHRAE Symposium on Calculation of Interzonal Heat and Mass Transport in Buildings.* 1989. Vancouver, B.C.: ASHRAE.
6. Axley, J. and R. Grot. *The Coupled Airflow and Thermal Analysis Problem in Building Airflow System Simulation.* in *ASHRAE Symposium on Calculation of Interzonal Heat and Mass Transport in Buildings.* 1989. Vancouver, B.C.: ASHRAE.
7. Walton, G.N., *CONTAM93 User Manual*, . 1994, National Institute of Standards and Technology (NIST).
8. Arens, E.A., *et al. A Study of Occupant Cooling by Two Types of Personally Controlled Air Movement.* in *Pan Pacific Symposium on Building and Urban Environmental Conditioning in Asia.* 1995. Nagoya, Japan.
9. Flourentzou, F., J. Van der Mass, and C.A. Roulet. *Experiments in Natural Ventilation for Passive Cooling.* in *Optimum Ventilation and Air Flow Control in Buildings: 17th AIVC Conference.* 1996. Gothenburg, Sweden: AIVC.
10. Alexander, D.K., H.G. Jenkins, and P.J. Jones. *Investigating the Effects of Wind on Natural Ventilation Desing of Commercial Buildings.* in *Sustainable Building: A BEPAC + EPSRC Conference.* 1997. Abingdon, England: BEPAC Web Site.
11. Givoni, B., *Passive and Low Energy Cooling of Buildings.* 1994, New York: Van Nostrand Reinhold. 263 Pages.

# VENTILATION AND COOLING
## 18TH ANNUAL AIVC CONFERENCE
## ATHENS, GREECE, 23-26 SEPTEMBER 1997

**Title**: Airflow through Horizontal Openings

Stairwell

**Authors**: A.A.Peppes , M. Santamouris and D.N.Asimakopoulos

**Affilitation**: Group Building Environmental Studies, Physics Dept., University of Athens, University Campus 15784, Athens, Greece.

**Airflow through Horizontal Openings**

**A.A.Peppes , M. Santamouris and D.N.Asimakopoulos**
**Group Building Environmental Studies**
**Department of Applied Physics, University of Athens,**
**Building PHYS-V, Athens 15784, Greece**

**Synopsis** - This paper deals with the interzonal air movement in a building, through horizontal openings, under natural convective conditions. These airflow phenomena are investigated experimentally, through a series of experiments in the stairwell of a full-scale building, using tracer gas technique. The resulting time-dependent concentration evolution offers a means of analyzing the flow field. These cases are also simulated by a CFD code, that uses the finite-volume method and incorporates a low-Reynolds k-ε two equation turbulence model. The simulations results regarding the concentration and velocity, are in good agreement with experimental data. Results indicate that the contaminant transmission and consequently the airflow pattern is quite complex and is affected by geometry, location of heat and contaminant sources, building materials and microclimate. The study also discusses the effectiveness of CFD modeling to describe airflow phenomena through horizontal openings, under various conditions. The results could be used to develop accurate algorithms for inclusion in existing mathematical models.

**List of Symbols**

d = distance from the nearest wall(m)
g = acceleration due to gravity ($msec^{-2}$)
$G_k$=stress production of turb.kin.energy
$G_B$ =buoyant generation of turb.kin.energy
H = height of the stairwell (m)
k=kin.energy of turbulence($Jkgr^{-1}$)
p = pressure (Pa)
Ra = Rayleigh number (dimensionless)
T = temperature (K)
To = reference temperature (K)
t = time (sec)
u,v,w = velocity components ($msec^{-1}$)
x,y,z = spatial coordinates
$\alpha$ = thermal diffussivity ($m^2 sec^{-1}$)
$\beta$ = coefficient of thermal expansion($K^{-1}$)
$\Gamma_\varphi$ = exchange coefficient of $\varphi$
$\varepsilon$=dissipation rate of kin.energy($Jkgr^{-1}sec^{-1}$)
$\mu_e$=effective dynamic viscosity($kgrm^{-1}sec^{-1}$)
$\mu_t$=turb.dynamic viscosity($kgrm^{-1}sec^{-1}$)
$\rho$ = density ($kgr\ m^{-3}$)
$\sigma$ = turb.Schmidt or Prandtl number
$\varphi$ = dependent variable

## 1. Introduction

In recent years there has been an increased interest in the study of airflow through large internal openings. This issue is of great importance due to its implication on energy saving, adequate ventilation, thermal comfort, pollutant transfer and dispersion of fire and smoke in the interior of buildings. However, little work has been done on the airflow through horizontal openings, such as ventilation shafts and stairwells. Indeed, very few authors have studied these phenomena and very few systematic experimental data are available in the literature.

A number of studies have been reported. Brown [1] have investigated airflow through small square openings in horizontal partitions. Reynolds [2], Zohrabian et al.[3] have conducted experiments and developed a model for the energy and mass transfer in a stairwell model, Riffat et al [5] has studied buoyancy-driven flow through a staircase in a two-floor house. In other studies Zohrabian et al.[4], S.Ergin-Ozkan et al. [7] and Riffat [6] used CFD modeling and compared predictions with experimental data.

There are studies involving air flow prediction in rooms (Haghighat et al. [8] ,Murakami et al. [9]) ,in atriums (Alamdari et al.[10]) and others involving measurements and CFD modeling of contaminant transmission in indoor spaces (Drangsholt [11] , Subrata et al.[12]).

Recent research in Computational Fluid Dynamics and tracer gas measurement permit to analyze these airflow phenomena, conducting extensive modeling.

The purpose of this study is to expand the existing knowledge on the physical phenomena related to natural convection in a stairwell and on the other hand to compare the CFD predictions and measurements and consequently to provide foundations for improving the existing predictive procedures.

## 2. Description of Experiments

A series of experiments have been performed in a building , in order to study the buoyancy-driven airflow between floors. Five experiments were held at the main stairwell located in the central building of the Department of Applied Physics of University of Athens. The stairwell extends to a height of about 16.5m as it connects the four floors of the building and a small basement. Each floor is about 3.7m high, while the basement is about 1.7m high. Since the geometry is rather complex, figures can describe the building in a more effective way.Figure 1, shows a section of the specific experimental site, while Figure 2 depicts a horizontal plan, which is identical for all floors, since the internal design is common. The rest of dimensions are illustrated in these figures. The entrance door, the doors connecting the stairwell with the offices located in the four floors and all the windows were kept closed and sealed during all the experiments. Some small openings and cracks were also sealed in order to reduce the infiltration as much as possible.

The thermal performance of the stairwell was constantly monitored. The air temperature was monitored by five Tiny Tag sensors (accuracy: ± 0.6%) which had already been calibrated. These sensors were distributed , one on each floor, and placed in specific locations which remained the same for all the experiments (Figure 1,2). Surface temperature on almost all the internal surfaces, was measured by PT100 sensors (accuracy: ± 0.1%).Air velocity measurements were also provided by two Dantec sensors (accuracy:± 0.4%),located in two specific points of the stairwell for all the experiments (Figure 1,2).

A single tracer gas technique was adopted. Several tracer gases are available , but $N_20$ was chosen for this work since it has desirable characteristics in terms of detectability, safety and cost and it has been used successfully in previous air movement studies. The concentration of gas was measured using an infrared gas analyzer(accuracy:± 1%).The tracer gas was injected in a specific position via three (3) injection points placed altogether, and eight (8) sampling points were carefully chosen and distributed so as to monitor its concentration variation with time at various heights of the stairwell. Samples were taken every 30 seconds for the total duration of each experiment.

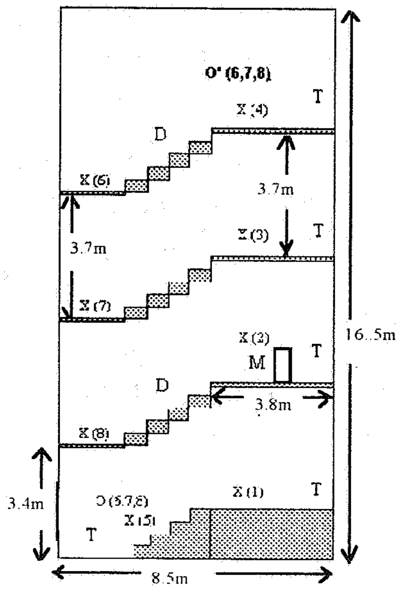


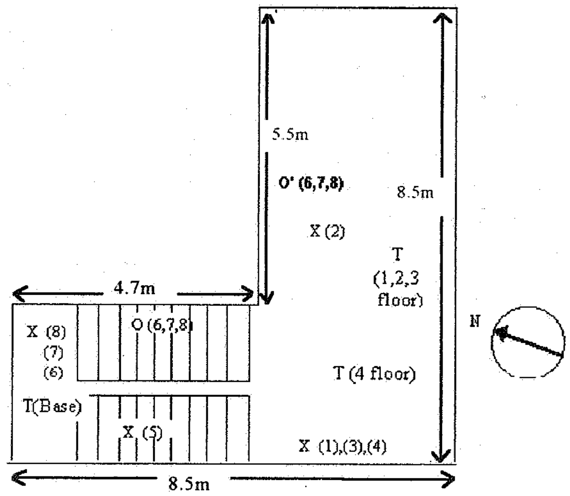


Fig. 1. Section of the stairwell.
(1m from the facade of building).
Location of injection and sampling points and sensors for all the experiments: X (sampling point),O( injection point for A,B,D exper.), O'(injection point for C,E exper.),M(main unit),T(air temp.sensor) D ( air velocity sensor).

Fig. 2. Horizontal plan of the stairwell (2m from the facade of building).
Location of injection and sampling points and sensors for all the experiments: X (sampling point),O( injection point for A,B,D exper.),O'(injection point for C,E exper.),M (main unit),T(air temp.sensor) D ( air velocity sensor).

Five experiments were carried out during January and February of this year, as it was mentioned before. From now on, they will be referred as experiment A, B, C, D, E. The duration of monitoring of gas concentration for each experiment was 75, 95, 75, 60, 58 minutes, respectively. In the first three experiments (A,B,C), monitoring of concentration at sampling points started as soon as the gas injection finished. For the experiments A and B, the gas was released in a specific position in the basement, while for experiment C , the injection took place in the fourth floor (Figures 1,2).

In the other experiments (D and E), the concentration of gas was monitored as soon as the gas release initialized, provided that the gas injection rate was nearly constant for the whole duration of experiments. This rate was initially measured by a flow-meter for an almost constant pressure level as written down on the display of main unit. Its value remained around 0.00030 kgr gas $m^{-3}$ for the D and E experiments.

For experiment D , the gas was injected in the basement, in the same position as in experiments A and B, while for experiment E , the release took place in the fourth floor, in the same position as in experiment C(Fig.1,2).The positions of sampling points were the same for all the experiments and for the total durations (Fig. 1,2).

### 3. Description of Numerical Computation

**Mathematical Model** - The mathematical model was a CFD code that generate approximate solutions to the Navier-Stokes equations, which are considered universally valid to describe the flow of a fluid, heat and concentration in a specific field. These equations are based on the conservation equations of mass, momentum, thermal energy and concentration species.

For Rayleigh numbers higher than $10^{6}$, a two equation k-ε model of turbulence was employed [13,14]. Since Rayleigh numbers were ranging from 3 $10^{12}$ to 4 $10^{12}$ during all the experiments, turbulence calculations were necessary to predict the flow. These equations can be represented by a general form of a differential equation for the dependent variable φ :

$$\frac{\partial}{\partial t}(\rho\varphi) + \frac{\partial}{\partial x}(\rho u\varphi) + \frac{\partial}{\partial y}(\rho v\varphi) + \frac{\partial}{\partial z}(\rho w\varphi) = \frac{\partial}{\partial x}\left(\Gamma_\varphi \frac{\partial \varphi}{\partial x}\right) + \frac{\partial}{\partial y}\left(\Gamma_\varphi \frac{\partial \varphi}{\partial y}\right) + \frac{\partial}{\partial z}\left(\Gamma_\varphi \frac{\partial \varphi}{\partial z}\right) + S_\varphi \quad (1)$$

where the first term stands for transiense , the remaining three terms in the left part of equation represent convection, the first three terms on the right part stand for diffussion ($\Gamma_\varphi$ stands for diffusivity for scalar variables and for effective viscocity $\mu_e$ for velocities) and finally $S_\varphi$ gives the source rate. It is obvious that φ can be any scalar variable (such as enthalpy h, kinetic energy k, energy dissipation ε,concentration c) or vector variable (u,v,w velocities components).Its value is equal to 1 for the continuity equation.The turbulent dynamic viscocity was determined as : $\mu_t = C_\mu \rho k^2 / \varepsilon$ (2)

where $C_\mu$ is determined experimentally. The standard k-ε model can obtain satisfactory results for forced convection configurations - high Reynolds number- as it incorporates the "wall function" method to bridge the rapid variations of velocity and temperature near the wall. The advantage of this approach is its computational economy as it eliminates the need for considering many grid points in the region near the wall.

Unfortunately, such wall laws are not adapted to natural convection problems as this specific one [15]. Therefore the viscous sublayer must be descretized and the behavior of turbulent variables must be damped within the whole domain through low-Reynolds modeling. The low-Reynolds extension of Lam and Bremhorst [16] to the two equation k-ε model, was used here. According to this model the empirical constants $C_\mu$ in the calculation of turbulent viscocity $\mu_t$ (equation (2)) and $C_1$, $C_2$ constants appearing in the source term of conservation equation of dissipation rate ε , were multiplied respectively by the functions :

$$F_\mu = [1-\exp(-0.0165\, R_k)]^2\, (1+20.5/R_t) \quad (3)$$
$$F_1 = 1+(0.05/F_\mu)^3 \quad (4)$$
$$F_2 = 1-\exp(-R_t^2) \quad (5)$$

where $R_k = k^2 / (v\, \varepsilon)$ and $R_t = k^{0.5}\, d / v$ are the turbulence Reynolds numbers and d is the distance to the nearest wall. For high Reynolds numbers $F_\mu$, $F_1$ ,$F_2$ tend to unity.

Separating and reattaching flow regions may occur in buildings which extend in height and have quite complex geometry. Yap [17] proposed an additional source term to the ε equation which takes into account these phenomena so as to avoid prediction of excessive heat transfer coefficient in such regions. His correction was also applied in these simulations.

**Solution Procedure** - The numerical resolution procedure of the calculations which couple the pressure, velocities, temperature and turbulent variables was the SIMPLE algorithm

(Semi-Implicit Method for Pressure Linked Equations) developed by Patankar [18]. The governing equations were spatially descretized over a 'staggered' grid using the Finite Volume Method (FVM). The Power-Law differencing which gives physically realistic solutions even for coarse grids, was used for the convective-diffusive fluxes and the source terms were linearized. These equations were solved using the line-by-line Tri-diagonal Matrix Algorithm (TDMA).

For the transient approach, the Fully Implicit Scheme was adopted [18].This scheme does not dictate any restrictions on the time-interval selection, as other schemes do, and satisfies generally the common requirements for simplicity and physical behavior. For the boundary conditions, the non-slip condition at the solid surfaces was applied for velocities. The k was zero at the solid surfaces and the gradient of $\varepsilon$ normal to the surfaces was considered zero. The temperature of the surfaces were taken from the measurements and considered constant for the duration of experiments.

The results were obtained for a 52 x 42 x 92 (x-,y-and z-directions, respectively) grid size. Since low-Reynolds number modeling requires that the equations are integrated right down to the wall, care was taken to ensure good numerical resolution in the near-wall region. So a non-uniform grid was adopted. Indeed, nearly five grid points were located in the region $y+ < 11.5$ where the laminar sublayer exists, with the first node positioned at $y+ = 1.0$, where $y^+ = u_T\, d_P / v$ is the dimensionless distance from the surfaces and $u_T = \sqrt{(\tau_w / \rho)}$ is the friction velocity ,while $d_P$ is the distance of point P from the wall and v is the kinematic viscocity. A similar approach is to concentrate several grid points inside the wall boundary layer. Its thickness $\delta$ is estimated by the relation $\delta/H = 4.86\ Ra^{-0.25}$ (6) with the first point located very close to the wall ( $y/H= 10^{-6}$) [13]. To conclude , dense grid was put near walls and other solid surfaces -although it was particularly difficult because of the presence of the stairs- for the selected grid size, and a relatively coarse grid arrangement in other regions. Negligible changes to the variables (~ 1%) were found when a larger grid size was adopted. However it is very significant to obtain results with sufficient accuracy , while achieving the best computational economy at the same time.

The criterion for convergence for all dependent variables was the following: $\max | \varphi^{n+1} - \varphi^{n} | \leq 10^{-4}$ between two successive sweeps. At this stage the sum of the mass residuals had to be less than a small value ($10^{-3}$ kgr $sec^{-1}$) . The convergence becomes quite problematic in low-Reynolds number flows. Therefore , strong under-relaxation was used - false Dt type - for all the variables ,except pressure [18]. Variable relaxation factors were applied during simulations in order to achieve convergence earlier.

## 4. Results and Discussion

Simulations of the cases corresponding to the five experiments, described before, were carried out. Care was taken to provide the initial field values for the concentration and temperature which are necessary for the simulations.

For the cases corresponding to the A,B,C experiments , the concentration levels measured at the various points just when the gas release finished, were considered as the initial values dominated in each zone-floor. For the rest of cases (D and E experiments) the concentration was considered zero for the whole domain with the existence of a static production source characterized by an almost constant injection rate. In a similar way, the initial values of temperature for each zone were taken from the measurements just the moment the monitoring started. The average value and the standard deviation of temperature for each floor are presented in Table 1 :

Table 1. Average air temperature ($_o$ C)

| Air Temp. (o C) | Exper. 1 | Exper. 2 | Exper. 3 | Exper. 4 | Exper. 5 |
|---|---|---|---|---|---|
| Basement | 11.18 ± 0.10 | 11.62 ± 0.09 | 9.45 ± 0.13 | 11.07 ± 0.08 | 9.30 ± 0.01 |
| Floor 1 | 15.82 ± 0.23 | 16.18 ± 0.13 | 14.99 ± 0.16 | 16.14 ± 0.10 | 14.40 ± 0.18 |
| Floor 2 | 17.28 ± 0.19 | 17.26 ± 0.24 | 15.49 ± 0.16 | 17.26 ± 0.19 | 14.89 ± 0.23 |
| Floor 3 | 16.80 ± 0.19 | 17.11 ± 0.18 | 15.20 ± 0.18 | 16.80 ± 0.09 | 14.50 ± 0.25 |
| Floor 4 | 17.82 ± 0.31 | 18.02 ± 0.14 | 16.63 ± 0.13 | 18.11 ± 0.11 | 16.02 ± 0.23 |

The temperature in each floor changed insignificantly with time.The relatively short duration of the experiments is the main cause.Comparison of data with the simulation predictions showed an average value of relative difference of about 2-3%.The greater values were measured on the fourth floor. This was expected , due to the buoyant motions and the fact that the air on the highest floor came to contact with warmer surfaces.

From the analysis of air velocity measurements at the two specific points in the staircase(ranging from 0.05 to 0.15 m sec$^{-1}$) and their comparison with the simulation results (ranging from 0.01 to 0.11 m sec$^{-1}$), it was observed an underestimation of values as calculated from the model. The air motion was rather weak due mainly, to the temperature distribution. The air velocity measurements were very limited in order to give a more detailed description of airflow. However, the simulations gave the overall features of flow patterns. Several vortexes were identified. These eddies promoted the heat transfer and the uniformity of temperature within each floor. The complex geometry of the stairwell produced a strong three-dimensional flow.

Comparison of the measured concentration evolution at all monitoring points with the model predicted one, showed relatively good agreement.

The average value of relative difference with its standard deviation and the correlation coefficient for each experiment are presented in Table 2 :

Table 2. Average Relative Difference of Concentration levels

| | Exper. 1 | Exper. 2 | Exper. 3 | Exper. 4 | Exper. 5 |
|---|---|---|---|---|---|
| Rel.Differ. | 0.12 ± 0.09 | 0.14 ± 0.10 | 0.24 ± 0.18 | 0.18 ± 0.14 | 0.22 ± 0.20 |
| Corr.Coef. | 0.91 | 0.90 | 0.95 | 0.96 | 0.96 |

The CFD model managed to predict the time variation of concentration with quite good accuracy, at least for the A and B experiments. The simulation of the third experiment depicted a significant deviation which must be attributed mainly to the strong-compared to the other cases- prevailing outdoor wind during this experiment. This fact reinforced infiltration inevitably. The last two simulations for the D and E experiment showed also an intense deviation. This can be attributed to the small deviation (1%) of the injection rate and partly to the infiltration which must not be negligible during these cases, as outdoor wind measurements revealed. Furthermore, the simplifications made for the determination of initial field of values of variables in every floor, contributed to the increase of the relative error for all runs. However, the model succeeded in predicting the trend of concentration evolution at all sampling points and for all experiments.

Figure 3 shows an example of this evolution as measured and as calculated during the experiment A and for the four floors.

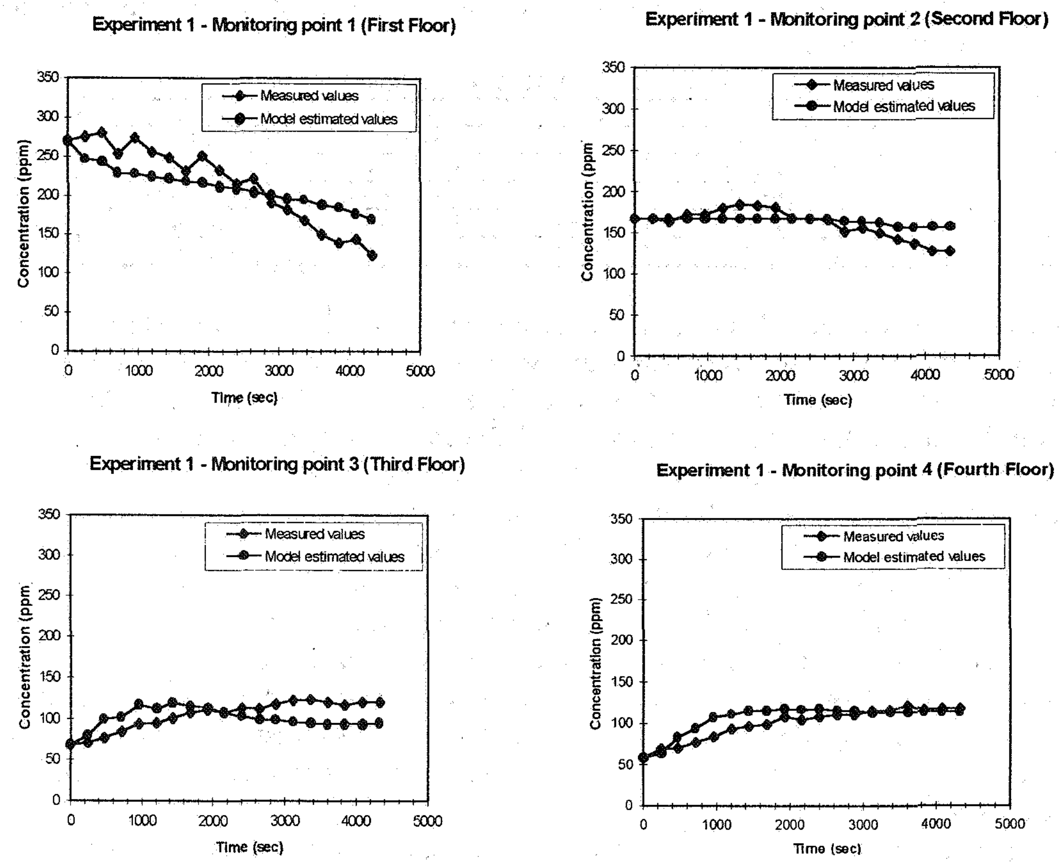


Figure 3. Measured and estimated concentration as a function of time ( experiment A)

Besides these problems that arose during the experiments, there are some other more basic difficulties. For instance, it must be noted , how difficult is to simulate full scale cases especially when this concerns quite large spaces. The detailed determination of thermal boundary conditions is very critical. This is very difficult when many surfaces with various thermal behavior exist, as in our case.In addition, in thermally-driven enclosures, a great difficulty comes from the turbulence models. These models are not strictly validated. Two different models usually show different results for the same configuration [19]. Much more experimental work is needed in order to better understand the phenomena and derive appropriate models for their description .Finally, the airflow through horizontal openings is physically highly transient , unstable and difficult to be described since it is driven by instability instead of a relatively stable distribution of pressure as through vertical openings.

## 5. Conclusions

A buoyancy-driven flow within the complex geometry of a stairwell was computed using Computational Fluid Dynamic simulation. Time-dependent computation revealed the airflow patterns which affects the contaminant transmission. The comparison between the experimental data and the estimations as mainly concern the time-dependent concentration evolution showed encouraging agreement despite the difficulties related with turbulence models, geometry, simplifications, experimental errors and boundary conditions.

Investigation of these factors is required so as to enhance the accuracy of this model. This fact will reinforce the already existing confidence for applying this computational model to further studies related to natural convection through horizontal openings. The final goal is to develop algorithms sufficient enough to be included in models using pressure networks so as to predict the interzone heat and mass transfer in the interior of multi-storey buildings.

## 6. References


1. Brown W G , 1962. " Natural convection through rectangular openings in partitions- 2 : Horizontal Partitions", Int. J. Heat and Mass Transfer, Vol 5, pp 869-881.
2. Reynolds A J , 1986. "The scaling of flows of energy and mass through stairwells" Build. And Envir. ,Vol 21,No 314,pp 149-153.
3. Zohrabian A S , Mokhtarzadeh M R ,Reynolds A J,1989. "Buoyancy-driven air flow in a stairwell model with through -flow"Brunel Univ.,UK.
4. Zohrabian A S , Mokhtarzadeh M R ,Reynolds A J,1988. "A numerical study of buoyancy-driven flows of mass and energy in a stairwell",9th AIVC Conf.Gent, Belgium, pp.1-21.
5. Riffat S B ,1989. " A study of heat and mass transfer through a doorway in a traditionally built house ", ASHRAE Trans., Vol 95, pp 584-589.
6. Riffat S B ,Kohal J S ,Shao L, 1994. " Measurement and CFD modelling of buoyancy-driven flows in horizontal openings " Proc. ASHRAE IAQ94,Conf.Engineering Indoor Environment, St Louis.
7. Ergin-Ozkan S, Mokhtarzadeh M R ,Reynolds A J, 1992. "Two- and Three-dimensional finite volume predictions of flow in a stairwell and comparison with experiment" Inter. Symposium on Room Air convection and ventilation eff.,Tokyo.
8. Haghighat,F.,Jiang,Z.,Wang,J.C.Y.,1989. "Natural convection and air flow pattern in a partitioned room with turbulent flow",ASHRAE Trans.Vol95,part2,pp155-161.
9. Murakami,S.,Kato,S.1990. "Numerical and experimental study on flow and diffusion field in room,11th AIVC Conf.,Italy.
10. Alamdari F.,Edwards S.C., Hammond,G.P.,1991. "Microclimate performance of an open atrium office building:a case study in thermo-fluid modeling.IMechE,pp81-92.
11. Drangsholt F. 1993. "Air flow pattern and pollutant transmission in auditoria - measurements and CFD simulations". Proc.6thConf. IAQ., Vol5,pp189-195.
12. Subrata R.,Baker A.J. and Kelso R.M.,1993."Airborne contaminant CFD modeling studies for two practical 3-D room air flow fields".Proc.6thConf.IAQ,Vol5,p349-358
13. Markatos ,N.C.,Pericleous ,K.A.,1984. "Laminar and turbulent natural convection in an enclosed cavity".Int.J.Heat Mass Transfer,Vol.27 ,No 5,pp755-772.
14. Launder,B.E.,and D.B. Spalding (1972) Mathematical models of turbulence. New York,Academic Press.
15. Beghein C., Allard F., Draoui A. 1992." Numerical modeling of turbulent convection in athermally-driven square cavity".Sem.22 Procc.J.M.Burgers Centre.
16. LamC.K.G., Bremhost K.,1981." A modified form of the k-ε model for predicting wall turbulence",ASME J.Fluids Eng.,Vol 103,p 456 .
17. Yap C.,1987. "Turbulent heat and momentum transfer in recirculating and impinging flows".PhD Thesis,Faculty of Tech., Univ. of Manchester.
18. Patankar,S.V (1980) Numerical Heat Transfer and Fluid Flow, Hemisphere, NY.

VENTILATION AND COOLING
18TH AIVC CONFERENCE, ATHENS, GREECE
23-26 SEPTEMBER, 1997

**Title:** Simulation of the Cooling Effect of the Night Time Natural Ventilation: A 3D Numerical Application to the "Maison Ronde" of Botta

**Author(s):** D Groleau, C Marenne, F Raymond

**Affiliation:** Lab CERMA, URA CNRS 1581, Ecole d'Architecture de Nantes, rue Massenet, 44300 Nantes, France

# 18th AIVC Conference

# VENTILATION AND COOLING

# Call for Papers

## Proposed Paper for submission by February 17th, 1997

**Title :** **Simulation of the cooling effect of the night time natural ventilation : a 3D numerical application to the « Maison Ronde » of Botta.**

**Authors :** GROLEAU Dominique , MARENNE Christian, RAYMOND Frank

**Address :** **Laboratoire CERMA, URA CNRS 1581, Ecole d'Architecture de Nantes rue Massenet, 44300 NANTES (FRANCE)**

**Tel :** (33)2 40 59 43 24 **Fax :** (33)2 40 59 11 77

### ABSTRACT

Natural ventilation can play an important role in the control of indoor temperature in summer, preventing overheating and favouring cooling of the structure of the building. But, highly variable features of parameters like wind conditions at the openings, indoor air motion and heat exchanges between air and walls, make prediction very difficult and complex. The research applies the 3D finite element CFD code, N3S, to the air flow simulation on a well-known dwelling building located in South of Swiss, the « Maison Ronde » of the famous architect Mario Botta. The refreshing effect is mainly examined, in a summer night, when crossing ventilation due to the wind is involved for creating indoor air motion and for cooling walls and ceilings surfaces.

To be realistic, the simulation takes simultaneously into account the three main aspects of the problem :

- determining boundaries conditions. To avoid to set artificial or irrealistic conditions at openings, the 3D mesh of the house was immersed in a numerical « wind tunnel », at the frontier of which the wind profile was imposed. Therefore, the incoming air flow is the result of the outdoor aerodynamical effect of the building geometry and of the location of opened windows.

- resolving air flow simulation with thermal conditions. The N3S code uses a thermal boundary layer at the walls that enabled to compute the wall temperature convective effect on the air flow, in mixed convection.

- calculating the cooling effect of the air flow into the structure of the wall. A finite difference model was integrated to the CFD code to modelize the transient thermal behavior of the mass inertia walls.

The presentation will focuse, firstly on the technical aspects of the implementation to the cooling effect of the summer night ventilation and, secondly, on its application to the « Maison Ronde » . From realistic initial conditions corresponding to the beginning of the night, the simulation will study the transient evolution of the air flow, internal air and wall surface temperatures. Obtained results will be analyze in relation to the architectural specificities of the house to explain its thermal behavior and appreciate the night cooling effect.

VENTILATION AND COOLING
18TH ANNUAL AIVC CONFERENCE
ATHENS,GREECE, 23-26 SEPTEMBER, 1997

# NUMERICAL SIMULATION OF IAQ AND ENERGY NEED BY COMIS MODEL:(OUTCOME FROM IEA ANNEX27: EVALUATION AND DEMONSTRATION OF DEMESTIC VENTILATION SYSTEMS)

Hiroshi Yoshino and Jing Liu
Department of Architecture, Faculty of Engineering, Tohoku University
Sendai 980-77, Japan

Yun Zhao
OM Solar Association, Nagaturu-cho 158-1,Hamamatsu City, 435, Japan

Lars-Goran Mansson
LGM Consult AB, Adler Salvius vag 87, S-146 53 TULLINGE, Sweden

Jean-Robert Millet
CSTB, Ventilation and Air Conditioning, Div84, Av. Jean Jaures, Champs -sur-Marne, BP 2-77421 Marne la Vallee, Cedex2, France

Helmut E. Feustel
Lawrence Berkeley Lab., Indoor Env. Program, Bldg. 90, Room 3074, Berkeley, CA 94 720, U.S.A

## Synopsis

The purpose of this research is to give an overall prospect of the performance of 4 kinds of ventilation systems for dwellings using numerical simulation under various conditions. The total number of combinations of various parameters for the calculation is 174.

Calculations for pollutant concentration, humidity and condensation, interior pressure and airflow rate, heat energy by ventiulation,etc. are performed hourly through the heating season.

In this paper, a new method was described to evaluate the effect of ventilation system under climatic conditions for each type of dwelling with an airtightness level from the points of view of indoor air quality and energy need. In addition, by means of statistical method, the impact of various parameters on IAQ and ventilaton systems was discussed.

## 1. Introduction

It's well known that most people spend most of their time within buildings. So ventilation of buildings is very important people to not only obtain acceptable indoor air quality but also avoid mould growth and condensation. On the other hand, the increase of ventilation rates may lead to exceeding energy consumption. Because evaluation of the performance of ventilation systems is directly linked to many design/control parameters, so it's very hard to get exact results up to now. Subtask 2 of IEA ANNEX27 'Evaluation and Demonstration of Domestic Ventilation Systems' has a purpose of statistical analysis using numerical simulation for airflow, indoor air pollution and energy load. In this paper, COMIS multi-zone infiltration and pollutant transport model was used for this research work, which had been developed by IEA ANNEX23 'Multi-zone Airflow Modelling'[1].

## 2. Assumption

### 2.1 Model house

A single-family house(D4c) and 4-story multi-family house(D4a) was chosen to represent different dwelling types. Room height was 2.5m and the living room always faced south. Their floor plans are shown in Fig 1. Leakages for 1, 2.5, 5.0[1/h@50Pa] were assumed to be concentrated in two parts on each exterior wall, one half located at 0.625m and the other half at 1.875m above the floor. For the 10[ach@50Pa] the additional cracks were located at the floor and ceiling. The standard family form and living schedule are based on European statistics[2]. Indoor air temperature was uniformly at 20℃. Except for the door between kitchen and hall, all the others were considered closed. Four main ventilation systems, i.e., natural, natural passive stack, mechanical exhaust and mechanical central supply and exhaust (represented as system 1 to 4 respectively in this paper). Installation of local fans in bathroom (weekdays: 6:00 - 8:00, weekends: 9:00 - 11:00) and/or kitchen (17:00 - 18:00) and supply air openings in habitable rooms was combined with ventilation system. The wind pressure values[3] are subject to different wind directions. Three regions were selected to represent the different climate conditions. Table 1 illustrates their main meteorologic parameters. Window airing was assumed at bedrooms only and the duration was 4h(8:00 - 12:00)

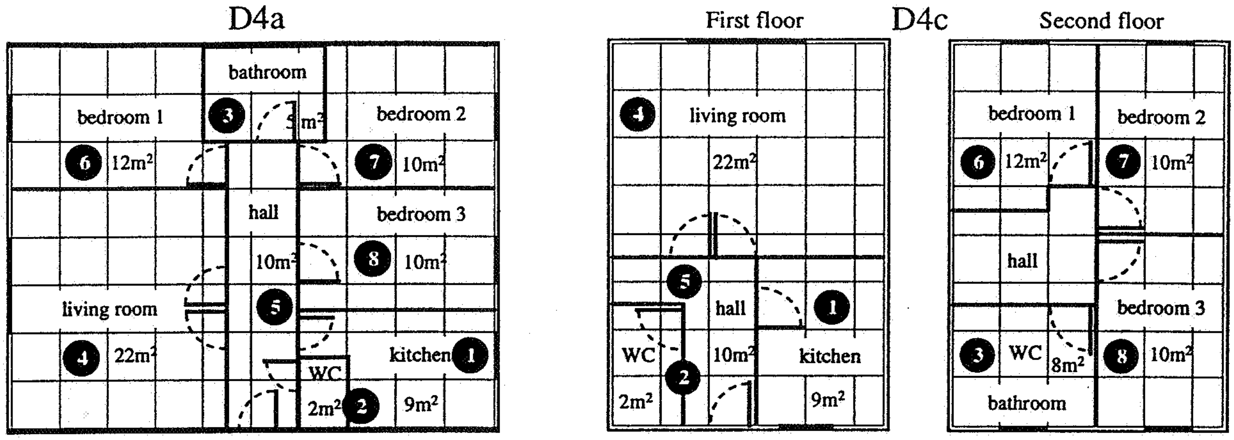


***Fig. 1: Floor plan of dwelling example***

***Table 1: Climate characteristic of three regions***

| Climate | Cold (Ottawa) | Moderate (London) | Mild (Nice) |
|---|---|---|---|
| *Heating Season* | 2 Oct-20 May | 24 Sep-20 May | 13 Nov-27 Apr |
| *Average temperature [ ℃]* | 1.44 | 7.51 | 10.1 |
| *Average humidity [g/kg']* | 2.97 | 5.22 | 5.31 |
| *Average wind speed [m/s]* | 4.44 | 1.97 | 4.34 |
| *Prevailing wind direction* | 186.8° (S) | 182.1° (S) | 264.9° (SW) |

during weekdays.

### 2.2 Indoor air pollutants

Except humidity, four kinds of air pollutants were simulated to reflect IAQ. They are described as the following: the pollutant generated from rooms themselves(Plt1), it is based on a constant emission related to the room area($1g/m^2h$); $CO_2$(Plt2); the pollutanat which is related to cooking activities(Plt3), it is considered to be proportional to the water production during cooking ($1g_{Plt3}=2g_{vapor}$); the pollutant which is related to passive smoking(Plt4), the emission source is set up as 20g/h for one smoker[3]. The metabolic $CO_2$ and water vapor (including showering and cooking) production of spacious case(2 persons) is given in Fig 2. The outdoor concentration of all pollutants was neglected. Since some kinds of indoor air pollutants' concentration is always low relatively, so a special index was introduced in terms of CV to show the cumulative effect of pollutant on occupancy during heating season[4]. It's the cumulated value for each occupancy on the basis of the number of exposured hours Nh above a certain indoor air pollutant concentration Ci: Nh(Ci). If 700ppm is defined as a threshold value of $CO_2$ for human's heath,

$$CV_{CO2(700)} = \int Nh(Ci) \quad \text{for } Ci>700ppm \qquad (1)$$

### 2.3 Combination of all the simulation parameters

As mentioned above, the related parameters for sensitivity studies are summarized in Table 2. A selection of critical combinations, at least 174, has been made on mathematical statistics.

## 3. Calculation example

### 3.1 Indoor air pollutant concentration variation

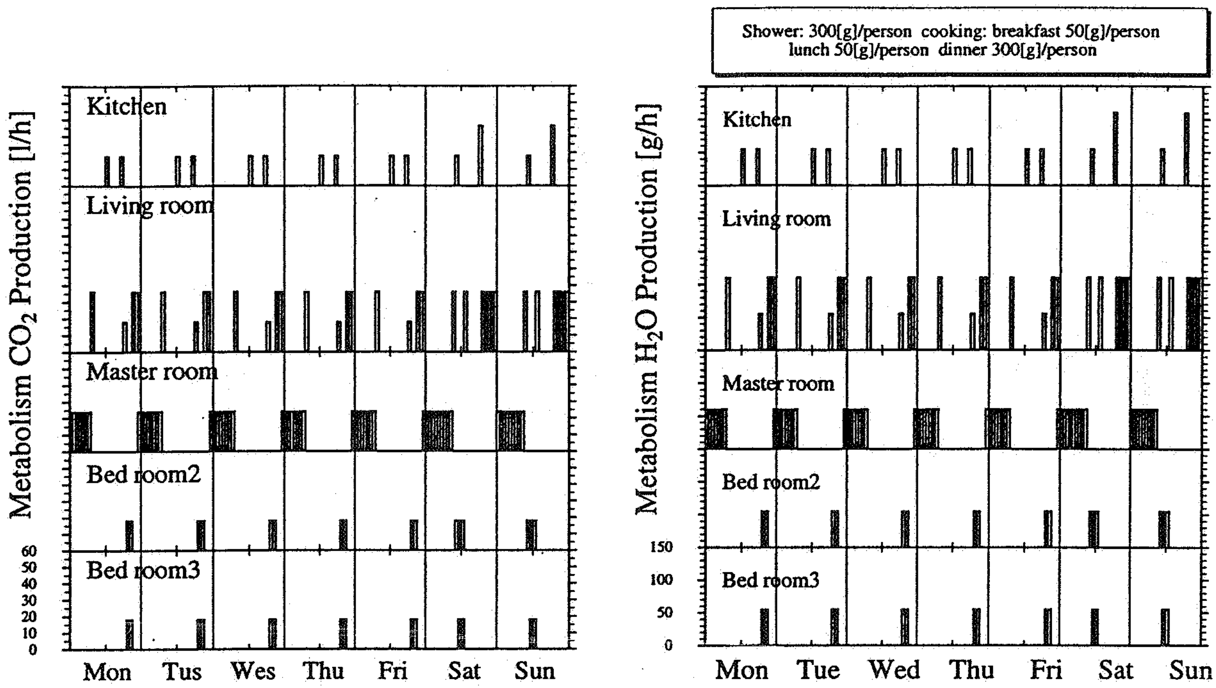


***Fig. 2: Metabolic $CO_2$ and water vapor generation schedule***

***Table 2: Entire parameters for simulation***

| Parameter | Level | | |
|---|---|---|---|
| *Dwelling type* | Single family house | Ground floor in 4 story multi-family house | Top floor in 4 story multi-family house |
| *Leakage* | 10(5) | 5(2.5) | 2.5(1) |
| *Occupancy* | 5(Crowded) | 4(Average) | 2(Spacious) |
| *Window Airing* | climate depending | 50% climate depending | Closed |
| *Climate* | Cold (Ottawa) | Moderate (London) | Mild (Nice) |
| *Supply Area (system 2,3)*<br>*(system 1)* | 400cm$^2$<br>410cm$^2$ | 100cm$^2$<br>101cm$^2$ | 0cm$^2$ |
| *Flow Rate (system 3,4)* | 45 *l/s* | 30 *l/s* | 15 *l/s* |
| *Local Fan Kitchen* | ON(100 *l/s*) | | OFF |
| *Local Fan Bath* | ON(25 *l/s*) | | OFF |
| *Comments* | ( ) for system 4 | | |

Table 3 describes two examples coded as N17 and N105. The former is system 1 while the latter is system 3. Fig 3 shows the indoor air pollutant concentration variation in the living room and the total fresh airflow rate during a certain week period(1 Jan～7 Jan). It can be found that owing to window airing and local fan, the variation in air flow rate becomes substantial. Especially when windows are opened, the fresh air rate increases up to 271[m$^3$/h] and can be more than 10 times the rate when closed and the consequencial effects on the indoor environment are obvious. The highest pollutants' level occurres in the living room between 6:00p.m. and 12:00p.m.. The $CO_2$ concentration during this period even exceedes 1.0g/kg'.

**3.2 Airflow distribution**

*Table 3: Detailed description of N105 and N17*

| Case No. | Dwelling type | Leakage [1/h@50Pa] | Occupancy [persons] | Window airing | Climate | Supply area [cm2] | Flow rate [l/s] | Local fan kitchen [l/s] | Local fan bathroom [l/s] |
|---|---|---|---|---|---|---|---|---|---|
| *N105* | D4c | 2.5. | 2 | open | Nice | 400 | 15 | 100 | 25 |
| *N17* | D4c | 2.5 | 2 | closed | Nice | 410 | no | no | no |

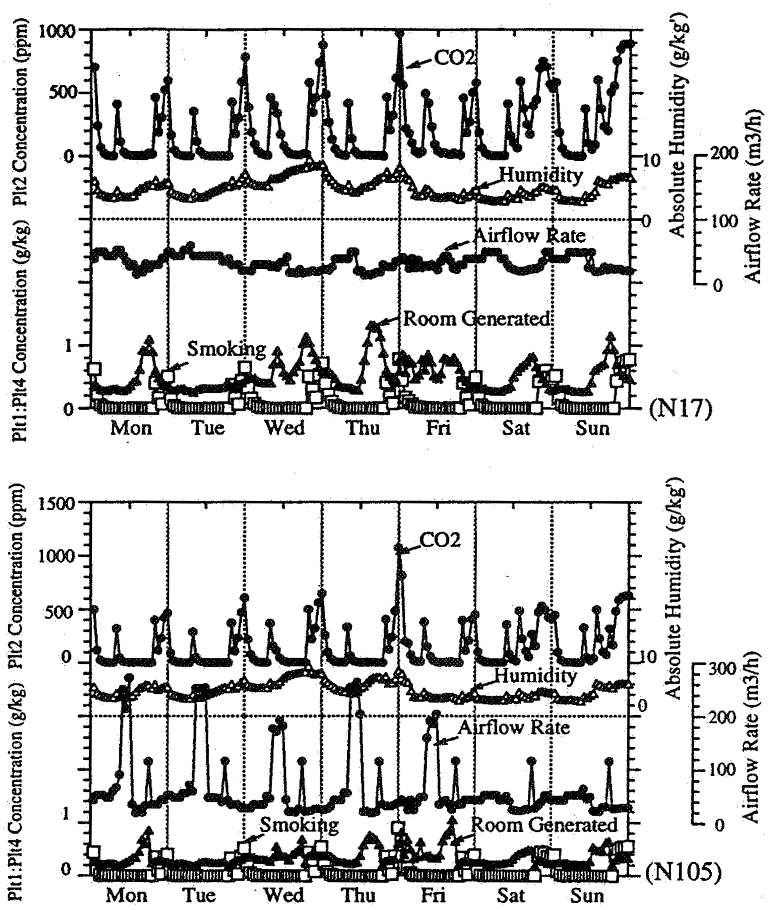


*Fig. 3: Variation of pollutant concentration and airflow rate (N17 and N105)*

From Fig 4 to Fig 7 two special times were selected to study the impact of window airing and kitchen hood on instantaneous airflow through all the zones for N17 and N105. The selected time and the instantaneous meteorological data are shown in Table 4. The figures show that due to mechanical sytem and local fan, airflow rates through habitable rooms increase to a great exent, especially when window airing is used at the same time. For example, at 9:00a.m., the airflow through bedroom 1,2 for system 3 is 6.26, 5.52 times as much as that for system 1. At 17:00p.m., the airflow through living room for system 1 is only 21.8[m$^3$/h], while for system 3 it increases up to 123.6[m$^3$/h] and the total flow pattern of this dwelling changes completely.

*Table 4: Description of the two selected time*

| Date/Time | Wind speed [m/s] | Wind direction [°] | Outdoor temperature [°C] |
|---|---|---|---|
| *07Nov / 9:00a.m.* | 5 | 0 (N) | 14 |
| *12Nov / 5:00p.m.* | 3 | 270 (NW) | 11.6 |

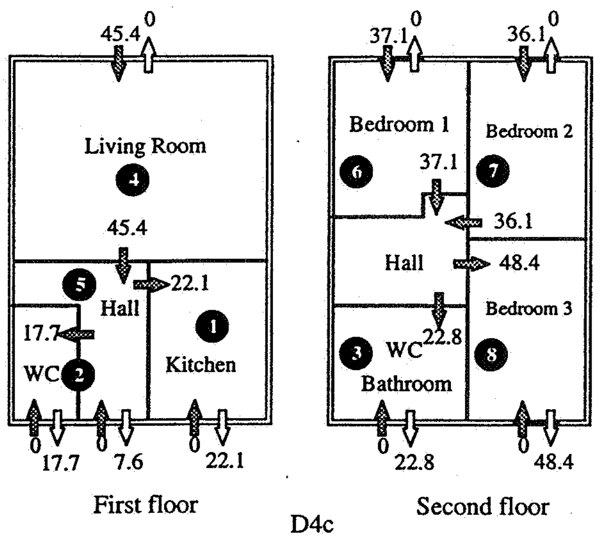


Fig. 4: Distribution of airflow rates at 9:00a.m.(N17)

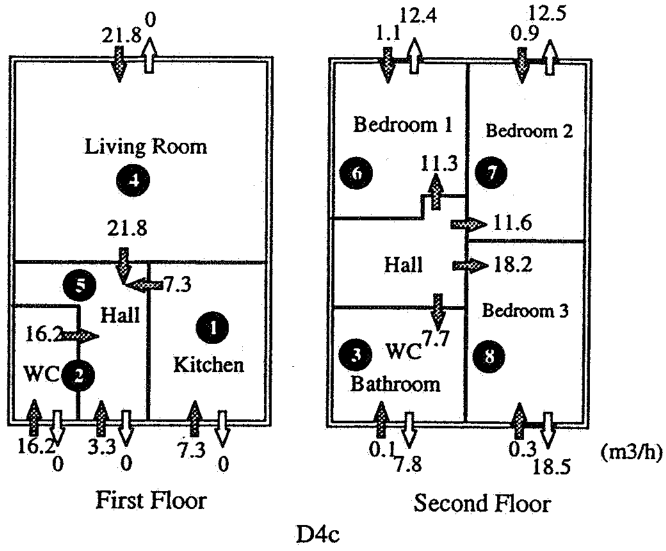


Fig. 5: Distribution of airflow rates at 5:00p.m.(N17)

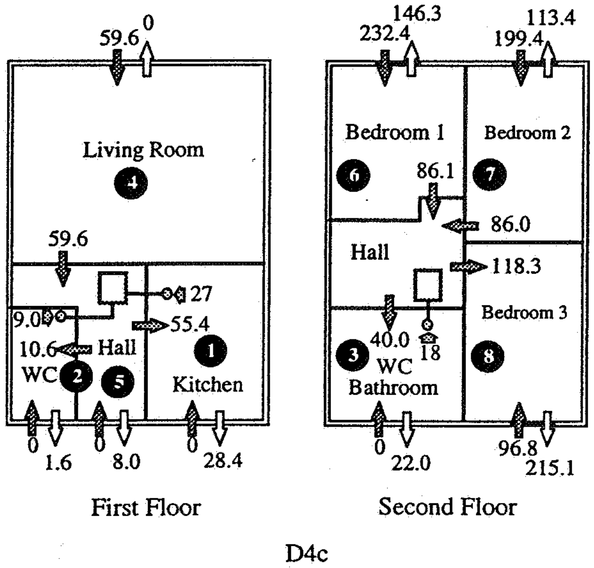


Fig. 6: Distribution of airflow rates at 9:00a.m.(N105)

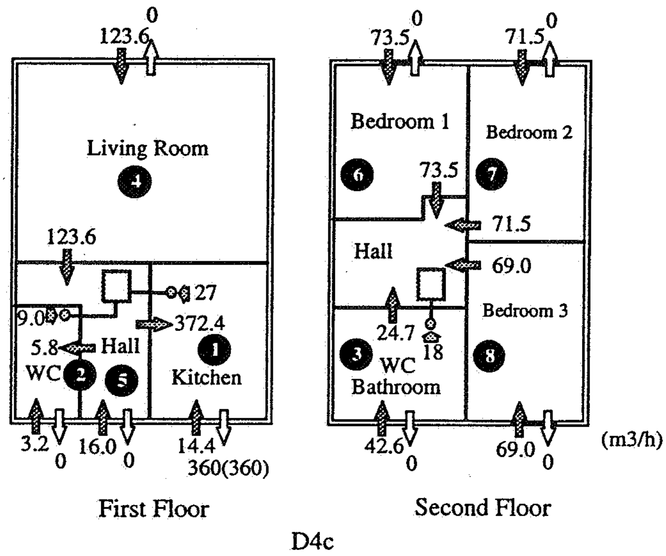


Fig. 7: Distribution of airflow rates at 5:00p.m.(N105)

# 4. Analysis of calculation result

## 4.1 Evaluation of ventilation system

Because the total energy consumption(due to both air exchange and fan's electrical need) during heating season and $CO_2$ concentration (represented by $CV_{CO2(700)}$ here) are the most important evaluation indexes associated with indoor environment, the combination of them will be an effective method to evaluate the synthetical performance of the ventilation system. Fig. 8 shows that $CV_{CO2(700)}$ of all the 174 cases is mainly in a range of 0 to 4000[g/kg × h] while the energy consumption within a range of 0 to 15000[kWh]. As an essential trend, the higher energy consumption results in lower $CV_{CO2(700)}$. Taking acceptable $CO_2$ level and energy conservation into account, limit values at 300[g/kg × h]and 3000[kWh] were derived to represent their threshold values respectively. The limit values were obtained from the average level of all the 174 cases. A rectangle is enclosed as shown in Fig 8 using the two limit values. Within this region, both $CO_2$

level and energy consumption are lower than the average level of total cases, thus this region can be considered as an 'Acceptable Region' for occupancy. Then an 'Acceptable Ratio' was derived based on the ratio of the case number of each ventilation system in the 'Acceptable Region' to the total case number of that system respectively. As shown in Table 5, when other parameters are assumed the same, the 'Acceptable Ratio' of system 4 is the highest. Apparently, using system 4, the $CO_2$ level and energy consumption are the most acceptable for occupancy. It can be attributed to the fact that indoor air quality and air distribution are good due to the force of central mechanism, and energy consumption is less than other systems because of heat recovery.

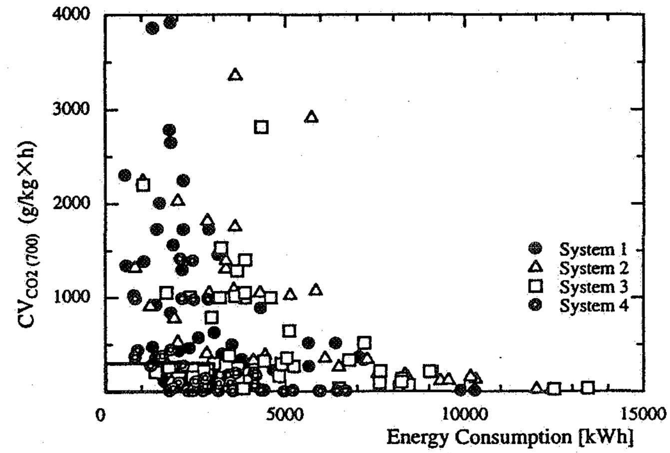


*Fig. 8: Impact of different ventilation systems on energy and IAQ*

*Table 5: 'Acceptable Ratio' for various systems*

| System | 1 | 2 | 3 | 4 |
|---|---|---|---|---|
| *Acceptable Ratio* | 0.14 | 0.16 | 0.16 | 0.33 |

### 4.2 Evaluation of related parameters

4.2.1 Predictable formulae

As indicated in Table 2, the related parameters and their corresponding categories are all represented by qualitative data. According to multivariate statistical theory, quantification I analysis method is available to analyze the relationship between these parameters and $CV_{CO2(700)}$. The calcuation results are summaried in Table 6. From this table, the predictable formula of every ventilation system for $CV_{CO2(700)}$ can be obtained. Equction 2 shows the predictable formula of natural ventilation system(system 1)as an example:

$$CV_{CO2(700)} = 997.3-118.34x_{11}+194.77x_{12}+204.7x_{13}-585.61x_{21}+118.7x_{22}+522.75x_{23}+274.62x_{31}-23.6x_{32}-262.08x_{33}-20.4x_{41}+11.2x_{42}+14.54x_{43}-77.92x_{51}+661.5x_{52}-277.34x_{53}-596.8x_{61}+80.8x_{62}+554.14x_{63}-27.99x_{81}+16.6x_{82}+11.21x_{91}-6.7x_{92} \quad (2)$$

Using these predictable formulae, the practical extent of indoor $CO_2$ level can be approximately expected upon any combinations of aforementional parameters. Because the adjusted R squared values in Table 6 are close to 1, these predictable formulae can be regarded to be valid for

*Table 6: Category scores of ventilation systems*

| Item / Category | | System 1 R'=0.775 $\alpha$<0.01 | System 2 R'=0.735 $\alpha$=0.03 | System 3 R'=0.707 $\alpha$=0.1 | System 4 R'=0.860 $\alpha$<0.01 |
|---|---|---|---|---|---|
| *Dwelling type* | *D4c (x11)* | -118.34 | -86.44 | -39.3 | 51.92 |
| | *D4agf (x12)* | 194.7 | 25.86 | 1.11 | -113.85 |
| | *D4atf (x13)* | 204.7 | 265.86 | 16.36 | -61.36 |
| | *range* | 323.04 | 352.3 | 55.66 | 165.77 |
| *Leakage area '/' for system 4 (n50)* | *10/5 (x21)* | -585.61 | -432.69 | -311.78 | -140.36 |
| | *5/2.5 (x22)* | 118.7 | -0.01 | 152.2 | 61.49 |
| | *2.5/1 (x23)* | 522.75 | 433.13 | 213.34 | 107.81 |
| | *range* | 1108.36 | 865.82 | 525.12 | 248.17 |
| *Family number* | *5 (x31)* | 274.62 | 312.53 | 272 | 231.96 |
| | *4 (x32)* | -23.6 | -253.2 | -328.73 | 59.91 |
| | *2 (x33)* | -262.08 | -178.47 | -59.3 | -263.68 |
| | *range* | 536.7 | 491 | 600.73 | 495.64 |
| *Window airing* | *open (x41)* | -20.4 | -27.01 | 79.49 | -5.54 |
| | *half open (x42)* | 11.2 | 40.14 | -157.59 | 61.49 |
| | *closed (x43)* | 14.54 | 5.75 | 22.49 | -27.02 |
| | *range* | 34.94 | 67.15 | 237.08 | 88.51 |
| *Climate* | *cold (x51)* | -77.92 | -117.19 | -101.95 | 41.88 |
| | *moderate (x52)* | 661.5 | 527.61 | 412.85 | 101.03 |
| | *warm (x53)* | -277.34 | -162.13 | -163.19 | -95.36 |
| | *range* | 938.84 | 689.74 | 576.04 | 196.39 |
| *Supply area '/' for system 1 (cm2)* | *400/410 (x61)* | -596.8 | -527.51 | -260.62 | |
| | *100/101 (x62)* | 80.8 | 188 | -9.88 | |
| | *0 (x63)* | 554.14 | 427.97 | 267.02 | |
| | *range* | 1150.94 | 955.48 | 527.64 | |
| *Mechanical flow rate (l/s)* | *45 (x71)* | | | -303.51 | -380.18 |
| | *30 (x72)* | | | 164.65 | -445.88 |
| | *15 (x73)* | | | 196.97 | 560.88 |
| | *range* | | | 500.48 | 1006.76 |
| *Kitchen fan* | *on (x81)* | -27.99 | -14.88 | 80.01 | -18.61 |
| | *off (x82)* | 16.6 | 8.82 | -44.15 | 11.03 |
| | *range* | 44.59 | 23.7 | 124.16 | 29.64 |
| *Bathroom fan* | *on (x91)* | 11.21 | 16.75 | -212.4 | -8.26 |
| | *off (x92)* | -6.7 | -9.93 | 117.19 | 4.89 |
| | *range* | 17.91 | 26.68 | 329.59 | 13.15 |
| *Constant* | | 997.3 | 705.86 | 518.76 | 255.26 |

application.

4.2.2 Evaluation from category scores

The category score in Table 6 can show how the variation of indoor $CO_2$ level changes from the average level. The following are the evaluation results:

1) $CV_{CO2(700)}$ is higher in multi-family house(D4a) than single-family house;

2) $CV_{CO2(700)}$ decreases with the increase of leakage or area of supple air, decrease of family number, operation of local fans and opening of windows.

3) $CV_{CO2(700)}$ in moderate weather condition seems the worst among the three weather conditions. In practice, the reason is perhaps due to $CV_{CO2(700)}$ depends on the number of exposured hours strongly and the heating season of London is much longer than Nice and Ottawa.

4.2.3 Evaluation of item range

According to quantification I analysis method, the item range in Table 6 can be used to show which parameter influences on indoor $CO_2$ level significantly and which one slightly. The following can be concluded:

1) System1: the impact of leakage, area of supply air and weather condition on $CV_{CO2(700)}$ looks far more greater than other parameters;

2) System2: the impact of leakage and area of supply air on $CV_{CO2(700)}$ looks a little greater than other parameters;

3) System3: the impact of leakage, area of supply air, weather condition, family number and mechanical air flow rate on $CV_{CO2(700)}$ looks roughly equal;

4) System4: mechanical air flow rate is the dominant parameter affecting $CV_{CO2(700)}$ among all the parameters;

5) The impact of window airing and local fan on $CV_{CO2(700)}$ looks week for every system.

## 5. Conclusions

In accordance with results from the 'Acceptable Ratio' proposed in this paper, mechanical central supply and exhaust system has been confirmed to lead to lower indoor $CO_2$ level and reduce energy consumption. On the base of quantification I analysis statistical method, the impact of related parameters with every system on $CV_{CO2(700)}$ respectively was studied quantitatively. Controlling these parameters appropriately can guarantee an adequate indoor air enveironment for occupancy.

**Acknowledgement**

This research work is one part of ANNEX27, 'valuation and Demonstration of Domestic Ventilation System' which is one of the international collaboration projects undertaken by IEA(International Energy Association). The authors would also like to acknowledge helpful advice and data presentation from the member of ANNEX23 — Hans Phaff (TNO Building and Construction Research, the Netherlands)

**References**

1)Hans P: "Final Report ANNEX23.Multizone Ventilation Models", TNO, July 1996.

2)L-G Mansson: "Annex27-Domestic Ventilation, Occupant Habits' Influence on Ventilation Need", 15th AIVC Conference, Sep 1994.

2)JR Millet, et al: "Assumptions for the Simulations of ANNEX27", CSTB, Nov 1996.

3)JG Villenave, et al: "Comparison of Ventilation Systems Performances Related to Energy Consumption and Indoor Air Quality", 2nd International Conference of IAQ, Ventilation and Energy Conservation in Buildings, Canada, May 1995

VENTILATION AND COOLING

18TH ANNUAL AIVC CONFERENCE
ATHENS, GREECE, 23-26 SEPTEMBER, 1997

# Performance of Series Connected Heat Exchangers with Liquid Circuit on Loop

Esa Marttila

Lappeenranta University of Technology
Department of Energy Technology

## ABSTRACT

The series connected heat exchangers - configured either as an arrangement of gas-gas, gas-liquid or liquid-liquid heat exchangers- are widely used in the process industry and air-conditioning where they can be found in a variety of heat (cool) recovery, in heating and cooling applications. The design of heat exchangers follows the conventional design procedures for compact heat exchangers, and involves computation of excanger dimensions to yield a prescribed heat exchanger efficiency and pressure drops for fluid streams.

This paper describes a procedure for calculating the performance of series connected heat exchangers, when heat tranfer fluid has been looped between heat exchangers. The heat excanger system consists of heat (cool) recovery heat exchanger(s), pre-heater(s) or pre-cooler(s) and a main heat exchager to heat or to cool a main stream to the aim temperature. The heat excangers are connected with the looped fluid circuit. The connecting fluid flow rate has to be determined to achieve optimum heat or cool recovery.

The following considerations has to be almost always made when the heat exchangers is designed for the application,

- Heat transfer requiremments
- Costs
- Physical size
- Pressure drop characteristics

In the main stream the heat transfer requirements for temperatures must be met in the selection or design of any heat exchanger. The way with which the requirements are met, depends on the relative weights placed on costs, physical size or pressure-drop characterristics. Economic plays a key role in the design and selection of heat exchanger equipment, and the engineer should bear this in his mind when embarking on any new heat transfer design problem.

For the used heat exchangers the presented procedure gives the looped fluid flow rate, with which the best possible heat recovery efficiency is achieved. In the other hand the procedure gives the performances for heat exchangers to achieve the end temperature of the main stream.

### List of Symbols

| | |
|---|---|
| $c_p$ | specific heat capacity of fluid, J/kgK |
| $E_e$ | value of energy transferred by the heat recovery system annually, FIM |
| $q_v$ | volume flow rate, $m^3/s$ |
| $q_{v1}$ | volume flow rate of supply air, $m^3/s$ |
| $q_{v2}$ | volume flow rate of exhaust air, $m^3/s$ |
| $\Phi$ | heat flux from exhaust air to supply air, W |
| $C_1$ | heat capacity rate of supply air, W/K |
| $C_2$ | heat capacity rate of exhaust air, W/K |
| $C_3$ | heat capacity rate of heat transfer liquid, W/K |
| P | electric capacity of compressor, W |
| R | ratio of heat capacity rates $C_1/C_2$ |
| $R_1$ | ratio of heat capacity rates$C_1/C_3$ |
| $R_2$ | ratio of heat capacity rates $C_2/C_3$ |
| $T_{11}$ | inlet temperature of supply air in heat recovery heat exchanger, K |
| $T_{12}$ | outlet temperature of supply air in heat recovery heat exchanger, K |

| | |
|---|---|
| $T_{21}$ | inlet temperature of exhaust air in heat recovery heat exchanger, K |
| $T_{22}$ | outlet temperature of exhaust air in heat recovery heat exchanger, K |
| $T_{31}$ | inlet temperature of liquid in the supply air heat exchanger, K |
| $T_{32}$ | outlet temperature of liquid in the supply air heat exchanger, K |
| $T_{33}$ | inlet temperature of liquid in the exhoust air heat exchanger, K |
| $T_{34}$ | outlet temperature of liquid in the exhoust air heat exchanger, K |
| $e_h$ | price of primary energy, FIM/MJ |
| $f_1$, $f_2$,$f_{11}$, | |
| $f_{12}$ | help functions, equations (32)-(35) |
| $q_{v3}$ | volume flow rate of heat tranfer liquid, $m^3/s$ |
| $\Delta T_V$ | change of temperature of heat tranfer liquid $T_{31}$-$T_{34}$ or $T_{34}$-$T_{31}$, K |
| $\varepsilon$ | thermal efficiency from exhaust air into supply air |
| $\varepsilon_1$ | thermal efficiency of supply air $(T_{12}-T_{11})/(T_{31}-T_{11})$ |
| $\varepsilon_2$ | thermal efficiency of exhaust air $(T_{21}-T_{22})/(T_{21}-T_{33})$ |
| $\varepsilon_j$ | coefficient of performance in the refrigeration cycle |
| $\theta_0$ | temperature difference, $T_{21}$-$T_{11}$ tai $T_{11}$-$T_{21}$ , K |
| $\theta_1$ | temperature difference, $T_{31}$-$T_{11}$ tai $T_{11}$-$T_{31}$, K |
| $\theta_2$ | temperature difference, $T_{21}$-$T_{33}$ tai $T_{33}$-$T_{21}$, K |
| $\theta^*$ | relative change of heat transfer liquid, $\Delta T_V/\theta_0$ |
| $\theta^{**}$ | relative change of supply air in heating $(T_{12}-T_{11})/\theta_0$ or in cooling $(T_{11}-T_{12})/\theta_0$ |
| $\phi_1$ | heat capacity to the supply air, W |
| $\phi_2$ | heat capacity from exhaust air, W |
| $\phi_3$ | heat capacity from primery energy source, W |
| $\phi_{max}$ | maximum possible transferrable heat flow, W |
| $\rho$ | density, $kg/m^3$ |

## DIMENSIONING THE HEAT RECOVERY HEAT EXCHANGER IN VENTILATION

The recovery of heat (cool) in ventilation systems forms a part of the production and distribution of heat in the whole of a building. Most commonly available sources of energy for satisfying the heating need of a building are fuel, district heating, or electricity, and, as an addition to primary energy, the waste heat flow of a building. The most common waste heat flow of a building which is possible to utilize is the entalpy content of exhaust air.

The utilization of the entalpy content of exhaust air for heating the supply air depends on the costs of utilization and the savings obtained through utilization. The object in the dimensioning of a heat recovery unit is at first to find the heat exchanger size with whicht it is possible to achieve the economically best final results.

The factors which determine the dimensioning of a heat recovery unit are: the saving of primary energy through heat recovery, the investment costs of carrying out the heat recovery system, and the operating costs of heat recovery and, in addition, the investment savings achieved through the carrying out of a heat recovery system.

### Value of Recovered Entalpy Content of Exhaust Air

The entalpy content recovered from exhaust air can be got with the aid of the recuperation ratio ($\varepsilon$) of a heat recovery heat exchanger. The restriction of recuperation ratio is possible in connection with protection against ice formation and overheating. Ventilation systems usually operate between certain times ( from $t_{1j}$ to $t_{2j}$, j = 1 to 365) of a day on certain days of week. The value of the entalpy content of exhaust air recovered then can be calculated from the following equation (1) (Marttila 1996).

$$E_e = \epsilon q_{V1} c_{p1} \rho e_h \sum_{j=1}^{365} \int_{t_{1j}}^{t_{2j}} \langle T_{21} - T_{11} \rangle_j \, dt \tag{1}$$

When only temperature difference is a function of time in Equation (1), the so-called degree-hour amount can be calculated as in integral on the basis of maximum temperature difference on operation time (Marttila 88)

$$\bar{\theta} t = \sum_{j=1}^{365} \int_{t_{1j}}^{t_{2j}} \langle T_{21} - T_{11} \rangle_j \, dt \tag{2}$$

The recuperation ratio of a heat recovery heat exchanger is defined as the ratio between the transferred heat flow and the largest possible transferrable heat flow (Kays and London 84).

$$\Phi_{max} = (q_{vi} c_{pi} \rho_i)_{min} (T_{21} - T_{11}) \tag{3}$$

$$\varepsilon = \frac{\Phi_c}{\Phi_{max}} = \frac{\Phi_h}{\Phi_{max}} \tag{4}$$

**Series Connected Heat Exchangers with Liquid Circuit on Loop**

In common application of the heat (cool) recovery (Figure 1) the thermal efficiency $\varepsilon$ can be defined as in the equation (5) (Kays ja London 1984).

$$\epsilon = \frac{\epsilon_1 \epsilon_2}{\frac{\epsilon_1 R_1}{R_2} + \epsilon_2 - \epsilon_1 \epsilon_2 R_1} \tag{5}$$

Next the thermal efficiency will be defined when the heat and cool coils in the figure 1 has been replaced with the plate heat exchaners as in the figure 2.
In the air conditioning system the supply air has to be cooled or to be heated to the certain temperature $T_{12}$. The heating or cooling capacity can be written as in the equation (6).

$$\phi_1 = C_1 (T_{12} - T_{11}) \tag{6}$$

The heating or cooling capacity from the exhaust air can be written as in the equation (7).

$$\phi_2 = C_2 (T_{21} - T_{22}) \tag{7}$$

The heating or cooling capacity from the primary source (fuel, district heating, electricity) can be written as in the equation (8).

$$\phi_3 = C_3 (T_{31} - T_{34}) \tag{8}$$

Now the heating capacity can be written as in the equation (9).

$$\phi_1 = \phi_2 + \phi_3 \tag{9}$$

The parameters for the thermal efficiency $\varepsilon$ are defined as $\varepsilon_1$, $\varepsilon_2$,.$\theta_o$, $\theta_1$, $\theta_2$, $\theta^{**}$ and $\theta^*$ (equations (10) - (15).

$$\epsilon_1 = \frac{T_{12} - T_{11}}{T_{31} - T_{11}} \tag{10}$$

$$\theta_o = T_{21} - T_{11} \tag{11}$$

$$\theta_1 = T_{31} - T_{11} \tag{12}$$

$$\theta_2 = T_{21} - T_{33} \tag{13}$$

$$\theta^{**} = \frac{T_{12} - T_{11}}{\theta_o} \tag{14}$$

$$\theta^{*} = \frac{T_{31} - T_{34}}{\theta_o} \tag{15}$$

Now the thermal efficieny can be written as in the equation (16).

$$\epsilon = \theta^{**} - \frac{1}{R_1}\,\theta^{*} \tag{16}$$

The paramter $\theta^{*}$ can be written as in the equation (17).

$$\theta^{*} = \theta^{**} R_1 \left( 1 + \frac{1}{R}\,\frac{\epsilon_2}{\epsilon_1} - \epsilon_2 R_2 \right) - R_2\,\epsilon_2 \tag{17}$$

Now the thermal efficiency can be written as in the equation (18) (Marttila, 1996).

$$\epsilon = \theta^{**} \left( \epsilon_2 R_2 - \frac{1}{R}\,\frac{\epsilon_2}{\epsilon_1} \right) + \frac{1}{R}\,\epsilon_2 \tag{18}$$

**Heat Exchanger network design in Cooling** (Figure 3)

Next the situation are dealed , where the condensation and vaporization heat exchaners are coupled in series with the heat recovery heat exchangers.

Cooling demand to the supply air can be written as the equation (19).

$$\Phi_1 = C_1 \, (T_{11} - T_{12}) \tag{19}$$

Heating capacity to the exhaust air consists of the cooling demand of the supply air and the electric capacity of the compressor. The heating capacity to the exhaust air can be written as the equation (20).

$$\Phi_2 = C_2 \, (T_{22} - T_{21}) \tag{20}$$

Electric capacity of the compressor can be written as the equation (21).

$$P = \frac{C_3 \, (T_{34} - T_{31})}{\epsilon_j} \tag{21}$$

Heating capacity to the exhaust air can be written as the equation (22)

$$\Phi_2 = \Phi_1 + P \tag{22}$$

The thermal efficiencies of the heat exchangers are defined as in the equations (23) and (24).

$$\epsilon_1 = \frac{T_{11} - T_{12}}{T_{11} - T_{34}} \tag{23}$$

$$\epsilon_2 = \frac{T_{22} - T_{21}}{T_{33} - T_{21}} \tag{24}$$

Caculation parameters $\theta_o$, $\theta_1$, $\theta_2$, $\theta^{**}$ and $\theta^{*}$ are defined as in the equations (25) - (29).

$$\theta_o = T_{11} - T_{21} \tag{25}$$

$$\theta_1 = T_{11} - T_{31} \tag{26}$$

$$\theta_2 = T_{33} - T_{21} \tag{27}$$

$$\theta^{**} = \frac{T_{11} - T_{12}}{\theta_o} \tag{28}$$

$$\theta^{*} = \frac{T_{34} - T_{31}}{\theta_o} = \frac{\Delta T_v}{\theta_o} \tag{29}$$

With the aid of these parameters the temperature differences $\Delta T_v$ ja $\theta_2$ can be written as in the equations (30) and (31).

$$\Delta T_v = R_1 \epsilon_1 \theta_1 + [\, \Delta T_v (1 + \frac{1}{\epsilon_j}) - R_2\, \epsilon_2\, \theta_2] \tag{30}$$

$$\theta_2 = \Delta T_v\, (1 + \frac{1}{\epsilon_j}) - \theta_1\, (1 - R_1\, \epsilon_1) + \theta_o \tag{31}$$

The funqtions $f_1$, $f_2$, $f_{11}$ ja $f_{12}$ have been defined as the equations (32) - (35).

$$f_2 = \frac{1}{\epsilon_j}\, (\, 1 - \epsilon_2\, R_2) - \epsilon_2\, R_2 \tag{32}$$

$$f_{11} = R_2 \, \epsilon_2 \tag{33}$$

$$f_{12} = \theta^{**} \, \frac{R_2}{\epsilon_1} \left( R \, \epsilon_1 + \epsilon_2 - \epsilon_1 \, \epsilon_2 \, R_1 \right) \tag{34}$$

$$f_1 = f_{11} - f_{12} \tag{35}$$

With the aid of equations (32) - (35) the temperature cahnge of the liquid flow ($q_{v3}$) can be defined as the equation (36).

$$\theta^* = \frac{\Delta T_v}{\theta_o} = \frac{f_1}{f_2} \tag{36}$$

REFERENCES

LONDON, A.L. and KAYS, W.M.
"Compact heat exchangers"
Mc Graw-Hill, New York, 1984 ,336 s

MARTTILA, E.
"Dimensioning of heat recovery heat exchangerS in an air conditioning system"
Lappeenranta University of Technology, Research papers 54, Lappeenranta 1996, p. 1 - 52.

MARTTILA, E
"Saved energy in heat recovery of an air conditioning system"
Lappeenrannan teknillinen korkeakoulu, Energiatekniikan osasto, Lappeenranta 1988, p. 1-35.

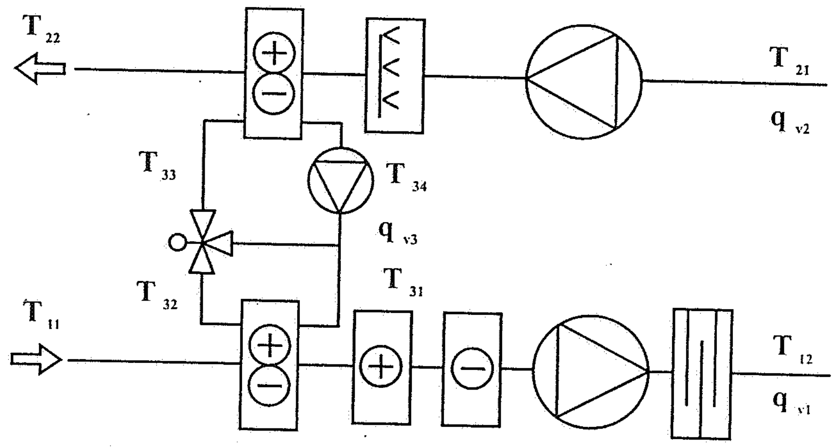


Figure 1 The indirect heat excanger system when primary energy has been carried for the system to the heating (cooling) coils.

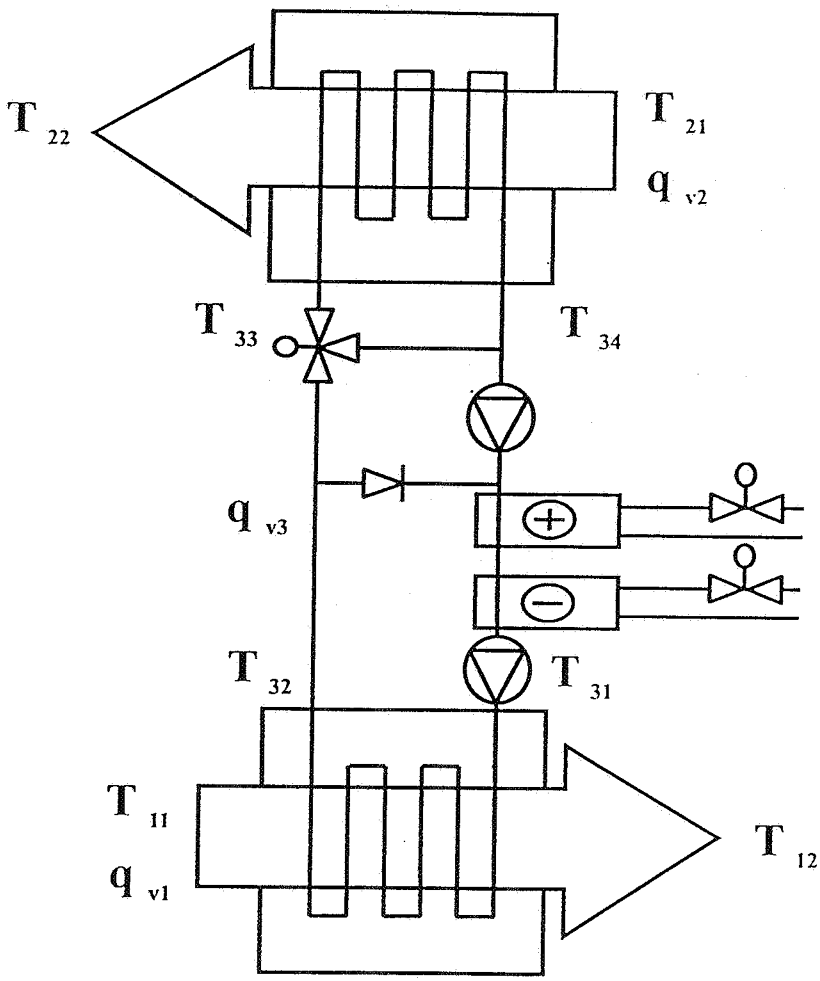


Figure 2. The indirect heat excanger system when primary energy has been carried for the system to the plate heat exchangers.

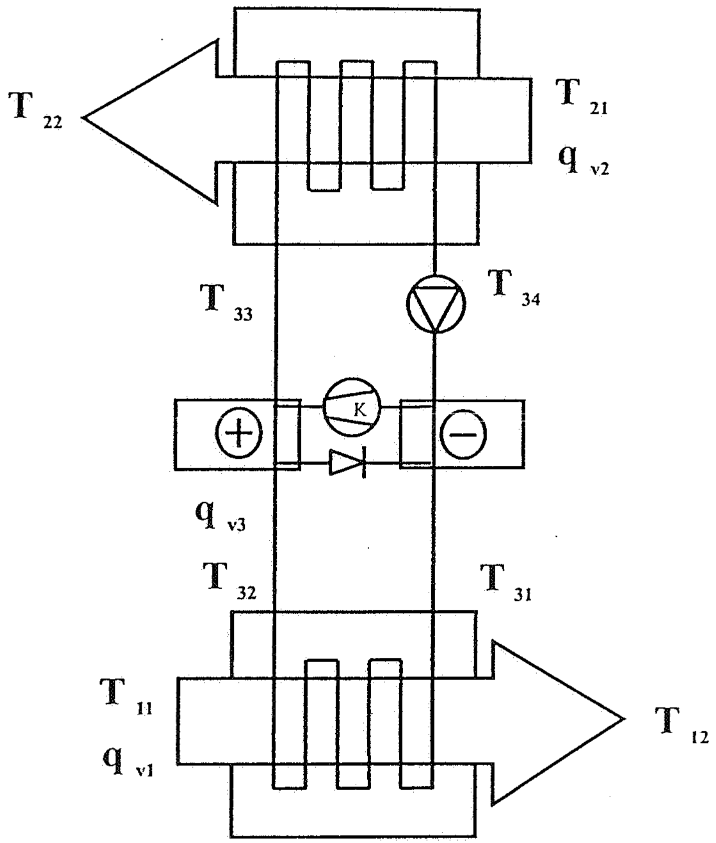


Figure 3. The indirect heat excanger system when condensation and vaporization heat exchangers are coupled in series with heat recovery heat exchangers.

# VENTILATION AND COOLING

18 TH ANNUAL AIVC CONFERENCE
ATHENS, GREECE, 23-26 SEPTEMBER, 1997

Methode die sneller gaat dan CFD, maar minder precies ook !!

Ergens tussen CFD en nodenetwork

## Zonal models : presentation and proposal of new expression of balance equations applied to the study of air flow and heat transfer in buildings.

MUSY M.*, WURTZ E.*, NATAF J.M.✧

* L.E.P.T.A.B. , Université de La Rochelle, 17042 La Rochelle, FRANCE.
✧ S.G.R. L.N.B.L., University of California, Berkeley 94720, U.S.A.

## SYNOPSIS

This paper presents an analysis of different possibilities of representing mass transfers in zonal models.
In this aim, formulations derived from the Navier-Stokes equations or from Euler's theorem are obtained. The models which result from them and empirical models are compared so that to define the best compromise between simplicity, accuracy and easy convergence.

## LIST OF SYMBOLS :

a : coefficient ($s^{-2}$)
b : coefficient ($s^{-2}$)
C : empirical constant ($m/s^1Pa^{1/2}$)
$\vec{F}_S$ : surface forces (N)
$\vec{F}_V$ : volume forces (N)
g : gravitation constant ($m/s^2$)
h : height of the cell (m)
$h_c$ : convection transfer coefficient ($W/m^2K^1$)
$\vec{i}$ : unit vector relative to the axe X
$\vec{k}$ : unit vector relative to the axe Z
l : width of the cell (m)
n : empirical exponent (-)
$\vec{n}$ : perpendicular unit vector
P : air pressure (Pa)
qm : mass flow rate (kg/s)
r : air molar constant ($m^2/s^2K$)
S : surface ($m^2$)
T : air temperature (K)
u : velocity along the axe X (m/s)
$\vec{V}$ : velocity vector (m/s)
w : velocity along the axe Z (m/s)
X : horizontal axe
Z : vertical axe
$\Delta P$ : pressure difference (Pa)
$\rho$ :air density ($kg/m^3$)

**Subscripts :**
0 : centre
Bottom : bottom neighbour
i : studied cell
North : north neighbour
South : south neighbour
Top : top neighbour

## 1. INTRODUCTION

The zonal method is a simplified tool which allows to study the air flow and heat transfers in buildings. Intermediate between one-node models, which results do not permit to predict accurately the thermal comfort or the air quality in a local, and CFD models, which are very slow and require large amount of memory, especially three dimensional, this approach is based on the partitioning of a room or group of rooms into a small number of sub-zones or cells. In these cells, energy and mass balance apply while the exchanges between cells are described at their interfaces.

In our study, SPARK environment is used to develop the zonal model. SPARK is based on object oriented environment and is designed to solve large systems of non-linear equations. The modularity of SPARK permit to test successively the different models without having to rebuild the whole simulation each time.

## 2. REDUCTION OF THE NAVIER-STOKES EQUATIONS

To make our approach clearer, we will carry out our calculations in two-dimensional cases only.
The purpose of this part is the description of mass flows which occur to the interfaces of a standard cell in a local (cell « i » in figure 2.1).

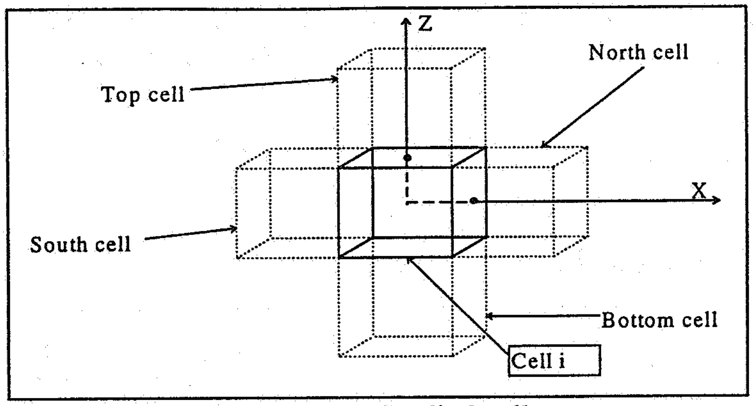

Figure 2.1 : Studied cell.

## 2.1. REDUCTION OF THE EQUATIONS

In steady state, the Navier-Stokes equations combined to the mass conservation equation in two-dimensional Cartesian coordinates (X,Z), applied to the air of a local, can be expressed as follows :

$$\begin{cases} -\dfrac{1}{\rho}\dfrac{\partial P}{\partial x} = u\dfrac{\partial u}{\partial x} + w\dfrac{\partial u}{\partial z} \\ g - \dfrac{1}{\rho}\dfrac{\partial P}{\partial z} = u\dfrac{\partial w}{\partial x} + w\dfrac{\partial w}{\partial z} \end{cases}$$

In these equations, air is assumed as an inviscid flow, only submitted to gravity forces.
To describe the mass flows that cross the frontiers of the cell i that are perpendicular to the axe X, the first Navier-Stokes simplified equation will be studied. In this equation, w is assumed to be equal to zero, it means that flow lines are considered parallel to the axe X. Furthermore, perfect gas law is supposed to apply to the air. The first Navier-Stokes equation becomes :

$$-\frac{rT}{P}\frac{\partial P}{\partial x} = u\frac{\partial u}{\partial x}.$$

By integrating this equation between the frontiers that separate the « cell i » from the « South cell » and the « North cell », with considering that temperature is homogeneous in the cell i and equal to à $T_i$, the following equation is obtained :

$$-rT_i \ln\left(\frac{P\left(\frac{l}{2},Z\right)}{P\left(-\frac{l}{2},Z\right)}\right) = \frac{1}{2}\left(u^2\left(\frac{l}{2},Z\right) - u^2\left(-\frac{l}{2},Z\right)\right).$$

Where P(l/2, Z) (respectively P(-l/2,Z)) is the pressure to the points included in the North (South) frontier which ordinate is Z.
The pressure is supposed to be hydrostatic in the cell and because of this in the frontiers too :

$$\begin{cases} P\left(\frac{l}{2},Z\right) = P_0\left(\frac{l}{2}\right) - \rho_i g Z \quad , \\ P\left(-\frac{l}{2},Z\right) = P_0\left(-\frac{l}{2}\right) - \rho_i g Z \end{cases}$$

where $P_0(-l/2)$ and $P_0(l/2)$ are the pressures in the centre of the frontiers.

Air density has been assumed constant and equal to $\rho_i$ in the cell. This can be justified by the fact that it varies more with temperature (assumed to be constant) than with pressure.

Introducing the new relations $\begin{cases} P_0\left(\frac{l}{2}\right) = \frac{1}{2}\left(P_{0North} + P_{0i}\right) \\ P_0\left(-\frac{l}{2}\right) = \frac{1}{2}\left(P_{0South} + P_{0i}\right) \end{cases}$, where $P_{0North}$, $P_{0South}$ and $P_{0i}$ are respectively the pressures in the centre of the North, South and i cells, the final equation is :

$$\boxed{u^2\left(\frac{l}{2}, Z\right) = u^2\left(-\frac{l}{2}, Z\right) - 2rT_i \ln\left(\frac{\frac{1}{2}\left(P_{0North} + P_{0i}\right) - \rho_i g Z}{\frac{1}{2}\left(P_{0South} + P_{0i}\right) - \rho_i g Z}\right)} \quad (1)$$

Knowing the velocity profile on the south frontier (X=-l/2) of the cell and the centre pressure of North, South and i cells, the velocity of the flow can be calculated in every point of the North frontier. The boundary conditions permit to solve the problem. Once the velocity profiles evaluated, flow rates to the interfaces can be determined.
A similar study allows to establish the equation for Z direction :

$$\boxed{w^2\left(\frac{h}{2}\right) = w^2\left(-\frac{h}{2}\right) - 2gh - 2rT_i \ln\left(\frac{\left(P_{0Top} + P_{0i}\right)}{\left(P_{0Bottom} + P_{0i}\right)}\right)} \quad (2)$$

## 2.2. MODEL

The discretization of the vertical interfaces is made with a small number of iso-altitude on which velocity is calculated. The velocity profiles are then approximated by linearization and the mass flows calculated from these profiles.
At the frontier separating a cell and a wall, the mass flow is set to zero (impermeable wall).

## 2.3. RESULTS AND DISCUSSION

This model did not permit to obtain 2D or 3D convergent simulations, but gives good results in trivial 1D cases as those presented in figure 2.2.

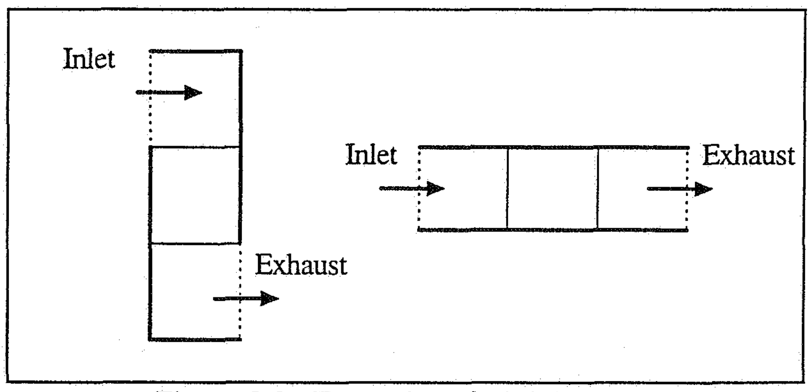

Figure 2.2 : Examples of trivial cases.

The non convergence in 2D cases, encouraged us to re-examine the equations 1 and 2 so that to replace the logarithmic expression with a simpler expression.
In equation the logarithmic term can also be written as follows :

$$-2rT_i \ln\left(\frac{\frac{1}{2}(P_{0North}+P_{0i})-\rho_i gZ}{\frac{1}{2}(P_{0South}+P_{0i})-\rho_i gZ}\right) = -2rT_i\left(\ln\left(1+\frac{(P_{0i}-P_{0South})-2\rho_i gZ}{(P_{0North}+P_{0South})}\right)-\ln\left(1+\frac{(P_{0i}-P_{0North})-2\rho_i gZ}{(P_{0North}+P_{0South})}\right)\right)$$

The terms $\frac{(P_{0i}-P_{0South})-2\rho_i gZ}{(P_{0North}+P_{0South})}$ et $\frac{(P_{0i}-P_{0North})-2\rho_i gZ}{(P_{0North}+P_{0South})}$ are small behind 1, what permits to simplify the expression :

$$-2rT_i \ln\left(\frac{\frac{1}{2}(P_{0North}+P_{0i})-\rho_i gZ}{\frac{1}{2}(P_{0South}+P_{0i})-\rho_i gZ}\right) \approx -2rT_i\left(\frac{(P_{0i}-P_{0South})-2\rho_i gZ}{P_{0North}+P_{0South}}-\frac{(P_{0i}-P_{0North})-2\rho_i gZ}{P_{0North}+P_{0South}}\right).$$

$$\approx -2rT_i\left(\frac{P_{0North}-P_{0South}}{P_{0North}+P_{0South}}\right)$$

Admitting that $P_{0North}+P_{0South}\approx 2P_{0i}$, and using perfect gas law, a simple expression is obtained :

$$-2rT_i \ln\left(\frac{\frac{1}{2}(P_{0North}+P_{0i})-\rho_i gZ}{\frac{1}{2}(P_{0South}+P_{0i})-\rho_i gZ}\right) \approx -\rho_i(P_{0North}-P_{0South}).$$

This expression included in equation 1 gives :

$$\boxed{u^2\left(\frac{l}{2},Z\right) = u^2\left(-\frac{l}{2},Z\right)-\rho_i(P_{0North}-P_{0South})}.$$

This is Bernoulli equation applicable along a horizontal flow line. The reduction of equation (2) leads to Bernoulli equation applicable along a vertical flow line.
These equations are therefore applicable to 1-D for which the flow lines that cross South (or Bottom) interface cross North (or Top) interface too. But this becomes false in 2-D and 3-D cases. It probably explains why the simulations did not converge.

## 3. EULER THEOREM APPLICATION

### 3.1. EQUATIONS DEVELOPMENT

In steady state, the expression of Euler's theorem is : $\iint_S (\rho\vec{V})(\vec{V}.\vec{n})dS = [\vec{F}_V]+[\vec{F}_S]$.

Applied in 2-D to the studied cell (figure 2.1), and projected onto X and Z axes it leads to :

$$\begin{cases} \iint_{South\_frontier} -\rho u^2 dS + \iint_{North\_frontier} \rho u^2 dS + \iint_{Bottom\_frontier} -\rho wudS + \iint_{Top\_frontier} \rho wudS = [\vec{F}_V.\vec{i}]+[\vec{F}_S.\vec{i}] \\ \iint_{South\_frontier} -\rho uwdS + \iint_{North\_frontier} \rho uwdS + \iint_{Bottom\_frontier} -\rho w^2 dS + \iint_{Top\_frontier} \rho w^2 dS = [\vec{F}_V.\vec{k}]+[\vec{F}_S.\vec{k}] \end{cases}.$$

Admitting that the force of gravity is the only volume force and surface pressures the only surface forces that act on the cell, the equations become :

$$\begin{cases} \iint\limits_{South\_frontier} -\rho u^2 dS + \iint\limits_{North\_frontier} \rho u^2 dS + \iint\limits_{Bottom\_frontier} -\rho wudS + \iint\limits_{Top\_frontier} \rho wudS = \iint\limits_{South\_frontier} -PdS + \iint\limits_{North\_frontier} PdS \\ \iint\limits_{South\_frontier} -\rho uwdS + \iint\limits_{North\_frontier} \rho uwdS + \iint\limits_{Bottom\_frontier} -\rho w^2 dS + \iint\limits_{Top\_frontier} \rho w^2 dS = \iint\limits_{Bottom\_frontier} -PdS + \iint\limits_{Top\_frontier} PdS + \iiint\limits_{cell\_i} \rho g dV \end{cases} \quad .(3)$$

## 3.2. APPLICATION TO A FLOW

To evaluate the integrals contained in equation (3), hypothesis on velocity profiles must be done. They are supposed to be plan :

$$\begin{cases} u_{South\_frontier}(Z) = u_{0\_South} + a_{South} Z \\ u_{North\_frontier}(Z) = u_{0\_North} + a_{North} Z \\ u_{Bottom\_frontier}(X) = u_{0\_Bottom} + a_{Bottom} X \\ u_{Top\_frontier}(X) = u_{0\_Top} + a_{Top} X \end{cases} \qquad \begin{cases} w_{South\_frontier}(Z) = w_{0\_South} + b_{South} X \\ w_{North\_frontier}(Z) = w_{0\_North} + b_{North} X \\ w_{Bottom\_frontier}(X) = w_{0\_Bottom} + b_{Bottom} X \\ w_{Top\_frontier}(X) = w_{0\_Top} + b_{Top} X \end{cases}.$$

In the interfaces, the air density is considered homogeneous and the pressure hydrostatic :

$$\begin{cases} -\rho_{South}\left(u_{0\_South}^2 + \dfrac{a_{South}^2 h^2}{12}\right) + \rho_{North}\left(u_{0\_North}^2 + \dfrac{a_{North}^2 h^2}{12}\right) - \rho_{Bottom}\left(w_{0\_Bottom} u_{0\_Bottom} + \dfrac{b_{Bottom} a_{Bottom} l^2}{12}\right) \\ + \rho_{Top}\left(w_{0\_Top} u_{0\_Top} + \dfrac{b_{Top} a_{Top} l^2}{12}\right) = -P_0\left(-\dfrac{l}{2}\right) + P_0\left(\dfrac{l}{2}\right) \\ -\rho_{Bottom}\left(u_{0\_Bottom}^2 + \dfrac{a_{Bottom}^2 l^2}{12}\right) + \rho_{Top}\left(u_{0\_Top}^2 + \dfrac{a_{Top}^2 l^2}{12}\right) - \rho_{South}\left(w_{0\_South} u_{0\_South} + \dfrac{b_{South} a_{South} h^2}{12}\right) \\ + \rho_{North}\left(w_{0\_North} u_{0\_North} + \dfrac{b_{North} a_{North} h^2}{12}\right) = -P_0\left(-\dfrac{h}{2}\right) + P_0\left(\dfrac{h}{2}\right) + \rho_i g V \end{cases}$$

Four unknowns per interface have been introduced while only two equations per cell have been obtained. Continuity equations between interfaces are needed.

## 3.3. CONCLUSION

This method leads to the introduction of many supplementary unknowns, (4 per interface in 2-D cases and 9 per interface in 3-D cases). The resolution will be all the slower. Furthermore, writing continuity equation between interface involves the addition in the model of new macro-objects linking the interfaces. These are the reasons why, for the moment, this method has been put aside.

# 4. EMPIRICAL MODEL

## 4.1. DESCRIPTION OF ZONAL MODEL

In the zonal model studied by E. WURTZ [5], mass exchanges between cells are calculated from the equation of flows across large enclosures K. LIMAM et al.[2] :

$q_m = \int_S C\rho(\Delta P)^n dS$ where c and n are empirical coefficients.

E. WURTZ [5] has shown that with C equal to 0.83 and n equal to 0.5 where the flow is turbulent (usual case) and equal to 1 where the flow is laminar (for example when crossing a permeable wall), the zonal model gives results similar to those obtained with FLUENT.

## 4.2. ADVANTAGES AND LIMITS

The aforementioned method yielded good results for certain typical physical configurations (openings, cases for which flow is easily predictable) but falls short in particular in the case of natural convection. It is thus quite hard to demonstrate a thermally stratified problem, and impossible to represent properly a decelerated flow.
Furthermore, it is sometimes difficult to obtain the convergence of the simulation. This must be due to the coefficient n=0.5 that makes mass exchange equation non-linear.

## 4.3. REDUCTION OF THE MODEL

Pressure differences that occur in rooms are very small. As shown in figure 4.1, the function $f(\Delta P)=0.83*\Delta P^{1/2}$, separated in three intervals can be approximated by linear functions :

- $f_1(\Delta P)=0.2*\Delta P-0.75$ if $\Delta P\in[-10,-0.75]$,
- $f_2(\Delta P)=1.2*\Delta P$ if $\Delta P\in[-0.75,0.75]$,
- $f_3(\Delta P)=0.2*\Delta P+0.75$ if $\Delta P\in[0.75,10]$.

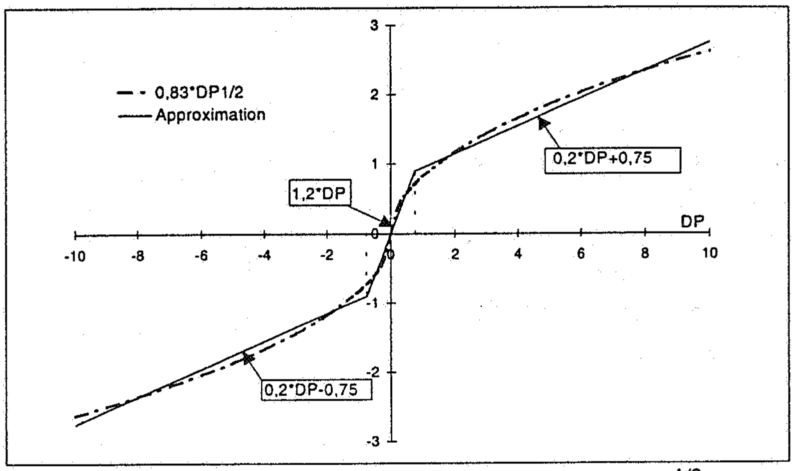

Figure 4.1 : Approximation of $f(\Delta P)=0.83*\Delta P^{1/2}$.

## 5. RESULTS
## 5.1. PRESENTATION OF SPARK

The Simulation Problem Analysis and Research Kernel (SPARK) is a modular environment that automates writing code for systems of non-linear equations. It was developed for building science but is applicable to other fields. First written for steady state problems, (J.L. ANDERSON [1]), it has been extended to handle transient problem by the addition of time integrator objects (E.F. SOWELL and al. [4]).
As TRNSYS, CLIM2000 and Allan Simulation, SPARK allows the user to build complex simulations by connecting smaller elements that can be objects (single equations) or macro-objects (equations subsystems).
Objects are automatically generated from equations expressed symbolically (J.M. NATAF and F. WINKELMANN [3])
SPARK use the graph-theoretic techniques to reduce the size of the equations system so that SPARK's Newton-Raphson solver words on the reduced equations set and, after convergence, the remaining unknowns are solved for.
The output is a C program that is automatically compiled and executed.

To build zonal models in SARK environment, two main object classes are created, they correspond to the cells and the interfaces between cells.

The cell class consists of the balance equations for the cell, the pressure drop equation and the perfect gas law while the interface class consists of the mass and energy flow calculations. These classes are used as many time as necessary to define the simulation and linked in the connection file.

## 5.2. COMPARISON ZONAL MODEL - SIMPLIFIED MODEL

Empirical zonal model and simplified one are studied from the simple configuration shown in figure 5.1 (ventilated room with heating floor (301K) and exterior wall (288K). The cells are 0,8m side squares. The results (flow rates, temperature density and pressure are represented in figure 5.2 and figure 5.3.

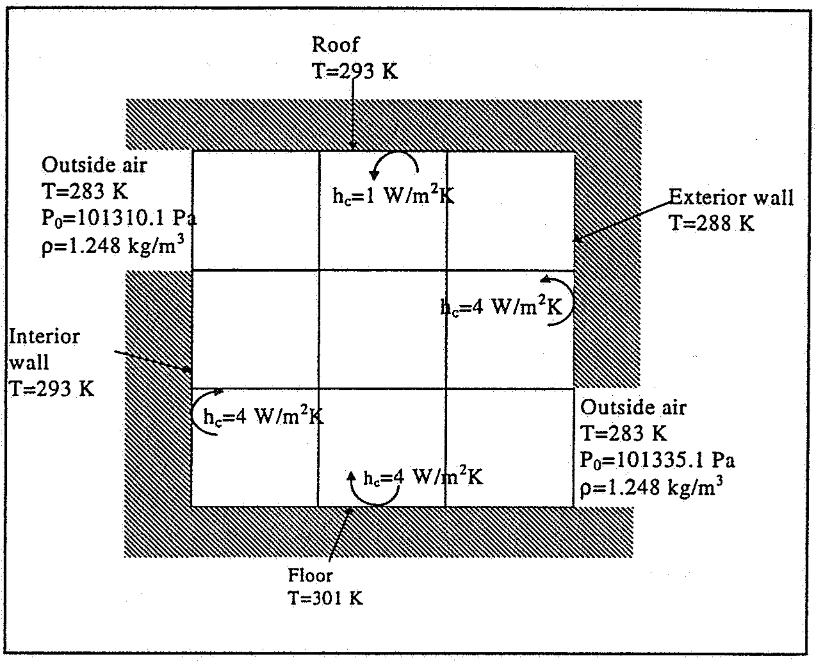


Figure 5.1 : Studied configuration

## 5.3. RESULTS AND CONCLUSION

The results given in figure 5.2 and figure 5.3 have been obtained with the simplified model and empirical model, they are presented as follows :

- *italic* : vertical and horizontal mass flow rates(kg/s),
- dotted outlined, from top to bottom : temperature (K), density (kg/m$^3$), pressure (Pa).

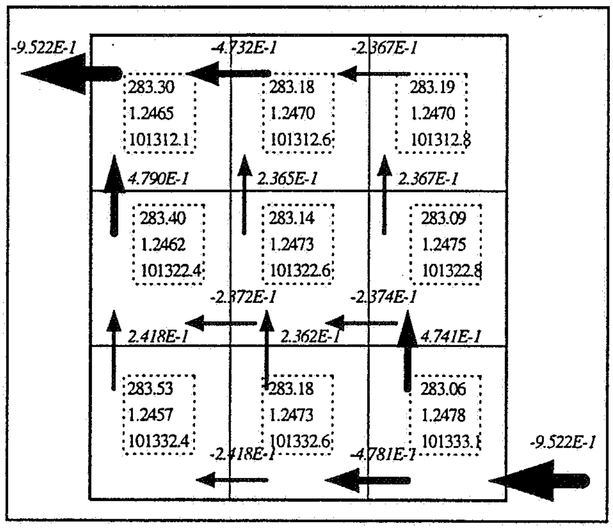


Figure 5.2 : Simplied model, results.

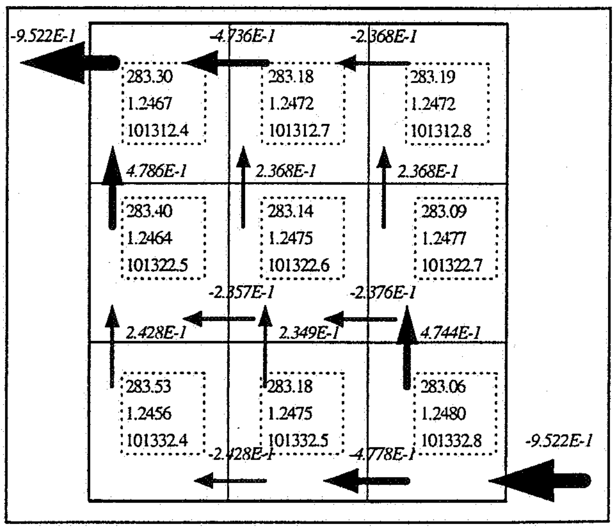


Figure 5.3 : Empirical model, results.

One can notice that the temperatures and mass flow rates obtained are very similar while the differences between pressures are more important. It does not really matter because pressure is not the most interesting result in thermal and mass transfers representation.

## 6. CONCLUSION

The best compromise between simplicity of the model, convergence of the simulation and calculation time seems to be the simplified model presented in chapter 3.3. This model gives as good results as the empirical one, thus in very short calculation times, so it will be possible to couple it with other models. The aim of the next studies will be the coupling of the simplified zonal model with wall models, comfort models, moisture and pollutants transport models. It is also projected to create new sorts of cells that represents plumes or jets.


## ACKNOWLEDGEMENTS :

The authors wish to thanks Mr Francis ALLARD for his help and discussion during this work


## REFERENCES :


1. ANDERSON J.L.
« A network definition and solution of simulation problems »
Technical Report 21522. Lawrence Berkeley Laboratory. September 1987.

2. LIMAM K., INARD C., ALLARD F.
« Etude expérimentale des transferts de masse et de chaleur à travers les grandes ouvertures verticales »
*Ventilation et renouvellement d'air.* Lyon. GEVRA, 1991.

3. NATAF J.M. WINKELMANN F.
« Symbolic modelling in building energy simulation »
LBL Report LBL-35439. Lawrence Berkeley Laboratory. April 1994.

4. SOWELL E.F., BULH W.F., NATAF J.M.
« Object-oriented programming, equation-based sub-models, and system reduction in spank. »
*Proceedings of Building Simulation' 89*, pages 141-146, Vancouver, British Colombia, Canada, June 1989.

5. WURTZ E.
« Modélisation tridimensionnelle des transferts thermiques et aérauliques en environnement orienté objet »
PhD Thesis. Ecole Nationale des Ponts et Chaussées. 1995.

## VENTILATION AND COOLING

18TH ANNUAL AIVC CONFERENCE
ATHENS, GREECE, 23-26 SEPTEMBER, 1997

# A MODIFICATION OF THE POWER-LAW EQUATION TO ACCOUNT FOR LARGE SCALE WIND TURBULENCE

$q = c \cdot \Delta p^n \rightarrow$ aanpassen voor turbulentie

Kai Sirén

Helsinki University of Technology
Finland

# A MODIFICATION OF THE POWER-LAW EQUATION TO ACCOUNT FOR LARGE SCALE WIND TURBULENCE


## SYNOPSIS
Existing infiltration and exfiltration calculation methods are mainly based on the stationary approach, where long term mean values are used for wind input data. The real wind speed is, however, varying continuously with time. Because the process of the crack flow is non-linear, using mean wind speed values will give erroneous results for the air flows. The goal of the research has been to develop a simple method to account for the effect of large scale wind turbulence on the calculated air flows.

A modification of the power-law equation has been derived based on the assumption of sinusoidal wind speed fluctuation. The equation is integrated over time to form a new turbulent power-law equation. The integration is carried out numerically using the simple trapezoidal rule approximation. This equation can be used in flow computation in the place of the ordinary power-law equation. The additional input data needed for such a computation is the wind turbulence intensity.

The performance of the turbulent power-law equation is tested computationally by comparing its results against the results of a theoretically far more detailed calculation method, which takes into account the dynamics of the air in the cracks and the capacity of the building space. The computations are carried out using Simnon, a program specially designed for simulation of non-linear systems. Real, with one second time interval measured wind speed has been used as input data. A simple building model with two floors and eight cracks in the walls has been used as a test case. The results show, that the error in the flow rates caused by the stationary approach is mainly dependent on the flow exponent and the turbulence intensity and varies roughly between 0 - 20 %. The higher the turbulence intensity and the more laminar the crack flow, the higher is the error. The turbulent power-law equation performs well and is capable to reduce this error by roughly one decade.


## LIST OF SYMBOLS

| | | |
|---|---|---|
| $a$ | amplitude | m/s |
| $C_p$ | pressure coefficient | - |
| $K$ | flow coefficient | $(m^3/s)/(Pa)^n$ |
| $I_t$ | intensity of turbulence | - |
| $n$ | flow exponent | - |
| $p_i$ | internal pressure | Pa |
| $p_w$ | wind pressure | Pa |
| $\Delta p$ | pressure difference | Pa |
| $q$ | volume flow rate | $m^3/s$ |
| $q_t$ | total infiltration volume flow rate | $m^3/s$ |
| $q_{tr}$ | total infiltration reference volume flow rate | $m^3/s$ |
| $R_w$ | proportionality factor | - |

| | | |
|---|---|---|
| $t$ | time | s |
| $T$ | period of integration | s |
| $v$ | wind velocity | m/s |
| $v_m$ | mean wind velocity | m/s |
| $V$ | volume | $m^3$ |
| $\rho$ | density | $kg/m^3$ |
| $\sigma_v$ | standard deviation of velocity | m/s |
| $\omega$ | angular velocity | rad/s |
| $\Im$ | integral term | $(m/s)^{2n}$ |

## INTRODUCTION

The usual procedure to compute the infiltration and exfiltration air flows implies fixed wind velocity values. This implies, that an average velocity representing one hour or a longer period of time is used as input value. The nature of crack flow through the building envelop is non-linear, which means that using average wind velocity as an input does not give correct average flow rate values and air exchange rates. The larger is the turbulence, the larger are the errors expected when applying the steady-state approach. The effect of wind velocity fluctuations on air exchange has been studied and different kinds of approaches to tackle the problem have been made [1-6]. In the following a modification of the power-law equation is derived, which is capable to account for the wind turbulence. The performance of the equation is shown by comparing the results with the results of a detailed dynamical infiltration/exfiltration computation.

## POWER-LAW EQUATION

The non-linear interdependence in crack flow between the pressure difference and the volume flow rate is usually described either by the quadratic equation or by the power-law equation [7]. Both equations have their advantages and disadvantages. In general they both, however, describe the crack flow very satisfactorily, as long as the coefficients included in the equations are chosen according to the properties of the crack or cracks the equation is representing. Here the power-law equation forms the basis for a further development. The power-law equation is usually presented in the following form:

$$q = K\,\Delta p^n \qquad (1)$$

where q is the volume flow rate, K is a flow coefficient, $\Delta p$ is the pressure difference and n is the flow exponent. The flow coefficient is related to the size of the opening and the flow exponent is dependent of the type of the flow. For a fully laminar flow n=1.0 and for a fully turbulent flow n=0.5. In real buildings the flow paths leading air through the building shell are usually combinations of several cracks and material layers. This means, that nor fully laminar neither fully turbulent flows computationally exist and effective values between the lower bound and the upper bound for the flow exponent in equation (1) have to be chosen. The non-linearity of equation (1) also clearly explains, why using mean velocity of some time period gives erroneous results for air flows during that period, when the wind velocity is temporally fluctuating.

## TURBULENT POWER-LAW EQUATION

With the turbulent power-law equation a trial is made to account for the problem described above. In a simplified approach the wind velocity as a function of time is approximated by a sine curve in the following manner

$$v(t) = v_m + a\sin(\omega t) \qquad (2)$$

fluctuating part of wind

where $v_m$ is mean velocity, a is amplitude, $\omega$ is angular velocity and t is time. When such a wind strikes a building, the pressure on the building external surfaces follow the velocity and the pressure difference over a crack located in the envelop is

$$\Delta p(t) = p_w(t) - p_i(t) = C_p \frac{1}{2}\rho\, v^2(t) - p_i(t) \qquad (3)$$

where $p_w$ is wind pressure, $p_i$ is internal pressure, $C_p$ is pressure coefficient and $\rho$ is air density. Substituting the wind velocity in equation (2) to equation (3) and further, substituting the pressure difference in equation (3) to the power-law equation (1) yields for the flow rate through a crack

$$q(t) = K\left[C_P \frac{1}{2}\rho\ (v_m + a\sin(\omega t))^2 - p_i(t)\right]^n \qquad (4)$$

aggregate power law equation

The temporal variation of the internal pressure inside the building $p_i(t)$ is unknown. Let's now set the following hypothesis: the internal pressure fluctuates proportional to the wind kinetic pressure

$$p_i(t) = R_w \frac{1}{2}\rho\, v^2(t) \qquad (5)$$

where $R_w$ is the proportionality factor having a constant value. Substituting (5) into (4) gives further for the flow rate as a function of time

$$q(t) = K\left[(C_P - R_w)\frac{1}{2}\rho\ (v_m + a\sin(\omega t))^2\right]^n \qquad (6)$$

The conservation of mass for the zone j in the building is

$$\frac{d(\rho_j V_j)}{dt} = \sum_{k=1}^{N} \rho_k q_k(t) \qquad (7)$$

where $\rho_j$ and $V_j$ are the density and the internal volume of zone j, and the sum is taken over all cracks k which are connected to the zone j. The density and the volume of the zone are now, as an approximation, set to be constant values, which yields for each zone a mass conservation equation of the type

$$\rho_1 q_1(t) + \rho_2 q_2(t) + \dots \rho_N q_N(t) = 0 \tag{8}$$

The aeraulic behaviour of the whole building is covered by a set of mass conservation equations of the type above, one written for each zone. This set of non-linear algebraic equations is usually solved by iterative methods. Now, however, the flow rates in equation (8) are not constant, but are varying with time. To be able to get a solution, we first integrate both sides of equation (8) over a period of time, which can be done term by term and then divide both sides by the period of integration

$$\frac{1}{T}\int_0^T \rho_1 q_1(t)\,dt + \frac{1}{T}\int_0^T \rho_2 q_2(t)\,dt + \dots + \frac{1}{T}\int_0^T \rho_N q_N(t)\,dt = 0 \tag{9}$$

If the period of time T is long enough, we get a new set of mass conservation equations, where the fluctuating, time depended flow rates q(t) are replaced by mean flow rates $q_m$

$$\rho_1 q_{m1} + \rho_2 q_{m2} + \dots \rho_N q_{mN} = 0 \tag{10}$$

According to this, equation (6) is now integrated for one period of the sine function

$$q_m = \frac{\omega}{2\pi} K\left[(C_P - R_w)\frac{1}{2}\rho\right]^n \int_0^{2\pi/\omega} (v_m + a\sin(\omega t))^{2n}\,dt \tag{11}$$

Because the flow exponent n is not an integer, there is no analytical solution for this equation. For this reason a numerical approach for integration is utilised. There are several alternatives available to do the numerical integration. Here the trapezoid rule with eight subintervals is used. Thus the integral term in equation (11), numerically integrated, yield

$$\Im = \frac{1}{8}(v_m + a)^{2n} + \frac{1}{4}(v_m + \frac{a}{\sqrt{2}})^{2n} + \frac{1}{4}v_m^{\ 2n} + \frac{1}{4}(v_m - \frac{a}{\sqrt{2}})^{2n} + \frac{1}{8}(v_m - a)^{2n} \tag{12}$$

and the mean flow rate, when the time of integration is set to T=1, is

$$q_m = K\left[(C_P - R_w)\frac{1}{2}\rho\right]^n \Im \tag{13}$$

In computation of infiltration and exfiltration air flows, the normal power-law equation can be replaced by the above turbulent power-law equation. The computation procedure is exactly the same than in the mean velocity approach. The internal mean pressures, which now are the unknowns, correspond to the mean velocity

$$p_{im}(t) = R_w \frac{1}{2} \rho\, v_m^{\,2}(t) \tag{14}$$

and are included in the turbulent power-law equation in the $R_w$ factor. Further, the amplitude a of the approximative sinusoidal velocity (2) has to be known to be able to compute a value for the integral expression (12) and the flow rates (13). The real wind velocity, however, is not sinusoidal and has no constant amplitude. On the other hand, the real wind velocity has a mean value and a standard deviation. The sinusoidal velocity, presented by an analytical function, can also imagined to have a standard deviation, which quite easily can be shown to be

$$\sigma_v = \frac{a}{\sqrt{2}} \tag{15}$$

where a is the amplitude of the fluctuation. The intensity of turbulence, which can be computed based on wind velocity measurements, is defined as the standard deviation divided by the mean velocity

$$I_t = \frac{\sigma_v}{v_m} \tag{16}$$

According to equations (15) and (16) we get for the amplitude of the sinusoidal velocity

$$a = \sqrt{2}\, I_t\, v_m \tag{17}$$

which now can be calculated by substituting the mean velocity and intensity of turbulence of the real wind into the equation (17).

## COMPUTATIONAL VALIDATION

Because of the many simplifying approximations and one hypothesis included in the concept above, the results can not be precise, even if all other factors like flow coefficients, flow exponents, pressure coefficients etc. would have exactly correct values. To test the performance of the turbulent power-law equation, a computational validation was done. The demand is, that the reference results, which form the base of the comparison, must have essentially higher quality than the results produced by the method under the test. Here the reference computations decided to be carried out using Simnon [8], a program specially designed for simulation of non-linear systems described with differential or difference equations. It contains a macro level language to define the system and a solver which gives the choice between several algorithms of numerical integration. The integration is done using an automatic step size adjustment.

The case used for validation is a simple building with two floors, having one crack in each wall in both floors, together eight cracks. Momentum equations for each crack and the opening between the floors and a conservation of mass equation for both zones (floors), together eleven differential equations describe the temporal characteristics of the system.

Measured wind velocity was used as input data for the Simnon computations. The input velocity data was measured on the roof level of a two storey building located in a sub-urban single-family house area in southern Finland. This way the characteristics of the local wind speed, which strikes the buildings, could be monitored. Each input data set consists a ten minutes sample recorded with one second time interval, together 600 velocity readings.

For the usual mean velocity computation approach the mean velocity of the ten minutes data sets was used as wind input. For the turbulent power law approach the information of the intensity of turbulence of each data set was added to the input data. For the Simnon reference computations all recorded 600 wind velocity values of each data set were used to perform the dynamic computations. In Fig. 1 the mean total infiltration air flows of the mean velocity approach and the turbulent power law approach are compared with the results of the reference computations.

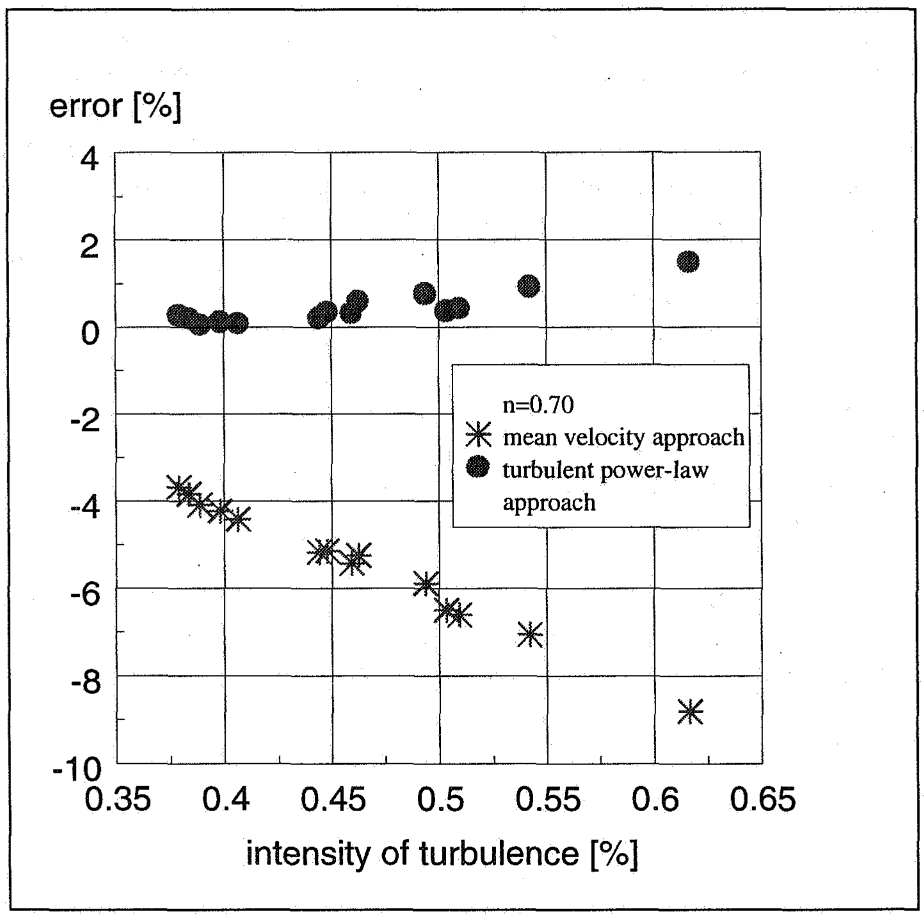


Fig. 1. Relative errors of the total infiltration air flows as a function of the intensity of wind turbulence.

The error terms in Fig. 1 are defined as follows:

$$error = 100 \frac{q_{mt} - q_{mtr}}{q_{mtr}} \tag{18}$$

where $q_{mt}$ is the temporal mean total infiltration volume flow rate into the two floor building, computed with either the mean velocity approach or the turbulent power-law approach and $q_{mtr}$ is the corresponding reference quantity, computed with SIMNON and representing the temporal mean of the time period of the wind input data set.

## DISCUSSION

There are two main factors influencing the prediction error shown above. One is the intensity of wind turbulence, as clearly can be seen from Fig.1. The other is the flow exponent. The results shown are computed using a typical medium size value n=0.7 for the flow exponent. If the flow exponent is reduced, which means a more turbulent flow in the cracks, the error of both approaches is also reduced and vice versa.

The turbulent power-law approach shown, does not take into account any temperature difference between indoors and outdoors. This feature can, however, be added easily.

The validation described, is comparison between two computational results. Even though the dynamical SIMNON approach is very detailed and gives, without any doubt, sufficiently reliable results, a more convincing and final validation should be done by using measured reference values. The question is, however, of quite small differences and a measurement based validation is a very demanding task.

## CONCLUSIONS

It has been shown, that the turbulent power-law approach performs well in the case of a simple computational exercise and is capable to reduce the error of the usual mean velocity approach by roughly one decade.

The error in computed results caused by wind velocity fluctuations, depends mainly on the intensity of wind turbulence and the nature of the crack flow. The higher the turbulence intencity and the more laminar the crack flow, the higher is the error.

According to the computations, the hypothesis of the indoor pressure to be proportional to the wind kinetic pressure seems to hold well.

**REFERENCES**

*1. Hill J.E. and Kusuda T.*
*"Dynamic Characteristics of Air Infiltration"*
*ASHRAE Transactions 81 Part 1, 1975, pp 168-185.*

*2. Potter I.N.*
*"Effect of fluctuating Wind Pressures on Natural Ventilation Rates"*
*ASHRAE Transactions 85 Part 2, 1979, pp 445-457.*

*3. Sasaki T., Hayashi M. and Aratani N.*
*"On the Ventilating Characteristics of the Space under the fluctuating Wind Pressure"*
*Proceedings of Roomvent-87 "Air Distribution in ventilated Spaces", Session 4a, 1987.*

*4. Haghighat F., Rao J. and Fazio P.*
*"The influence of Turbulent Wind on Air Change Rates - a Modelling Approach"*
*Building and Environment, Vol. 26, No 2,1991, pp. 95-109.*

*5. Sharples S. and Palmer R.G.*
*"Modelling fluctuating Air Flows through Building Cracks"*
*Proceedings of the 15'th AIVC Conference, 1994, pp. 216-222.*

*6. Sharples S. and Thompson D.*
*"Experimental Study of Crack Flow with varying Pressure Differentials"*
*Proceedings of the 17'th AIVC Conference, 1996, pp. 343-351.*

*7. Liddament M.*
*"Air Infiltration Calculation Techniques - An Applications Guide"*
*Air Infiltration and Ventilation Centre, 1986.*

*8. Simnon for Windows, Version 2.0, May 1995. SSPA Maritime Consulting AB, Göteborg, Sweden.*

**VENTILATION AND COOLING**
**18TH AIVC CONFERENCE, ATHENS, GREECE**
**23-26 SEPTEMBER, 1997**

**Title:** **Simulation of Non-Passive Particle Dispersion in Ventilated Rooms**

nt gepresenteerd

**Author(s):** **Sture Holmberg*, Yuguo Li****

**Affiliation:** *** National Institute for Working Life, S-171 84 Solna, Sweden**
****CSIRO, Building Construction and Engineering, P O Box 56, Highett, Vic.3190, Australia**

# Simulation of Non-Passive Particle Dispersion in Ventilated Rooms

Sture Holmberg
National Institute for Working Life
S-171 84 Solna, Sweden

Yuguo Li
CSIRO, Building, Construction and Engineering
P.O. Box 56, Highett, Vic. 3190, Australia

**Synopsis**
Concentrations of indoor air contaminants are normally calculated by assuming that they fully follow airflow paths in a room. This assumption is also used to predict the local residence time of contaminants in a room, which may further be used to characterise the ventilation effectiveness. In this paper, a different methodology has been adopted, in which indoor airborne particles do not always follow the main airstream induced by the ventilation system. Dispersion of particles is predicted by a drift-flux model. The model assumes that the settling velocity of each particle is sufficiently small when compared to the high inflow velocity and the volumetric concentration of particles is also very low. This assumption has justified the use of a drift-flux multi-phase model rather than a fully coupled multi-fluid model. Additionally, the effect of the particles on turbulence can be neglected. In the drift-flux model, a settling term is added to the concentration equation, and the body force term in the momentum equation is treated using the principle of a Bousinnesq approximation, similar to that in a thermal-buoyancy-driven flow.

The model has been previously validated by comparing numerically calculated results with those measured in an aerosol chamber. In the examples in this paper, particles with diameters ranging from 0.5 $\mu$m to 5 $\mu$m are supplied into a room through a ventilation and air-conditioning register. Local particle concentrations are calculated for different particle size groups. It is shown that in the air-conditioning situations considered, the thermal-buoyancy-introduced flows provide an additional mixing mechanism for particle dispersion in the room. The developed model can be a useful tool for minimising particle concentrations in the air by evaluating and selecting an optimum air distribution and air-conditioning system.

## 1. Introduction

Contaminant and particle concentrations have often been used as a direct measure of indoor air quality in buildings. In ventilation and industrial hygiene, many design guidelines and regulations specify the threshold of a particular contaminant concentration. Thus, there has been considerable interest in the literature in attempting to predict the contaminant concentration and turbulence dispersion of contaminants and particles. Indeed, the particle concentration is closely related to the flow pattern in a flow system. In the 1950's, a tracer concentration history in a flow system was used to introduce the concepts such as residence time and age of the fluids in chemical engineering. These concepts have been further developed in the field of ventilation to evaluate ventilation performance. In ventilation engineering, one very useful modification to the concentration equation is the steady state transport equation for the mean age of the air (see for example [1] and [2]). In all the situations considered, the particles of the tracer are assumed to be passive, i.e. they follow the airflow path in an enclosure.

In this paper, a new concentration equation is suggested for non-passive (settling) particles. By modifying the general concentration and momentum equations, particle settling velocities can be considered when movement of indoor air pollutants in rooms is simulated. This allows the settling rates of dust and other solid pollutants to be estimated.

The new model, where air velocity turbulence is calculated by a k-ε model, is expected to give a better understanding of the relationships between room geometries, ventilation airflow rates and ventilation principles on one hand, and pollutant characteristics and concentration levels on the other. Simulations can be used to find the optimal air distribution principle to eliminate/minimise identified harmful indoor air particles in built environment. A particular area of interest is the human near-body zone, where the particle behaviour and local concentrations are of particular importance from an occupational health point of view. The work to be presented in this paper has been a close collaboration between the two authors who represent two separate organisations with a strong interest in dust and pollutant control.

## 2. Governing equations for particle dispersion

The general governing equation for continuity and transport is:

$$\frac{\partial(\rho u_j \varphi)}{\partial x_j} = \frac{\partial}{\partial x_j}\left(\Gamma \frac{\partial \varphi}{\partial x_j}\right) + S \tag{1}$$

where subscript j stands for coordinate directions. The equation components are given in Table 1. From Equation (1) the z direction momentum equation is given by:

$$\frac{\partial(\rho u_j w)}{\partial x_j} = \frac{\partial}{\partial x_j}\left(\Gamma \frac{\partial w}{\partial x_j}\right) + S + F_{\Delta\rho} + F_{\Delta T} \tag{2}$$

where body forces due to particle/fluid density differences ($F_{\Delta\rho}$) and thermal differences ($F_{\Delta T}$) are modelled by using a Boussinesq approximation. A particle settling velocity $w_s$ is included in the concentration equation, giving the following equation for concentration calculations of non-passive particles in the air:

$$\rho\left(u\frac{\partial c}{\partial x} + v\frac{\partial c}{\partial y} + (w+w_s)\frac{\partial c}{\partial z}\right) = \frac{\partial}{\partial x_j}\left(\Gamma \frac{\partial c}{\partial x_j}\right) \tag{3}$$

**Table 1**. General transport parameters for Equation (1). The pressure component is given by p, temperature by T, laminar Prandtl number (Schmidt number) by $\sigma$, fluid viscosity by $\mu$ and density by $\rho$. Subscripts c, i and t indicate concentration, coordinate direction and turbulence.

| EQUATION | $\varphi$ | $\Gamma$ | S |
|---|---|---|---|
| Continuity | 1 | 0 | 0 |
| Momentum | $u_i$ | $\mu + \mu_t$ | $-\partial p/\partial x_i$ |
| Particle concentration<br>Energy | c<br>T | $\mu/\sigma + \mu_t/\sigma_c$<br>$\mu/\sigma + \mu_t/\sigma_t$ | 0 |
| Turbulent kinetic energy | k | $\mu + \mu_t/\sigma_k$ | $P_k - \rho\varepsilon$ |
| Dissipation of k | $\varepsilon$ | $\mu + \mu_t/\sigma_\varepsilon$ | $\varepsilon(C_{\varepsilon 1}P_k - C_{\varepsilon 2}\,\rho\varepsilon)/k$ |
| $P_k = \mu_t(\partial u_i/\partial x_j + \partial u_j/\partial x_i)\partial u_i/\partial x_j$, $\mu_t = C_\mu\,\rho k^2/\varepsilon$, $C_\mu = 0.09$, $C_{\varepsilon 1} = 1.44$, $C_{\varepsilon 2} = 1.92$, $\sigma = 0.72$, $\sigma_c = 0.9$, $\sigma_t = 0.9$, $\sigma_k = 1.0$, $\sigma_\varepsilon = 1.3$ | | | |

### 3. Boundary conditions

Particles were supplied into the room with incoming air. The particle concentration in the supply air as well as the room's initial concentration was set to 10 ppm for all particle sizes. For non-isothermal calculations (the air-conditioning case), the temperatures of all wall surfaces were 25°C and that of the supply air was 17°C. The standard k-ε turbulence model [3] was used together with wall functions for near-wall grid points. The boundary conditions for the k-ε turbulence model used at supply registers are determined by using an assumption of the isotropic turbulence. This gives the following boundary condition for the supply turbulent kinetic energy [4], k:

$$k = \frac{3}{2} I^2 u^2 \tag{4}$$

where I is the supply turbulence intensity and u is the supply velocity.

The energy dissipation rate, ε, is given by:

$$\varepsilon = 0.1643\, k^{1.5}/d \tag{5}$$

where d is the supply inlet diameter. At the outlet a zero streamwise gradient is prescribed, i.e.:

$$\frac{\partial u_i}{\partial x} = \frac{\partial T}{\partial x} = \frac{\partial c}{\partial x} = \frac{\partial k}{\partial x} = \frac{\partial \varepsilon}{\partial x} = 0 \tag{6}$$

where x is the coordinate direction normal to the outlet.

## 4. Model evaluation

A preliminary validation of the numerical particle dispersion model has been reported by the authors in a previous paper, [5]. Briefly, the validation was carried out by comparing numerically calculated velocity profiles and particle settling on wall surfaces with those measured in an aerosol chamber. The use of a drift-flux model for predicting particle dispersion has also been demonstrated for a liquid-solid separation problem in an industrial vessel, [6].

## 5. Application and results

A finite volume computer code Ventair 1 was used in the present three-dimensional numerical simulations, [7]. For moderate computing times, a grid of (32x22x22) was used in the ventilation and air-conditioning examples to be presented here. A second-order QUICK scheme is used for discretising the convection terms in the momentum equations, and a first-order hybrid scheme is used for discretising the convection terms in the k, ε and concentration equations. The room configuration used for all calculations here is shown in Figure 1.

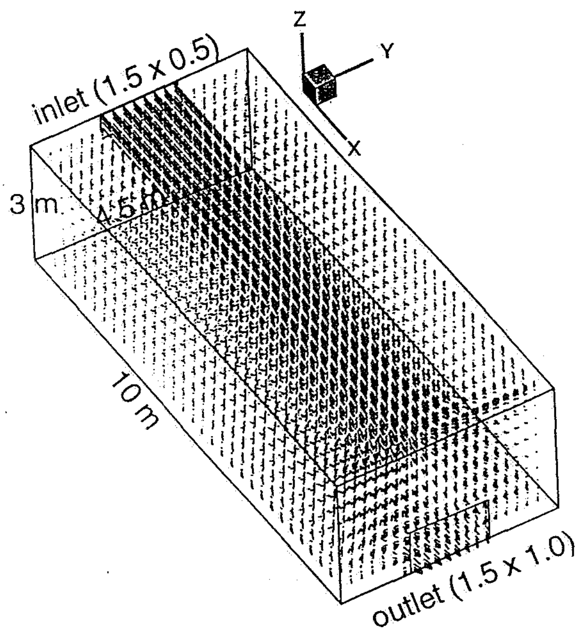


**Figure 1.** Room configuration showing geometries and locations of air and particle supply and exhaust.

Particle settling for the flow situation in Figure 2 are given in the Figures 3-5, which show the behaviour of particles with three different aerodynamic diameters (0.5 $\mu$m, 2.0 $\mu$m and 5.0 $\mu$m).

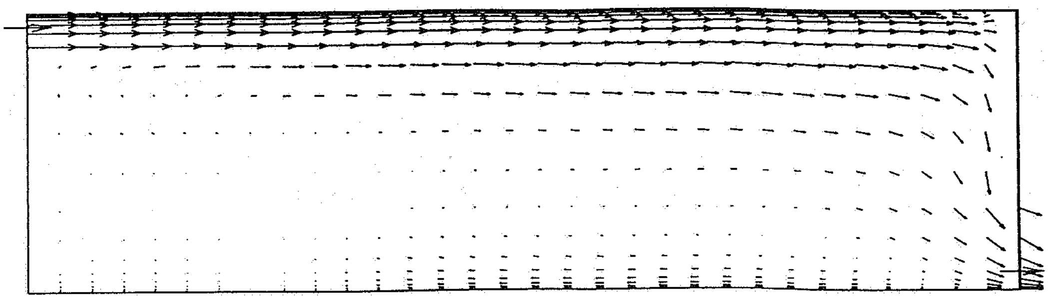

**Figure 2.** Isothermal velocity field in the middle of the room (x-z). Low air flow velocities in the low-left recirculation zone allows settling of airborne particles. Supply velocity, u = 1 m/s.

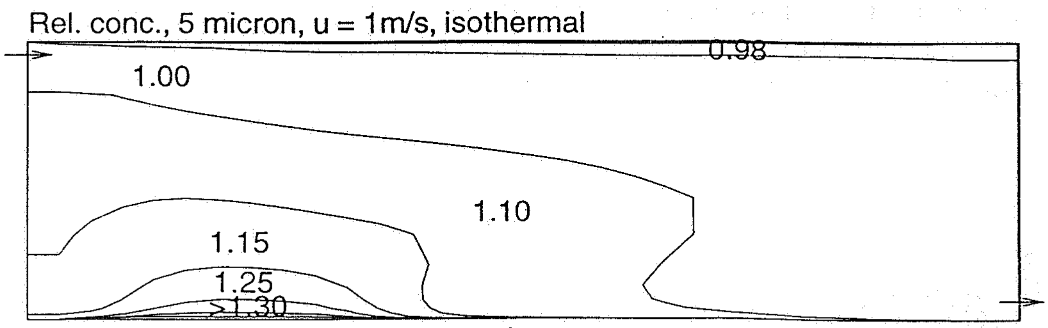


**Figure 3.** Settling of 5 $\mu$m particles in an isothermal ventilation situation with recirculation.

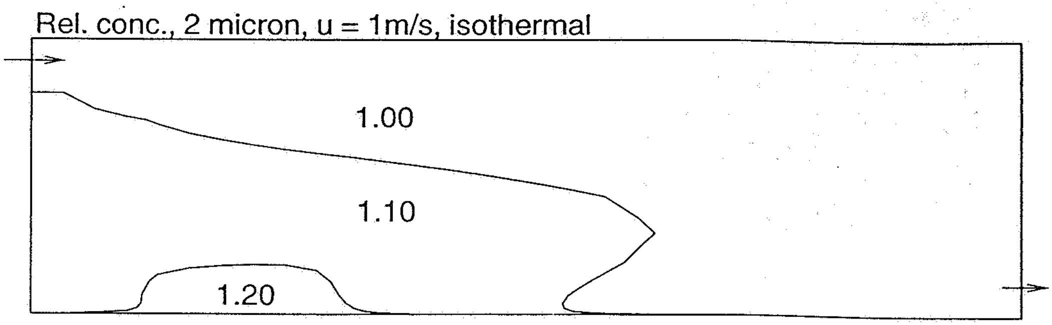


**Figure 4.** Settling of 2 $\mu$m particles in an isothermal ventilation situation with recirculation.

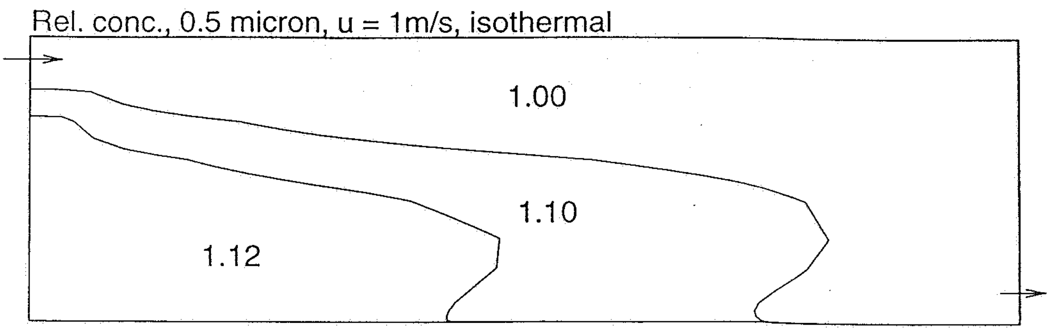


**Figure 5.** Settling of 0.5 $\mu$m particles in an isothermal ventilation situation with recirculation.

Acording to the numerical results, areas of high pollutant concentration were found where air slowly recirculates. In these low air velocity regions, particles have a chance to settle and higher concentrations than room mean concentrations resulted. Larger particles settle easily, while smaller particles tend to be mixed, as expected. It should be noted here that the particle deposition at wall surfaces was modelled as a perfect deposition situation, i.e. once a particle goes to a wall, it becomes a part of the wall.

Air-conditioning
An isothermal case may be ideal in realistic ventilation applications. The presence of thermally driven flows has been shown to produce additional mixing in a room. The most important basic natural convection airstreams are boundary layer flows along wall surfaces and plumes above a heat source. In the mixing ventilation system considered in this paper, natural convection airstreams are generally used, if possible, to interact with the dominant air supply jets to improve the mixing effectiveness. A further numerical test is carried out to study the effect of such a mixing flow system on particle dispersion.

The supply air temperature is assumed to be 17°C, while all wall surfaces are assumed to be 25°C. The wall natural convection flows and the relatively cold supply air have modified the flow pattern significantly (see Figure 6). This has resulted in a flow pattern with less low velocity recirculation and, as a result, almost no settling of particles in the room occurred even for the largest particles considered (see Figure 7).

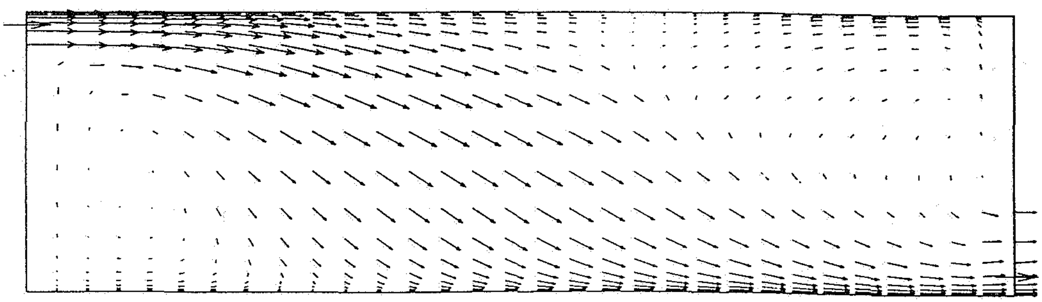

**Figure 6**. Non-isothermal flow pattern with a 17°C air supply temperature and 25°C wall surface temperatures.

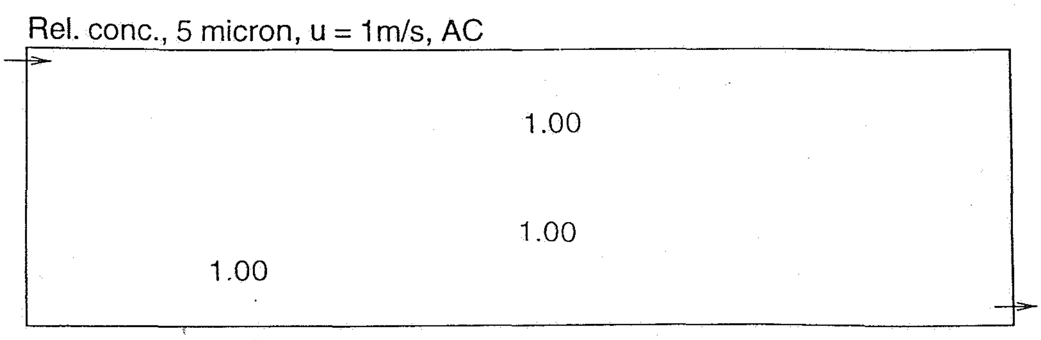


**Figure 7**. Constant (relative) local concentrations of 5 $\mu$m particles in the room. Non-isothermal ventilation (air-conditioning) with cold air supply and warm room surfaces.

The non-isothermal flow was here more efficient than the isothermal flow in removing particles from the room. The absence of stagnant airflow zones has minimized the particle settling and resulted in an unvaried particle concentration in the room. The particle settling situations may be very different in a room ventilated by displacement, as mixing is minimized in the occupied region in that system. A future study will be carried out on displacement ventilation systems.

## 6. Conclusions

A drift-flux model is used to simulate non-passive particle dispersions in a ventilated (air-conditioned) room. The model assumes that the settling velocity of each particle is sufficiently small when compared to the high inflow velocity and the volumetric concentration of particles is also very low. A settling term is added to the concentration equation, and the body force term in the momentum equation is treated using the principle of a Bousinnesq approximation, similar to that in thermal-buoyancy-driven flows.

Particles with diameters ranging from 0.5 $\mu$m to 5 $\mu$m are supplied into the room through a ventilation and air-conditioning supply register. It is shown that in the isothermal case, particle settling occurs in the low velocity recirculating zone for larger particles. In the air-conditioning case, the additional mixing effect introduced by natural convection flows along wall surfaces provides an efficient flow pattern for removal of all sizes of particle considered.

## 7. References

[1] Davidson, L and Olsson, E.
''Calculation of Age and Local Purging Flow Rates in Rooms''
Building and Environment, Vol. 22, No. 2, pp. 111-127

[2] Li, Y., Fuchs, L. and Holmberg, S.
''Methods for Predicting Air Change Efficiency''
Proceedings, Air Distribution in Rooms (Roomvent '92), Third Int. Con., September 2-4, 1992, Aalborg, Denmark

[3] Launder, B.E. and Spalding, D.B.
''The Computation of Turbulent Flows''
Computational Methods of Applied Mechanical Engineering 3, 1974

[4] Awbi, H. B.
''The Role of Numerical Solutions in Room Air Distribution Design''
Proceedings, Roomvent '90, Second Int. Conf., June 13-15, 1990, Oslo, Norway

[5] Holmberg, S and Li, Y.
''Modelling of Indoor Environment - Particle Dispersion and Deposition''
Submitted to the Int. Journal of Indoor Air Quality and Climate (Indoor Air), 1997

[6] Li, Y., Rudman, M. and Brown, G.
"Particle transport in a bottom-feed separation vessel"
Proceedings, Computational Fluid Dynamics in Mineral & Metal Processing and Power Generation, Ed: M. P. Schwarz, M. R. Davidson and A. K. Easton, Melbourne, 3-4 July, 1997

[7] Li, Y.
''Ventair 1 - A General Computer Program for Transient, 3D, Turbulent and Buoyant Flows with Surface Radiative Effect'', Department of Mechanics, KTH, Stockholm, 1992

VENTILATION AND COOLING

18TH ANNUAL AIVC CONFERENCE
ATHENS, GREECE, 23-26 SEPTEMBER, 1997

interessant !!
of TIPVENT

# QUALIFICATION OF VENTILATION SYSTEMS

VOORAL
room ventilation efficiency

DANIEL MARCHAL(*), M-L. BAUMANN (**), PIERRE BARLES (*)

(*) CENTRE TECHNIQUE DES INDUSTRIES AERAULIQUES ET THERMIQUES
CETIAT
27 - 29, Boulevard du 11 Novembre 1918
BP N° 2042
69603 VILLEURBANNE CEDEX
FRANCE

(**) GAZ DE FRANCE - Direction de la Recherche - CERUG - Service EHT
361, Avenue du Président Wilson
93210 LA PLAINE SAINT DENIS
FRANCE

# QUALIFICATION OF VENTILATION SYSTEMS

D. MARCHAL (*), M.-L. BAUMANN (**), P. BARLES (*)

(*) Centre Technique des Industries Aérauliques et Thermiques (CETIAT)
27 - 29, Boulevard du 11 novembre 1918 - BP N° 2042 - 69603 Villeurbanne (France)

(**) Gaz de France - Direction de la recherche - CERUG - Service EHT
361, Avenue du Président Wilson - 93210 La plaine Saint-Denis (France)

## SYNOPSIS

The results presented here supply values for the room ventilation efficiency of a number of configurations covering as many as possible of ~~the ventilation systems en~~countered in actual practice.

The study is based on experimental results and numerical simulation. Using a few configurations experimented-on, simulations were performed using CFD code, which in particular allowed the reliability of calculations to be checked. The simulation tool was then used in such a way as to arrive at results that could be applied in practice.

It was thus found that the air renewal rate has little effect on efficiency, whereas the combined effects of the thermal behaviour of the air stream, and the position of the inlet and outlet orifices, play a decisive role.

## LIST OF SYMBOLS

$C$ : pollutant concentration (mass fraction)
$\Delta\theta$ : temperature difference between air inlet and local ambiance (K)
$\eta$ : ventilation efficiency
$\tau$ : air renewal rate (volume/hour)

Subscripts :
$i$ : air inlet
$o$ : air outlet
$l$ : local

## 1. PURPOSE OF THE WORK PRESENTED

While the criteria for efficiency rating of a room ventilation system are precisely defined, work seeking to determine their values in ordinary field situations remains sparse, and information is therefore lacking on the subject. The study reported-on here was undertaken with the purpose of quantifying the performance of various systems that can be used to ventilate a room of which the atmosphere is liable to be polluted by a gaseous emission.

The method used is based on both experiment and numerical simulation using CFD code. These two differing means were closely combined, with experiment supplying the means to verify the reliability of the computed results, while computation allowed the scope of the investigation to be widened.

The results obtained were compared with those published in reference [1], the only source of practical values currently available to our knowledge.

## 2. EXPERIMENTAL STUDY

The experimental study was conducted in a test facility of oblong shape, diagrammatically represented in figure 1. In the configuration represented, air sweeps through the room from top to bottom (top → bottom). Also studied were diagonal sweeping from bottom to top (bottom → top) and so-called air-displacement ventilation, with fresh air introduced at low velocity at a low height, and extraction at the top of the opposite wall (displacement). In all these cases, on account of the porosity of the side walls, a fraction of the order of 20 % to 30 % of the ventilation flow rate entered the room by infiltration through those walls.

The effect of the air renewal rate ($\tau$) was also studied (from 0.5 to 3 volumes per hour), as was the effect of the temperature difference ($\Delta\theta$) between the fresh air and the atmosphere inside the room (0, +5 and -5°C).

The pollution was provoked by a point-source injection in the middle of the room, and at a height of 0.80 m, of nitrous oxide ($N_2O$), a tracer chosen because it can be detected at small concentrations. Concentration measurements were taken at the various points represented in figure 1 (four on a central vertical line at different heights, one control point at the air inlet and one at the outlet) where samples were taken and the data routed to an analyser.

The experiments were conducted in two stages : first, a fresh-air ventilation situation was established, then the pollutant was injected in a continuous stream until a steady-state situation was obtained ; from then on, the pollutant injection was halted and the ventilation maintained until the system returned to the initial nil-concentration field. The recordings obtained thus provide both continuous-injection concentrations, and transitional situations for the pollution and depollution phases.

Table 1 lists the results in the steady-state situation for the various configurations studied, where they are expressed in terms of ventilation efficiency, defined as follows :

$$\eta = \frac{C_o - C_i}{C_l - C_i}$$

in which $C$ is the pollutant concentration and the indices $i$, $o$ and $l$ refer respectively to the fresh-air inlet, the outlet, and the local zone of which the air quality is measured.

**Table 1: measuring ventilation efficiency**

| Mode | top → top | | top → bottom | | bottom → top | | Displacement |
|---|---|---|---|---|---|---|---|
| $\tau$ | 0.5 | 1 | 1 | 0.5 | 1 | 0.5 | 3 |
| | $\eta$ | $\eta$ | $\eta$ | $\eta$ | $\eta$ | $\eta$ | $\eta$ |
| $\Delta\theta = 0$ | 0.30 | 0.31 | 0.72 | 0.86 | 1.08 | 0.92 | 1.09 |
| $\Delta\theta = +5$ | 0.49 | 0.41 | 1.02 | 0.80 | 1.08 | 0.68 | 1.09 |
| $\Delta\theta = -5$ | 0.91 | 0.81 | 0.93 | 0.8 | | | |

These results point to the predominant effects of the ventilation method and the type of thermal operation. On the other hand, the ventilation rate has only fairly little effect on efficiency.

## 3. PERFORMING OF THE NUMERICAL SIMULATION ; RESULTS

Simulation was performed using CFD code available on the market (FLUENT), and it consisted of numerically integrating the Navier-Stokes equations in the field under study. The use for this purpose of the finite-volumes method requires prior meshing of the three-dimensional space represented. Other factors taken into account are turbulence, using a two-equation model ($k$-$\varepsilon$), the diffusion of the pollutant in the air (molecular and turbulent diffusion), heat transfer and the effects of gravity which entail gravity forces differing according to the local content of a pollutant which is denser than air.

The results of the comparison between the calculations and the measurements were presented in reference [2] for steady-state and transitional situations ; satisfactory concordance warranted the use of the numerical tool for purposes of systematic processing. The latter was performed so as to obtain practical results that could be applied as generally as possible. Furthermore, the attempt was made to cross-check the results with reference [1], leading to the following data, as set out in table 2 :

- steady-state operation in a dwelling room or office of average dimensions (4 x 3 x 2.6 m) ;
- heavier-than-air pollutant ($CO_2$), introduced uniformly in the whole of the volume of the room lying below one metre above the floor ;
- study of three ventilation modes : top → bottom, bottom → top and displacement ;
- two air renewal rates ($\tau$) : 1 and 2 volumes per hour ;
- four types of thermal operation, differing in the temperature difference ($\Delta\theta$) between the inlet and the extraction point (0, -5, +5 or 10 K) ; in the non-isothermal cases, the heat source is distributed uniformly throughout the occupied zone ;
- air velocity with moderate blowing (1.7 or 3.5 m/s, depending upon the air renewal rate, and 0.5 m/s with ventilation by displacement).

The combining of these different parameters leads to the study of 14 cases, of which table 2 summarises the data and results, expressed in terms of ventilation efficiency : either as an average value ($\overline{\eta}$) for the occupied zone, or as a minimum value ($\eta_{min}$) for the most polluted point, with its coordinates indicated (in the key to figure 2).

**Table 2 : numerical simulation of ventilation efficiency**

| Venti-lation mode | $\tau$ (vol.h$^{-1}$) | $\Delta\theta$ (K) | $\overline{\eta}$ | $\eta_{min}$ | x (m) | y (m) | z (m) | CEN TC 156 ref. [1] |
|---|---|---|---|---|---|---|---|---|
| top → bottom | 1 | 0 | 0.99 | 0.76 | 0.5 | 0 | 0 | 0.9 to 1 |
| top → bottom | 2 | 0 | 0.99 | 0.82 | 0.5 | 0 | 0 | 0.9 to 1 |
| top → bottom | 1 | -5 | 0.99 | 0.89 | 0.5 | 0 | 0 | 0.9 |
| top → bottom | 1 | 5 | 1.38 | 0.61 | 0.5 | 0 | 0 | 1 |
| top → bottom | 2 | 10 | 1.43 | 0.64 | 0.5 | 0 | 0 | 1 |
| top → top | 1 | 0 | 0.86 | 0.65 | 0.5 | 0.33 | 0 | 0.9 |
| top → top | 1 | -5 | 0.98 | 0.88 | 1.2 | 0 | 0 | 0.9 to 1 |
| top → top | 1 | 5 | 0.60 | 0.35 | 0.5 | 0 | 0 | 0.8 |
| top → top | 1 | 10 | 0.59 | 0.35 | 0.5 | 0 | 0 | 0.4 - 0.7 |
| bottom → top | 1 | 0 | 0.93 | 0.80 | 0.5 | 1 | 0 | 0.7 to 0.9 |
| bottom → top | 2 | 0 | 0.94 | 0.68 | 0.5 | 0.70 | 0.92 | 0.7 to 0.9 |
| bottom → top | 1 | -5 | 1.06 | 0.97 | 3.5 | 1 | 0 | 1.2 to 1.4 |
| bottom → top | 1 | 5 | 0.94 | 0.59 | 3.5 | 0 | 0 | 0.2 to 0.7 |
| bottom → top | 1 | 10 | 0.93 | 0.60 | 3.5 | 0 | 0 | |

The average values in the occupied zone are little different from one, as a rule, showing that the air is relatively homogeneous in that zone on account of its being mixed by the input stream. Exceptions to this are the cases where both orifices are located at the top (top → top situation), when the fresh air tends to leave untouched the occupied zone containing polluted air that is denser, so making for reduced efficiency. In all the cases studied, average efficiency is found to be independent of the air renewal rate.

Local extreme values observed in the occupied zone always lie at the lower angles or corners of that zone. The difference between the average and maximum ventilation efficiency generally ranges between 10 and 50%, except in the bottom → top case with the input stream warmer than the ambient atmosphere in which the high average efficiency (0.94) is penalised by a high degree of unevenness in the occupied zone and maximum pollution of more than twice the average value.

Working Group WG5 of CEN TC 156 [1] has provisionally allowed certain values for ventilation efficiency according to the system used. These values were compared to our own findings and are also shown in table 2. The comparison shows that with the exception of some very isolated discrepancies (particularly in the the case of cross-ventilation systems with warm air jets), they concur to a very large extent with the simulation results.

## 4. CONCLUSIONS

The study discussed here provides concrete results concerning the ventilation efficiency of a number of configurations that differ from each other by the arrangement of the air inlet and outlet orifices, the flow rate, and the temperature difference between the air blown in and the ventilated atmosphere. In addition to this efficiency rating relating to the average value of the pollutant concentration in the occupied zone, the results also provide information on the heterogeneousness of the ambient air, particularly as regards the maximum concentration of the pollution and its location.

The ventilation efficiency values obtained were compared with those advocated by the CEN TC 156 [1] standardising committee for the same configurations, showing that apart from a few corrections of detail, the values in the draft standard were correctly estimated.

## 5. ACKNOWLEDGEMENTS

The authors would like to express their thanks to the *Agence Française de l'Environnement et de la Maîtrise de l'Energie (ADEME)* for its financial contribution to this work.

## REFERENCES

[1] Design criteria for the indoor environment, CEN TC 156 WG6 Draft standard Pr 1752 (1996)

[2] M.-L. Hanrion, P. Barles, D. Marchal. Efficiency characterisation of various ventilation configurations. 17th AIVC annual conference. Gøteborg (1996)

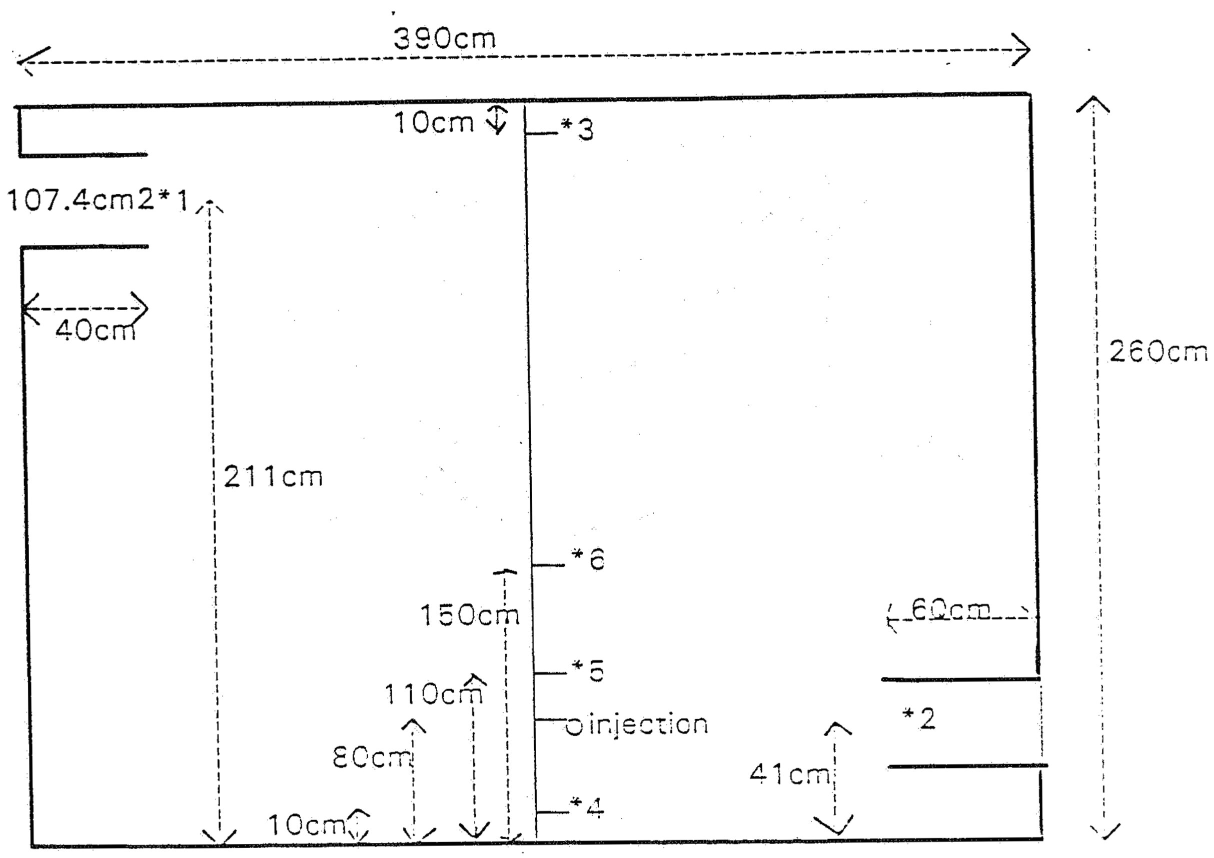

390cm
10cm
*3
107.4cm2*1
40cm
260cm
211cm
*6
150cm
60cm
*5
110cm
oinjection
*2
80cm
41cm
*4
10cm


Figure 1

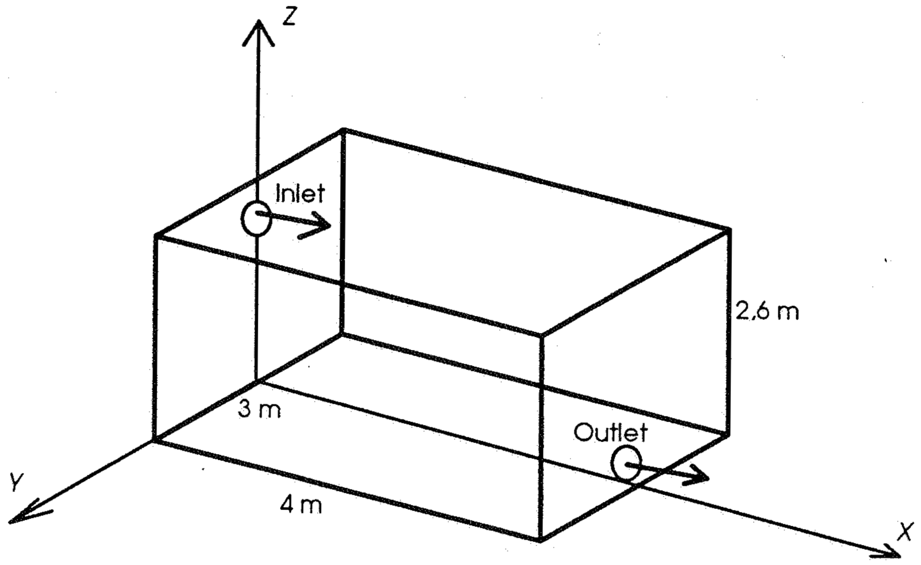


Figure 2

## VENTILATION AND COOLING

**18TH ANNUAL AIVC CONFERENCE**
**ATHENS, GREEC, 23-26 SEPTEMBER, 1997**

# Checking of simulation models in a ventilation test room

CFD

A. Weber*
Dr. Th. Rüegg*
Dr. A. Schälin**

*EMPA
Swiss Federal Laboratories for Materials Testing and Research
Section 175 Building Equipment
CH - 8600 Dübendorf, Switzerland

**ETHZ
Swiss Federal Institut of Technology
Research in Building Technology
Air & Climate Group
CH-8092 Zürich, Switzerland

# Checking of simulation models in a ventilation test chamber

A. Weber, Th. Rüegg, A. Schälin

## Synopsis

Checking models of thermal behaviour or ventilation of a room can be performed in special test cells. At EMPA a ventilation test chamber with several experimental facilities has been designed and built. The inside wall surface temperatures of the chamber can be controlled using a software model which simulates the thermal behaviour of a real wall. As a test case a heated office room was calculated with TRNSYS and compared with measurements made in the chamber.

As an example of checking ventilation models the validation of a CFD-model of a horizontally pivoted window is presented. A parameter analysis was made with this model and the result were compared with the results of a simplified model which is included in the multizone airflow calculation programm COMIS. This simplified model is based on the Bernoulli equation and therefore it needs a discharge coefficient $C_d$. As a result of the parameter analysis a linear function for the $C_d$ value was found.

## List of symbols

| | |
|---|---|
| $\alpha$ | tilting angle [°] |
| $C_d$ | discharge coefficient [-] |
| $c_1$ | concentration before window was opened in room 1 [ppm] |
| $c_2$ | concentration before window was opened in room 2 [ppm] |
| $\Delta c$ | average of the changes of the concentrations in room 1 and 2 [ppm] |
| $\Delta c_1$ | change of the concentration in the room 1 [ppm] |
| $\Delta c_2$ | change of the concentration in the room 2 [ppm] |
| $H$ | height [m] |
| $H_a$ | height of the pivoting axis [m] |
| $\dot{m}$ | massflow [kg/s] |
| $\dot{m}_{12}$ | massflow from room 1 to room 2 [kg/s] |
| $\dot{m}_{CFD}$ | massflow calculated with the CFD-model [kg/s] |
| $\dot{m}_{Bernoulli}$ | massflow calculated with the Bernoulli-model [kg/s] |
| $\Delta p$ | pressure difference [Pa] |
| $\rho$ | air density [kg/m$^3$] |
| $t$ | opening time period [s] |
| $V$ | volume of one room [m$^3$] |
| $w(z)$ | width of the opening at the level z [m] |
| $W$ | width of the window [m] |
| $z$ | level [m] |

# 1 The ventilation test chamber

For the investigation of room ventilation a test chamber was built at EMPA. This chamber can be used to model the thermal and aerodynamic behaviour in real size.

## 1.1 Chamber and conditioning equipment

The chamber has a maximum floor area of 6.1m x 4.6m and a maximum height of 3m and can be adjusted to smaller length, width or height. Two walls, the floor and the ceiling are constructed of water carrying metal panels. The other two walls are transparent to allow for air flow visualization viewed from outside the room. These walls are built with two plexiglas sheets forming a channel through which conditioned air is flowing. By controlling the water- or air-temperatures respectively it is possible to adjust the inside surface temperatures. The whole surface is devided in 10 separate temperature zones. An air handling unit delivers conditioned air to the room through air terminals which can be placed anywhere between the metal panels of the room envelope. An overview of the conditioning equipment is given in figure 1.

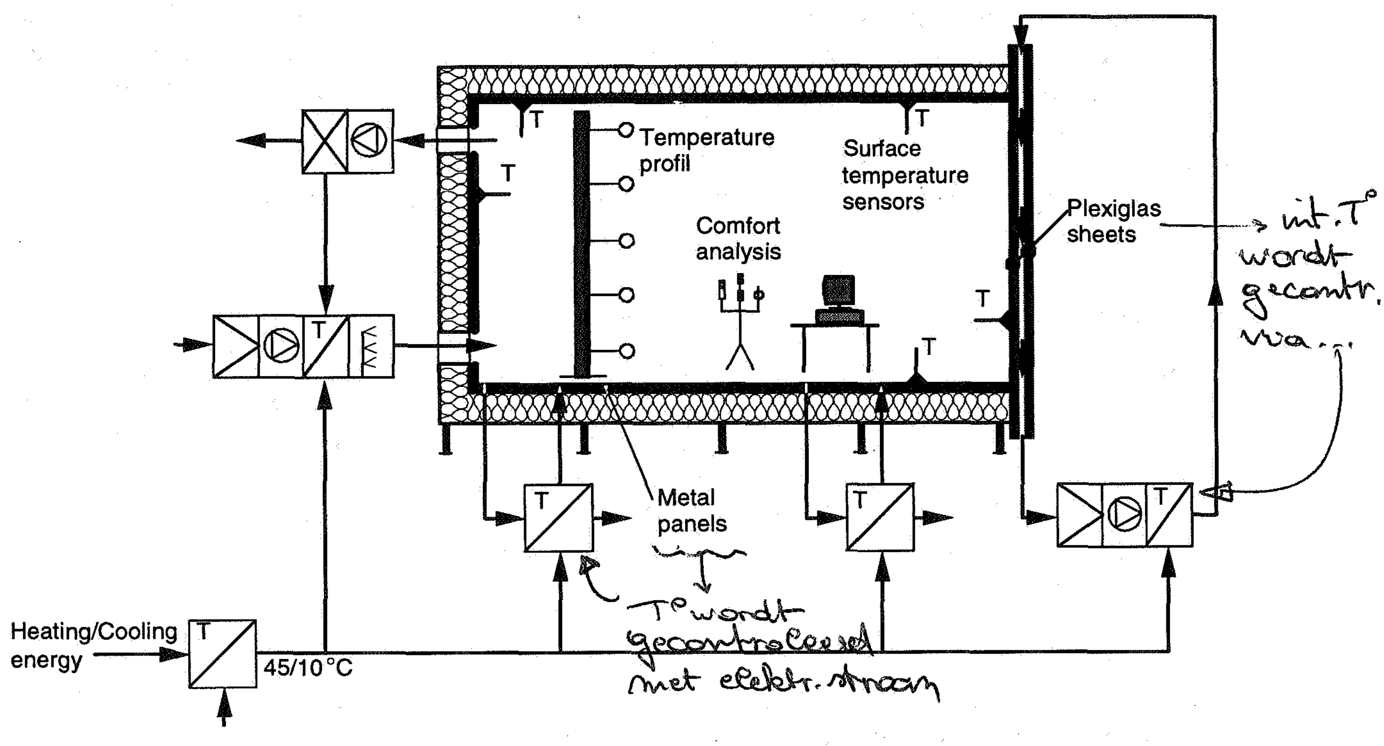


*Fig. 1: Conditioning equipment and measuring systems*

## 1.2 Control system and data acquisition

All the conditioning parameters appear on a PC monitor and can be controlled manually or by a time step program. The wall surface temperatures are measured directly on the surfaces and are used for the closed-loop control of the water supply temperatures. In addition each surface temperature zone is equipped with heat flow sensors. This allows to control the surface temperature dynamically as if it would be the surface of a thermally heavy wall making up the envelope of the test room. The heat flow values are used in a finite differences model containing the thermal capacity and conductivity parameters of the wall. The temperature of

the wall layers is calculated with the software model giving the actual surface temperature which is the setpoint of the water conditioning equipment.
Measuring systems in the room include temperature and velocity sensors and a tracer gas system. The data acquisition stores the measurements in a database from where they can be retrieved in the desired combinations.

### 1.3 Investigation possibilities - a test case

The thermal and ventilation characteristics of different rooms can be established in the test chamber on 1:1 scale. This allows studies of thermal comfort and ventilation effectiveness of a variety of different rooms. Also very important is the possibility to investigate the convective interaction of the air with the simulated thermal mass of the envelope.
As a test case a heated office room was calculated with the TRNSYS simulation software and also investigated in the laboratory. Several time varying energy transfers like transmission and infiltration loss to the outside, a solar input and a thermostatic heating element as a balance of the total energy were taken into account. In the laboratory the dynamic surface temperature of the exterior wall was controlled by the time varying outside temperature of the wall model and the solar energy was established by light bulbs radiating on the heatflow sensors which control the dynamic temperature of the floor. The comparison between calculation and experiment showed agreement in the wall and room temperatures and partly in the heating power, but during the time phases of low heating power discrepancies were observed. This experiment showed that the dynamic wall surface conditioning with a thermal model is a very efficient feature for the investigation of the thermal behaviour of ventilated rooms.

## 2 Model validation of a horizontally pivoted window

Measurements in the ventilation test chamber were used to validate a CFD-model of a horizontally pivoted window. Results from this model were compared with the results from a simplified model based on the Bernoulli equation. This was made to find correct values for the discharge coefficient $C_d$ for the Bernoulli-model. The multizone airflow calculation program COMIS includes the Bernoulli-model for different types of large openings [1], [2]. The discharge coefficient $C_d$ is well known for large rectangular openings, but not for horizontally pivoted windows [3], [4].

### 2.1 Measurements

The chamber was divided into two rooms, one with cold air representing the outside and one with warm air representing the inside. The partition-wall included the investigated horizontally pivoted window. As the test room does not have two separate air conditioning systems, the different air temperatures in both rooms were enforced by controlling the wall panel temperatures. Such, a maximum temperature difference of 17°C could be achieved.
At the beginning of each experiment, the investigated window in the partition was closed. Then the window was opened and the time was measured until the front of the cold airstream passes the point b (figure 2). This was made by filling the cold room with smoke before the window was opened, to visualize the cold airflow entering the warm room.
To determine the airflow quantitatively, $SF_6$ was injected and mixed by a fan in the warm room until a homogenous concentration of about 6 ppm was reached. Then the window was opened during a short time period. After closing the window the air in both rooms was mixed up by a fan until the concentrations were homogenous again (figure 3).

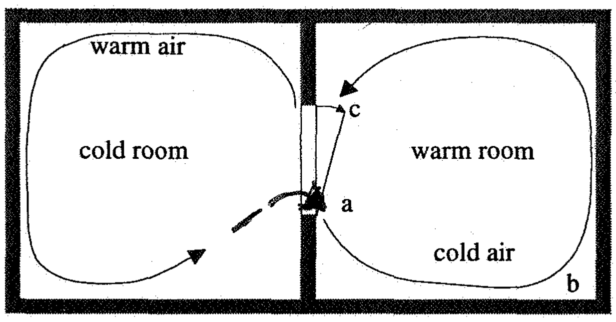


*Fig. 2: Trace of the air after the window has been opened*

Selected opening times were below the time measured as described above to ensure a constant tracergas concentration and massflow of the airstream during the experiment.
The massflow can be determined using:

$$\dot{m} = \frac{\Delta c \cdot V \cdot \rho}{(c_1 - c_2) \cdot \Delta t} \qquad \text{with:} \qquad \Delta c = \frac{\Delta c_1 + \Delta c_2}{2} \tag{1}$$

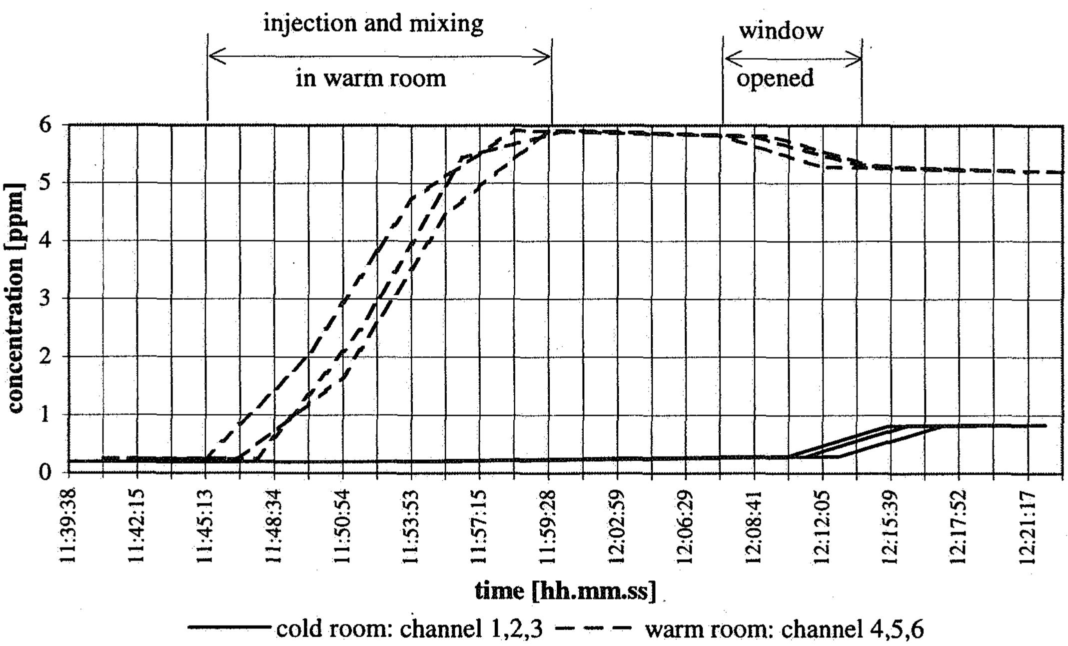


*Fig. 3: Example of a tracergas ($SF_6$) measurement during an experiment*

## 2.2 CFD-model

The CFD-model was made using the program FloVent [5], [6]. The whole test chamber including the partition and the investigated window was modeled. The window was modeled without the frame. The tilted side of the window had to be represented by small rectangular elements (figure 4). Turbulent flow was modeled using the k-ε-model and walls were adiabatic. Start temperatures in the two rooms have been input. In the real test chamber start temperatures were established by heat transfer from inside wall surface. Therefore in the model the airflow pattern of the room is not the same as shown in figure 2, were the incoming flow is warmed up on the floor surface and then rises up. In the model the incoming air stays on the floor and warms up much slower by heat transfer from the warm air above. As the opening time period were selected short enough, this has no effect to the flow in the window. The transient flow after the window has been opened shows also some differences to the reality: In the model, the temperature of that volume of air which is between the tilted side of the window and the plane of the wall is at the start equal to the inside temperature. As a result the flow will be in the first seconds the same like the flow in a totally opened window. In reality, opening the window will cause some turbulence which mixes up cold and warm air in that region right from the beginning. As we took an average massflow over the whole opening time, this effect did not influence the result significantly. Figure 4 shows the temperature distribution calculated with the CFD-model for the situation 4 seconds after the window has been opened.

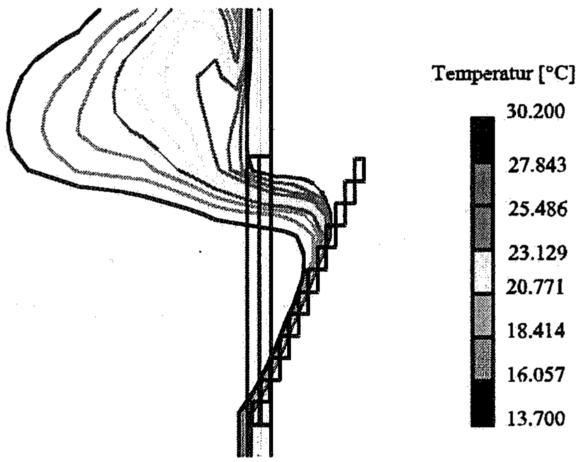


*Fig. 4: Temperatures calculated with FloVent*

### 2.3 Validation of the CFD-model with results of the measurement

The dimensions of the investigated window are: Height = 1.14m; Width = 0.78 m
Results from measurement and CFD-calculation are shown in the following table:

| $\alpha$ [°] | 90 | 18.67 | 13.6 | 8.55 | 90 | 18.67 | 13.6 | 8.55 |
|---|---|---|---|---|---|---|---|---|
| $\Delta T$ [°C] | 10 | 10 | 10 | 10 | 17 | 17 | 17 | 17 |
| $\dot{m}$ Measurement [kg/s] | 0.147 | 0.050 | 0.036 | 0.024 | 0.175 | 0.070 | 0.047 | 0.014 |
| $\dot{m}$ CFD [kg/s] | 0.149 | 0.047 | 0.037 | 0.017 | 0.196 | 0.059 | 0.044 | 0.023 |
| relative difference [%] | 1.3 | 6.4 | 5.5 | 41.2 | 10.7 | 18.6 | 6.4 | 39.1 |

Analysis of the measurement data showed that in cases with more than 10% relative difference between measurement and CFD-calculation, the measurement values were not correct due to several reasons. That means the CFD-model is well calibrated for the comparison with the Bernoulli-model. For small tilting angles ($\leq 10°$) convergence was more difficult to achieve using the current code.

## 2.4 Bernoulli-model

The massflow in large openings based on the Bernoulli equation is:

$$\dot{m}_{12} = C_d \int_0^H \sqrt{2\rho(z) f_{12}(z)} \cdot w(z) \cdot dz \qquad \text{with:} \qquad f_{12}(z) = \begin{cases} \Delta p(z), & if \quad \Delta p(z) > 0 \\ 0 & , if \quad \Delta p(z) < 0 \end{cases} \tag{2}$$

$$\dot{m}_{21} = C_d \int_0^H \sqrt{2\rho(z) f_{21}(z)} \cdot w(z) \cdot dz \qquad \text{with:} \qquad f_{21}(z) = \begin{cases} \Delta p(z), & if \quad \Delta p(z) < 0 \\ 0 & , if \quad \Delta p(z) > 0 \end{cases} \tag{3}$$

The geometry of the large opening is described with w(z). Figure 5 shows the geometry of a horizontally pivoted window. In the used model it is assumed that the flow is strictly horizontal. That means air at height z flows through two rectangular apertures in series as shown in the figure 5. The width of the equivalent aperture is as follows:

$$w(z) = \begin{cases} W & , \quad if\ (z < H_1)\ or\ (z > H_2) \\ \sqrt{\dfrac{(|H_a - z| \cdot \tan\alpha)^2 \cdot W^2}{(|H_a - z| \cdot \tan\alpha)^2 + W^2}} & , \quad if \quad H_1 < z < H_2 \end{cases} \tag{4}$$

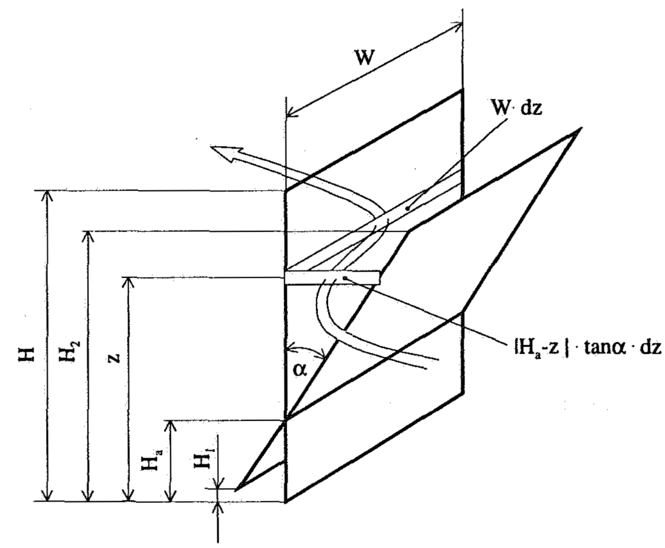


*Fig. 5: Geometry of a horizontally pivoted window*

## 2.5 Comparison between CFD- and Bernoulli-model

The tilting angle, the ratio of height and width of the window, and the temperature difference has been varied for the comparison of the two models. Setting $C_d = 1$ in the Bernoulli-model the correct $C_d$ could be identified as:

$$C_d = \frac{\dot{m}_{CDF}}{\dot{m}_{Bernoulli}} \tag{5}$$

With linear regression the following relation was found as:

$$C_d = 0.0147 \cdot \alpha - 0.0928 \cdot \frac{H}{W} + 0.04116 \qquad (6)$$

The $C_d$-value is not dependent on the temperature difference, which means the Bernoulli-model is describing correctly the effect of the temperature difference.
In the current version 2.1 of COMIS this relation can be input by the user, but in future versions equation (6) will be included in the code.

## 3 Conclusions

- The ventilation test chamber has shown to be suitable for checking the results of ventilation and thermal simulations.
- The dynamic wall surface conditioning with a thermal model is a very efficient feature for the investigation of the thermal behaviour of ventilated rooms.
- The discharge coefficient $C_d$ for the Bernoulli-model of a horizontally pivoted window is found to be a function of tilting angle and the ratio of height and width of the window with values between 0.36 and 0.58. With this function, the simplified model can be applied with more reliability, since up to now mostly $C_d$ values for rectangular openings were used alsc for horizontally pivoted windows.

## Acknowledgments

Thanks to Beat Lehmann, who made the test case with the heated office room. Further thanks to Mauro Cadloni and Mattia Ferrazzini, who performed all the experiments and the calculations for the horizontally pivoted window.

## References

[1] COMIS Workshop: *Fundamentals of the Multizone Air Flow Model* -COMIS, AIVC TN 29, may 1990

[2] Dorer V.: *New Large Vertical Opening and Single Sided Ventilation Routines in COMIS*, IEA-ECB Annex 23 technical report , EMPA 175, April 1995

[3] van der Maas J.: *Airflow through large openings in buildings*, IEA-ECB Annex 20 Report, 1992

[4] van der Maas J., Roulet C.A., Fürbringer J.-M., Hertig J.-A.: *Thermocinetique*, ERL-B 2.3 Raport final, EPFL LESO LASEN, December 1992

[5] Flometrics Ltd: *How to use FloVent for software version 1.2*, England, 1992

[6] Flometrics Ltd: *Reference Manual, New Features for Version 1.3*, England, 1992

[7] Cadloni M., Ferrazzini M.: *Natürlicher Luftaustausch durch Kippfenster,* Diplomarbeit 1997, ETH Zürich

VENTILATION AND COOLING
18TH AIVC CONFERENCE, ATHENS, GREECE
23-26 SEPTEMBER, 1997

Title: **Experimental Approach Towards Air Flow Through A Door Connecting Rooms of Different Temperature**

Author(s): N. Papamanolis*, M Santamouris**, E.Dascalaki**,
A. Argiriou***, D.N. Asimakopoulos**

Affiliation: *Department of Civil Engineering, Univ.of Thessaly, 38334 Volos
** Lab.of Meteorology, Univ of Athens, 15784 Athens
***Inst.of Meteorology & Physics of the Atmospheric Environment, National Observatory of Athens, 11810 Athens

# EXPERIMENTAL APPROACH TOWARDS AIR FLOW THROUGH A DOOR CONNECTING ROOMS OF DIFFERENT TEMPERATURE

**N. Papamanolis[1], M. Santamouris[2], E. Dascalaki[2], A. Argiriou[3], D.N. Asimakopoulos[2]**

1. Department of Civil Engineering, Univ. of Thessaly, 38334 Volos,
2. Laboratory of Meteorology, Univ. of Athens, 15784 Athens
3. Institute of Meteorology and Physics of the Atmospheric Environment, National Observatory of Athens, 11810 Athens

## 1. SYNOPSIS

Air flow through doors, windows and other large openings constitutes a major factor in building ventilation. However, due to the complexity of the physical processes involved, relevant physical phenomena are not yet fully understood.

The paper presents data obtained from five consecutive experiments concerning air flow through a large opening (door) connecting two rooms (volumes 28.3 $m^3$ and 38.1 $m^3$ respectively) with different air temperatures. The experiments were conducted within the two chambers (Service and Test Room) of a PASSYS Test Cell, a fully equipped outdoor facility for thermal and solar monitoring. The experiments involved the heating of one room (Test Room) until there was a significant temperature difference between the rooms. After that, the door was opened, and the mass and heat exchanges between the two rooms were measured using the available equipment. More specifically, the experimental data, corresponding to 30 sec -step records, concerns the measurement of tracer gas (N2O) concentrations, indoor temperatures, air speed and direction in the middle of the door opening, outdoor temperature and wind speed and direction.

This paper attempts a qualitative analysis of the experimental results as a first step towards a more comprehensive study of the physical processes in operation in relevant phenomena.

## 2. INTRODUCTION

Ventilation, as an air change process in a building interior, is advantageous provided that the properties of the environmental air, which are related to the hygiene and comfort of the inhabitants (temperature, humidity, air pollutant concentration), are favourable compared with corresponding indoor air properties. Otherwise, a correction of the unfavourable properties of the inflowing air is necessary using energy consuming processes.

The above commentary comprises the correct framework for the study of the qualitative and quantitative characteristics of building ventilation processes. An important section of this study concerns the air flow through various opening types in construction elements. The corresponding air flow processes through large openings under steady state conditions have long ago been investigated. However, what is of great importance are the transient processes taking place during the establishment of communication between two spaces through a large opening. Relevant physical phenomena occurring during the opening of a door or window is empirically known to produce sudden and significant changes in the qualitative and quantitative ventilation characteristics of internal rooms. More specifically, the study is important both for external openings (windows, balcony doors) and internal openings (doors) between adjacent rooms. The prediction of these phenomena was, until recently, possible using empirical and simulation models. The recent work of Daskalaki *et al* (1996) has experimentally studied the establishment of communication between a room and the environment through a large opening (Single Sided Ventilation). In this paper the results are presented from a similar experiment concerning the establishment of communication between two rooms with different air temperatures. The experiment was designed (Argiriou *et al*, 1993) and theoretically analysed (Santamouris *et al*, 1993) under the PASCOOL Programme in order to contribute to the understanding of the processes involved in such phenomena.

## 3. METHOD

The experiments on which this paper is based took place in Athens during October 1993. They were conducted in the interior of a PASSYS Test Cell, a fully equipped outdoor facility for thermal and solar monitoring (Vandaele and Wouters, 1994). The Test Cell is divided into two rooms, namely the "Test Room" and the "Service Room" (Figure 1). The Test Room is highly thermally- insulated and airtight with its dimensions (Length = 5.00 m, Width = 2.76 m, Height = 2.75 m) based on an average room. The Service Room, with dimensions of 2.40 m, 3.58 m and 3.29 respectively, is the place where the cell equipment, such as the heating and cooling systems, control units etc., is installed. The two rooms are connected by a 1.01 m by 2.00 m internal door.

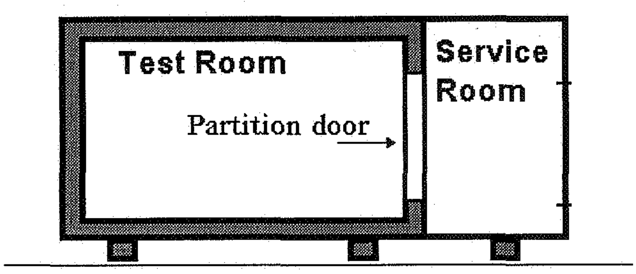


Figure 1: PASSYS Test Cell cross-sectional view

For the experiment, the Test Room was heated until a significant temperature difference between it and the Service Room was reached. At the same time, as the tracer gas decay technique was used to estimate the air exchange rate between the two rooms, N2O was injected into the Test Room and the concentration, in both rooms, was monitored by an infrared gas analyser. When the concentration of N2O in the Test Room was sufficiently high, the heating was stopped and the communication door was slowly opened.

The experiment was repeated five times. Each time it lasted about 25 minutes, with the door being opened after about 10 minutes. Throughout the entire experiment, a long list of physical parameters was constantly recorded. Namely, 74 parameters were recorded at 30 -sec steps. Among them are:

- Tracer gas (N2O) concentration measurements at six points inside the adjoining rooms,
- Indoor temperature measurements at different points inside both rooms,

- Surface temperatures at different points on the interior walls
- Air speed and direction measurements at seven fixed heights in the middle of the partition door opening (2.02 m2 area)
- Outdoor temperature and wind speed and direction measurements at heights of 1.5 m, 2 m and 10 m.

The instrumentation used included the following sensors, with corresponding accuracy in parenthesis:
Temperature: PT100 (0.01 °C), PT1000 (0.1 °C), T-fast (0.1 °C)
Air speed: DANTEC (0.4 %), Hot wire (2 %)
Wind speed: 3 cup anemometer (2 %)
Wind direction: vane (5 °)

## 4. RESULTS

Figure 2 - based on the first experimental data - presents the speeds of the air masses, at different heights on the layer of the partition door opening, during the air exchange processes which are triggered by the establishment of communication between the two rooms.

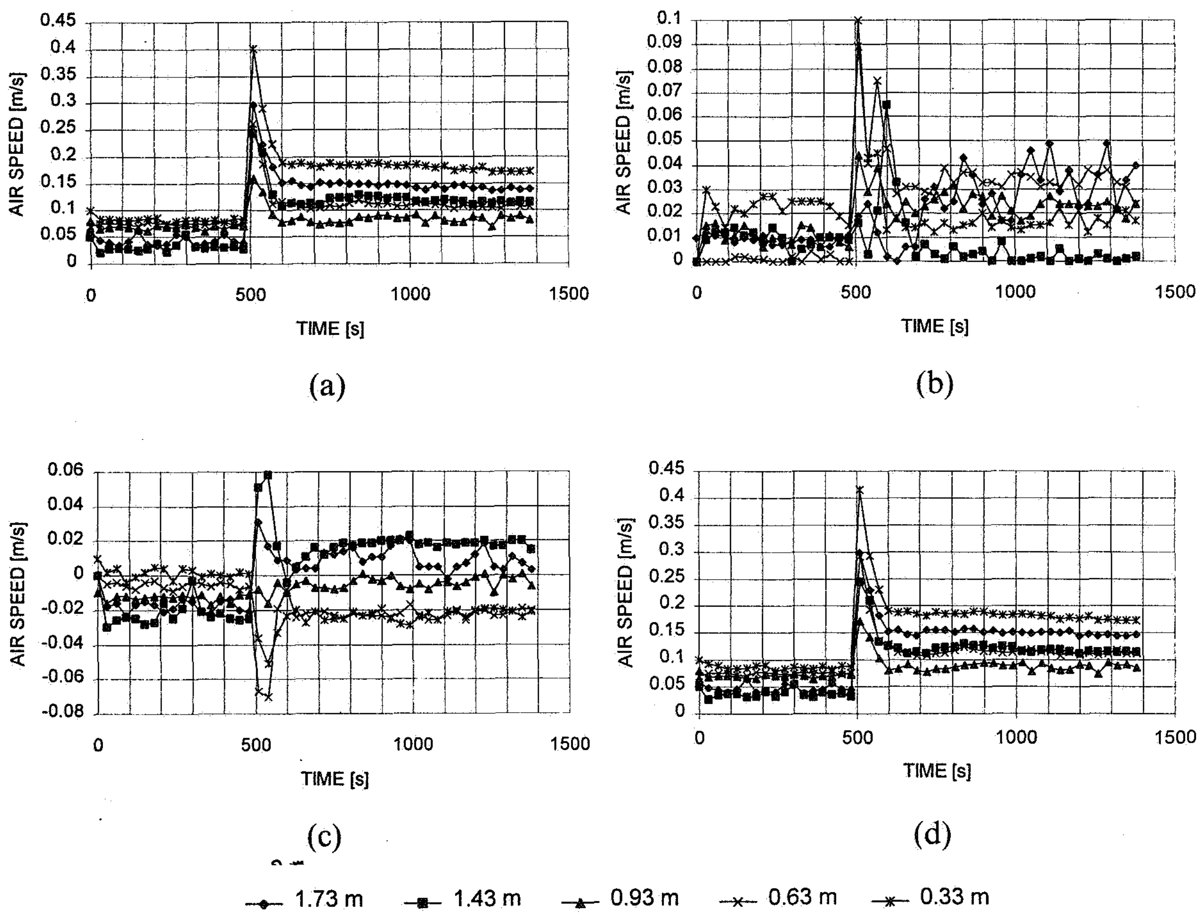


Figure 2: Air speed measurements on x (a), y (b) and z (c) axes, and total speed (d), at different heights on the partition door opening.

Air speeds records correspond to the directions of the x, y and z axes of an orthogonal system, with the x axis along the long dimension of the test cell. Based on this data, the total speed is calculated mathematically. From these diagrams we can observe that a sudden increase in air circulation is produced by opening the door which, after a short peak period, returns to a higher speed than before. The air flow is mainly along the x axis, with its magnitudes reaching values up to 0.5 m/s.

This finding is seen more clearly in Figure 3 where the consecutive speed profiles of the air moving through the door opening are displayed on 30 sec step intervals. Profiles 1 and 2, which are almost identical, correspond to the closed door. Profile 3 represents the sudden increase in air speed, while the next profiles, 4 and 5, represent the drift towards a more turbulent than before condition, with increased speeds at the upper and lower edges of the opening.

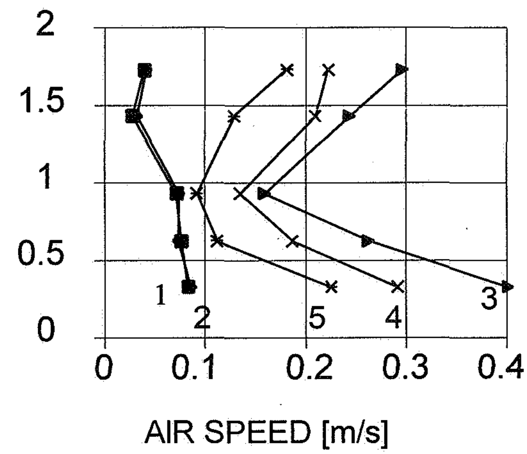


Figure 3: Consecutive air speed profiles - from 1 to 5 - vertical to the partition door, corresponding to 30 sec step recordings during the door opening

The air speed measurements represent absolute values in x and y directions with the direction of the flow only identifiable in the z direction (positive values represent motion upwards). In the x direction it is also possible to identify the direction of the air flow only at a height of 1 m, which corresponds to the midheight of the door opening. In all cases, as shown in the experimental results, at this particular layer, the flow was from the Test Room to the Service Room, which means that the neutral zone was always lower.

This circulation causes the air changes between the two rooms which is depicted in the diagrams in Figure 4, where the variation in the tracer gas concentrations with time are presented for all the experiments. From these diagrams, it is clear that after the door is opened there is a sudden and rather extensive bi-directional transfer of air masses between the two rooms which even results in the reversion of relative gas concentrations. This sudden and rather extensive air exchange, and the accompanying increased air circulation, is obviously not only caused by thermal convection forces but is also affected by the pressure forces imposed by the door opening process (Papamanolis, 1992).

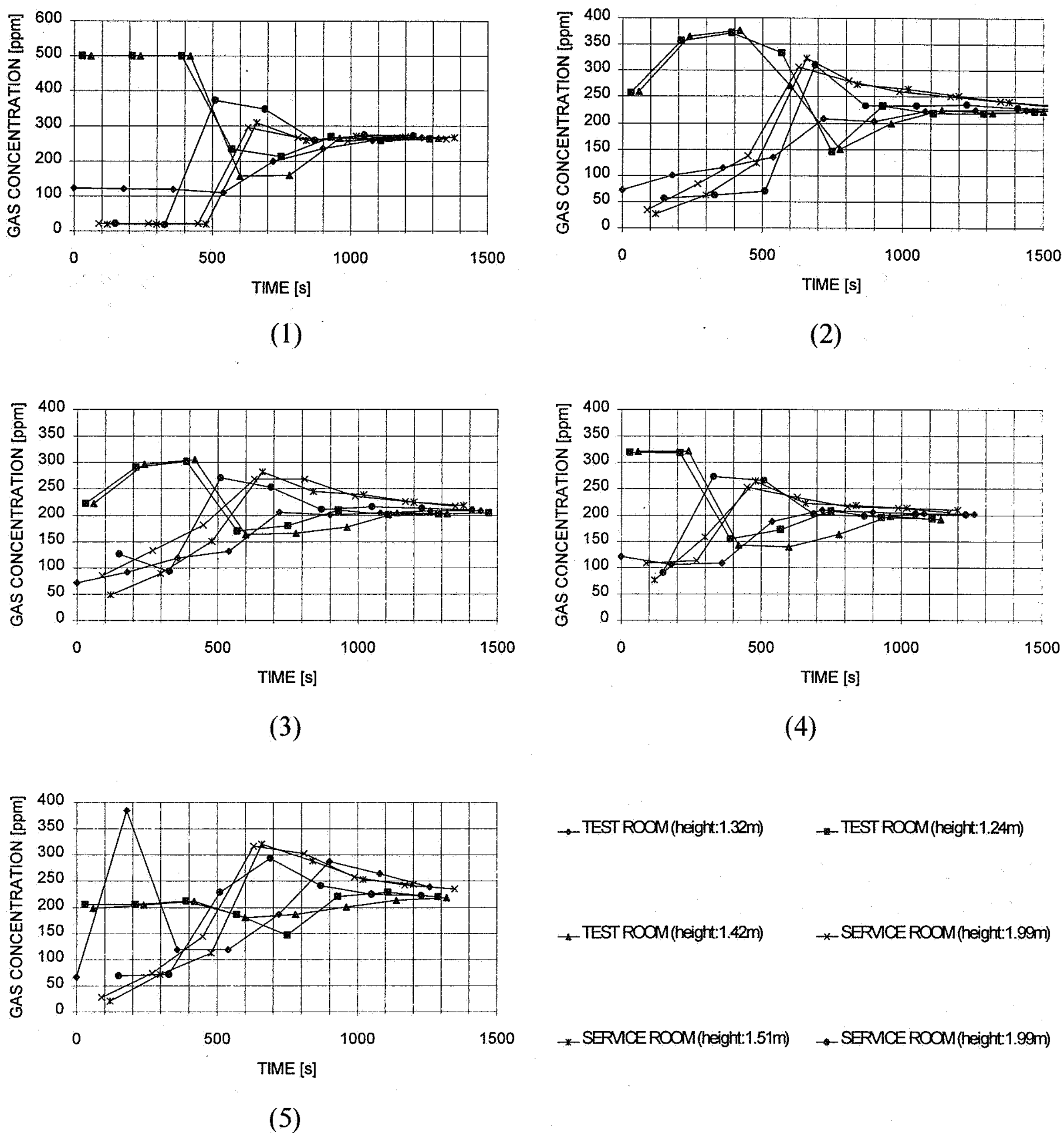


Figure 4: Tracer gas concentration measurements at fixed points in the Test and Service Room.

This phase of the phenomenon, which may be likened to a pulse, is of relatively short duration and is followed by a rapid convergence of tracer gas concentrations in the two rooms which denotes an adequate mixing of the corresponding air masses. More specifically, based on the results of the first experiment (Diagram 1 in Figure 4), we can calculate that during the first 500 s (approximately equal to 8 min) after the door opening we have this sudden air exchange phase and after that we have an almost complete mixing of corresponding air masses. Almost similar are the results coming from all the experiments.

The air exchange processes result in air temperature changes in both rooms. Figure 5 shows the temperature variation at different heights on the partition door opening. From these diagrams, it is clear that the temperature change is more pronounced at the lower layers where the cooler air masses form the Service Room are inflowing. However, even at higher layers, where at the first stages of the phenomenon the flowing air masses are substantially the same as before the door opening, there is a significant temperature reduction which at least makes the timing of the triggering event (door opening) obvious.

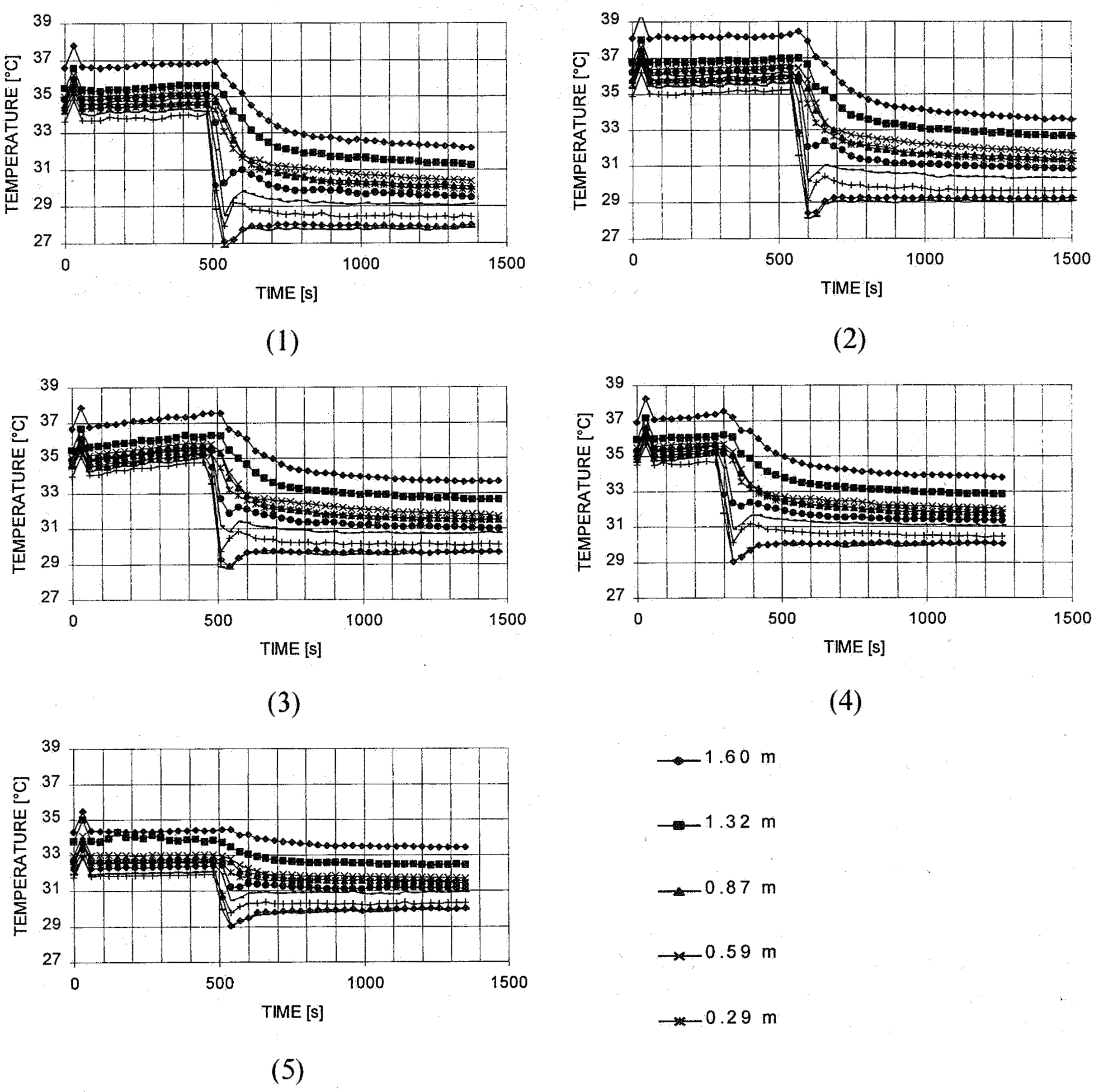


Figure 5: Air temperature measured with PT1000 sensors at various heights on the partition door.

In contrast to the temperature sensors at the opening layer, the air temperature sensors in the middle of the rooms do no reveal so clearly the mixing process initiated by the establishment of communication between the two rooms. In Figure 6, the air temperature changes are presented at different points in the middle of the rooms.

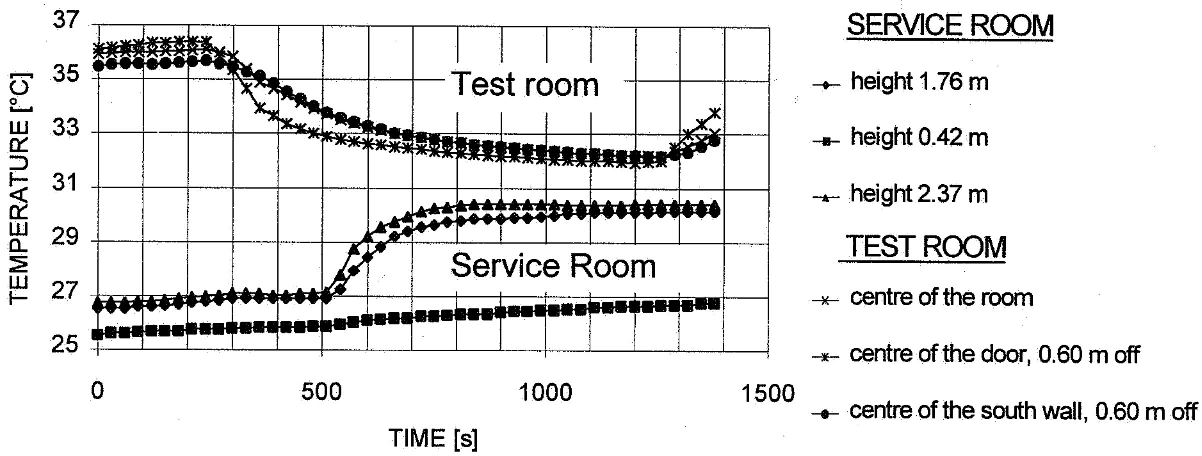


Figure 6: Air temperatures at different points inside the Service Room and the Test Room during the first experiment

It is easy to observe that air temperatures in both rooms are changing slowly and tend asymptotically to be identical. It is also apparent that at least some of the sensors do not respond well to the starting of the air mixing processes, which in the case of the diagram in Figure 6, which is based on the first experiment data, is located very close to 500 s.

## 5. CONCLUSIONS

From the data which was collected during the five consecutive experiments and which was presented in this particular paper, it can be concluded that the establishment of communication between two spaces of different temperature through a large opening is accompanied by processes of air mass exchange, which involve the mixing of the air masses and the balancing of their temperature. This exchange takes place in both directions of the air currents which are created through the opening. The greater the distance from the neutral zone, which is located approximately in the centre of the opening, the greater the respective air speeds become.

From the experimental data, it can be concluded that while the mixing of the air masses takes place for relatively short periods, the air temperature balance between the two spaces, in contrast, continues at a slow rate. This is obviously due to the influence of other factors, excluding convection, which control this balance (conduction)

The above conclusions which are drawn from the initial elaboration of the available experimental data are the most conspicuous. They offer an introductory qualitative approach to the phenomenon, as within the scope of this paper. A more complete and systematic analysis will enrich and better document relevant phenomena aimed at a more detailed and comprehensive understanding of the mechanisms involved and the transient processes taking place.

**6. REFERENCES**


*1. ARGIRIOU, A., SANTAMOURIS, M., DASCALAKI, E., HELMIS, C. and ASIMAKOPOULOS, D.N*
*"Description of the Air Flow Experiments to be Carried Out in the PASSYS Test Cells"*
*PASCOOL Report, MDS PASCOOL Meeting, Glasgow, 1993.*

*2. DASCALAKI, E., SANTAMOURIS, M., ARGIRIOU, A., HELMIS, C., ASIMAKOPOULOS, D.N., PAPADOPOULOS, K. and SOILEMES, A.*
*"On the Combination of Air Velocity and Flow Measurements in Single Sided Natural Ventilation Configuration"*
*Energy and Building, 1996.*

*3. PAPAMANOLIS, N.*
*"Theoretical and Experimental Research towards the Optimal Utilisation of Natural Ventilation to Building Design" (in Greek)*
*Ph.D. Thesis, Aristotelian University of Thessaloniki, 1992.*

*4. SANTAMOURIS, M., DASCALAKI, E., ARGIRIOU, A., HELMIS, C. and ASIMAKOPOULOS, D.N.*
*"Analysis of Heat and Mass Flow due to Temperature Difference in a Two-zone Test Cell"*
*PASCOOL Report, MDS PASCOOL Meeting, Florence, 1993.*

*5. VANDAELE, L. and WOUTERS, P.*
*"The PASSYS Services"*
*Summary Rep., PASSYS Project, Belgian Building Research Institute, EC DG XII, Brussels, 1994.*

**VENTILATION AND COOLING**
**18TH AIVC CONFERENCE, ATHENS, GREECE**
**23-26 SEPTEMBER, 1997**

**Title:** **Identification and Validation of a Model to Predict the 3-D Distribution of Temperature in a Ventilated Test Room**

**Author(s):** **K Janssens, D Berckmans, V Goedseels**

**Affiliation:** **Laboratory for Agricultural Buildings Research, K U Leuven, K Mercierlaan 92, B-3001 Heverlee, Belgium**
**and National Fund for Scientific Research, Belgium**

# IDENTIFICATION AND VALIDATION OF A MODEL TO PREDICT THE 3-D DISTRIBUTION OF TEMPERATURE IN A VENTILATED TEST ROOM

**JANSSENS K. (1,2), BERCKMANS D. (1,2), GOEDSEELS V. (1)**

(1) Laboratory for Agricultural Buildings Research
K.U.Leuven, K. Mercierlaan 92,
B-3001 Heverlee, Belgium
(2) National Fund for Scientific Research, Belgium

## Abstract

In ventilated air spaces such as offices, industrial workplaces, greenhouses and livestock buildings the ventilation rate is often used to control the indoor temperature. Up to now, the indoor temperature is mostly considered to be uniform in space. However, measurements indicate that important 3-D gradients of temperature often occur, which are due to an imperfect mixing of the air in the ventilated space. In these cases of imperfect mixing the 3-D gradients of temperature must be taken into account in order to realise a better climate control.
In the laboratory a test room was built to analyse the process of imperfect mixing in more detail and under controlled conditions. In the test room with a volume of 9 m3 the ventilation rate can be varied between 80 and 300 m3/h, resulting in rather high air exchange rates (8.9 - 33.3 refreshments each hour). Different air flow patterns can be generated and measured using the ventilation rate as control input. A hot water basin and 5 heating elements at low temperature are positioned at the floor of the test room to simulate the moisture and heat production of a living organism. The test room is furthermore provided with 36 temperature sensors which are positioned in a 3-D grid to measure the 3-D distribution of temperature.
A model has been developed to predict the dynamic response of temperature at an arbitrary sensor position to non-linear variations of the ventilation rate as input. From physical laws it has been derived that the model has the structure of a second order model with a slow and a fast time constant. The fast time constant can be related to the 'local mean age of air' at the corresponding sensor position and to the fast heat losses through the walls. The slow time constant can be related to the slow heat losses through the walls.
The second order model has been identified for the 36 sensor positions in the test room. Therefore, an unbiased identification algorithm was applied to 50 step up experiments in the test room. After the model identification step, 4 validation experiments were performed in the test room to validate the model. From the validation experiments it can be concluded that the dynamic response of temperature at the 36 sensor positions resulting from non-linear variations of the ventilation rate can be predicted with an average accuracy of 0.3 °C.

VENTILATION AND COOLING

18TH ANNUAL AIVC CONFERENCE
ATHENS, GREECE, 23-26 SEPTEMBER, 1997

# Use of Computational Fluid Dynamics for Modelling Passive Downdraught Evaporative Cooling

M. A. Mansour*, M. J. Cook*, A. H. Taki+, and K. J. Lomas*

*Institute of Energy and Sustainable Development, De Montfort University
Leicester, LE1 9BH, UK
Tel: +44 116 257 7417 Fax: +44 116 257 7449
http://www.iesd.dmu.ac.uk

+Department of Building Studies
School of the Built Environment, De Montfort University
Leicester, LE1 9BH, UK
Tel: +44 116 257 7048 Fax: +44 116 257 7440

# Use of Computational Fluid Dynamics for Modelling Passive Downdraught Evaporative Cooling

M. A. Mansour, M. J. Cook, A. H. Taki, and K. J. Lomas


## Synopsis

The air flow in a Passive Downdraught Evaporative Cooling (PDEC) tower has been modelled using a Computational Fluid Dynamics (CFD) code. Water is injected into dry warm air and the interaction between the water and the air is represented using a particle transport model. This models the transfer of mass, momentum and heat between the water particles and the air in addition to predicting individual particle trajectories. The CFD code successfully produced predictions for the air flow in such a cooling system and the results are comparable with those obtained from a one dimensional finite difference model. The CFD results however, provide much more spatial information, in particular, individual particle trajectories. CFD also offers far greater potential for modelling full PDEC systems in which the evaporatively cooled air is delivered to occupied spaces.


## List of Symbols

| | |
|---|---|
| $C_p$ | specific heat (J/kgK) |
| $D$ | diffusivity of water vapour in air ($m^2$/s) |
| $d$ | particle diameter (m) |
| $g$ | gravity vector (m/$s^2$) |
| $H$ | enthalpy (J/kg) |
| $h_{fg}$ | latent heat of evaporation (J/kg) |
| $k$ | turbulent kinetic energy ($m^2/s^2$) |
| $m$ | particle mass (kg) |
| Pr | Prandtl number |
| $p$ | pressure (Pa) |
| $S_\phi$ | source term |
| Sh | Sherwood number |
| $T$ | temperature (K) |
| $T_G$ | temperature of continuous phase (K) |
| $T_P$ | temperature of water particle (K) |
| $t$ | time (s) |
| $U$ | velocity vector (m/s) |
| $v_r$ | relative velocity of the particle and the continuous phase (m/s) |
| $W_c$ | molecular weight of water vapour (kg/kmol) |
| $W_G$ | molecular weight of the mixture in the continuous phase (kg/kmol) |
| $X$ | the ratio of the saturated vapour pressure to the continuous phase vapour pressure at a given temperature |
| $X_G$ | molar fraction of water vapour in the continuos phase |
| $x$ | displacement vector (m) |
| $Y_{wv}$ | mass fraction of water vapour(kg/kg) |
| $\Gamma_{wv}$ | molecular diffusion coefficient (kg/ms) |
| $\Gamma_\phi$ | diffusion coefficient for $\phi$ |
| $\phi$ | arbitrary variable |
| $\lambda$ | thermal conductivity (W/mK) |
| $\mu$ | dynamic (laminar) viscosity (kg/ms) |
| $\mu_T$ | turbulent viscosity (kg/ms) |
| $\mu_{eff}$ | $\mu + \mu_T$ (kg/ms) |
| $\theta$ | azimuth angle (radians) |
| $\rho$ | density (kg/$m^3$) |
| $\rho_{Bref}$ | buoyancy reference density (kg/$m^3$) |
| $\rho_p$ | particle density (kg/$m^3$) |
| $\sigma_H$ | turbulent Prandtl numbers for $H$ |
| $\zeta$ | bulk viscosity (kg/ms) |

## 1. Introduction

Passive Downdraught Evaporative Cooling (PDEC) is an energy efficient method of producing cool air in hot dry climates. The process involves injection of a very fine mist of water particles, produced by micronisers, into a warm dry air stream. As the water evaporates, the air temperature decreases by an amount dependent on the amount of water which is evaporated. This cooled air can then be delivered to occupied spaces. A PDEC system can be readily divided into three distinct zones: (i) a wind catcher; (ii) a cool air production zone (or evaporation zone) where water droplets are sprayed into the air stream; and (iii) a region in which the cooled air is delivered to the occupied spaces [1]. It is the modelling of zone two using computational fluid dynamics (CFD) that is the subject of this paper.

The work is part of a three year research project which began in January 1996 under the EC Joule programme [1]. It is a multi-disciplinary project involving architects: Brian Ford & Associates and Mario Cucinella Architects; building physicists and simulation experts at De Montfort University and the University of Malaga; monitoring experts at the Conphoebus Institute in Sicily, and microniser and control specialists Microlide SA. The objective is to study the application of PDEC systems to non-domestic buildings.

In this paper CFD simulations of evaporative cooling is discussed. A very simple, two dimensional case has been considered in which water is injected, evenly distributed, along a horizontal line. The total flow rate is set equal to that from a single (typical) microniser. In order to gain confidence in the CFD predictions, the results are compared with a one dimensional 'tower model' of Rodríguez et al. [2,3] and Alvarez et al [4].

## 2. Modelling the Evaporation Zone in CFD

### 2.1 The CFD package

The CFD package used for this work is CFX-F3D [5], version 4.1. This a multiblock code in which geometries are defined using one or more topologically rectangular blocks. Each block is then covered with a mesh and the governing equations solved using the finite volume method on a co-located grid [6].

### 2.2 Modelling the Evaporation Zone

A particle transport model was used to represent the evaporation zone. In this model, water droplets are considered as a source of mass, momentum and energy in the continuous phase. The model begins by solving the equations of the continuous phase assuming no particles are present. Particles are then tracked through the continuous phase and particle equations are solved for particle velocity, temperature and mass, using the continuous phase parameters already calculated. The particle source terms are then calculated and the continuous phase equations solved again. This sequence is repeated until satisfactory convergence is attained (fig. 1).

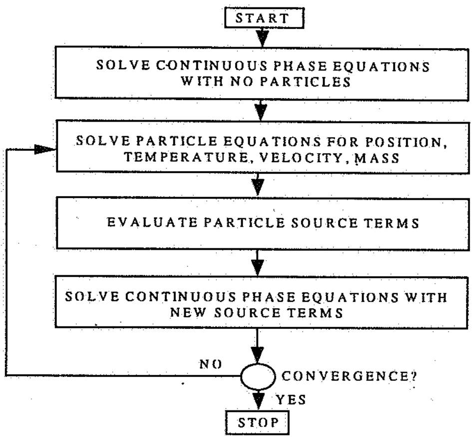


**Figure 1.** Flow chart for particle transport model computational sequence.

### 2.3 Continuous Phase Governing Equations

The code solves the following conservation equations for mass, momentum and energy (enthalpy) in the continuous (air) phase:

$$div(\rho U\phi) - div\left(\Gamma_\phi grad\phi\right) = S_\phi + S_\phi^p \tag{1}$$

**Table 1.** Terms in the governing equations when using an eddy viscosity turbulence model.

| Conservation equation | $\phi$ | $\Gamma_\phi$ | $S_\phi$ |
|---|---|---|---|
| Mass | 1 | 0 | 0 |
| Momentum | $U$ | $\mu + \mu_T$ | $-gradp_0 + div(\mu_{eff}\, gradU) + \rho g$ |
| Enthalpy | $H$ | $\frac{\lambda}{C_P} + \frac{\mu_T}{\sigma_H}$ | 0 |
| Mass Fraction of water vapour | $Y_{wv}$ | $\Gamma_{wv}$ | 0 |

Note that in equation (1) there are two source terms, $S_\phi$ is the continuous phase source term and $S_\phi^p$ is the source term due to the particles. The continuous phase source terms and diffusion coefficients are given in table 1 for the (arbitrary) variable $\phi$. All transient terms have been omitted since the work sought steady-state solutions.

$p_0$ is a 'modified' pressure given by

$$p_0 = p + \frac{2}{3}\rho k + \left(\frac{2}{3}\mu_{eff} - \zeta\right) gradU - \rho_{Bref}\mathbf{g}.\mathbf{x} \tag{2}$$

The turbulence model used in this work was the standard $k$-$\varepsilon$ model [7].

### 2.4 The Particle Equations:

#### Momentum Equations

The equations for the rate of change of velocity of the particles come directly from Newton's second law:

$$m\frac{dU}{dt} = \underbrace{\frac{1}{8}\pi d^2 \rho C_D |v_r| v_r}_{\text{Drag force}} - \underbrace{\frac{1}{4}\pi d^3 \nabla P}_{\text{Pressure gradient}} + \underbrace{\frac{1}{6}\pi d^3 (\rho_p - \rho)\mathbf{g}}_{\text{Buoyancy force}} - \underbrace{\frac{1}{6}\pi d^3 \rho \frac{dU}{dt}}_{\text{Added mass force}} \tag{3}$$

where the drag factor $C_D$ is given by : $C_D = 24\frac{(1+0.15\mathrm{Re}^{0.687})}{\mathrm{Re}}$

and Re is the particle Reynolds number: $\mathrm{Re} = \frac{\rho|v_r|d}{\mu}$

**The Heat Transfer Equations**

The particle rate of change of temperature is governed by two physical processes, convective heat transfer ($Q_C$) and latent heat transfer ($Q_M$) associated with mass transfer, where:

$$Q_C = \pi d\lambda \mathrm{Nu}\,(T_G - T_P) \tag{4}$$

and

$$Q_M = \frac{dm}{dt}h_{fg} \tag{5}$$

where the Nusselt number is given by $\mathrm{Nu} = 2 + 0.6\,\mathrm{Re}^{1/2}\,\mathrm{Pr}^{1/3}$

The total heat transfer is thus given by

$$mC_p\frac{dT}{dt} = Q_C + Q_M \tag{6}$$

**Mass Transfer Equations**

Particle mass transfer is modelled using the 'Spray Drier Model' [5]. This controls the amount of mass transfer depending on whether a particle is above or below the 'boiling point'. A particle is said to be 'boiling' if the saturation vapour pressure at a given temperature, $p_{sat}$, is greater than the gaseous vapour pressure, where

$$p_{sat} = \exp\left[A - \frac{B}{T+C}\right] \tag{7}$$

$A$, $B$ and $C$ are constants and their values for water are 23.196, 3816.44 and -46.13 respectively.

When the particle is below the boiling point, mass transfer is given by

$$\frac{dm}{dt} = \pi d D \mathrm{Sh}\frac{W_C}{W_G}\log\left(\frac{1-X}{1-X_G}\right) \tag{8}$$

and when it is above the boiling point by

$$\frac{dm}{dt} = -\frac{Q_C}{h_{fg}}. \tag{9}$$

**Boundary Conditions**

Three types of boundary condition were used in this investigation: WALL boundaries, PRESSURE boundaries, and SYMMETRY PLANE boundaries.

WALL boundary conditions are placed at fluid-solid interfaces and enable the specification of velocities (normally zero), heat fluxes, and temperatures. Conventional wall functions [6] are imposed at WALL boundaries.

Fluid may flow into or out of the domain across a PRESSURE boundary. If fluid flows *into* the domain, Neumann conditions (i.e. zero normal gradient) are imposed on velocity and turbulence quantities, and values assigned directly to pressure and temperature (Dirichlet conditions). When fluid flows *out* of the domain across a PRESSURE boundary, Dirichlet conditions are imposed on pressure, and Neumann conditions on all other variables.

At SYMMETRY PLANE boundaries, all variables are set to be mathematically symmetric, except the component of velocity normal to the boundary which is *anti*-symmetric. In 2D axi-symmetric flows a SYMMETRY *AXIS* is imposed at $r = 0$ at which the azimuthal (swirl) component of velocity is anti-symmetric.

## 3. The Problem being modelled

A cylindrical PDEC tower of 8.0m height and 1.0m diameter was modelled with adiabatic walls. Water droplets (diameter of $30\,\mu m$) were injected at 0.25m from the top of the tower with a temperature of 24°C and a volume flow rate of 6 l/h (speed = 30m/s). External conditions were zero wind, air temperature of 40°C, and relative humidity of 26.2% (water content of 12g water per kg dry air). These conditions are typical of those experienced in southern-European regions during the summer season.

## 4. CFD Representation of the Problem

In CFX-F3D two dimensional problems are defined by specifying a slice of the geometry which is one cell thick in the direction normal to the plane of the slice and imposing SYMMETRY PLANE boundaries on the two faces parallel to the slice. Consequently the PDEC tower was represented using a one radian slice with SYMMETRY PLANE boundaries set at the $\theta = 0$ and $\theta = 1\,\text{rad}$ faces. A PRESSURE boundary was placed at some (finite) distance from the tower to represent the exterior domain (figure 2). The external air conditions specified in section 3 are imposed at the PRESSURE boundaries.

The slice was divided into 20 cells in the radial direction and 120 cells in the longitudinal direction.

Water injection was represented using twenty vertically downward particle trajectories. Particles were injected from the centre of each cell along the tower width at 0.25m below the top of the tower with a mass flow rate directly proportional to the starting cell area. This ensured that the water was distributed evenly.

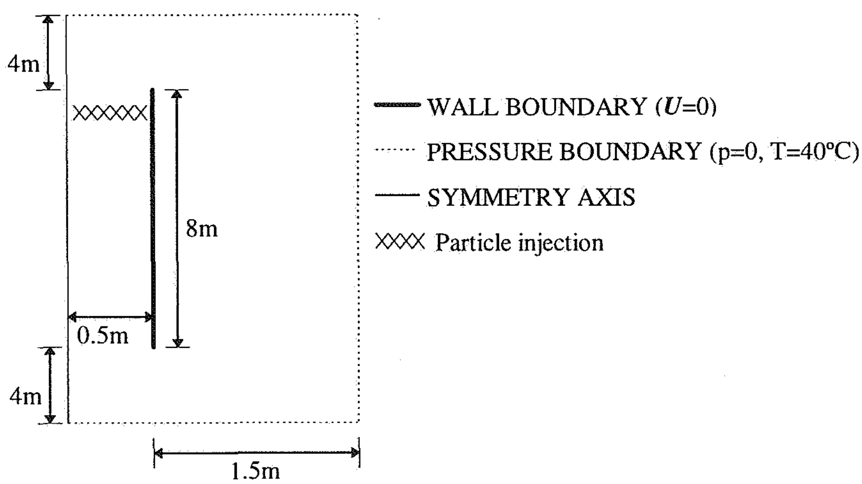


**Figure 2.** Geometry and boundary conditions used in the simulations.

## 5. Results and discussion

Injection of the water particles induces a downdraught shown in figure 3. The resulting particle tracks (fig. 4) are of uniform length and direction except in the vicinity of the wall where lower air speeds (due to wall friction effects) result in shorter tracks and small outward radial velocity component. Figures 5 and 6 illustrate the cooling effect produced by the particles. As expected, no further cooling occurs once the particles have evaporated.

The CFD results have been compared with those predicted by the one dimensional 'tower model' described in [2], [3] and [4]. In that model the flow variables are solved along the tower length. The tower was discretised into 100 elements and the flow variables calculated in each. In order to compare the CFD results with the tower model results, averaged values of the flow variables predicted by the CFD code were calculated at each height corresponding to the elements defined in the tower model.

The discrepancies between the CFD predictions and those of the 'tower model' suggest that the CFD code predicts a lower flow rate through the tower (fig. 7). This is thought to be due to 2D effects, in particular, turbulence, that are not present in the 'tower model'. As a result, in the CFD model, energy is given up in the production of turbulence and so less energy is available to bring about the mean flow parameters, thus yielding a lower flow rate. A reduced flow rate means there is less dry air available per unit mass of moisture and this yields a higher mass fraction of water (fig. 5) and cooler air which is also reflected in the CFD results (fig. 6). Another contributing factor to the higher flow rate in the 'tower' model is the assumption of zero pressure loss at the inlet.

The difference in the velocities between the CFD and 'tower model' at the top of the tower (fig. 7) is thought to be due to the momentum transfer between the particles and the air which is neglected in the 'tower' model. In the CFD code, momentum is transferred from the relatively fast moving water particles to the surrounding air. This causes acceleration of the air between the top of the tower and the injection point with a pressure drop in the same region (fig. 8). In the 'tower' model, particles are assumed to take the velocity of the surrounding air immediately after injection. Consequently there is no upstream acceleration, just a constant velocity equal to that at the tower inlet which ensures the mass entering the tower is equal to that leaving.

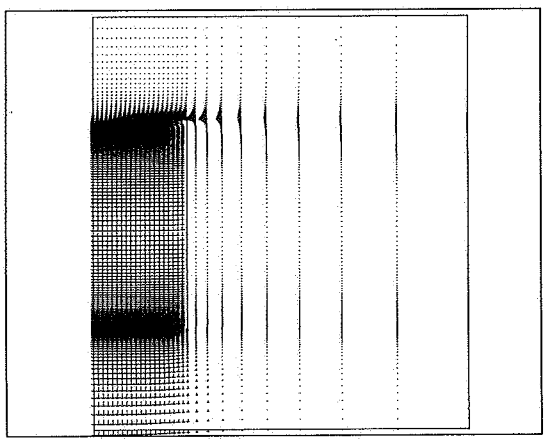

**Figure 3.** Flow pattern predicted by the CFD model.

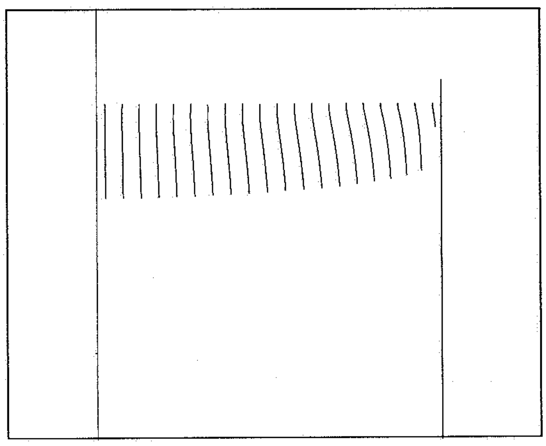

**Figure 4.** Particle tracks predicted by the CFD model (longest particle trajectory is 1.08m).

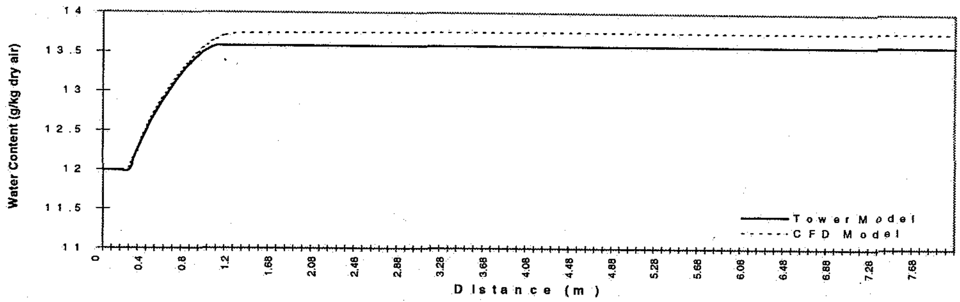


**Figure 5.** Water content along the tower length.

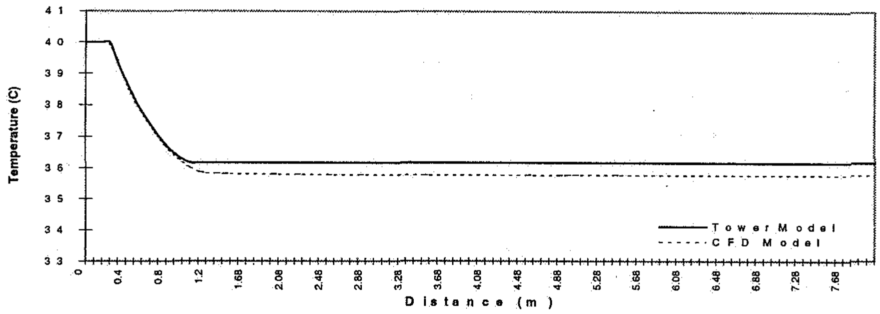


**Figure 6.** Air temperature along the tower length.

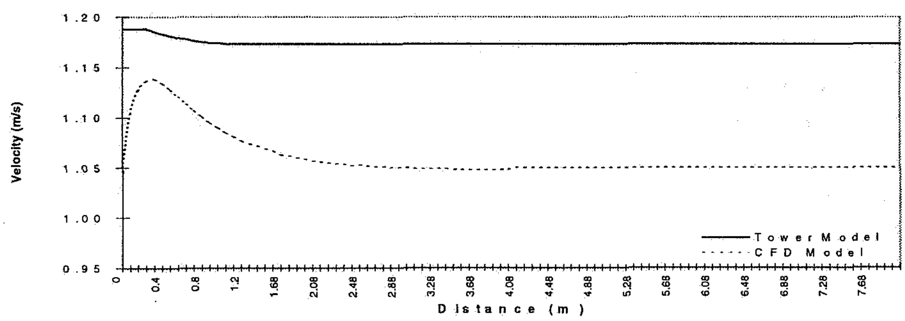


**Figure 7.** Vertical velocity magnitude of the flow along the tower length (0 = top of tower).

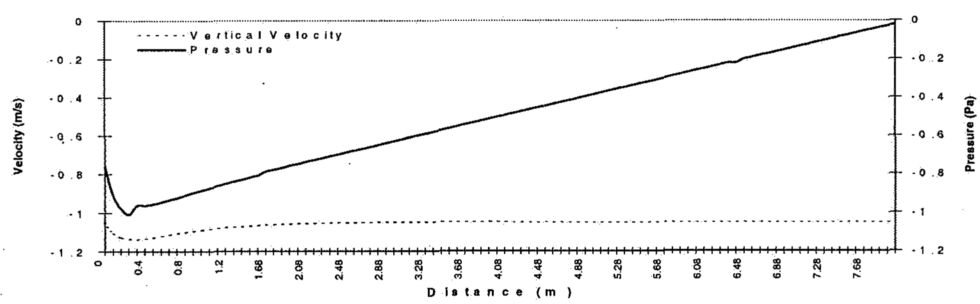


**Figure 8.** Vertical velocity and modified pressure along the tower length (CFD model).

## 6. Conclusions and Further Work

Predictions have been produced for a Passive Downdraught Evaporative Cooling (PDEC) system using CFD. In order to quantify the accuracy of the results, comparisons have been made with a one dimensional 'tower model'. The results compare favourably giving increased confidence in the CFD predictions. Some differences are explained and reasons for these are suggested.

It is now the intention to progress to a more accurate CFD model of the individual micronisers that are used for injecting the very fine mists of water. The work will identify optimum modelling techniques such as the number of particle trajectories required to accurately represent a single microniser and how to model size distribution of particles. Various numerical parameters used for obtaining convergence will also be investigated. It is then the intention to model a full (3D) PDEC system with wind catcher devices and delivery of cooled air into occupied spaces. The predictions will be compared with results from experiments currently under way in a test building at the Conphoebus Institute in Catania, Sicily.

## 7. Acknowledgment

The authors wish to thank Prof. E. Rodríguez for his comments and advice in the final stages of writing this paper.

## 8. References

1. Bowman, N., et al.
   "Application of Passive Downdraught Evaporative Cooling (PDEC) to Non-Domestic Buildings". Renewable Energy, Vol. 10., No. 2/3, 1997, pp.191-196.
2. Rodríguez, E. A., Alvarez, S., and Martin, R.
   "Direct Air Cooling From Water Drop Evaporation"
   Architecture and Urban Spaces, PLEA '91, 1991, pp.619-624.
3. Rodríguez, E. A., Alvarez, S., and Martin, R.
   "Water Drops As a Natural Cooling Resource. Physical Principles"
   Architecture and Urban Spaces, PLEA '91, 1991, pp. 499-504.
4. Alvarez, S., Rodríguez, E. A, and Molina, J. L.
   "The Avenue of Europe at EXPO '92: Application of Cool Towers"
   Architecture and Urban Spaces, PLEA '91, 1991, pp.195-201.
5. Computational Fluid Dynamics Services
   CFX 4.1 Flow Solver User Guide,1995 (AEA Harwell).
6. Versteeg H. K. and Malalasekera W.
   "An Introduction to Computational Fluid Dynamics - the Finite Volume Method"
   (1995) (Longman Group Ltd.)
7. Launder, B. E. and Spalding, D. B.
   "The numerical computation of turbulent flows"
   Computer Methods in Applied Mechanics and Engineering volume 3, 1974, pp269-289.

Rapport SMITS

idee van afwegen ≠ karakt.
uit slecht !!

zie ook in
andere paper

Compare < natural / HVAC

* reliability ⟶ reliab v/h systeem
* comfort
* cost ⟶ cost of install. plaatsen
* energy cons.
* reliability of calculations !!
↳ uitrekenen op comfort

lijst van ≠ karakt : +/-
(nog uit te breiden)

wegen !!

proberen zoveel mogelijk cijfers op te kleven

# VENTILATION AND COOLING

## 18 ANNUAL AIVC CONFERENCE
## ATHENS, GREECE, 23-26 SEPTEMBER 1997

# Characteristic values of natural ventilation and air conditioning

A.H.C. van Paassen, S.H. Liem, and B.P. Groninger

Delft University of Technology
Faculty of Mechanical Engineering and Marine Technology
Process and Energy Department
Laboratory of Refrigeration and Indoor Climate Technology
The Netherlands

# Characteristic values of natural ventilation and air conditioning

A.H.C. van Paassen, S.H. Liem and B.P. Gröninger
Delft University of Technology
The Netherlands

**Summary**

This investigation is part of project NATVENT™, a concerted action of nine institutions of seven European countries under the Joule-3 program. It aims to open the barriers that blocks the use of natural ventilation systems in office buildings in cold and moderate climate zones.

The choice to apply natural ventilation in office buildings is very arbitrary: it depends very much on the personal preference of the architect or taken for budgetary reasons, even sometimes not considered at all. This article proposes a method to compare natural ventilation with more complicated mechanical ventilation systems based on reliability, comfort, initial and maintenance costs and energy consumption. It shows clearly the strong points (cheap, reliable) and the weak points (limited cooling capacity) of natural ventilation.

## 1. Introduction

NATVENT™ is a Pan-European project under the Joule-3 program. It aims to open the barriers that block the use of natural ventilation in office buildings. One of its actions is the integration and maintenance of natural ventilation systems.

In practice the choice to apply natural ventilation with night cooling is very arbitrary: it depends very much on the personal preference of the architect or taken for budgetary reasons, even sometimes not considered at all. In many cases natural ventilation can still be a very competitive alternative. One reason for this ignorance for natural ventilation is the lack of tools to compare it with other ventilation systems.

This article proposes a method to develop such a tool. First the basic concepts of reliability and maintainability will be discussed. Afterwards other performance characteristics are introduced, such as air quality (AQ), comfort performance ($CP_x$), where 'x' stands for the maximal allowable internal load per square meter, budgetary performance (BP) and energy performance (EP)

Finally these performance characteristics are used to choose the appropriate ventilation system for certain conditions.

## 2. Performance features

A (ventilation) system can be assessed by the success at which it will obtain the design objectives. These objectives can be reached completely or sometimes only to a certain extend. By giving each system a characteristic value (between 0 and 1), one can rank the success of that system for that specific feature. By summing up these characteristic values an overall performance characterization is obtained that can be used to compare the different systems. Performance features that can be used to categorise a ventilation system are: reliability, overall comfort criteria, costs (first and maintenance), energy consumption and safety features.

* Reliability: Without any numerical calculation it can be said that traditional natural ventilation systems are far more reliable, because they do not need power and have a small number of components. Of course when these systems will become more complicated by adding motors and sensors for better control, the performance may increase but the reliability will eventually approaches that of ordinary mechanical ventilation systems.

* Overall comfort criteria: The factors that are typical in natural ventilation systems and that should be discussed in relation with air conditioning systems, are air motion (draught), space humidity, noise level, air cleanness, and psychological effects (acceptance of higher temperatures with openable windows).

* Costs: The costs can be divided in first costs and maintenance costs. For automatic controlled natural ventilation systems the actuators and control system require maintenance. Because the actuators are not concentrated in one place, but spread out through the whole building, the personal costs are higher then the component cost.

* Energy consumption: The outside air supplied by the ventilation system should be heated to room temperature. Here natural systems have the drawback that heat recovery is very difficult to apply. Mechanical ventilation and air conditioning systems can be equipped with heat recovery units. But on the other hand mechanical ventilation systems need fans to transport the air and therefore they use electricity. Air conditioning systems not only need energy for transport, but also use a substantial amount of energy for conditioning the air. In general the energy costs of air conditioning systems are about three times higher than for mechanical ventilation systems [1].

* Safety features: Other features that are difficult to quantify are fire and smoke control and safety against burglary. These are very complex and beyond the scope of this paper.

## 3. Theoretical background [2]

A system that cannot fulfill the function for which it is designed, fails. The reliability of the system depends on the period in its life cycle, in which it fails; when this occurs in the first period of its life cycle, the system is not reliable. On the other hand, when it fails at the end or over it's (theoretical) life cycle, the system is said to be reliable.

The reliability R(t) of a system or a component is defined as the probability of failure free functioning in a certain time interval (0 to t) under defined conditions. When f(t) is the failure probability density function (the probability that the system fails in time interval (t, t+dt)), then

$$F(t)=\int_0^t f(t)*dt$$

is the unreliability function. The reliability R(t) is defined as the complementary function of the unreliability function F(t):

$$R(t)=1-F(t)$$

The conditional probability density function or failure degree z(t) is the probability that the system fails in the time interval (t, t+dt), given, that it has not failed till time t under certain conditions. It is defined as:

$$z(t)=\frac{f(t)}{R(t)}$$

The discussed quantities above are related to distribution functions, which can be characterized by certain parameters. One of the most important distributions is the negative exponential distribution, given by

$$R(t) = e^{-\lambda * t} \qquad \text{with} \qquad \lambda = \frac{1}{MTBF}$$

$\lambda$ is the failure rate, defined as the fraction with failure of tested pieces within a period dt. MTBF is Mean Time Before Failure.

The main characteristic of this distribution is that failures occur at random. This means that the probability of failure in each interval of the duration of its life time is the same, so the failure degree is a constant. When the MTBF is reached, there are only 37% survivors of the initial population, see figure 1 for some examples of the negative exponential distribution.

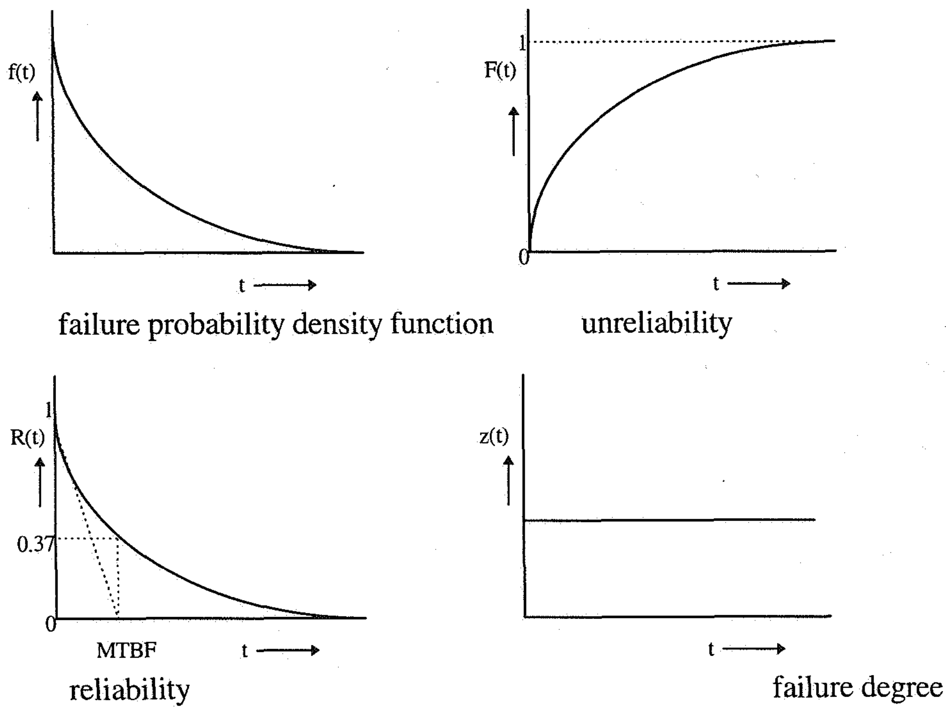


Figure 1 The negative exponential distribution

## 4. Reliability analysis

For every function of a technical system the demand for reliability needs to be described in the demand specification. When the reliability's of all the separate components of the system are known, the reliability on system level can be determined with a reliability model and rules from mathematics. Fig 2 shows the reliability's of the components of a simple system.

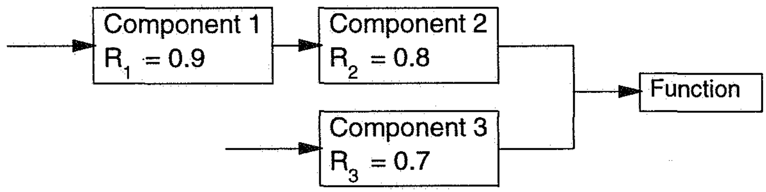


Figure 2 Example of a reliability model for a simple system

This system functions when the components 1 and 2 function or when component 3 functions or when all 3 components are functioning. The reliability of the branch that consists of component 1 and 2 is:

$$R_{1,2}(t) = \prod_{i=1}^{n} R_i(t) = R_1 * R_2 = 0.9{*}0.8 = 0.72$$

The system reliability now becomes:

$$R_{syst}(t) = 1 - \prod_{i=1}^{n} F_i(t) = 1 - (0.28{*}0.3) = 0.92 \qquad (F=1-R)$$

This procedure is called a reliability analysis.

The reliability of the separate components can be determined with historical data, by registration of occurred failures or by testing of the components in a laboratory under simulated operation circumstances. In [2] are given life spans and failure rates (failures per $10^6$ h) of some selected components and equipment's. In this study reliability is considered as a measure for maintenance costs.

## 5. Reliability analysis of HVAC systems

Based on the procedure described in the foregoing paragraph four HVAC systems will be analyzed. These systems are:

1. Natural ventilation with radiators for heating
2. Same as 1 but with motorized windows and vents for night cooling
3. Mechanical ventilation with radiators
4. Variable Air Volume (VAV) system

The reliability analysis is based on the following assumptions:

* The system only functions when all components are functioning
* The system is used non-stop 24 hours a day, 365 days a year
* All components have an exponential reliability distribution
* The components which are not likely to fail have a reliability of 1
* Only components which are considered important are included

The reliability for a period of 1 year is calculated. This means that the installation is used for 1 * 365 * 24 = 8760 hours. So the reliability of a component is given by: $R(8760) = e^{-\lambda \cdot 8760}$, with $\lambda$ is the failure rate of the component.

The reliability of the entire system is the product of the reliability's of its components.

To illustrate the procedure, the reliability of a natural ventilated system with motorized windows and vents for night cooling and radiators for heating (see figure 3) is determined.

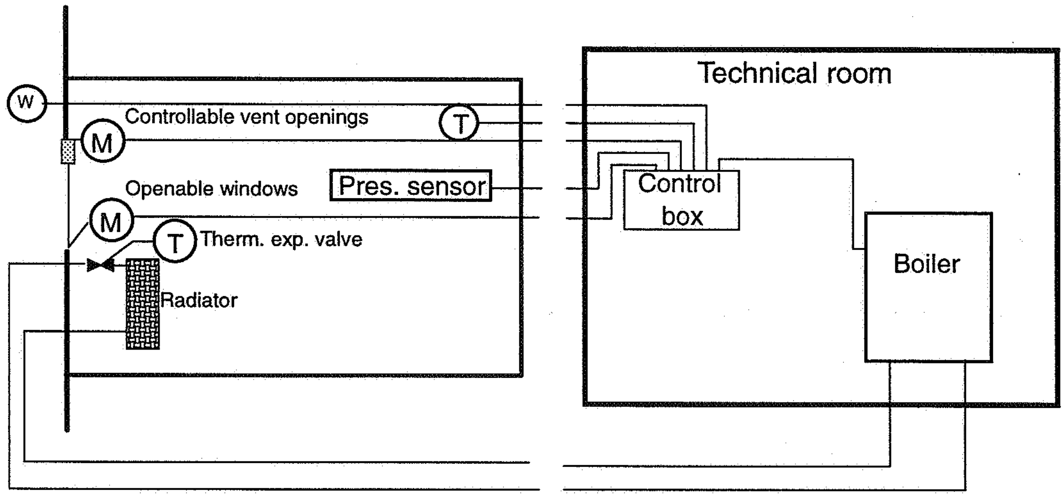


Figure 3. The ventilation system with motorized windows and vents and radiators for heating

| Components | Failure rate : λ | Reliability |
|---|---|---|
| controllable ventilation opening | | 1 |
| openable windows | | 1 |
| tubes | | 1 |
| radiator | | 1 |
| boiler | | |
| elec. controller | | |
| thermostatic expansion valve | $10^{-5}$ | 0.916 |
| elec. servo motors (2 x) | $2 \times 10^{-5}$ | 0.839 |
| presence sensor | $10^{-6}$ | 0.991 |
| weather sensor | $10^{-6}$ | 0.991 |
| temp. sensor | $10^{-6}$ | 0.991 |

Total system reliability (rough estimate !): R= 0.648

In the same manner the reliability's of the other systems are determined. The results are given in Table I. As expected, the reliability of the Variable Air Volume System drops dramatically because the number of its components is much higher.

Table I. Reliability's of some HVAC systems → open mechanic.

| System | Description | Reliability |
|---|---|---|
| 1 | Natural ventilation + radiator heating | 0.8 |
| 2 | As 1 + controlled windows and vents for night cooling | 0.6 |
| 3 | Mechanical ventilation + radiator heating | 0.6 |
| 4 | Variable Air Volume System | 0.3 |

## 6. Other characteristic values

Other features that can be used to compare the system performance besides reliability are:

Air Quality: $$AQ = \frac{\text{Fresh air supplied by the system}}{\text{Fresh air required according specifications}}$$

Although simulation studies showed that well-designed natural ventilation systems in general can easily satisfy the specifications, there are periods with too low/too high rates [3]. Considering the number of hours with too low ventilation rates the AQ-value is set at 0.8. System 2 has an AQ-value equal to 1. It has a rule based control system [4] that adjusts the window opening as a function of wind speed and wind direction, so that on average a constant flow of outside air is supplied. Because mechanical- and VAV-systems deliver the right ventilation rates under all circumstances, AQ = 1 for these systems.

Comfort Performance: $$CP_x = \frac{\text{Cooling delivered}}{\text{Cooling required}}$$

x = the internal load per square meter floor area

With natural ventilation without night cooling the maximal internal load is only 15 W/m$^2$ (see Table II); this means, that at $CP_{25}$ (internal load is 25 W/m$^2$) the comfort performance is only $CP_{25}=15/25=0.6$. When the internal load is increased to 40 W/m$^2$, the comfort performance drops to $CP_{40}=0.375$. With system 2 it has been experimentally found [5], that with night cooling the internal load can be increased to 30 W/m$^2$; consequently $CP_{25}=1 (0 <= CP_x => 1)$ and $CP_{40}=0.75$.

Budgetary Performance: $$BP = \frac{\text{Cost of the cheapest system}}{\text{Cost of the system considered}}$$

The budgetary performance (BP) can be determined with Table II

Table II. Costs and allowable internal load (use of outdoor shading)

| System | | per m$^2$ net occupied area | | |
|---|---|---|---|---|
| | | Investment cost | Maintenance cost | Internal load (max) |
| | | NLG | NLG /year | W |
| 1 | Natvent+rad | 154 | 4.4 | 15 |
| 2 | As 1 + controlled windows and vents for night cooling | 300 | 9 | 30 |
| 3 | Mech. vent+rad | 330 | 8.8 | 30 |
| 4 | VAV system | 680 | 18 | >50 |

Energy Performance: $$EP = \frac{\text{Primary energy of natvent - system}}{\text{Primary energy of system considered}}$$

Table III shows typical values of primary energy consumption's for a well isolated, medium heavy office building facing south with outside shading. With these values EP can be determined for the various systems. It is clear, that the air conditioning system has the highest energy consumption. It uses approximately three times more energy than the other systems.

Table III. Energy consumption of some HVAC systems

| | System | Yearly energy consumption [MJ/m$^2$] | | | |
|---|---|---|---|---|---|
| | | Heating | Cooling | Transport | Total |
| 1 | Natural ventilation+radiators | 447 | 0 | 0 | 100% |
| 2 | As 1 + controlled windows and vents | 447 | 0 | 0 | 100% |
| 3 | Mechanical ventilation + radiators | 447 | 0 | 35 | 108% |
| 4 | Variable Air Volume system | 756 | 399 | 420 | 350% |

## 7. Characteristic values

Table IV. Characteristic values with an internal load of 25 W/m$^2$

| | System | R | AQ | $CP_{25}$ | BP | EP |
|---|---|---|---|---|---|---|
| 1 | Natural ventilation +radiators | 0.8 | 0.8 | 0.6 | $\frac{154}{154}=1.0$ | 1.0 |
| 2 | As 1 + controlled windows and vents | 0.7 | 1.0 | 1.0 | $\frac{154}{300}=0.5$ | 1.0 |
| 3 | Mechanical ventilation + radiators | 0.6 | 1.0 | 1.0 | $\frac{154}{330}=0.5$ | 0.9 |
| 4 | Variable Air Volume System | 0.3 | 1.0 | 1.0 | $\frac{154}{680}=0.2$ | 0.3 |

Table V. Characteristic values with an internal load of 40 W/m$^2$

| | System | R | AQ | $CP_{40}$ | BP | EP |
|---|---|---|---|---|---|---|
| 1 | Natural ventilation+radiators | 0.8 | 0.8 | 0.4 | 1.0 | 1.0 |
| 2 | As 1+controlled windows and vents | 0.7 | 1.0 | 0.7 | 0.5 | 1.0 |
| 3 | Mechanical ventilation+radiators | 0.6 | 1.0 | 0.7 | 0.5 | 0.9 |
| 4 | Variable Air Volume System | 0.3 | 1.0 | 1.0 | 0.2 | 0.3 |

Je kan van maken als
alle factoren even heel! zijn
Ander weegfactoren
(bvb comfort, x5)

The characteristic values as defined in the preceding paragraphs can be determined for the various ventilation systems for different conditions and locations. Tables IV and V shows the characteristic values of four ventilation systems for a well isolated, medium heavy office building facing south with outside shading and with internal loads of respectively 25 $W/m^2$ and 40 $W/m^2$. It must be emphasized, that these values are rough estimates, based on generally accepted data [1] and personal experience [5]. It shows that natural ventilation with night cooling can still be used with an internal heat load of 25 $W/m^2$

These tables forms a simple tool for architects and developers to choose the appropriate ventilation system for a certain condition, included natural ventilation.

## 8. Conclusions

In the preceding paragraphs the characteristic values of various ventilation systems such as reliability, air quality, comfort, budgetary features and energy performance are defined. After these values are tabulated, they can be used to choose the appropriate ventilation system, ranging from simple natural ventilation to more sophisticated air conditioning systems and in doing so bring natural ventilation in the focus of the architect or developer as a comparable ventilation system with its strong (cheap, reliable) and weak points (limited cooling capacity)


## Acknowledgment

This work is part of the Pan-European NatVent™ project funded in part by the European Commission under the JOULE-3 program and coordinated by the Building Research Establishment Ltd (BRE-UK). The participating organizations are: Belgian Building Research Institute (BBRI-B), TNO Building & Construction Research (TNO-NL), Danish Building Research Institute (SBI-DK), J&W Consulting Engineers AB (J&W-S), Willan Building Services (Willan-UK), Sulzer Infra Laboratory (Sulzer-CH), Delft University of Technology (TUD-NL) and Norwegian Building Research Institute (NBI-N).


## References


1. SBR-publication 213, Ontwerp van energie-efficiënte kantoorgebouwen. R'dam 1994.
2. Bloch, H.P. and Gaitner, F.K., Practical Machinery Management for Process Plants. Volume 2, 1983.
3. Galen, P.J.M., Automatische raamopeningen als bruikbaar onderdeel van de klimaatregeling, report KK-1070, TUD, June 1994.
4. Paassen, A.H.C., and P.J.M. van Galen, Rules for Cooling through motorized vent windows, 19th Congress IIR, August 20-26, 1995, The Hague, The Netherlands.
5. Paassen, A.H.C. van and Lute, P.J. Performance and feasibility of Passive Climate Systems, CLIMA 2000, November 1-3, 1993, London CD-Rom.

ENQUÊTE

intéressante paramètres

VENTILATION AND COOLING

18TH ANNUAL AIVC CONFERENCE
ATHENS, GREECE, 23-26 SEPTEMBER, 1997

# Barriers to Natural Ventilation Design of Office Buildings

*Søren Aggerholm*

Danish Building Research Institute, SBI
P.O. 119
Dr. Neergaards Vej 15
DK-2970 Hørsholm
Denmark
Tel: +45 42 86 55 33
Fax: +45 42 86 75 35
E-mail: soa@sbi.dk

# Barriers to Natural Ventilation Design of Office Buildings

*Søren Aggerholm*
Danish Building Research Institute, SBI

## Synopsis

Perceived barriers restricting the implementation of natural or simple fan assisted ventilation systems in the design of new office type buildings and in the refurbishment of existing such buildings have been identified in seven central and north European countries with moderate or cold climate: United Kingdom, Belgium, The Netherlands, Switzerland, Norway, Sweden and Denmark.

The barriers were identified in an in-depth study with structured interviews based on questionnaires among leading designers and decision makers: architects, consultant engineers, contractors, developers, owners and governmental decision makers. The study is part of the ***NatVent***™ project being carried out under the EC JOULE programme.

The interviews identified a significant lack of knowledge and experience on special designed natural ventilation in office buildings compared to the knowledge and experience on mechanical ventilation. In addition there is a lack of sources to natural ventilation knowledge in standards, guidelines and building studies and a desire for new design tools on natural ventilation including calculation rules and easy-to-use, simple and advanced computer programmes.

## 1. Introduction

Mechanical ventilation systems are often installed in office buildings where good natural ventilation would have been sufficient to obtain comfortable indoor climate and good air quality. It is important to identify the barriers seen by designers and decision makers which restrict the implementation of natural ventilation systems and lead to the decision to install mechanical ventilation plants in office buildings where it is not strictly necessary. Knowing the barriers is the first step in providing solutions to overcome them.

## 2. Interviews

A total number of 107 designers and decision makers were interviewed. In general the interviews in each country were performed with: 5 architects, 3 HVAC consultant engineers, 2 developers, 2 owners, 2 contractors and a governmental decision maker responsible for regulations and standards in the country. The interviewees were selected with the intention of also identifying the variety in opinions and viewpoints on natural ventilation in office buildings among people with the same profession.

The interviews were based on two questionnaires as follows:

- <u>General view on natural ventilation in office buildings.</u>
  General knowledge, viewpoints, experience and perceived problems with natural ventilation systems in office type buildings.
- <u>Specific building project.</u>
  Decisions actually made during the design or refurbishment of an office type building.

A specific 5 point scale was used where possible. The questionnaires were not too tight and there was ample space for additional comments, remarks and viewpoints not included in the questions. The questionnaires were completed by the interviewee and the interviewer together. In general both parts of the interview were performed with all interviewees. The only exception is the governmental decision makers, where only the general view was relevant.

## 3 Main results

The main results from the interviews are given in this paper. Details can be found in the references. The results in the figures are given as the average for each group of professions interviewed. *All* is the average of all profession groups except for the governmental decision makers.

### 3.1 Knowledge on ventilation

Nearly all the interviewees have less knowledge on special designed natural ventilation compared to their knowledge on mechanical ventilation in offices, see figure 1. Especially in Belgium, Denmark, Switzerland and Norway the knowledge on special designed natural ventilation is very low compared to the knowledge on mechanical ventilation, see figure 2.

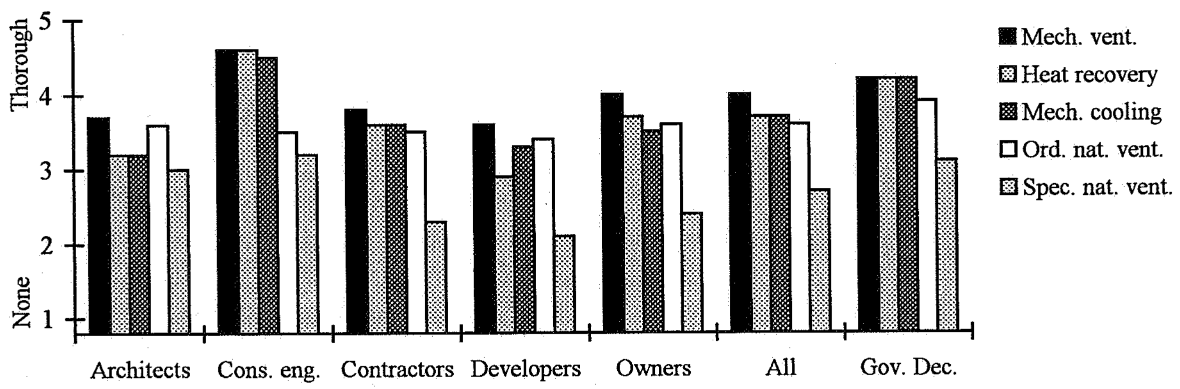


*Figure 1. The interviewees perception of own knowledge, by profession.*

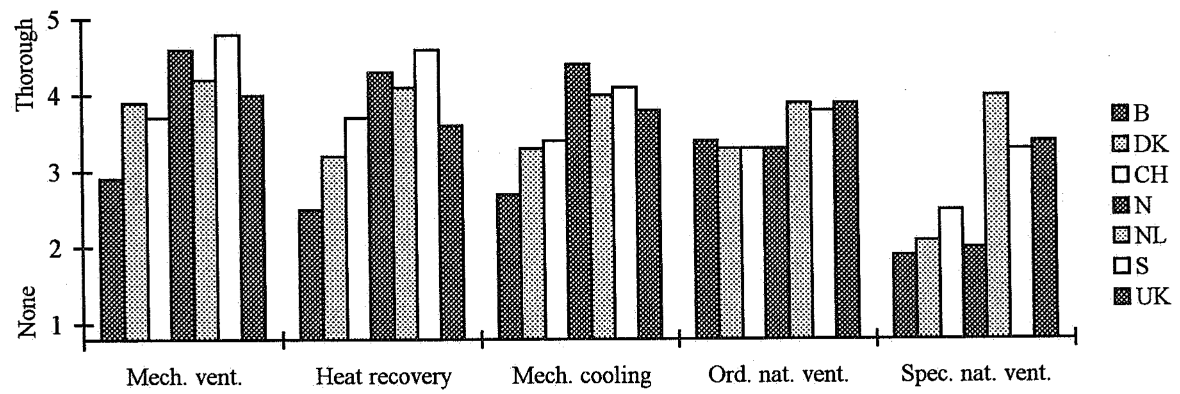


*Figure 2. The interviewees perception of own knowledge, by country. B=Belgium, DK=Denmark, CH=Switzerland, N=Norway, NL=The Netherlands, S=Sweden, UK=United Kingdom*

On average the interviewees have the same level of knowledge on ordinary natural ventilation as on mechanical ventilation. The exception is the consultant engineers who in general have less knowledge on ordinary natural ventilation compared to their knowledge on mechanical ventilation. The interviewees have indicated their level of knowledge on the five topics based on the knowledge necessary to perform their normal task in the design or decision process and relative to their profession. It is therefore not possible to compare the absolute level of knowledge between the professions based on the results.

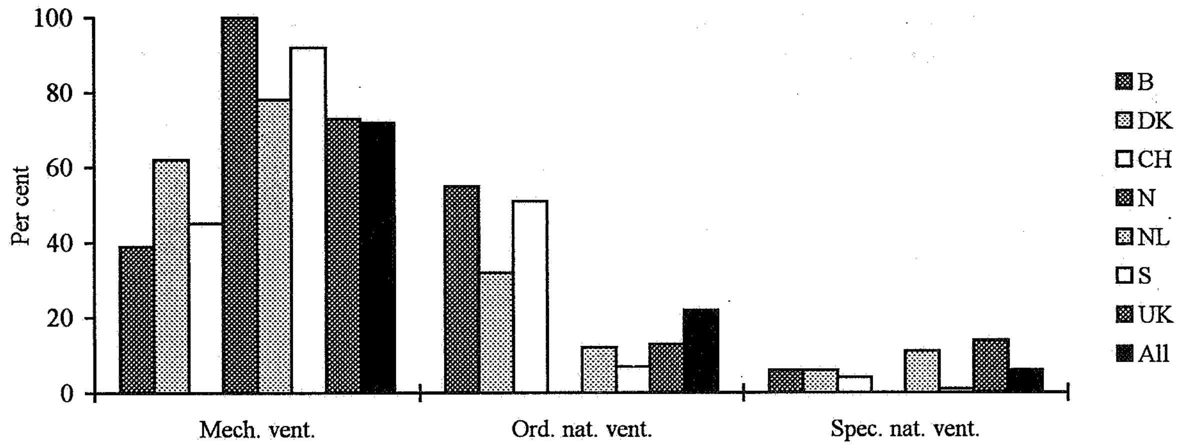


*Figure 3. The interviewees relative experience with mechanical, ordinary and special designed natural ventilation in new offices. The scale is the per cent of offices designed, constructed or owned.*

### 3.2 Experience

Most of the interviewees have much experience on mechanical ventilation in offices, whereas the experience with special designed naturally ventilated offices is very limited, see figure 3. Many of the interviewees have worked with ordinary natural ventilation in office buildings, but the actual number of buildings designed, constructed or owned varies significantly. The exception is Norway where none of the interviewees had designed, constructed or owned an office building with natural ventilation. The experience with ventilation in refurbished offices was about the same as in new offices.

### 3.3 Project fee

In many of the countries most of the interviewed architects and consultant engineers are normally paid according to design fee rules of the national Counsel of Practising Architects or Counsel of Consultant Engineers, and with the fee for the detailed design fixed based on a percentage of the estimated construction costs.

### 3.4 Design

In general there is no significant difference in the interviewees perception of the *ease of design* in the four cases: natural ventilation in cellular offices, natural ventilation in open plan offices, mechanical ventilation in cellular offices and mechanical ventilation in open plan offices, see figure 4. Many of the interviewees emphasised that the ease of design also depends on the demands of the indoor climate and on the complexity of the ventilation system.

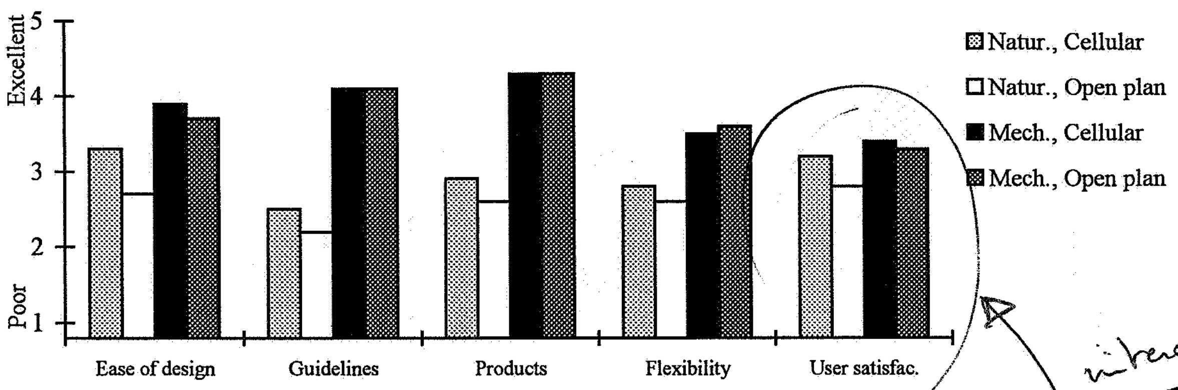


interessant

*Figure 4. The interviewees perception of the design of ventilation offices.*

Nearly all interviewees found that the availability of design *guidelines* and *products* were better on mechanical ventilation systems when compared with natural ventilation systems. The interviewees also expected a higher *flexibility* in mechanical ventilated offices than in natural ventilated offices.

The interviewees expect the same *user satisfaction* in natural and mechanical ventilated cellular offices. They expect higher user satisfaction in natural ventilated cellular than in natural ventilated open plan offices. In mechanical ventilated offices the expected user satisfaction is the same in cellular and in open plan offices. It was mentioned that user satisfaction also depends on the expectations, which are normally higher in mechanical ventilated offices.

### 3.5 Performance in practice

In general the interviewees expect a better performance of mechanical ventilation systems than of natural ventilation systems regarding cooling effectiveness, draught minimisation, ability to remove odours and pollutants, ability to prevent ingress of odours and pollutants and insulation against external noise, see figure 5. Regarding generation or transmission of internal noise the interviewees on average expect the same performance level by natural and mechanical ventilation. Several of the interviewees emphasised that the performance also depends on how well the system is designed.

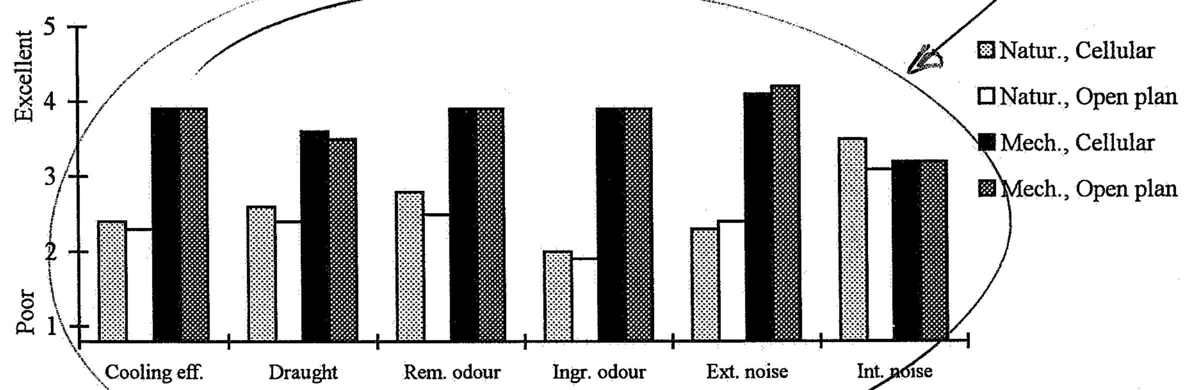


*Figure 5. The interviewees perception of the performance in practice of office ventilation.*

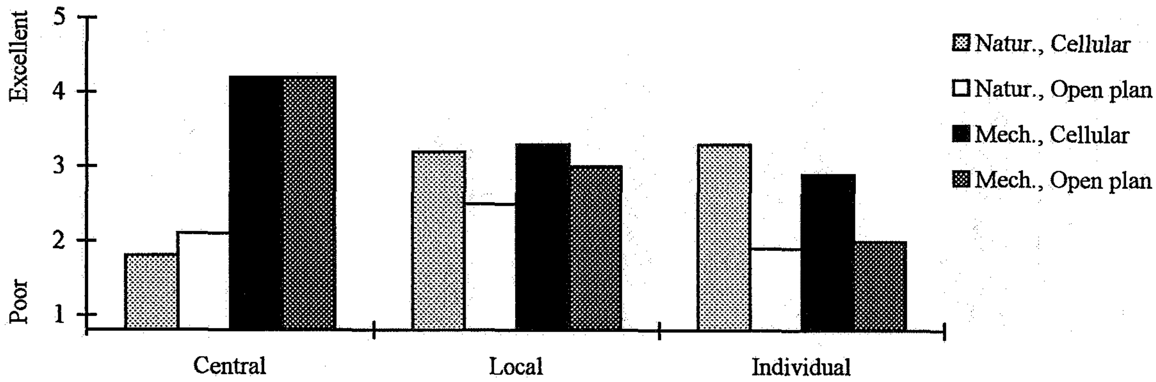


*Figure 6. The interviewees perception of the controllability of office ventilation.*

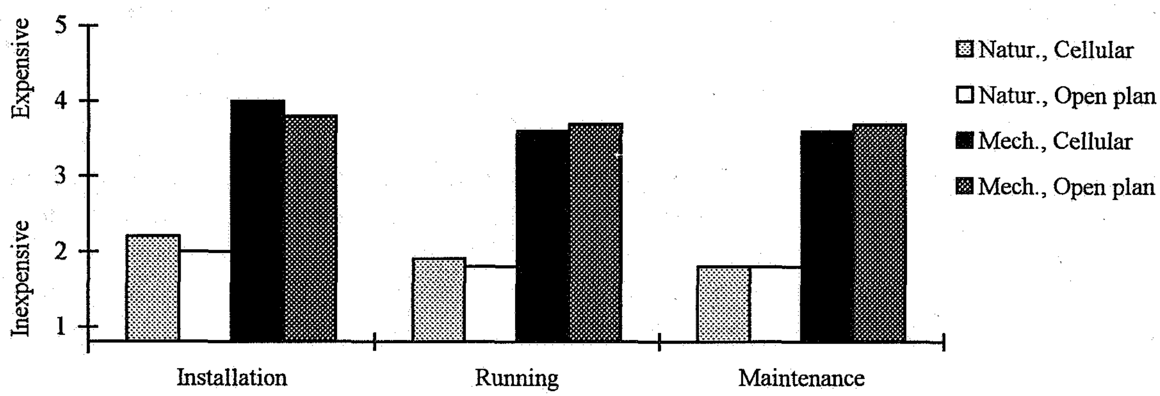


*Figure 7. The interviewees perception of the costs for office ventilation.*

### 3.6 Controllability

In general the interviewees expected a high degree of central controllability of mechanical ventilation systems and a low degree of central controllability of natural ventilation systems especially in cellular offices, see figure 6. The expected degree of local and individual controllability of the ventilation is a little higher in cellular offices than in open plan offices.

### 3.7 Costs

Most interviewees expect higher installation, running and maintenance costs for mechanical ventilation systems than for natural ventilation systems, see figure 7. Several of the interviewees emphasised that if mechanical ventilation is installed in a building a perceptible percentage of the total construction costs would be for the mechanical ventilation systems. It was also mentioned that the installation costs for natural ventilation systems is high if additional floor area or space is required.

### 3.8 Source to natural ventilation knowledge

The general opinion among the interviewees is that there is huge lack of good sources to natural ventilation knowledge. The mentioned sources are very sporadic and nearly no specific sources were mentioned by more than one or two of the interviewees.

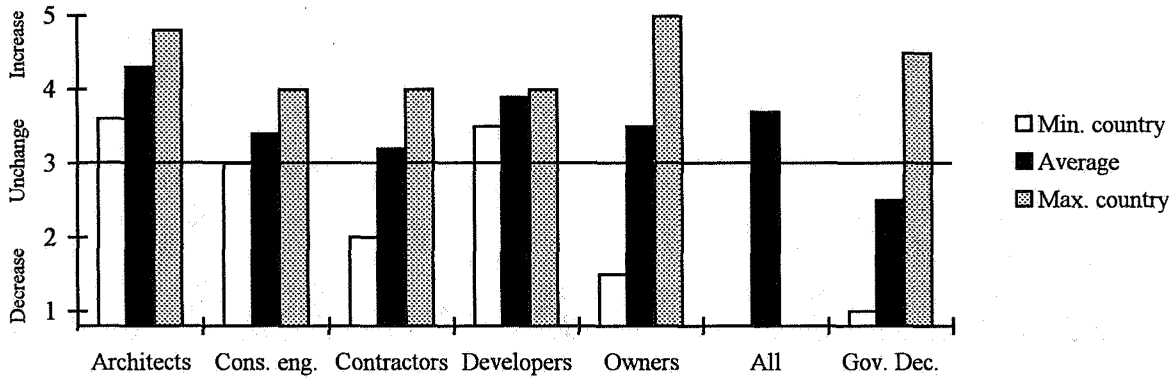


*Figure 8. The interviewees expectations on the future use of natural ventilation in offices.*

### 3.9 Expected future use of natural ventilation

The architects in general have the highest expectations of an increase in the use of natural ventilation in offices, see figure 8. On average only the governmental decision makers expect a decrease in the use of natural ventilation. The Swiss and Swedish governmental decision makers expected a significant decrease in the use of natural ventilation in offices. In Norway the interviewed governmental decision maker saw no future for natural ventilation. Also the HVAC consultant engineers and contractors expected natural ventilation to continue to be non-existent in Norwegian office buildings.

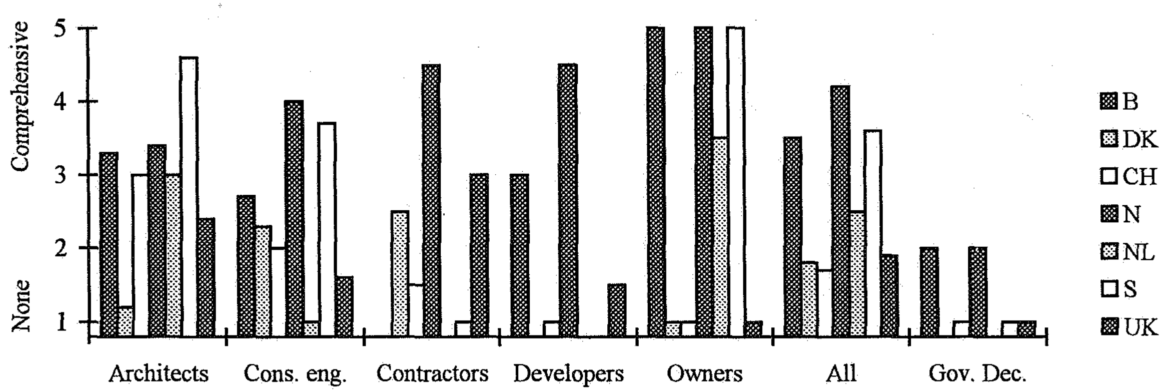


*Figure 9. The interviewees perception of restricting requirements in regulations, codes etc.*

### 3.10 Restricting requirements in codes

In Belgium, Norway and Sweden the interviewees perceived significant restrictions in building regulations, codes, norms and standards to the use of natural ventilation, see figure 9. In the other countries restrictions exist but they are perceived to be more limited. In general it is the architects and the owners that see the largest restrictions. The governmental decision makers perceived the restrictions from the requirements in building regulations, codes, norms and standards to be much more limited than the rest of the interviewees in a country.

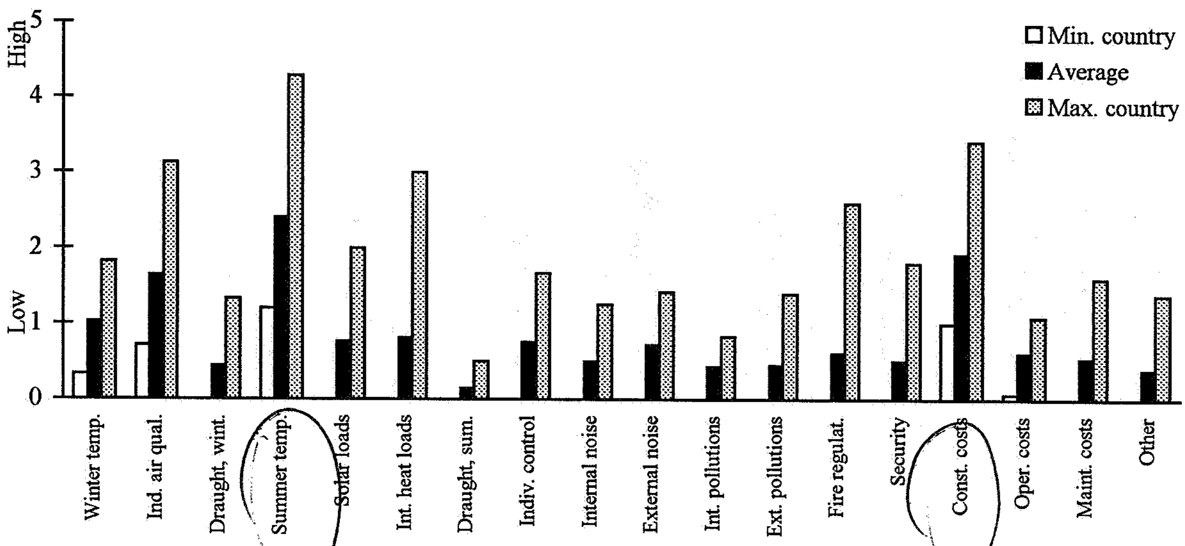


*Figure 10. Critical parameters in the design of the buildings.*

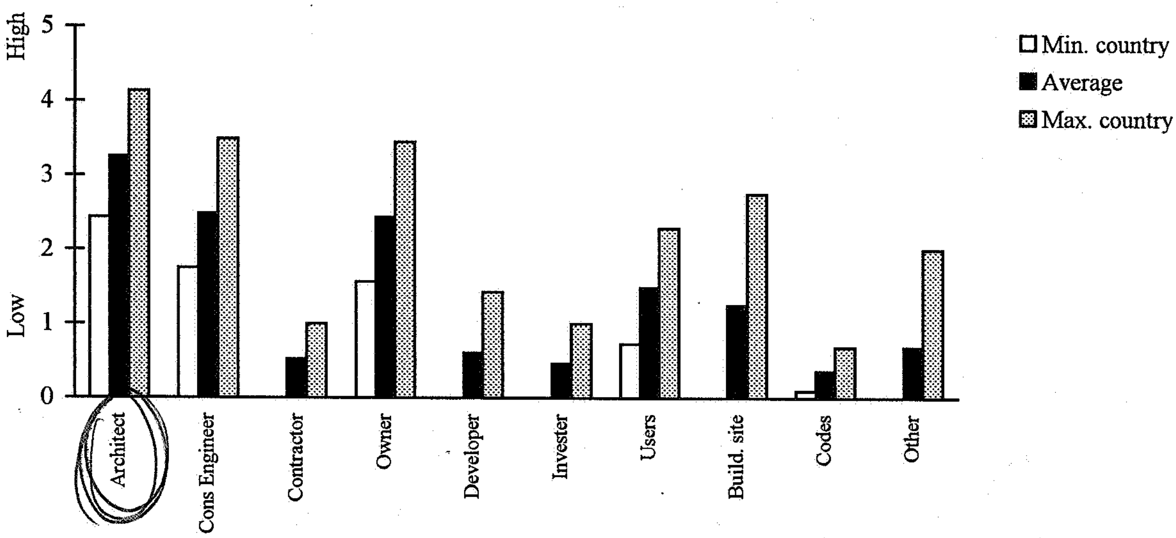


*Figure 11. Influence on the design of the buildings.*

### 3.11 Critical parameters

The interviewees perceived summer temperature, construction costs and indoor air quality to be the most critical design parameters in the specific building projects, see figure 10. The projects included buildings with natural ventilation in the offices and buildings with mechanical ventilation in the offices.

### 3.12 Influence

The architects, the consultant engineers and the owners were the ones with the highest influence on the chosen design in the specific building projects, see figure 11.

# 4. Conclusions

It is necessary with further improvement of natural ventilation system concepts, components, controls and design tools to encourage the wider uptake of natural ventilation in office buildings and to accelerate natural ventilation as a main design option in new and refurbished office buildings.

Simple, energy efficient, low cost natural ventilation system concepts for new and refurbished office buildings have to be developed and tested so that the use of natural ventilation in the majority of ordinary office buildings is not a technical and architectural challenge but a simple and well approved design solution.

Standards and guidelines have to be improved to be a better technical and legal background for the design of naturally ventilated office buildings. The standards and guidelines should also include generally accepted, simple and easy-to-use calculation rules for the design of natural ventilation.

Simple design tools need to be developed e.g. diagrams or easy-to-use computer programmes, that can be used in the early design process by architects, consultant engineers or design teams for analysis of the advantages and disadvantages of different ventilation systems.

The development of better components and control systems for natural ventilation need to be improved in order to enlarge the number of types of office buildings and geographic locations where natural ventilation would be the best choice.

The general knowledge on natural ventilation has to be improved. Among architects, consultant engineers and possibly also contractors the improved knowledge must come from basic education, post education, source books and building studies. Among developers and owners the improved knowledge must be obtained through simple, easy-to-understand descriptions and examples.

It may also be necessary to adjust the fee structure for the design of office buildings so that the designers are payed for the energy, indoor climate and total cost advantages of their design solutions and not for the amount of equipment installed in the building.

# 5. Acknowledgements

This paper is an output from the *NatVent™* project which is part funded by the European Commission DGXII within the JOULE programme 1994-1998 and under contract: JOR3-CT95-0022. The work in the project is also funded by national sources in the participating countries.

# 6. References

Aggerholm, S. "Barriers to Natural Ventilation Design of Office Buildings. *NatVent™* European Report". Danish Building Research Institute. (To be published autumn 1997)

Aggerholm, S. "Barriers to Natural Ventilation Design of Office Buildings. National Report: Denmark". Danish Building Research Institute. (To be published autumn 1997, together with similar national reports from the other participating countries)

you've hit the nail on the head

involve control engineers in the design → is control possible?

* lot of knowledge about control systems !!

↳ DATABASED (intell.) systems

(not MODEL for the building) no build. physics!

least square technique /

maybe neural network

# VENTILATION AND COOLING

18TH ANNUAL AIVC CONFERENCE
ATHENS, GREECE, 23-26 SEPTEMBER, 1997

CONTROL of natural ventilated buildings!

(Title)

# Feedback On The Design of Low Energy Buildings

(Authors)

Djamel Azzi and Gurvinder S Virk

(Affiliation)

E.E.Eng Dept. University of Portsmouth
Anglesea Building, Anglesea Road
Portsmouth. PO1 3DJ. UK

# Feedback On The Design Of Low Energy Buildings

D Azzi and G S Virk
Department of Electrical and Electronic Engineering, University of Portsmouth,
Anglesea ~~Rd Anglesea Road,~~ Portsmouth Hampshire, PO1 3DJ. UK
☎ (01705) 842762 E-✉: dazzi@ee.port.ac.uk

Research Fellow

## Synopsis

This paper presents results from the monitoring of a low energy building, namely, the Portland Building (University of Portsmouth - UK) during February and July 1997. The BMS ~~Research Group~~ at the University of Portsmouth has instrumented the building so that its performance can be compared with the predictions obtained at the design stage. The Building has been operational since July 1996 and the monitoring exercise commenced in January 1997. Sensors monitor air temperature, air relative humidity and slab temperature in selected areas of the building. Analysis of the data collected shows that the $CO_2$ and water vapour levels are acceptable during the winter period and that the number of air changes per hour in the office and seminar room under consideration are adequate. The variations of air temperature in July 1997 inside a seminar room are compared with predictions from a simulation exercise carried out using ESP-r (simulation package) at the design stage and found to be in agreement. The underlying work is on-going and aims at providing feedback on the design on naturally ventilated buildings as well as improving the operational control aspects.

## 1 . Introduction

Building designers in the UK and increasingly in other parts of Europe currently consider natural ventilation as their first option to achieve required indoor conditions. The main reason for this is the concern over energy bills incurred by conventional HVAC equipment. Although natural ventilation might be perceived as an easy alternative, it is not. It requires careful consideration at the design stage even for the simplest building. In many instances, it has to be used in conjunction with alternative strategies (resulting in a mixed mode and/or hybrid system), since it will have been predicted at the design stage that natural ventilation will have difficulty in satisfying all the operational demands; for example a large lecturing theater may necessitate the installation of a conventional HVAC system. This use of mixed technologies makes the problem more difficult as it is the designer's responsibility not to fall into a situation where the overall design is more expensive to run than a conventional HVAC installation.

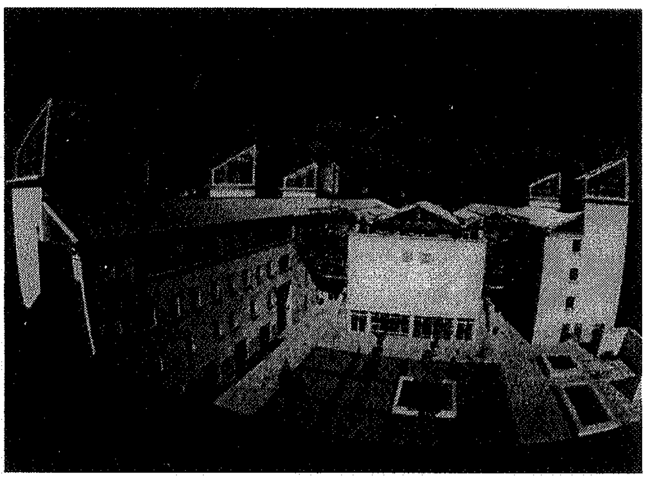

Figure 1. The Portland Building

The main problem associated with natural ventilation is the different requirement between the heating season and summer. In the former case, the concerns are over the maintenance of appropriate ventilation rates to ensure a safe and pollutant free working environment. In the summer the requirement is for high ventilation rates in order to maintain low (with respect to outside conditions) internal temperatures. Increasingly, sophisticated design calculations are called upon to help produce performant naturally ventilated buildings. As a result, there is a growing need for guidance on the design procedures and operation of naturally ventilated buildings. Part of the information required to build up such intelligence will eventually come from monitoring buildings which already implement natural ventilation. This would provide useful feedback for designers and building operators alike. In this context, several schemes are underway to monitor the performance of naturally ventilated buildings [1,2,3] and this paper presents early results from a monitoring exercise being carried out by the authors on the Portland Building [4] on campus at the University of Portsmouth, which is a mixed mode and hybrid building implementing natural ventilation, forced mechanical ventilation and HVAC plants.

## 2 . The Portland Building

The Portland Building (Figure 1) was built to house the Environment Faculty at the University of Portsmouth. It was commissioned during the summer of 1996 and is being monitored by the authors as part of an exercise aimed at assessing the effectiveness of the ventilation process and developing model based solutions to assist in the operation of the buildings. The Portland Building has been described by its designer, Professor Sir Colin Stansfield Smith as "...'a hands on laboratory' for experiencing a whole host of issues that can moderate and control an internal environment.", it is felt to be a valuable teaching aid for students to learn about natural ventilation and the factors which affect it.

The building is L-shaped and has five energy towers which provide staircase access, as well as house the electric ventilating fans and boilers for the under-floor heating. These towers are capped with glazed tops with controllable openings to take advantage of the effects of solar irradiance and the wind. The towers are linked to plenums on the different floors, and allow the air displaced by the stack effect to cross ventilate some of the rooms in the building; the air is discharged to the outside at the highest point in the towers through the motorised windows. The ventilating fans are used in extreme situations (summer time) where the stack effect alone is not sufficient. The Portsmouth BMS Research Group has, in conjunction with the BRE, instrumented sections of the building located between Towers 4 and 5 as described in the following section.

(under floor heating system!)

## 3 . Instrumentation

In order to assess the performance of the building from the comfort and ventilation points of view it was necessary to install required sensors in offices, corridors, rooms and towers. The monitored area in the building is shown in Figures 2 and 3. The emphasis was placed on measuring temperature both inside the space (air) and of

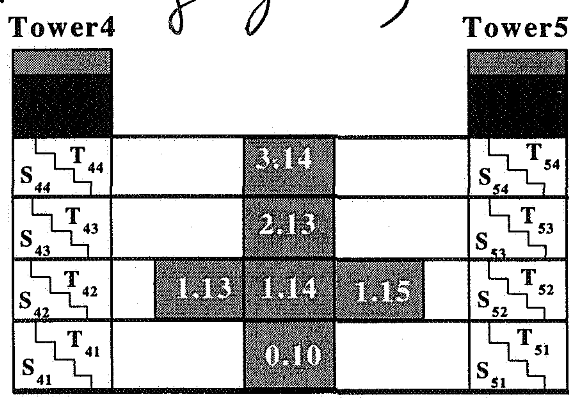


Figure 2. Portland Building - V-section

season). Air temperature inside Room 0.10 displays rapid oscillations on Thursday which can be explained by the fact that the two occupants in this office used a fan heater with a built in thermostat hence the temperatures oscillations.

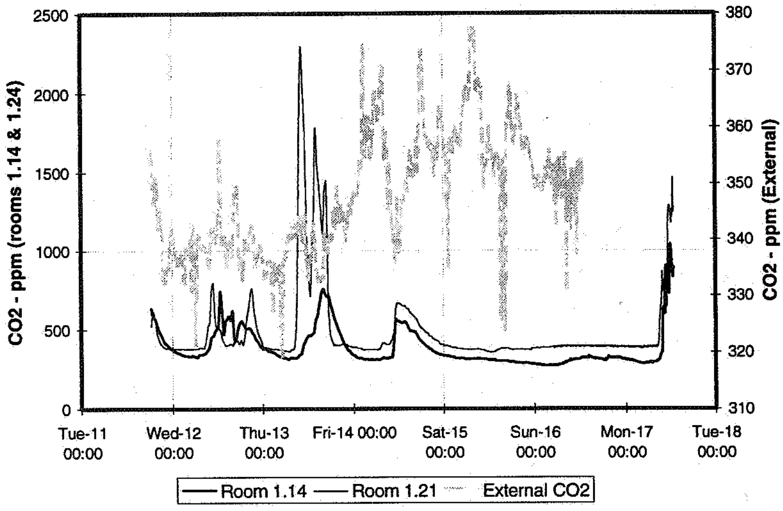

Figure 5. $CO_2$ concentration variations

***February 97- Air $CO_2$ and water vapor content***

Next, we look at the indoor air quality. Since the activities carried out inside the office and the seminar room are those undertaken by sedentary occupants engaged in clerical type work, it is reasonable to consider $CO_2$ and water vapour air content as comfort indicators.

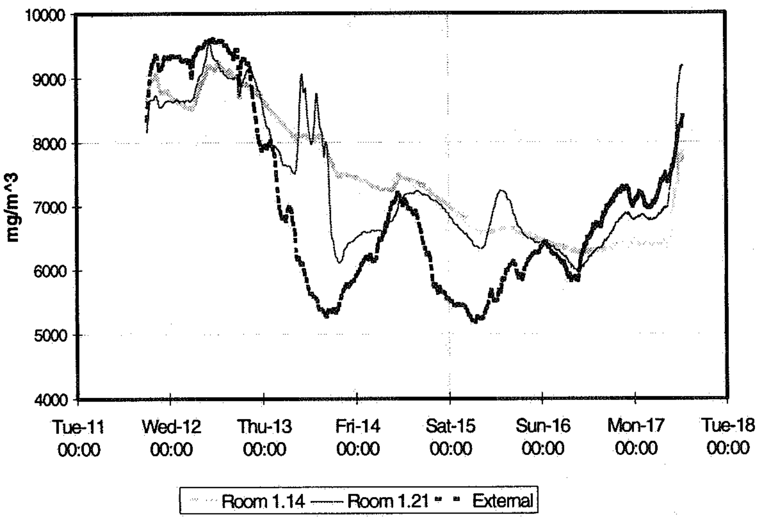

Figure 6. Water vapour content variations

Figure 5 shows the variations $CO_2$ content indoors (rooms 1.14 and 1.21) and outdoors. The latter remains fairly constant throughout the week at an average of ≅350 ppm. The indoor $CO_2$ concentration varies with occupancy as discussed in [5]. The high levels attained in 1.21 (seminar room) on Thursday are due to a class being held in it on that day. The levels are still under 3000 ppm which is below the recommended maximum level of 5000 ppm. Figure 6 shows the variations of water vapour content indoors and outdoors. Again the effect of occupancy can be clearly seen on Thursday-13th. A visual inspection of the graph shows the internal water vapour content is affected in a similar way by the external water vapour variations and the input from occupants, whereas the indoor $CO_2$ in the seminar room 1.21 rises to about 5 times its normal level while a class is being held inside it. The suitability of the $CO_2$ and water vapour levels for occupants is discussed in detail in [5]. Correlation analysis was carried out to assess quantitatively the influence of external $CO_2$ and water vapour content on internal air contents. Figures 7 and 8 show the correlation between the internal (cross ventilated seminar room) and the external water vapour and $CO_2$ air content. We can see that in the case of the water vapour content the behaviour of the external content is more influential than any other source (occupants), whereas in the case of the $CO_2$ content the correlation is not as well defined as in the case of water vapour. This is because the effect of occupancy takes a few hours to dissipate and is in proportion larger than the effect from the occupants on the internal water vapor content. The



Volgende pagina's fout

the walls (structural). Room $R_C$ is at the centre of the monitored section and the rooms on either side, below, above and across the corridor from it are also being monitored.

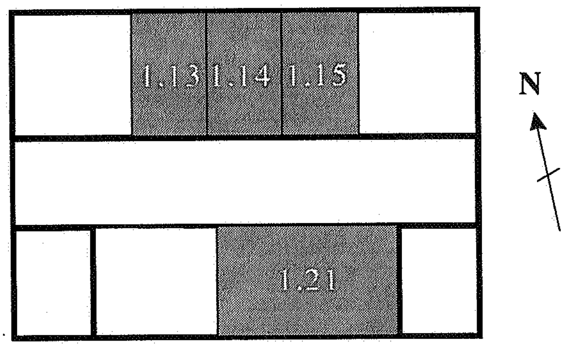


Figure 3. Portland Building - H-section

On the first floor (room $R_C$ and adjacent rooms) the relative humidity was also measured. The information from these sensors is continuously recorded at 5 minute intervals. In addition to this, the ventilation rates in Room $R_C$ (single sided ventilation) and the seminar room $R_S$ across the corridor from it, have been monitored by the BRE in February 1997 (as described in [5]) and more recently in July 1997 using tracer gas (SF6) techniques. Besides this continuous monitoring it is hoped that in the near future funding will be secured to carry out a subjective analysis of comfort conditions by circulating questionnaires among the building occupants.

# 4 . Discussion and analysis of data collected

## 4 . 1 . Winter Period

*February 97- Space temperatures*

Figure 4 shows the variations of air temperature inside single side ventilated offices on four floors and external air temperature. A visual inspection shows a good correlation between the latter and the indoor room temperatures. As can be seen, room 3.14 is the most sensitive to weather variations. This is explained by the fact that the offices on the top floor are heavily glazed and obviously more subject to the wind cooling effect (solar irradiance in the summer

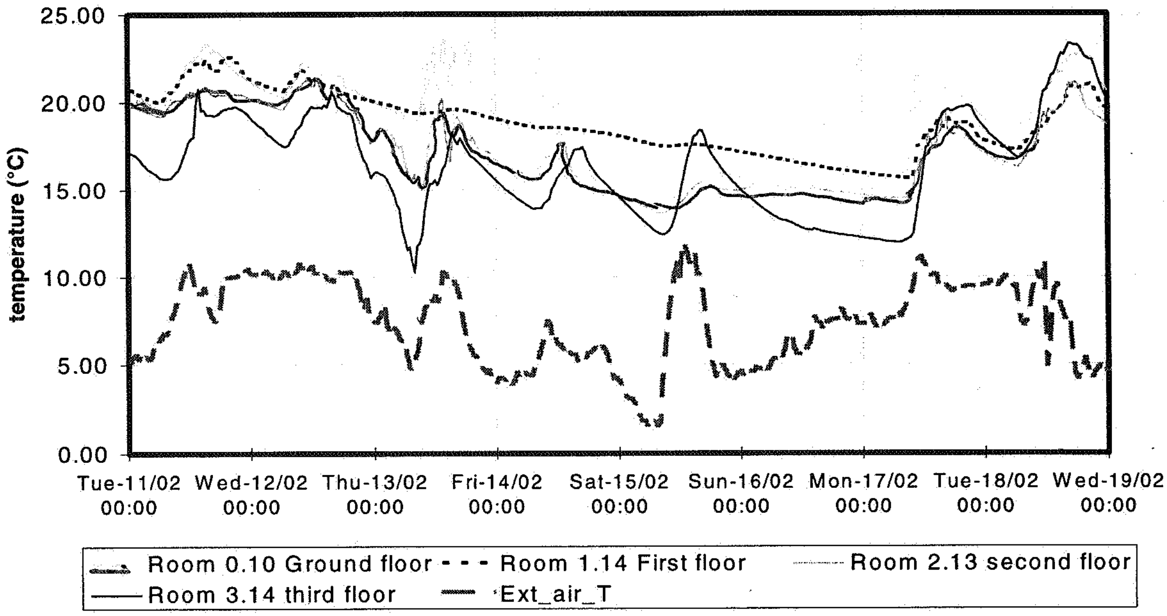


Figure 4. Air temperature on different floors.

computed correlation between the $CO_2$ and water vapour levels inside the room spaces shows that for room 1.21 (seminar room) the correlation is close to 1, but that for room 1.14 it is in the region of 0.5. This can be justified by the fact that the input in terms of water vapour from one occupant in the office does not show itself as strongly as in the case of a class.

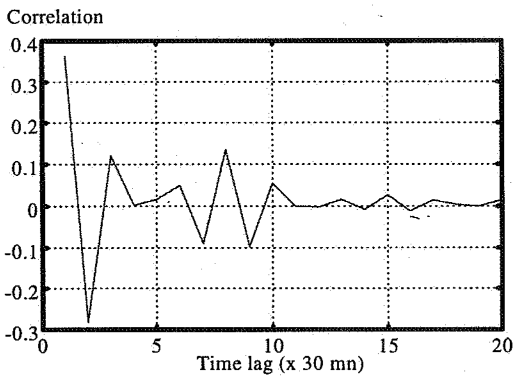


Figure 7. Correlation between outdoor and indoor air $CO_2$ content (seminar room).

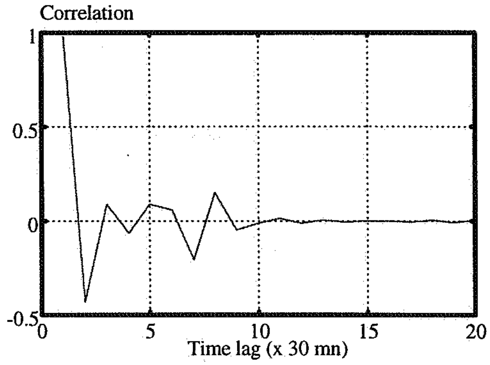


Figure 8. Correlation between outdoor and indoor air water vapour content (seminar room).

*February 97- Air change rate*

Analysis of the correlation between wind speed and direction and the number of ach in the rooms monitored is described next. Figure 9 shows the number of air changes in rooms 1.14 (office) and 1.21 (seminar room). The wind data (speed and direction) for the same period is shown in Figure 10. Visual examination of the curves does not reveal any obvious correlation, therefore, the correlation was computed using the data and is shown in Figure 11. As can be seen the data is uncorrelated. The number of air changes inside the monitored spaces seems to be independent of the variation of wind characteristics. However, the period covered is too short to draw any definitive conclusions; longer monitoring periods might show some dependence between the wind and rate of ventilation. Correlation was also calculated to identify any dependence between tower differential air temperature (between top and bottom of tower) but showed no conclusive results. The large peak in the ach in the seminar room (1.21) on Thursday night is thought to be due to a window left open overnight. The average rate of ventilation for Thursday (9am-5pm) was calculated to be 8 l/s for the office (room 1.14 with one occupant) and 17 l/s per person in the seminar room (room 1.21 - assuming 20 occupants). This shows the effectiveness of the cross ventilation process over the single side equivalent. Although on the border line in the case of the office space, the figures are acceptable and should be higher in the summer.

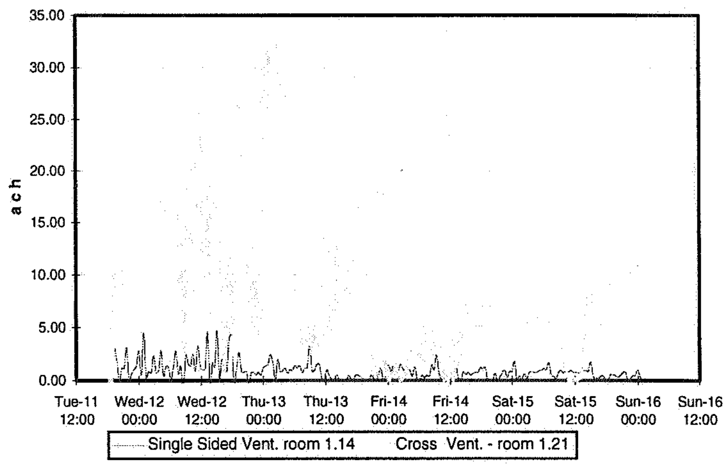


Figure 9. ach in office (1.14) and seminar room (1.21)

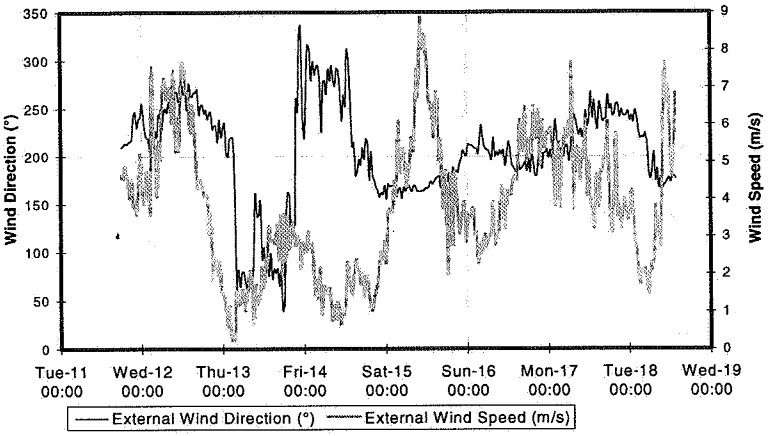


Figure 10 . Wind data

## 4 . 2 . Summer period

### *July 1997 - Maximum air temperature.*

At the design stage The ESP-r package was used to carry out several simulations in order to predict the performance of the Portland Building under extreme conditions and also in order to determine parameters such as the maximum openable area for the vents at the top of the towers. One of the predictions made was that the air temperature inside the studios during the month of July would not exceed 25°C for more than 13 hours during working time, that is 9am to 8pm, Monday to Friday. Figure 12 shows the variations of air temperature in seminar room 1.21 during the month of July 1997. Inspection of the data revealed that the air temperature in this room exceeded the 25°C threshold only by a maximum of 0.5°C for just over 24 hours during the working month, which confirms the predictions made at the design stage. Figure 13 shows the variations

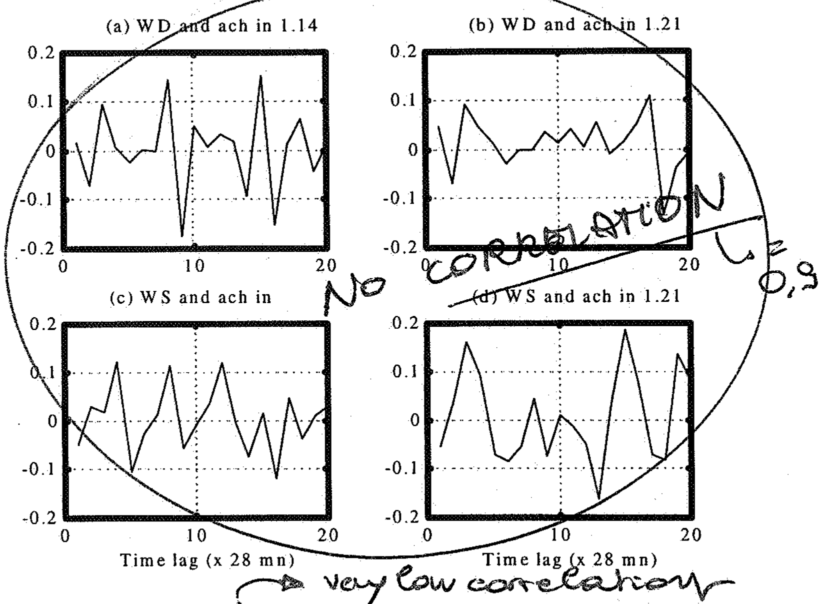


Figure 11. Correlation analysis of ach and wind data.

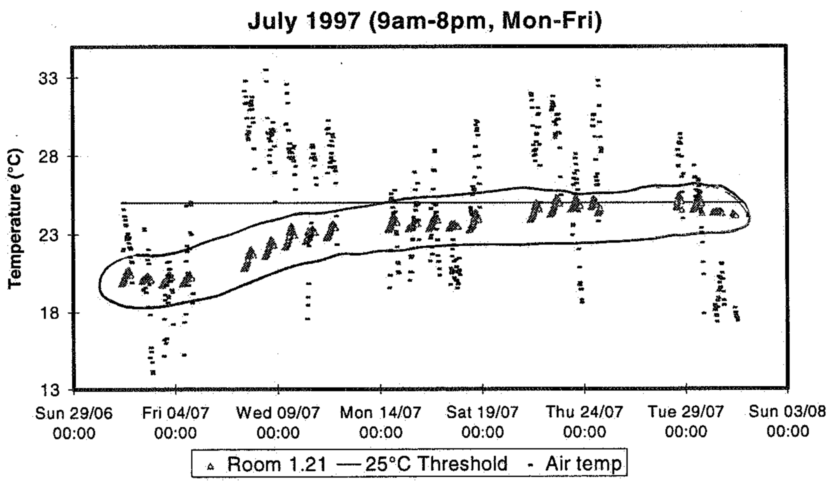


Figure 12. July 1997 air temperature variations room 1.21

or the air temperature in room 3.14 (top floor) during the same period and here the air temperature inside room 3.14 exceeded 25°C for more than 55 hours during the working month by a maximum of 3.2°C. In this case one must bear in mind that this room was possibly unoccupied and that the windows could have been closed at all times thus making ventilation rate minimal if not non-existent.

## 5 . Conclusions

The paper presented initial feedback on the performance of a naturally ventilated building, namely the Portland Building at Portsmouth University (UK). Winter data suggest that pollutant levels inside are well within the suggested limits. A correlation analysis confirmed the effect of occupancy on $CO_2$ and water vapour level, but no correlation was found between wind speed and the number of air changes per hour in either of the monitored rooms (office or seminar room). Finally the room air temperatures for the month of July 1997 were checked against a prediction made at the design stage and it was found out that on the first floor temperature hardly rose above the threshold of 25°C, but that on the third floor in room 3.14 the temperature was higher (maximum 3°C) than the threshold for just over 55 hours. A possible explanation for the latter could be the fact that the room is not occupied during the summer and that the windows could have been closed during most of the month. The monitoring of the Portland Building by the BMS Research Group at the University of Portsmouth is ongoing and the collected data is still being analysed and will be published in the near future.

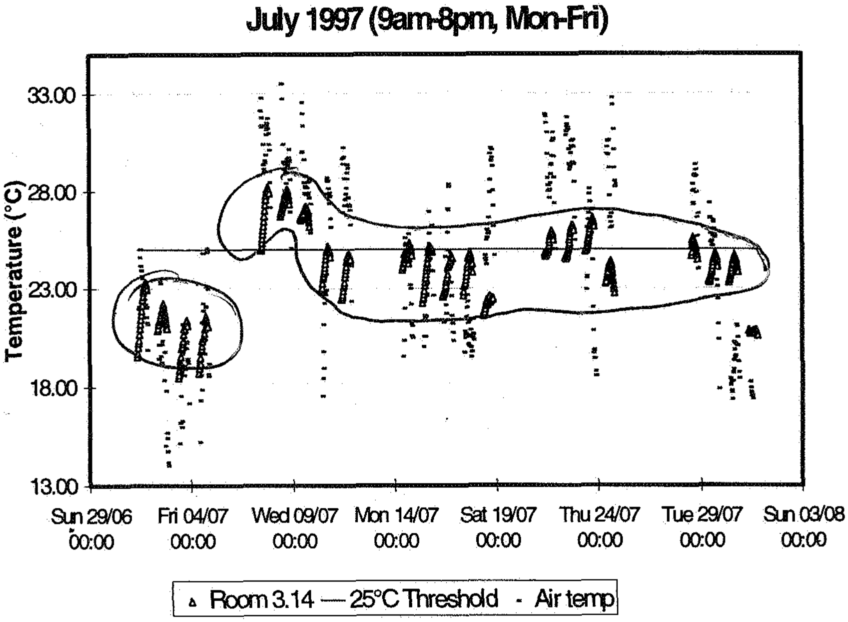


Figure 13. Air temperature variations room 3.14

## Acknowledgments

The authors wish to thank Mr. K Woodward of Hampshire County Council, Dr. M Kolokotroni, Mr. Brian Webb and Dr. Earle Perera of the BRE for their continued help with this work.

## References

1. *Kolokotroni M, Kukadia V and Perera E, "NATVENT - European project on overcoming technical barriers to low-energy ventilation", CIBSE National Conference, Harrogate, September 1996.*
2. *Clancy EM, Howarth A and Walker R., "Measurement of case study buildings:(1) De Monfort University Auditorium", BEPAC, Ventilation Towers Conference, 30th October 1996.*
3. *Happy J, "The energy efficient office of the future at BRE", Energy Management pp26-27, July/Aug 1995.*
4. *"Sense of enclosure: the Portland Building" , Architecture Today 71, September 1996, pp 16-22.*
5. *Kolokotroni M, Shaw R, Webb B and Perera E, Winter ventilation monitoring at the Portland Building", Building Services Journal (CIBSE) pp 47-49, July ~~1987~~.*

1997

# VENTILATION AND COOLING

## 18th ANNUAL AIVC CONFERENCE
## ATHENS, GREECE, 23-26 SEPTEMBER, 1997

constant injection
ipv constant
concentration!

(Title) **Ventilation efficiency measurements in real time using the method of homogeneous tracer emission**

( in mechanical ventilated
( buildings

(Author) **M R Bassett**[1]

nieuwe methode
wordt o.a. vglen met
de 'pulse method'

(Affiliation) 1 Building Research Association of New Zealand
Private Bag 50908 Porirua City
New Zealand

## 1. Synopsis

Trouble shooting air distribution problems in mechanically ventilated offices often has to be carried out in limited "after hours" periods. The method of applying a pulse of tracer to the fresh air supply has been found to be too time consuming to map the local mean age of air over complex floor plans. In response an automated gas chromatograph has been developed to make air change efficiency measurements in real time using the method of homogeneous emission. The equipment described here measures $SF_6$ concentrations at a large number of locations while the tracer is released constantly and as uniformly as possible within the ventilated space. The entire process (including analysing the output from the gas chromatograph) is controlled with a purpose designed computer programme in Visual Basic.

Ventilation efficiency measurements have been completed on twelve separate floors in eight mechanically ventilated buildings. The homogeneous emission method and the pulse method were used and were shown to give the same result in one building and to indicate that the dilution ventilation model most closely describes the ability of common ventilation configurations to deal with pollutants in the breathing zones. Some spatial differences in ventilation performance were evident. It was possible to explain many of these in terms of the distribution of ventilation supply and extract points in relation to internal partitioning.

## 2. Experimental approach

A schematic diagram of the automated tracer gas dosing and detection system is given in Figure 1. The equipment consists of a gas chromatograph (GC) and electron-capture detector (ECD) with a tracer delivery and sampling system automated to monitor ventilation performance simultaneously at up to 20 locations in a building. In this study, the breathing zones were dosed continuously with $SF_6$ through as many as 20 equal length small bore tubes supplied with tracer from a single dosing manifold. Tracer released by the flow regulator into the manifold was diluted with room air and pumped to the dosing points. The floor plan was divided into equal area zones coinciding with partitions where possible and a dosing point was located centrally in each zone about 1.5 m above floor level. Air was sampled continuously from a similar number of locations through small bore tubes using a separate pump to that used for dosing. Transport times were kept to less than a minute to ensure that samples selected by the computer controlled scanning valve and analysed by the gas chromatograph were current. The response of the GC to $SF_6$ was checked every 2-3 days using certified reference gases at 5 ppb and 20 ppb, and the rate of emission of tracer from the dosing regulator was measured by positive displacement several times in each building investigation.

The method used to map the mean age of air in the breathing zones on buildings has been described as the homogeneous emission or constant and uniform emission technique. Sandberg [1] developed a relationship between the mean age of air at a point $\tau_p$ and the local concentration of tracer $C_p$ on the basis that tracer was released into the ventilated space of volume $V$ continuously and uniformly at a rate $S$.

$$\tau_p = C_p/(S/V) \qquad 1$$

The mean age of air is often more easily communicated as an effective ventilation rate $r_p$ analogus to the conventional air change rate, as follows:

$$r_p = 1/\tau_p \qquad 2$$

The homogeneous emission method has been used mostly with passive sampling and dosing systems to measure long term average ventilation performance in naturally and mechanically ventilated spaces. Recent applications by Stymne [2], Walker et al [3] and Stymne and Boman [4] have used passive perfluorocarbon dosing techniques with either passive or pumped samples collected on an absorbing material such as charcoal. In this study a gas chromatograph working in real time has been used to record a time history of tracer concentrations at sampling points. This has given a clearer view of the dynamics of tracer concentrations in spaces where ventilation systems run for only part of the day, and ensured that concentrations $C_p$ could be averaged over periods of stability.

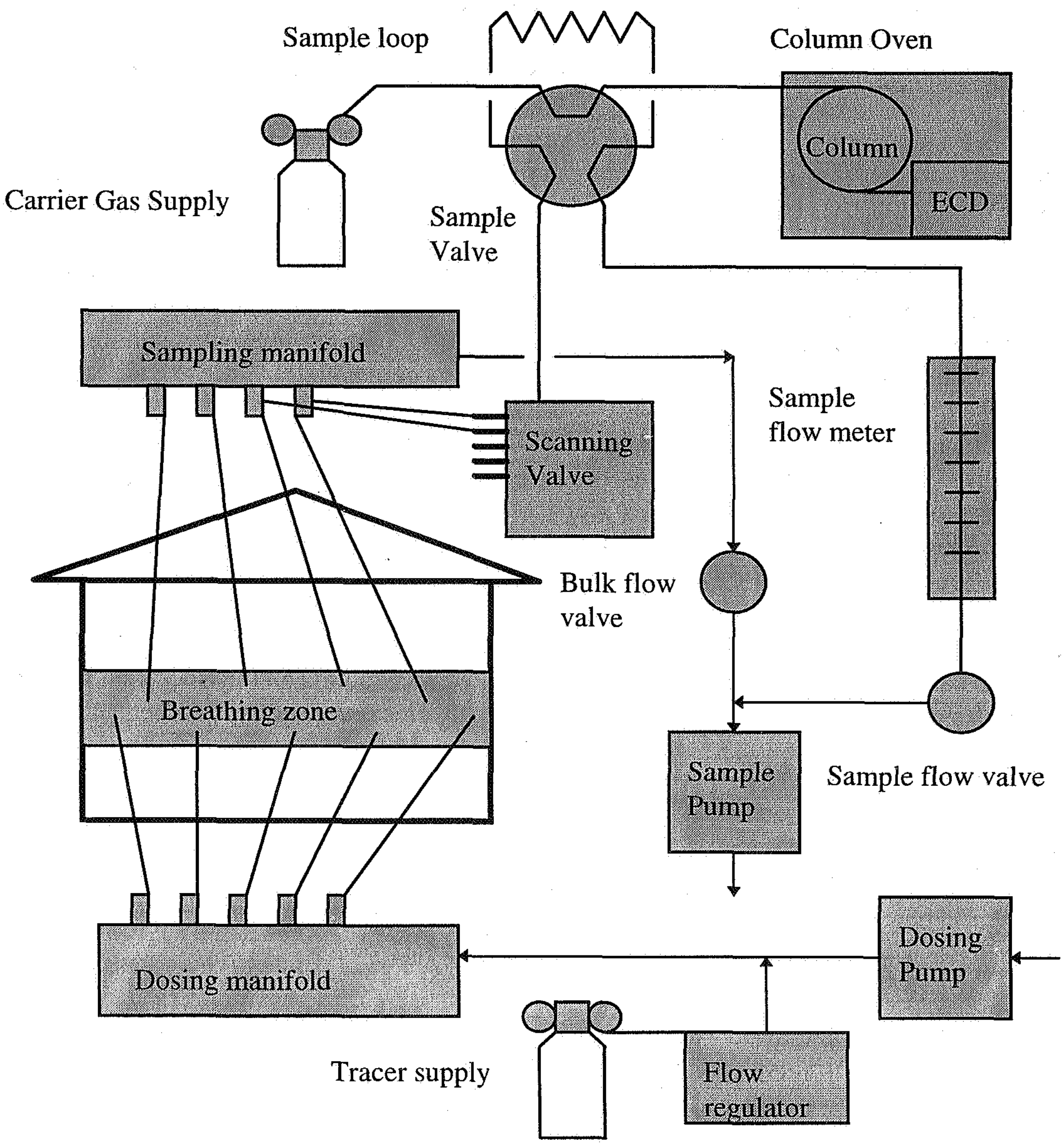


Figure 1: Outline of tracer dosing and sampling equipment for measuring ventilation performance.

## 3. Building and mechanical system descriptions

The ventilation performance measurements described here were carried out in eight buildings (labelled A to H) located in the central business district of Wellington New Zealand. Buildings A to D are the same as A to D in earlier papers [5,6] and buildings D (level 6) to H provide new data. All were office buildings with varying degrees of internal partitioning ranging from open plan to individual offices.

Buildings A B C and D have previously been described in detail [5,6] and only the key ventilation system characteristics are summarised here. All four buildings were provided with a constant air volume (CAV) air supply of 100% fresh air. In buildings B C and D fresh air was supplied onto the floor from a central duct and ducted from here to the proximity of plenum-mounted fan coil units. The efficiency with which fresh air was supplied to the breathing zones was previously determined by mapping the mean age of air over the floor plan using the pulse method. The important floor plan and air handling system details for buildings A to H are presented in Table 1.

Building E was built in the mid 1980's but the ventilation system was extensively refurbished in 1996. Air was supplied to core zones by a variable air volume (VAV) supply with recirculation, while a (CAV) induction system provided 100% fresh air around the glazed perimeter. In common with buildings F and H, the VAV supply was held at maximum air delivery during the tracer measurements so that effective ventilation rates could be compared with the delivered air supply.

Building F was completed in 1990 to provide high quality office space on 29 levels. It employs a sophisticated building management system to control the ventilation system which delivers CAV air to perimeter zones and VAV air to core areas. In common with buildings E and H, recirculation was at a minimum during the summer months when this tracer study was completed.

Building G was completed in 1996 and level 3 was still in un-tenanted open plan form at the time of these measurements. The ventilation system is the same as building D except that fresh air was discharged into the plenum at only four points along one side of the building. The main point of interest in this building was the uniformity with which the plenum mounted fan coil units distributed fresh air over the floor plan.

Building H was completed in the 1970's and only minor changes to the location and type of ceiling diffusers had been carried out since then. VAV air was supplied at 29 points on the floor plan with the highest density of supply points close to the perimeter. The 1st floor was mostly in open plan form during tracer measurements.

| **Building descriptions and air handling system capacities** | | | | | | |
|---|---|---|---|---|---|---|
| Building | Level | Floor area $m^2$ | Volume $m^3$ | Ventilation system type | Air supply rate $m^3/h$ maximum | Exhaust rate $m^3/h$ |
| A | 3 | 1,526 | 4,731 | CAV no recirculation | n/d | n/d |
| A | 2 | 521 | 2,553 | CAV no recirculation | 1,826 | 3,219 |
| B | 2 | 454 | 1,438 | CAV local recirculation | 1,750 | n/d |
| B | 3 | 469 | 1,486 | CAV local recirculation | 1,573 | n/d |
| C | 5 | 1,476 | 4,723 | CAV local recirculation | 3,563 | 2,600 |
| C | 6 | 1,476 | 4,723 | CAV local recirculation | 4,183 | 2,540 |
| D | 7 | 499 | 1,536 | CAV local recirculation | 1,092 | Nil |
| D | 6 | 544 | 1,671 | CAV local recirculation | 1,730 | Nil |
| E | 6 | 532 | 1,430 | VAV core CAV perimeter | 4,745 | n/d |
| F | 27 | 864 | 2,324 | VAV core CAV perimeter | 4,778 | n/d |
| G | 4 | 368 | 1,114 | CAV local recirculation | 1,012 | n/d |
| H | 1 | 450 | 1,248 | VAV non local recirculation | 8,802 | n/d |

Table 1: Building descriptions and air handling system capacities (n/d = not determined).

## 4. Air distribution efficiency

Effective ventilation rates have been measured in all 8 buildings. In buildings A to D (level 7) the pulse method was employed over several weeks to map out the mean age of air on the floor plan. In Buildings D (level 6) to H, the method of homogeneous emission was used, taking three days to accumulate data for at least 30 sample locations on the floor plan. Examples of results for a day are given in Figure 2 for building F and in Figure 3 for building G. Here the ventilation performance is expressed as an effective ventilation rate in air changes per hour (ac/h) according to Equation 2. Figures 2 and 3 have been simplified to show data from only four sampling locations, together with a central fine line representing the mean of 10 sampling locations.

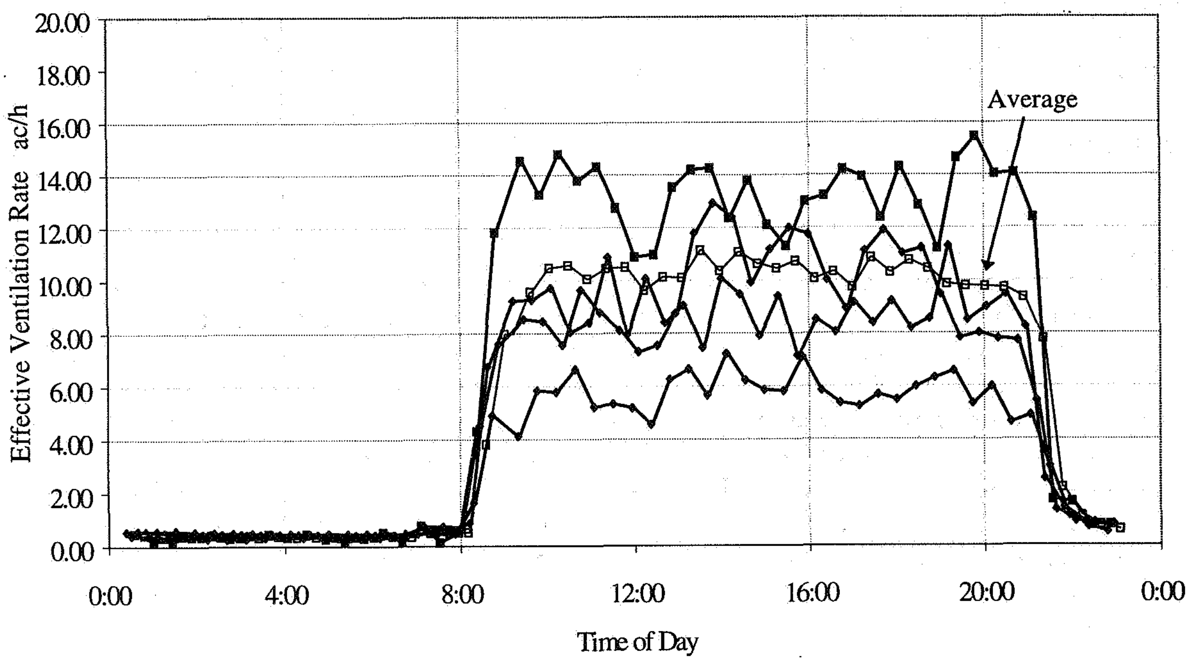


Figure 2: Effective ventilation rates in the breathing zones of building F.

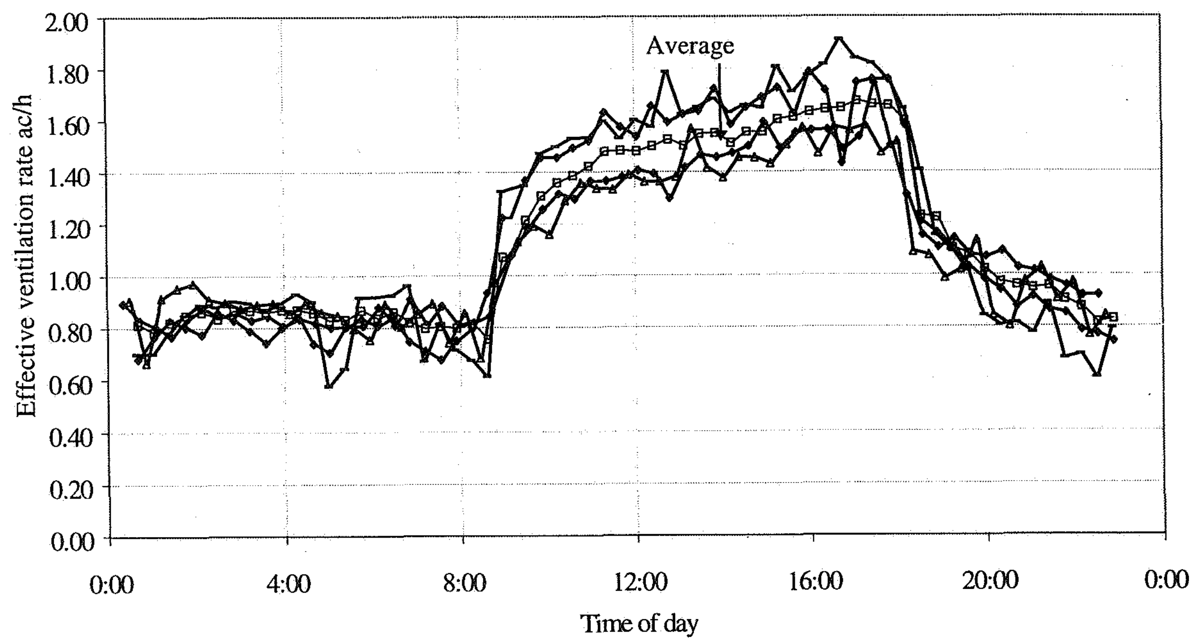


Figure 3: Effective ventilation rates in the breathing zones of building G.

Figures 2 and 3 clearly show how the tracer concentration responded to step changes caused by the ventilation system turning on and off. In building G the nominal time constant of the fresh air supply rate was about 0.6 h and Figure 3 shows that it took several time constants for tracer concentrations to approach steady state. In building F (and in buildings E and H) the time constant was much shorter because the VAV boxes were artificially set to maximum air flow to allow measured air deliveries to be compared with effective ventilation rates. Recirculation was at a minimum in the summer period to provide cooling in all buildings and as a consequence little tracer was detected returning to the floor. In winter with high recirculation fractions this would be reflected as different absolute and relative air change effectiveness results.

With the mechanical ventilation off at night, infiltration rates on floors of buildings E to H were measured and recorded as average mean age of air (infiltration) results in Table 2. In building F the infiltration rates were only weakly dependent on wind speeds, indicating that the measured infiltration was mostly a stack driven vertical air flow through the building. Infiltration and its interaction with mechanical ventilation systems is still relatively poorly understood in office buildings in New Zealand.

The effective ventilation rate was measured at 30 to 50 locations in the breathing zone of each building and the data presented as approximate contours on a floor plan. On the 27th floor of building H there were 61 CAV and 90 VAV terminals so that it was possible to plot both the effective ventilation rate in the breathing zone (Figure 4) and the measured fresh air delivery (Figure 5). The effective ventilation rates in the breathing zone form a similar pattern to the fresh air delivered at ceiling level with highest values around the perimeter. Overall, the effective ventilation rates tend to be higher than would be expected from the dilution ventilation model, especially in the core areas close to the exhaust points at either end of the stair shaft. This indicates that bulk air flows from the perimeter effectively sweep tracer from the core breathing zones. In building G there were grounds for expecting higher effective ventilation rates near fresh air delivery points but in fact air was recirculated sufficiently by the plenum mounted air handlers to eliminate this expected distortion. Figure 6 shows the effective ventilation rates for building G.

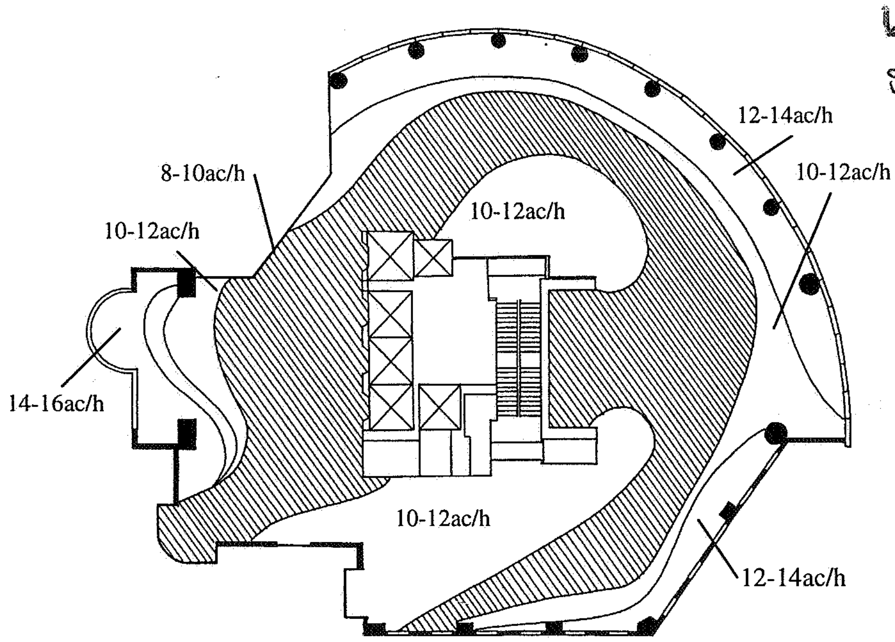


building with recirculation
↓
ACM high?

Figure 4: Approximate contours of effective ventilation rate in the breathing zones of building F

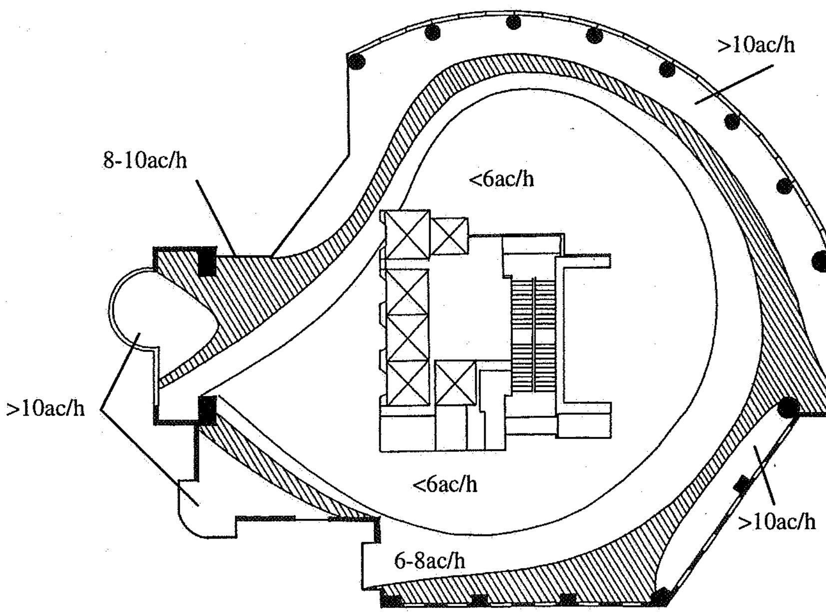


Figure 5: Approximate contours of air flow discharged through the ceiling in building F.

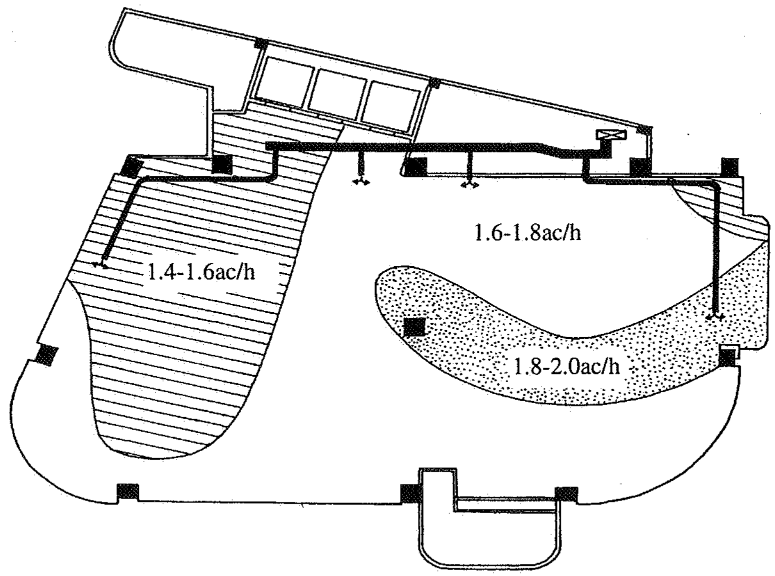


no recirculation ↓ AEM ↓

Figure 6: Approximate contours of effective ventilation rate in the breathing zones of building G.

The mean age of air in the breathing zone of each building floor and the air change efficiency have been calculated and recorded in Table 2. These have been calculated from the nominal time constant for the space and the breathing zone averaged mean age of air using the relationships presented by Sutcliffe [7]. In all cases the nominal time constants indicate that air flows delivered to the floor exceeded the requirements in force when the buildings were constructed.

| Measured ventilation characteristics in 8 New Zealand office buildings | | | | | | |
|---|---|---|---|---|---|---|
| Building | Level | Tracer method | Nominal time constant (h) | Mean age of air (infiltration) h | Mean age of air (ventilation) h | Air change efficiency % |
| A | 3 | Pulse | 0.79 | n/d | 0.75 | 53% |
| A | 2 | Pulse | - | n/d | 0.60 | - |
| B | 2 | Pulse | 0.82 | n/d | 0.76 | 54% |
| B | 3 | Pulse | 0.95 | n/d | 0.64 | 74% |
| C | 5 | Pulse | 1.33 | n/d | 1.65 | 40% |
| C | 6 | Pulse | 1.13 | n/d | 1.31 | 43% |
| D | 7 | Pulse | 1.40 | n/d | 1.41 | 50% |
| D | 6 | Constant | 1.03 | n/d | 1.03 | 50% |
| D | 6 | Pulse | 1.03 | n/d | 1.02 | 50% |
| E | 6 | Constant | 0.28 | 3.8 | 0.24 | 59% |
| F | 27 | Constant | 0.13 | 2.7 | 0.10 | 62% |
| G | 4 | Constant | 0.59 | 1.3 | 0.60 | 49% |
| H | 1 | Constant | 0.12 | 1.0 | 0.098 | 63% |

Table 2: Measured ventilation characteristics in 8 New Zealand office buildings.

Where it was possible to measure the nominal time constant, the air change efficiency for the breathing zones was between 40% and 75%. There was no strong link between these results and the type of ventilation system although there is a suggestion that buildings E, F and H with non local mixing and bulk air flows from perimeter to core areas may be more effective at dealing with pollutants in the breathing zone.

Overall, the study has shown that common ventilation configurations in New Zealand office buildings can be regarded as providing dilution ventilation in the breathing zones. The trend in ventilation standards eg. the draft ASHRAE 62 Standard "Ventilation for Indoor Air Quality" [8] is to include the ventilation effectiveness parameter in design calculations for fresh air supply rates. The measurements available from this study will provide supporting information and experience when New Zealand ventilation standards begin to require a consideration of ventilation effectiveness. Other workers, e.g. Fisk and Faulkner [9], have measured ventilation effectiveness parameters in mechanically ventilated buildings and developed a picture of the effectiveness of systems in a range of buildings. In their data, similar conclusions are reached concerning the description of mechanical ventilation in office buildings as primarily dilution ventilation.

## 5. Sensitivity to dosing strategy

The method of homogeneous emission rests on the assumption that tracer gas can be administered constantly and uniformly through the entire ventilated space. While it is relatively easy to deliver tracer at a constant rate, any realistic number of dosing points will fall short of the infinite number required for uniform emission. The systematic error associated with finite dosing will depend on detailed air flow patterns in relation to dosing and sampling points and this will vary from one building to the next. In this study an indication of the sensitivity to dosing arrangement has been determined by repeatedly measuring the effective ventilation rate at 10 or more fixed points in buildings D to H, while moving the dosing points each day to different sites within the equal volume zones. The pooled standard deviation of the repeated effective ventilation rate measurements in five buildings has been determined as 17%. This is comparable to the systematic error [6] of 20%

associated with pulse method measurements but rather more than a 5% reproducability error determined for homogeneous emission results by repeating effective ventilation rate measurements in building D. This data was collected with unchanging dosing and sampling sites. An overall uncertainty of 20% has been allocated to the effective ventilation rates measured in buildings D to H.

## 6. Conclusions

An automated gas chromatograph has been developed to measure the effectiveness of mechanical ventilation systems in real time. The method of homogeneous tracer emission has been used to explore ventilation performance in 5 buildings at the same time as developing an understanding of the limitations of the method and its sensitivity to different dosing strategies. The following conclusions are drawn from the study:

- Equipment for applying the method of homogeneous emission to mapping the efficiency of mechanical ventilation has been developed and trialed in 5 building floors. The method was shown to give the same mean age of air on one floor as that measured by the pulse method. The main advantage of the homogeneous emission method was that results were collected over three days in comparison with more than a month required for the pulse method.

- Sensitivity to the placement of dosing points was explored in five buildings. Between 10 and 20 dosing points releasing a constant flow of diluted tracer were located centrally in equal volume zones. Altering the dosing strategy by moving dosing points around in the equal volume zones influenced the effective ventilation rates measured at fixed locations by 17% (pooled standard deviation from 5 buildings).

- The air change efficiency in the breathing zones of 12 floors in 8 New Zealand office buildings has ranged from 48% to 75% indicating the dilution ventilation model most closely describes the ability of common ventilation configurations ~~to deal with pollutants~~ in the breathing zones.

↳ almost no short circuiting)


## 7. Acknowledgments

This work was funded by the Building Research Levy and the Public Good Science Fund of the Foundation for Research, Science and Technology. The assistance of the building owners for access to the buildings, Roger Stanford from BRANZ, Ron Conders from Advanced Building Services Ltd and Mark Sinclair from Colliers Jardine is also greatfully acknowledged.


## 8. References


1 Sandberg, M. 1984. *"The multichamber theory reconsidered from a view point of air quality studies"*. Building and Environment 19, 221.

2 Stymne, H. 1995. *"Method to determine local mean ages of air exchange efficiency in large buildings and buildings with many rooms"*. NORDTEST, Final report project No. 1165-94. Helsinki.

3 Walker, R. White, M.K. and Bergsøe, N., 1994. *"Application of new strategies for measuring ventilation rates in office buildings as part of an assessment if indoor air quality and energy use."* Healthy Buildings 94, Proceedings of the 3rd International Conference, Vol. 1, pp319-324, Budapest, Hungary.

4 Stymne, H and Boman, C.A., 1996. *"Application of a passive tracer technique in naturally and mechanically ventilated school buildings."* Proceedings of 17th AIVC Conference, Vol. 1 pp284-291, Gothenburg. Sweden.

5 Bassett, M.R. and Isaacs, N., 1994. *Preliminary ventilation effectiveness measurements by a pulse tracer method.* Proceedings of the 15th AIVC Conference, pp644-655, Buxton, England.

6 Bassett, M.R. and Isaacs, N., 1994. *Ventilation effectiveness measurements in selected New Zealand office buildings.* Proceedings of the 16th AIVC Conference, pp115-124, Palm Springs, USA.

7 Sutcliffe, H. (1990). *"A guide to air change efficiency".* Air Infiltration and Ventilation Centre, Technical Note 28. Coventry.

8 American Society of Heating, Refrigeration and Air-conditioning Engineers, Inc. 1996. *"BSR/ASHRAE Standard 62-1989R".* Public review draft standard. Atlanta.

9 Fisk, W. J. and Faulkner, D., 1992. *Air change effectiveness in office buildings: Measurement techniques and results.* Proceedings of the International Symposium on Room Air Convection and Ventilation Effectiveness, pp282-294. Tokyo.

# VENTILATION AND COOLING

18TH ANNUAL AIVC CONFERENCE
ATHENS, GREECE, 23-26 SEPTEMBER, 1997

# Impacts of air distribution system leakage in Europe: the SAVE-DUCT project

**F.R. Carrié[1], Peter Wouters[2], David Ducarme[2], Johnny Andersson[3], Jean-Claude Faÿsse[4], Pierre Chaffois[4], Marc Kilberger[5] and Vincent Patriarca[5]**

[1] Ecole Nationale des Travaux Publics de l'Etat
Dpt Génie Civil et Bâtiment - URA CNRS 1652
Laboratoire des Sciences de l'Habitat (LASH)
2 rue Maurice Audin
F - 69518 Vaulx en Velin Cedex - France

[2] Belgian Building Research Institute
Division of Building Physics and Indoor Climate
Rue de la Violette 21-23
1000 Brussels - Belgium

[3] SCANDIACONSULT
PO BOX 4205
SE 10265 Stockholm - Sweden

[4] ALDES Aéraulique
20, Boulevard Juliot Curie
F - 69200 Vénissieux - France

[5] Centre d'Etudes Techniques de l'Equipement de Lyon
Groupe Habitat Economie Bâtiment
46, rue Saint Théobald - BP 128
F - 38081 L'isle d'Abeau Cedex - France

CEN TC 156 "Ductwork"

Class A (lowest)
$f_A$ = 1,32 l/s m2 @ 400Pa
↓
ELA = 0,34 cm²/m² @ 25 Pa

Class C $f_A$ = 0,15 l/s m2 @ 400 Pa

SWEDEN
Lindab
↓
Good
Round system
↓
Cost + 25 à 50 %
MAIS installé réel ampelé

Françoise

# Impacts of air distribution system leakage in Europe: the SAVE-DUCT project

**F.R. Carrié[1], Peter Wouters[2], David Ducarme[2], Johnny Andersson[3], Jean-Claude Faÿsse[4], Pierre Chaffois[4], Marc Kilberger[5] and Vincent Patriarca[5]**

[1] Ecole Nationale des Travaux Publics de l'Etat
Dpt Génie Civil et Bâtiment - URA CNRS 1652
Laboratoire des Sciences de l'Habitat (LASH)
2 rue Maurice Audin
F - 69518 Vaulx en Velin Cedex - France

[2] Belgian Building Research Institute
Division of Building Physics and Indoor Climate
Rue de la Violette 21-23
1000 Brussels - Belgium

[3] SCANDIACONSULT
PO BOX 4205
SE 10265 Stockholm - Sweden

[4] ALDES Aéraulique
20, Boulevard Juliot Curie
F - 69200 Vénissieux - France

[5] Centre d'Etudes Techniques de l'Equipement de Lyon
Groupe Habitat Economie Bâtiment
46, rue Saint Théobald - BP 128
F - 38081 L'isle d'Abeau Cedex - France

## Synopsis

This paper gives an overview of duct leakage issues in Europe. A literature review indicates a lack of ductwork air tightness measurement data in the member states. However, based on a few papers and above all on a field study on 22 duct systems in France, we conclude that the ventilation and energy use implications of leaky ducts are large and merit further examination. To this end, we have started the SAVE-DUCT project (1997-1998) aiming at studying the potential implications of a tight air duct policy at the European level. Our work entails an overview of existing codes and standards, a review of available information on ductwork air tightness, and a field measurement campaign. On this basis, data analyses and simulations will be performed. In addition, a two-day workshop will be held in Brussels (June 10-11, 1998) so as to better interact with manufacturers, installers and consultant engineers as well as standardisation and governmental bodies.

## List of symbols

| | |
|---|---|
| $A$ | (tested) duct surface area ($m^2$) |
| $ELA$ | effective leakage area ($m^2$) |
| $f$ | leakage factor ($m^3 s^{-1} m^{-2}$) |
| $K$ | leakage coefficient per $m^2$ of duct surface area ($m\ s^{-1}\ Pa^{-0.65}$) |
| $n$ | flow exponent (-) |
| $Q$ | (leakage) flow rate ($m^3 s^{-1}$) |
| $Q^*$ | $Q$ divided by regulation airflow rate (-) |
| $\Delta P$ | pressure drop across the leaks (Pa) |
| $\Delta P_{ref}$ | reference pressure differential (Pa) |
| $\rho$ | density of air ($kg\ m^{-3}$) |

## Introduction

Mechanical ventilation systems are widely used in European buildings to provide fresh air to the occupants and also to avoid an accelerated deterioration of materials. However, many unanswered questions remain about the performance of these systems. One aspect of particular interest regards the leakiness of the ductwork which has been identified as a major way of wasting energy in US residences (Modera, 1989; 1993). According to Modera, a typical California house with ducts located in the attic or crawl-space wastes approximately 20% of heating or cooling energy through duct leaks and draws approximately 0.5 kW more electricity during peak cooling periods.

Based on a literature review and mainly on a field study conducted in France, this paper presents how duct leaks can impact on the performance of commonly used ventilation systems in Europe, and briefly describes the SAVE-DUCT project.

## Literature review

just part of SAVE-DUCT

It is commonly accepted that the ductwork air tightness is not a major issue for proper functioning of duct systems and thus leakage tests are viewed as an unnecessary expense. However, as stated in Eurovent Guidelines 2/2 a limited ductwork air tightness may be required to minimise the cost and the energy penalty due to an over-sized or inefficient plant, and/or to ease the flow balancing process, and/or to have control over the leakage noise (see Laine (1990)). Other impacts such as the entry or release of pollutants through leaks[1] or the in/ex filtration to unconditioned spaces can be foreseen. To provide a general (however simplified) picture, we have represented schematically duct leakage implications in Figure 1.

Among the member states, Sweden is probably the most advanced on this issue. Nearly every duct system is leak-tested, and air tightness class C (see Eurovent 2/2) is commonly required and fulfilled in new installations. The situation appears to be quite different in the other European countries. Tests are very seldom performed in standard buildings, and thus the knowledge on the ductwork air tightness mainly relies on a few studies.
In the UK, Babawale *et al.* (1993) have investigated one forced air-heating system and have come to worrying conclusions in terms of energy use and comfort conditions. They recommend a research effort to ascertain the extent and impact of duct leakage in new and old building stock in the UK, especially when the ducts run through unconditioned spaces. However, such installations are not very much used in European countries in general.
In Belgium, Ducarme *et al.* (1995) monitored a demand controlled ventilation (DCV) system recently installed in an office building. It was shown that the ductwork air tightness is a key aspect for fully benefiting from the energy savings offered by the DCV. In this specific case, the initial ductwork air tightness was so poor that no savings at all could be achieved: whatever the demand was, the same air flow rate was supplied the building, either to the occupied offices or to the corridor through the leaks. Afterwards, it proved to be very difficult and time consuming to improve the ductwork air tightness so as to meet Eurovent Class A. !!

[1] To our knowledge this issue has not been examined in the European context.

Pittomvils *et al.* (1996) investigated in detail the balanced ventilation system used in more than 170 very low energy houses built in the Flemish Region of Belgium by field and laboratory testing. They showed that the ductwork was so leaky that about one third of the air supplied by the fan at medium speed escapes through leaks before reaching the ventilated room.

In France, Riberon *et al.* (1992) found "insignificant" duct leakage in 19 new single-family houses. However, Carrié *et al.* (1996) measured very large leakage rates in 9 duct systems of multi-family buildings, 8 of schools, 2 of a day-care centre, and 3 of office buildings. Their analyses show that potentially large indoor air quality and energy use impacts at a national level.

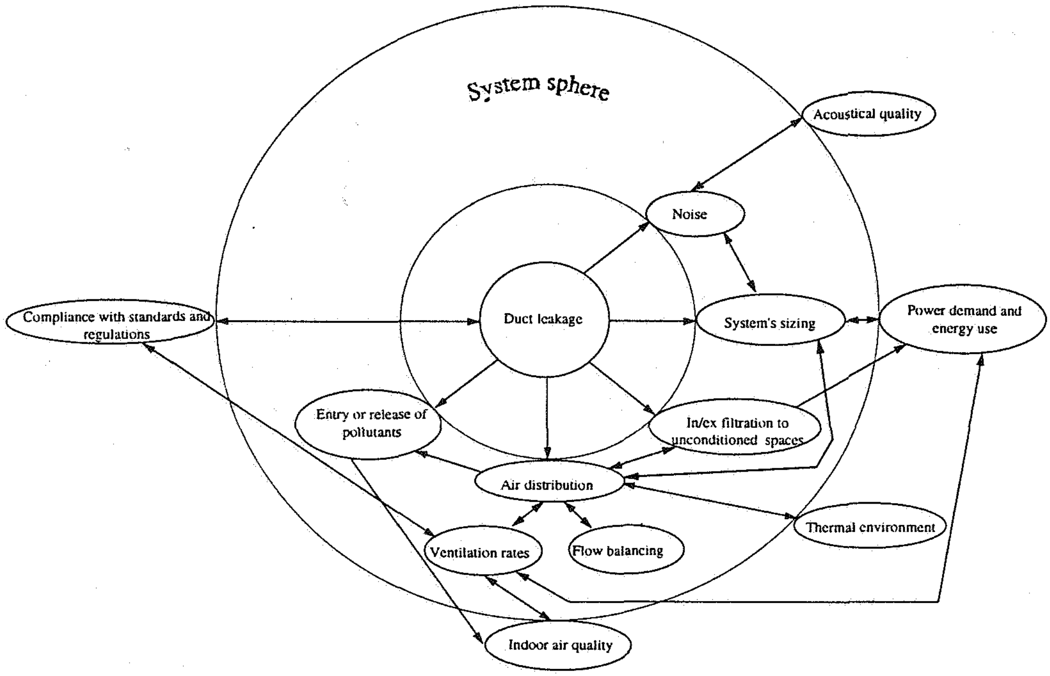


**Figure 1: Schematic diagram of duct leakage implications.**

## Field measurements on 22 duct systems in France

To provide a more detailed picture of ductwork air tightness issues, we propose to focus the field study reported by Carrié *et al.* (1996) that was funded in part by Ademe, and which is the basis of the SAVE-DUCT project described hereafter.

### *Measurement method*

In Europe, most ductwork air tightness standards propose a one-point measurement of the leakage flow rate at a given pressure differential and classify the installations similarly to Eurovent 2/2, i.e. in terms of the leakage coefficient per square meter of duct surface area defined in Equation 1:

$$\frac{Q}{A} = f = K\,\Delta P^{0.65} \qquad \text{(Equation 1)}$$

It is noteworthy that this classification relies on an arbitrary flow exponent of 0.65 which according to DW/143 (HVCA, 1986) is justified by Swedish tests performed on a variety of constructions. As this assumption may not hold in other countries, Carrié *et al.* performed the leakage measurement at several pressure stations which enabled them to assess $K$ as well as the Effective Leakage Area ($ELA$) and the flow exponent defined as follows:

$$Q = ELA\sqrt{\frac{2\,\Delta P_{ref}}{\rho}}\left(\frac{\Delta P}{\Delta P_{ref}}\right)^{n} \qquad \text{(Equation 2)}$$

### *Results*

The sample included 9 duct systems of multi-family buildings (4 to 5 levels), 8 of schools, 2 of a day-care centre, and 3 of office buildings. All of the buildings were located in the vicinity of L'Isle d'Abeau. Significant flaws were observed as shown in Figure 2.

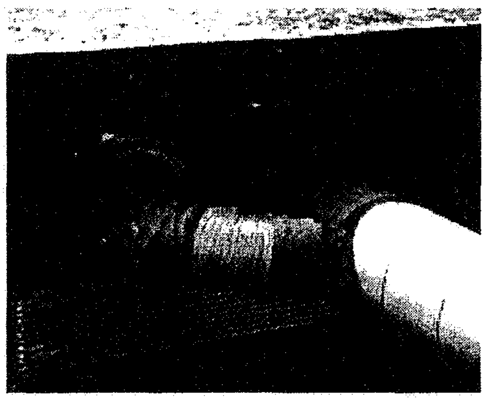

**Figure 2: Photograph of poorly installed duct connections.**

The results are represented Figure 3, and summarised in Table 1. It appears that the flow exponent has an average value considerably different from 0.65. Furthermore, it is found that except for one system, none can be classified according to the Eurovent 2/2 air tightness classes. $K$ is in average well above that of class A ($K < 0.027\ 10^{-3}\,\mathrm{m\ s^{-1}\ Pa^{-0.65}}$).

| | Flow exponent $n$ (-) | $K$ ($\mathrm{m\ s^{-1}\ Pa^{-0.65}}$) | $ELA/A$ ($\mathrm{cm^2/m^2}$) |
|---|---|---|---|
| Multi-family buildings | 0.59 (0.05) | 0.125 (0.050) | 1.9 (0.8) |
| Non-residential buildings | 0.57 (0.04) | 0.066 (0.035) | 1.0 (0.5) |

**Table 1: Duct leakage field measurements results (Carrié *et al.*, 1996). Average values of *n*, *K*, *ELA/A*. The standard deviations are shown in parenthesis.**

invloed op
power installe;

dus voor power
A of D niet zo veel,
wel voor andere zaken
consumpt, quality (iAQ), ...

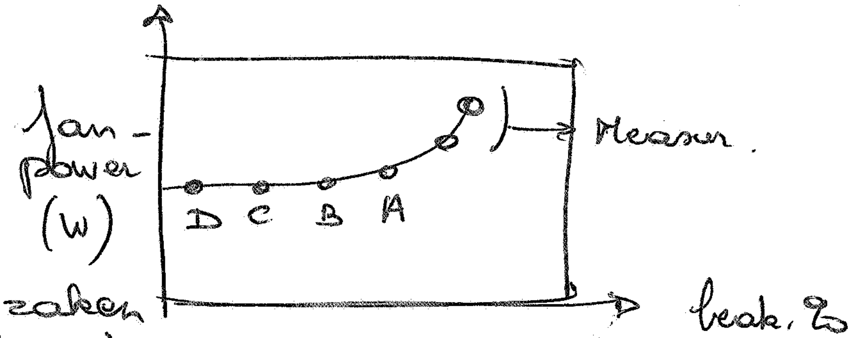


cost
effective!
(class C)

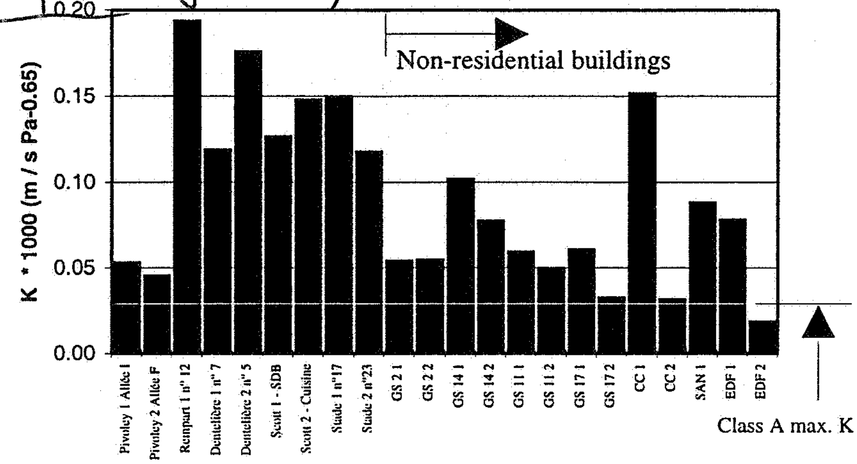


**Figure 3: Duct leakage field measurements (Carrié *et al.*, 1996) - Leakage coefficients.**

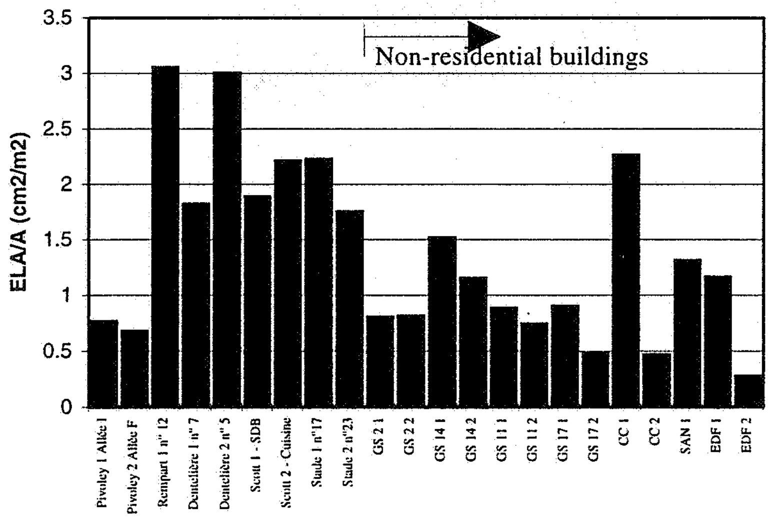


**Figure 4: Duct leakage field measurements (Carrié *et al.*, 1996) - ELA at 80 Pa normalised by the (tested) duct surface area.**

The leakage airflow rate divided by the regulation airflow rate ($Q^*$) is in average of 13% for residential buildings (Figure 5). These leakage rates result in a significant additional fan energy use at a national level given that in France 1 600 000 multi-family housings have been equipped with a mechanical ventilation system between 1981 and 1994 to comply with the regulation airflows. Thus, based on a mean (fan) power consumption estimate of 33 W per housing (see Barles *et al.* (1995)), the additional electricity energy consumption due to duct leakage would be of about 140 millions of kWh per year (16 MW during peak and off-peak periods alike). These energy implications are expected to be even greater as leaky ducts impact on the ventilation rates in a building, which in turn modifies the energy used for heating or cooling.

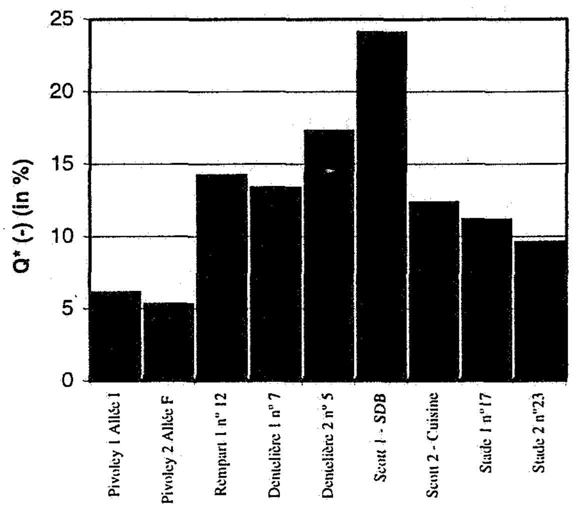


**Figure 5: Leakage airflow rate at 80 Pa divided by regulation airflow rate ($Q^*$) (from (Carrié *et al.*, 1996)).**

## Scope of the SAVE-DUCT project

All of this calls into question the applicability of ductwork air tightness standards and also the quality of the installation of ventilation systems in the member states. On this basis, we have started the SAVE-DUCT project (1997-1998) whose objectives may be summarised as follows:

1. Quantify duct leakage impacts
2. Identify and analyse ductwork deficiencies
3. Propose and quantify improvements
4. Propose modifications to existing standards

This programme is funded in part by the SAVE programme of Commission of the European Communities - Directorate-General for Energy (DG XVII). It is divided in 4 phases:

1. State of the art
    1.1 Existing codes and standards (Task 1)
    1.2 Existing duct leakage in Europe (Task 2)
    1.3 Survey of HVAC manufacturers and contractors (Task 3)

There exists a number of designs of air duct systems, commercially-available ventilation products, and traditions in practice that can potentially affect the leakiness of these systems. This phase is aimed at giving better knowledge about all of those aspects.
A survey of HVAC manufacturers will be done in Sweden, Belgium and France so as to know what types of systems are most used and what could be their air tightness weaknesses. This information will be cross-examined with a survey of HVAC contractors.

2. Field measurements (Task 4)
   Leakage data should be obtained from different states according to a well-defined protocol so as to quantify the impact of different practice traditions and policies. Our sample will include 60 buildings split between Sweden, Belgium and France.
   Existing rehabilitation techniques such as that developed by Modera and Carrié (1996) shall be tested on a few buildings.

3. Data analysis and simulation work (Task 5)
   The data collected in phases 1 and 2 will be analysed to back out estimates of energy use and ventilation rates implications of duct leakage.
   We will also analyse the origins of ductwork permeability. Particular attention will be given to the quality of the installation and that of the commercially-available products. The issue of the compliance with existing standard will also be addressed.

4. Implementing the results
   4.1 Workshop in Brussels (Task 6)
   4.2 Publication (Task 7)

Existing standards will be analysed by quantifying their impacts similarly to what will be done in phase 3. Several improvements will be proposed to manufacturers, HVAC designers and contractors, and standardisation committees.
A workshop will be held in Brussels on the 10th and 11th of June 1998. It is intended to implement the results of the SAVE-DUCT project and allow an exchange of views with the practice (producers, installers, consultant engineers, etc.) and the standardisation bodies. Also, a book reporting the major findings of this project shall be published.

## Conclusion

From this review, there appears an evident lack duct leakage measurement data in Europe (except for Sweden). Impact studies are also very limited. Still, based on a few studies, we can conclude that the ventilation and energy use implications of leaky ducts are large and merit further examination. To this end, we have started the SAVE-DUCT project (1997-1998) whose main objective is to better quantify the potential impacts of a tight air duct policy at the European level. It includes a field study on about 60 buildings to provide a more accurate picture of the ductwork air tightness status. The interaction with manufacturers, installers and standardisation bodies appears to be key to the success of this project. As for this, much is expected from the two-day workshop that will be held in Brussels (June 10-11, 1998).

## Acknowledgements

The research reported here is funded in part by the SAVE programme of the Commission of the European Communities - Directorate-General for Energy (DG XVII). The field study reported (Carrié *et al.*, 1996) was funded in part by Ademe (Agence de l'Environnement et de la Maîtrise de l'Energie) and conducted by CETE (Lyon) and ENTPE.

## References

1. Babawale, Z.A., Serive-Mattei, L., and Littler, J. Domestic ducted forced air heating: duct system leakage and heating energy use. Building serv eng res technol. 1993, Vol. 14, N° 4, p. 129-135.
2. Barles, P., Martin, C., and Yazigi, P. Consommation électrique des ventilateurs. In Séminaire GEVRA 95 - Ventilation des bâtiments. Sophia-Antipolis. Ademe. 1995.
3. Carrié, F.R., Balas, E., and Patriarca, V. Perméabilité des réseaux aérauliques. Ademe / CETE de Lyon, 1996. 22 p. Convention n° 4.04.0189.
4. Ducarme, D., Wouters, P., and L Heureux, D. Evaluation of an IR-controlled ventilation system in an occupied office building. In 16th AIVC Conference - Implementing the results of ventilation research. Palm Springs, CA, USA. AIVC. 1995. p. 517-526.
5. Eurovent 2/2. Air leakage rate in sheet metal air distribution systems. Eurovent / Cecomaf. 1996. 6 p.
6. HVCA. DW 143 - A practical guide to ductwork leakage testing. Heating and Ventilating Contractor's Association, London, 1986. 18 p.
7. Laine, J. Demand controlled air ductwork. In 10th AIVC conference. Espoo, Finland. AIVC. 1990. p. 397-411.
8. Modera, M.P. Residential Duct System Leakage: Magnitude, Impacts, and Potential for Reduction. ASHRAE Transactions. 1989, Vol. 95, N° 2, p. 561-569.
9. Modera, M.P. Characterizing the Performance of Residential Air-Distribution Systems. Energy and Buildings. 1993, Vol. 20, N° 1, p. 65-75.
10. Modera, M.P. and Carrié, F.R. Method and device for producing and delivering an aerosol for remote sealing and coating. The Regents, University of California. USA, US Patent N° 5,522,930. Jun. 4, 1996.
11. Pittomvils, J., Hens, H., and Bael, F.v. Evaluation of ventilation in very low energy houses. In 17th AIVC conference - Optimum ventilation and air flow in buildings. Gothenburg, Sweden. AIVC. 1996. p. 513-520.
12. Riberon, J., Villenave, J.-G., Simeon, R., and Millet, J.-R. Measurement of actual performances of ventilation systems in buildings. In 13th AIVC conference. Nice, France. AIVC. 1992. p. 233-245.